ORP-48628
Revision 0

Tests with High-Bismuth HLW Glasses

Final Report VSL-10R1780-1, Rev. 0; 12/13/10

Prepared for the U.S. Department of Energy
Assistant Secretary for Environmental Management

Office of River Protection

P.O. Box 450
Richland, Washington 99352

ORP-48628
Revision 0

Tests with High-Bismuth HLW Glasses

Final Report VSL-10R1780-1, Rev. 0; 12/13/10

K. S. Matlack
Vitreous State Laboratory
The Catholic University of America

A. A. Kruger
Department of Energy - Office of River Protection

I. Joseph
Energy*Solutions* Federal EPC, Inc.

H. Gan
W. K. Kot
M. Chaudhuri
R. K. Mohr
D. A. McKeown
T. Bardakei
W. Gong
A. C. Buecchele
I. L. Pegg
Vitreous State Laboratory
The Catholic University of America

Date Published
December 2010

Prepared for the U.S. Department of Energy
Assistant Secretary for Environmental Management

Office of River Protection

P.O. Box 450
Richland, Washington 99352

Release Approval Date 01/05/2011

TRADEMARK DISCLAIMER

Reference herein to any specific commercial product, process, or service by trade name, trademark, manufacturer, or otherwise, does not necessarily constitute or imply its endorsement, recommendation, or favoring by the United States Government or any agency thereof or its contractors or subcontractors.

This report has been reproduced from the best available copy.

Printed in the United States of America

VSL-10R1780-1

Final Report

Tests with High-Bismuth HLW Glasses

prepared by

Keith S. Matlack, Hao Gan, Wing K. Kot, Malabika Chaudhuri, Robert K. Mohr, David A. McKeown, Tevfik Bardakci, Weiliang Gong, Andrew C. Buechele, and Ian L. Pegg

Vitreous State Laboratory
The Catholic University of America
Washington, DC 20064

and

Innocent Joseph

Energy*Solutions* Federal EPC, Inc.
Columbia, MD

for

Department of Energy
Office of River Protection

December 6, 2010

Rev. 0; 12/13/10

Document Title: Tests with High-Bismuth HLW Glasses

Document Number and Revision: VSL-10R1780-1, Rev. 0

Issue Date: 12/13/10

Performing Organization: Vitreous State Laboratory, The Catholic University of America

Test Plan: Tests with High-Bismuth HLW Glasses, VSL-09T1780-1, Rev. 0

This report describes the results of testing specified by the above Test Plan. The work was performed in compliance with the quality assurance requirements specified in the Test Plan. Results required by the Test Plan are reported. The test results and this report have been reviewed for correctness, technical adequacy, completeness, and accuracy.

I.L. Pegg: _____ **Date:** 12/13/10
VSL Program Director/Principal Investigator

I. Joseph: _____ **Date:** 12/13/10
Energy*Solutions* Sub-Contract Manager

TABLE OF CONTENTS

List of Tables

List of Figures

List of Abbreviations

ADS	Air Displacement Slurry
ANL-LRM	Argonne National Laboratory – Low Activity Waste Reference Material
AOD	Air Operated Diaphragm
ASME	American Society for Mechanical Engineering
ASTM	American Society for Testing and Materials
BNI	Bechtel National, Inc.
CCC	Canister Center Line Cooling
DCP-AES	Direct Current Plasma Atomic Emission Spectroscopy
DF	Decontamination Factor
DM	DuraMelter®
DOE	Department of Energy
DWPF	Defense Waste Processing Facility
EA	Environmental Assessment
EPA	Environmental Protection Agency
EDS	Energy Dispersive X-Ray Spectroscopy
FTIR	Fourier Transform Infrared Spectroscopy
HEPA	High-Efficiency Particulate Air Filter
HEME	High-Efficiency Mist Eliminator
HLW	High Level Waste
IC	Ion Chromatography
IHLW	Immobilized High Level Waste
LAW	Low Activity Waste
M	Molarity
N	Normality
NIST	National Institute of Standards and Technology
NQA	Nuclear Quality Assurance
ORP	Office of River Protection
PBS	Packed Bed Scrubber
PCT	Product Consistency Test
QAPP	Quality Assurance Project Plan
QARD	Quality Assurance Requirements and Description
RPP	River Protection Project
SBS	Submerged Bed Scrubber
SCR	Selective Catalytic Reduction
SEM	Scanning Electron Microscopy
SOP	Standard Operating Procedure
SRM	Standard Reference Material
TCLP	Toxicity Characteristic Leaching Procedure
TCO	Thermal Catalytic Oxidation
TDS	Total Dissolved Solids
TSS	Total Suspended Solids
VGF	Vertical Gradient Furnace
VSL	Vitreous State Laboratory
W.C.	Water Column
WESP	Wet Electrostatic Precipitator
WTP	Hanford Tank Waste Treatment and Immobilization Plant
XRD	X-ray Diffraction
XRF	X-Ray Fluorescence Spectroscopy

SECTION 1.0
INTRODUCTION

This Final Report describes the testing of glass formulations developed for Hanford High Level Waste (HLW) containing high concentrations of bismuth. In previous work on high-bismuth HLW streams specified by the Office of River Protection (ORP), fully compliant, high waste loading compositions were developed and subjected to melter testing on the DM100 vitrification system [1]. However, during heat treatment according to the Hanford Tank Waste Treatment and Immobilization Plant (WTP) HLW canister centerline cooling (CCC) curves, crucible melts of the high-bismuth glasses were observed to foam [1]. Clearly, such an occurrence during cooling of actual HLW canisters would be highly undesirable. Accordingly, the present work involves larger-scale testing to determine whether this effect occurs under more prototypical conditions, as well as crucible-scale tests to determine the causes and potentially remediate the observed foaming behavior. The work included preparation and characterization of crucible melts designed to determine the underlying causes of the foaming behavior as well as to assess potential mitigation strategies. Testing was also conducted on the DM1200 HLW Pilot melter with a composition previously tested on the DM100 and shown to foam during crucible-scale CCC heat treatment. The DM1200 tests evaluated foaming of glasses over a range of bismuth concentrations poured into temperature-controlled, 55-gallon drums which have a diameter that is close to that of the full-scale WTP HLW canisters. In addition, the DM1200 tests provided the first large-scale melter test data on high-bismuth WTP HLW compositions, including information on processing rates, cold cap behavior and off-gas characteristics, and data from this waste composition on the prototypical DM1200 off-gas treatment system. This work builds on previous work performed at the Vitreous State Laboratory (VSL) for ORP on the same waste composition [1]. The scope of this study was outlined in a Test Plan [2] that was prepared in response to an ORP-supplied statement of work [3].

The HLW waste processing rate at the WTP depends on the glass production rate and waste loading in the glass, both which have been the focus of on-going work for ORP by VSL/Energy*Solutions*. That work has demonstrated substantial improvements in waste loadings and glass production rates for a number of HLW compositions and has the potential for further improvements when applied across the spectrum of Hanford HLW compositions. The WTP HLW melter design, unlike earlier DOE melter designs, incorporates an active glass bubbler system. The bubblers create active glass pool convection and thereby improve heat transfer and glass melting rate. The WTP HLW melter has a glass surface area of 3.75 m^2 and depth of ~1.1 m. The two melters in the HLW facility together are designed to produce up to 7.5 MT of glass per day at 100% availability. Further increases in HLW waste processing rates can potentially be achieved by increasing the melter operating temperature above 1150°C and by increasing the waste loading in the glass product. Increasing the waste loading also has the added benefit of decreasing the number of canisters for storage.

The estimates and glass formulation efforts for WTP have been conservative in terms of achievable waste loadings. These formulations have been specified to ensure that the glasses are

homogenous, contain little crystalline phases, are processable in joule-heated, ceramic-lined melters and meet WTP contract terms. The WTP's overall mission will require the immobilization of tank waste compositions that are dominated by mixtures of aluminum (Al), chromium (Cr), bismuth (Bi), iron (Fe), phosphorous (P), zirconium (Zr), and sulfur (S) compounds as waste-limiting components. Glass compositions for these waste mixtures have been developed based upon previous experience and current glass property models. In addition, however, DOE has initiated a testing program to develop and characterize HLW glasses with higher waste loadings [4]. Results of that work have demonstrated the feasibility of increases in waste-loading from about 25 wt% to 33-50 wt% (based on oxide loading) in the glass depending on the waste stream. It is expected that these higher waste loading glasses will reduce the HLW canister production requirement by about 25% or more. In addition, tests conducted with various HLW waste streams on the DM100 and DM1200 melters have demonstrated increases in glass production rates from 0 to 225 percent while increasing the processing temperature from 1150°C to 1175°C [1, 5]. Further increases to higher operating temperatures (1200°C) have the potential to further increase both processing rate as well as waste loadings, both of which translate into significant cost savings.

Under a separate contract to support the Hanford Tank Waste Treatment and Immobilization Plant (WTP), VSL has developed and tested glass formulations for WTP HLW waste compositions to provide data to meet the WTP contract requirements and to support system design activities [6-8]. That work is based upon small-scale batch melts ("crucible melts") using waste simulants. Selected formulations have also been tested in small-scale, continuously fed, joule-heated melters (DM100) [9-12] and, ultimately, in the HLW DM1200 Pilot Melter [5, 11-18]. Such melter tests provide information on key process factors such as feed processing behavior, dynamic effects during processing, secondary phase formation, processing rates, off-gas amounts and compositions, foaming control, etc., that cannot be reliably obtained from crucible melts. This sequential scale-up approach in the vitrification testing program ensures that maximum benefit is obtained from the more costly melter tests and that the most effective use is made of those resources.

The present glass formulation and melter testing work was aimed at one of the four waste streams previously specified by ORP [4]. Such testing supports the ORP basis for projection of the amount of Immobilized High Level Waste (IHLW) to be produced at Hanford and evaluation of the likely potential for future enhancements of the WTP over and above the present well-developed baseline. It should be noted that the compositions of the four ORP-specified waste streams differ significantly from those of the feed tanks (AZ-101, AZ-102, C-16/AY-102, and C-104/AY-101) that have been the focus of the extensive technology development and design work performed for the WTP baseline. In this regard, the work on the ORP-specified compositions is complementary to and necessarily of a more exploratory nature than the work in support of the current WTP baseline.

1.1 Test Objectives

The principal objective of the work reported here is to determine whether the foaming observed in crucible tests during canister centerline cooling of a glass formulated for a

high-bismuth HLW stream also occurs in large-scale tests, and to identify the causes of foaming upon cooling and potential mitigation strategies. The investigation was conducted at both the crucible and pilot scale (DM1200). The DM1200 unit was selected for these tests since it is able to support pour rates that are prototypical of the WTP HLW melters, and the 55-gallon drums into which the glass from the DM1200 is poured have a diameter that is close to that of the full-scale WTP HLW canisters. The DM1200 melter was also used previously with a variety of HLW glass compositions [5, 11-21] thus allowing comparisons with the previously collected data. These tests provided information on melter processing rates, processing characteristics, off-gas characteristics, melt foaming, and formation of secondary phases.

The objectives for the testing are [2]:

- Determine whether the foaming observed during CCC heat treatment in crucible tests also occurs in more prototypic large-scale tests.
- Investigate the underlying cause of foaming upon CCC of a high bismuth glass at the crucible scale.
- Investigate the effect of waste loading and waste components on foaming upon CCC of a high bismuth glass at the crucible scale.
- Investigate the effects of bismuth concentration on foaming in glass poured from the DM1200 during prototypical cooling conditions.
- Collect melt rate, off-gas, and processing data on the DM1200 while processing a high bismuth HLW composition.

The glass composition development work and foaming evaluation was based on one of the HLW waste compositions specified by ORP that has a high concentration of bismuth and that was previously processed on the DM100 [1].

1.2 Quality Assurance

This work was conducted under a quality assurance program that is based on Nuclear Quality Assurance (NQA)-1 (2000 and 2004) and NQA-2a (1990) Part 2.7 that is in place at the VSL. The program is compliant with applicable criteria of 10 CFR 830.120; Office of Civilian Waste Management DOE/RW-0333P, Quality Assurance Requirements and Description (QARD) Revision 20; the American Society of Mechanical Engineers (ASME) NQA-1, 2000 and 2004; and DOE Order 414.1 C, Quality Assurance. This program is supplemented by a Quality Assurance Project Plan (QAPP) for ORP work [22] that is conducted at VSL. Test and procedure requirements by which the testing activities are planned and controlled are also defined in this plan. The program is supported by VSL standard operating procedures that were used for this work [23]. In addition, the requirements of DOE/RW-0333P, Rev. 20, were applicable to the following specific aspects of this work:

- Crucible melt preparation
- Analysis of crucible melt glasses
- PCT
- Glass transition temperature measurement.

1.3 DM1200

1.3.1 Feed System

The feed material for these tests was prepared and controlled according to VSL specifications by a chemical supplier, as detailed in Section 2. Each batch of feed slurry was shipped to VSL in lined 55-gallon drums, which were staged for unloading into the mix tank. Both the mix tank and the feed tank are 750-gallon polyethylene tanks with conical bottoms that are fitted with mechanical agitators; the feed tank is also fitted with baffles to improve mixing. Any required feed additive can be added to the mix tank. Five calibrated load cells directly mounted on the legs of the feed tank are used to measure additions to, and removal from, the feed tank and are electronically monitored to determine the feed rate to the melter. The requisite amount of feed is pumped to the feed tank from the mix tank; measured amounts of water are combined by weight with the feed at this point to adjust the concentration of the melter feed. The material in the feed tank is constantly recirculated from the feed tank discharge outlet, at the tank bottom, to the tank inlet at the top, which provides additional mixing.

The feed is introduced into the melter using an air displacement slurry (ADS) pump, which is the present WTP baseline. The feed transfer line extends from the outlet of the ADS pump in the feed tank to the top of the melter. Feed is introduced into the melter through an un-cooled feed nozzle that is located above the center of the glass pool. Only one feed tube is used to represent the planned number of feed tubes per unit melt surface area in the full-scale WTP HLW melter. The operation of the ADS pump is controlled from the melter computer control system. The ADS pump works by opening the pump reservoir to the feed tank using a double-acting air cylinder and mechanical link to actuate the poppet. The reservoir is filled with slurry by gravity. After sufficient time is allowed to fill the reservoir (a few seconds), the poppet is toggled to close the reservoir to the tank and open the transfer line. After a desired delay time (dependent on the desired feed rate) the reservoir is pressurized with air to transfer the slurry (about 1.6 liter/shot) to the melter. This cycle is repeated at the rate required to provide the desired feed rate.

When necessary, a backup system is used to introduce feed into the melter with an air operated diaphragm (AOD) pump system that simulates the pulsed feeding action of an ADS pump. The recirculation loop extends to the top of the melter where feed is diverted from the recirculation loop into the melter through a Teflon-lined feed line and water-cooled feed tube. Two computer-operated pinch valves, one on the feed line and one on the recirculation loop, are activated in a timed sequence to introduce feed into the melter at the desired rate. The feed rate is regulated by adjusting the length of each pulse, the time between each pulse, and the pressure applied to the recirculation loop.

1.3.2 Melter System

The DuraMelter 1200 (DM1200), which is the HLW Pilot Melter, was used for these tests. Cross-sectional diagrams of the melter illustrating the discharge chamber and electrode configuration are provided in Figures 1.1 and 1.2. The DM1200 is a Joule-heated melter with Inconel 690 electrodes and thus has an upper operating temperature of about 1200°C. The melter shell is water-cooled and incorporates a jack-bolt thermal expansion system. The footprint of the melter is approximately 8 ft. by 6.5 ft. with a 4 ft. by 2.3 ft. air-lift discharge chamber appended to one end; the melter shell is almost 8 ft. tall. The melt surface area and the melt pool height are approximately 32 percent and 57 percent, respectively, of the corresponding values for the full-scale HLW melter. The discharge riser and trough are full-scale to verify pouring performance. Other aspects of the discharge system are also prototypical such as the chamber ventilation scheme. The glass contact refractory is Monofrax® K-3 while the plenum area walls are constructed of Monofrax® H refractory. The surface of the glass pool is 34" by 54" with a nominal glass depth of 25". The resultant melt volume is approximately 45,000 cubic inches (735 liters), which represents a glass tank capacity of more than 1.7 metric tons of glass. However, since the typical operating glass level is closer to 29 inches, the effective glass volume during testing is actually about 849 liters, giving an inventory of about 2.0 metric tons. The DuraMelter™ 1200 is fitted with one pair of electrodes placed high on opposite walls of the melter as well as one bottom electrode. The side electrodes are 11" by 34" giving an electrode area for the pair of about 750 sq. in. Depending on the glass level, the plenum space extends about 33" to 36" above the melt surface resulting in a plenum volume ranging from about 43 to 46 ft^3.

The single-phase power supply to the melter electrodes (250 kW design power) is derived from the DuraMelter 1000 transformers by wiring them in parallel and using a single large silicon controlled rectifier. Current can be passed either from the side electrodes to the bottom electrode or between the two side electrodes only, by rearranging jumpers; only side-to-side operation was used for the present tests. Programmable process controllers are installed and can be used to control temperature or power. The melt temperature is controlled by configuring the process controller to maintain constant power and adjusting the power set-point as needed to maintain the desired operating temperature. Alarms can be set to detect out-of-range temperatures or power in the melter. Backup process controllers are installed to be used in case of failure of the main controllers. The entire system is supported by a back-up generator that is tripped on in the event of a power outage.

The DuraMelter 1200 has several other features. The lid refractory is prototypic and also includes a two-piece construction, which simulates the seam needed for the LAW lid that was planned to be fabricated in three pieces. Nozzles are provided for the off-gas film cooler, a standby off-gas port, discharge airlift, along with 11 ports available for top-entering bubblers, start-up heaters and other components as needed. In addition, a bubbler arrangement is installed in the bottom electrode with the objective of developing permanent bubblers for possible use on future melters. For the present tests the optimum bubbler configuration established during previous tests with HLW simulants [5] consisting of two double-outlet, top-entering bubblers

was used, located in positions to mimic conditions in the WTP HLW melter. Figure 1.3 shows a schematic of the prototypical double-outlet bubbler design that is based on the combination of the results from these DM1200 tests [5] and room-temperature tests that were performed in a transparent fluid simulating the properties of the glass melt [24]. These bubblers have outlets 8 inches apart and were placed on the melter floor. The orientation of the bubblers in the melter, as shown in Figure 1.4, results in one of the bubbling outlets being 11.3 inches from the feed tube.

1.3.3 Off-Gas System

The melter and entire off-gas treatment system are maintained under negative pressure by two Paxton external induced draft blowers. This negative pressure is necessary to direct the gases from the melter to the prototypical off-gas system. The off-gas treatment system, shown schematically in Figure 1.5, consists of a submerged bed scrubber (SBS); a wet electrostatic precipitator (WESP); a high-efficiency mist eliminator (HEME), a high-efficiency particulate air (HEPA) filter; a thermal catalytic oxidation unit (TCO); a NO_X removal system (SCR); a caustic packed-bed scrubber (PBS); and a second HEME. Note that the PBS and the second HEME are not part of the WTP off-gas train, which effectively ends at the SCR. The HEME is used to limit entrained particle carryover into the balance of the VSL ventilation system. The system can be functionally divided into four subsystems:

Particulate Removal: Components from the SBS to the HEPA serve to remove essentially all of the particulate from the gas stream with an estimated removal efficiency of greater than 99.9999% for particles greater than 0.3 μm in size. In the WTP facility, this provision serves to segregate the radioactive from the non-radioactive components in the system for maintenance and handling purposes.

VOC Control/Acid Gas: The TCO unit is designed to oxidize any hazardous organics that are present in the off-gas stream. This is followed by a SCR to remove NO_X gases and a PBS to remove remaining acid gases.

Stack System: The emergency/bypass exhaust system, which includes a second HEPA, and the primary off-gas system both feed into the building stack system for exhausting to the atmosphere.

Liquid Processing: Components including the water spray lines, liquid sampling and water storage tanks, as well as the effluent evaporator, function to sample and process the system liquids for recycle or discharge.

With minor exceptions, the DM1200 off-gas system processing sequence follows the design for the full-scale WTP HLW melter system, except for cooling of the off-gas stream discharged from the SCR unit (which is present in the WTP off-gas train, but absent in the DM1200 system). Per WTP direction, the SBS unit that was used for previous DM1200 testing was modified in early 2004. Installation of the new system was completed in March 2004 and

that unit was used for the present tests. The changes were implemented to reflect modifications to the WTP SBS design that have taken place since the original DM1200 unit was installed. These modifications included changes to the diffuser plate design, down-comer jacket and connection to the diffuser plate, bed diameter, bed packing materials, cooling coils, and liquid overflow level.

Initial quenching of the melter exhaust gas stream is effected by the film cooler. Immediately upstream of the film cooler is the injection point for control air, which is used to regulate melter pressure. The gas entering the balance of the off-gas system is at a temperature of about 250 to 350°C and a flow rate of about 100-250 scfm, of which about 10-80 scfm is water vapor. The off-gas is then rapidly quenched by direct liquid water contact in the SBS, which also effects removal of most of the larger particulates. The piping between the film cooler and SBS has a high superficial gas velocity to minimize particulate deposition. The gas stream leaving the SBS is at a low temperature (typically between 40-50°C). Further mist and particulate removal is effected in the WESP, HEME and HEPA. The TCO and SCR follow the particle removal components and serve to destroy organic compounds and nitrogen oxides. These two units were off-line during the present tests due to the low concentrations of these components in the exhaust stream. Finally, the PBS provides acid gas removal. Water sprays are located in the WESP, PBS, and facility HEME to wash down deposits and dissolved species into their respective collection sumps from which they can be sampled. The system components are fabricated from corrosion resistant materials, including AL6XN and 316L stainless steel, and various plastics in less demanding locations. There are extensive provisions for sampling both the gas and liquid streams throughout the system in order to collect mass balance information and removal efficiency data for each treatment stage.

The off-gas system maintains the melter plenum under slight negative pressure, typically about -5 in. W.C. The plenum pressure is controlled by means of an air injection system that introduces a controlled air flow into the off-gas jumper just after the film cooler. The air is supplied by a blower through a diverter valve. The setting of the diverter valve, and therefore the air flow rate, is controlled by a process controller that responds to the signal from a melter pressure transducer. When the plenum pressure becomes more positive, the air injection flow rate is decreased, which tends to restore the pressure to the set-point. Conversely, the flow rate is increased when the plenum pressure becomes more negative.

1.3.4 Drum Cooling System

Crucible tests conducted at VSL using the canister centerline cooling curve measured during the Energy*Solutions* HLW canister filling tests indicated that, for high Bi content glasses, foaming occurred at some point during cooling [1]. To reproduce that cooling history for glass discharge from the DM1200 melter, a cooling system was built mimicking as nearly as practical the discharge conditions used by Energy*Solutions* [25], which in turn were intended to represent those at the WTP. The HLW canisters are 24" in diameter and 176.75" tall. The typical DM1200 discharge is into a 55 gallon drum which is nominally 23" in diameter and 34" tall. An examination of the centerline cooling curves for the HLW pour tests indicate that the radial cooling effects dominate any end effects. That is, with a buffer of hot glass from previous pours

below the current pour, cooling curves were relatively independent of height in the canister, as can be seen in Figure 1.6 from the report [25]. That figure shows temperature vs. time curves measured at four different heights in the canister before and after the glass pour that covered a particular thermocouple. The cooling system used in the present work was designed to create environmental conditions at the surface of the 55 gal drum similar to that of the HLW canisters during filling and cooling. This is facilitated by the similar diameters of the HLW canisters and the 55 gallon drums used on the DM1200.

The filling procedure for the HLW canisters at the LAW Pilot plant consisted of a nominally 30 minute discharge of about 150 kg of glass at about 1050°C, followed by about a 60 minutes delay before the next pour. The environment around the canister was cooled by forced air convection, with the flow rate adjusted to control the temperature rise of the discharged air. An insulating fiber enclosure 5' on a side surrounded the majority of the canister with the top two feet left exposed. The air was fed into the bottom of the enclosure and exited at the top of the enclosure. In the present DM1200 tests, because of limited space, the insulating fiber enclosure was 2.5' to 3' on a side, leaving the top 6 to 8 inches exposed. The wall temperatures of the canisters during the HLW pour tests are known and similar temperatures on the 55 gal drums should produce similar centerline cooling. Therefore the cooling airflow was adjusted to obtain the desired wall temperatures of the drums. To obtain a buffer of hot glass below the pour of interest, an initial pour of about 150 kg was performed. This was allowed to cool until its centerline temperature reached approximately 900°C, thereby providing a bed of glass for the test pour similar to that seen in the Energy*Solutions* canister filling. The test pours correspond to a level increase of about 14" in the drum, or about 270 kg of glass. A thermocouple tree similar to that employed by Energy*Solutions* was used to monitor the temperatures along the centerline, 3" from the centerline, 9" from the centerline, and at the exterior of the drum. The temperature vs. time curves were monitored by a data logger. The drum cover on the DM1200 had a view port that was fitted with a camera to view the glass during the pour. This allowed the observation and recording of any foaming that occurred.

1.4 Feed Sample Analysis

Feed samples were taken directly from the feed recirculation line during each test. Feed samples were poured into a platinum/gold crucible that was placed into a programmed furnace for drying and fusion to form a glass. The glass produced from this fusion was ground to less than 200 mesh and sealed in 20-ml vials for subsequent analysis by x-ray fluorescence spectroscopy (XRF), or by acid digestion followed by direct current plasma - atomic emission spectroscopy (DCP-AES) on the resulting solution. The feed samples were also characterized for their rheological properties, density, pH, water content, and glass yield.

1.5 Glass Product Analysis

The glass product from the DM1200 tests was discharged from the melter into 55 gallon drums periodically using an air-lift system. The discharged product glass was sampled by removing sufficient glass from the top of the cans for compositional analysis after the cooling

period and visual inspection (see Section 4.0). Samples were also taken from the center of drums and other locations after the drum was sawed in half. Glasses produced during crucible melt testing underwent heat treatments as well as measurements of processability (viscosity, conductivity and crystal content) and chemical durability (PCT and TCLP) to ensure their compliance with the present WTP contract requirements. All of these procedures are routinely conducted at VSL and, therefore, standard operating procedures (SOPs) are in place.

Sample preparation for chemical analysis typically involves size reduction and sieving. All samples were subjected to XRF to determine the concentration of all elements except boron and lithium. A series of National Institute of Standards and Technology (NIST) reference materials were used for confirmation of the XRF data. Boron and lithium were determined by total acid dissolution of ground glass samples in HF/HNO_3 and subjecting the resulting solutions to DCP-AES analysis.

1.5.1 Viscosity

The melt viscosity, η, was measured using a Brookfield viscometer. Measurements are performed in the temperature range of 950-1250°C and the data are interpolated to standard temperatures using the Vogel-Fulcher equation: $\ln \eta = [A/(T-T_o)]+B$, where A, B, and T_o are fitting parameters. The equipment is calibrated at room temperature using standard oils of known viscosity and then checked at 950-1250°C using a NIST standard reference glass (SRM 711). Both precision and accuracy of the viscosity measurements are estimated to be within ±15 relative%.

1.5.2 Electrical Conductivity

The electrical conductivity, σ, of each glass melt was determined by measuring the resistance of the glass melts as a function of frequency using a calibrated platinum/rhodium electrode probe attached to a Hewlett-Packard model 4194A impedance analyzer. Measurements are performed over similar temperature ranges to those employed for the melt viscosity measurements. The results are analyzed and modeled to obtain the DC electrical conductivity. The electrical conductivity data are then interpolated to standard temperatures using the Vogel-Fulcher equation: $\ln \sigma = [A/(T-T_o)] + B$, where A, B and T_o are fitting parameters. Estimated uncertainties in the electrical conductivity measurements are ± 20 relative%.

1.5.3 Product Consistency Test (PCT)

The product consistency test (PCT; ASTM C 1285) is used to evaluate the relative chemical durability of glasses by measuring the concentrations of the chemical species released from 100-200 mesh crushed glass (75-149 μm) to the test solution (de-ionized water in this case). PCT on the HLW glasses are performed at 90°C, in accordance with the current WTP contract requirement. The ratio of the glass surface area to the solution volume for this test is about 2000 m^{-1} (typically, 10 g of 100-200 mesh glass is immersed in 100 ml deionized water). All tests are

conducted in triplicate, in 304L stainless steel vessels, and in parallel with a standard glass included in each test set. The internal standard is the Argonne National Laboratory – Low Activity Waste Reference Material (ANL-LRM) reference glass [26] and/or the Defense Waste Processing Facility (DWPF)-Environmental Assessment (EA) glass, both of which have undergone round-robin testing. The leachates are sampled at predetermined times, the first of which is seven days. One milliliter of sampled leachate is mixed with 20 ml of 1M HNO_3 and the resulting solution is analyzed by DCP-AES; another 3 ml of sampled leachate is used for pH measurement.

1.5.4 Toxicity Characteristic Leaching Procedure (TCLP)

The TCLP was performed at VSL using SW-846 Method 1311, which employs leaching of crushed glass (< 3/8") in a sodium acetate buffer solution for 18 hours at 22°C with constant end-over-end agitation. A mass of about 100 grams of glass is leached in 2 liters of TCLP extract, according to the extraction method for non-volatiles. The surface area to volume ratio for this test is about 20 m^{-1}, which is about two orders of magnitude lower than that in the PCT. The leachates are analyzed by DCP-AES according to VSL standard operating procedures.

1.5.5 Secondary Phases

Secondary phases in the glass samples were determined by optical microscopy and scanning electron microscopy coupled with energy dispersive x-ray spectroscopy (SEM-EDS). Secondary phases due to crystallization and phase separation can be identified using these methods. Quantitative determination of the amount of crystals in glass samples were made by SEM in conjunction with image analysis.

1.6 Emission Samples

Melter emission fluxes were measured to complete the mass balance for each melter test. Isokinetic melter exhaust samples (exhaust gas flow velocity equal to velocity through the gas sample probe tip) were combined with the fourier transform infrared (FTIR) spectroscopy continuous monitoring data for gaseous species to characterize fluxes from the melter. In the DM1200 system, independent sampling ports for particulate and FTIR sampling are available throughout the off–gas treatment train (see Figure 1.5). Standard EPA isokinetic off-gas sampling trains and methods (EPA Methods 1A, 2, 4, 5, 26, 29), composed of particulate filters and liquid impingers, were used to collect materials that were subjected to chemical and physical analyses using the techniques described in Sections 1.4 and 1.5.

1.7 DM1200 Off-Gas System Sump Solutions

Sump solutions from the SBS, WESP, HEMEs, and PBS were taken throughout testing to verify material balances and unit efficiency. Total suspended solids (TSS) and total dissolved

solids (TDS) were determined on select samples using standard ASTM methods. The filtered solids and liquids derived from this procedure were analyzed to determine the total inorganic composition using methods similar to those used in glass and feed analysis. Anion concentrations were determined by ion chromatography and ion selective electrode analyses on filtered solutions. Select sump samples were also characterized for pH and density.

SECTION 2.0
WASTE SIMULANT AND BASE GLASS COMPOSITION

2.1 Waste Simulants

The waste stream compositions previously provided by ORP are given in Table 2.1 on an oxide basis [4]. The work described in this report focuses exclusively on the bismuth limited waste stream in response to the foaming observed at crucible scale during CCC [1]. Actual HLW Hanford tank wastes are aqueous solutions with suspended solids and dissolved salts including hydroxides, nitrates, nitrites, halides, and carbonates. For the purpose of the previous [4] and present work, the concentrations of the volatile components (i.e., carbonate, nitrite, nitrate, and organic carbon) are assumed to be similar to those found for the AZ-102 HLW waste [16]. With the waste compositions defined, formulation of the HLW waste simulant proceeds in a straightforward fashion. In general, oxides and hydroxides are used as the starting materials, with a slurry of iron (III) hydroxide (13% by weight) as one of the major constituents. Volatile inorganic components are added as the sodium salts, whereas organic carbon is added as oxalic acid. Although crucible melts using the appropriate radioactive components (i.e., thorium and uranium) were prepared and evaluated previously, radioactive components were omitted and the waste composition was renormalized in the simulated waste used for melter testing. Finally, the water content was adjusted to target a glass yield of 500 g of glass per liter of feed. The composition of the waste simulant formulated to produce 100 kg of waste oxides is given in Table 2.2.

2.2 Base Glass and Melter Feed Formulation

The composition and properties of the high-Bi glass selected for melter testing are given in Table 2.3. The selected glass formulation, HLW-E-Bi-6, meets all of the processing and product quality requirements imposed for these tests and has a waste oxide loading of 50 wt%. This exceeds both the minimum and maximum expected waste loadings provided in the previous scope of work [4] of 15 wt% and 40 wt%, respectively. The glass contains 6.7 wt% Bi_2O_3 and close to 5 wt% P_2O_5. The Bi_2O_3 content is more than three times the WTP contract minimum for Bi_2O_3 (2 wt%), PCT leach rates are over an order of magnitude lower than those of the DWPF-EA glass, and the TCLP leachate concentrations are all below the WTP delisting limits. The measured processing parameters are within acceptable ranges. As noted above, the viscosity is towards the high end of the acceptable range, which was appropriate in view of the fact that a portion of the testing was performed at elevated temperature on the DM100 [1]. The same formulation was used for the DM1200 tests to determine whether the foaming behavior observed in the crucible tests during CCC heat treatment was evident in prototypical large scale tests.

Melter feeds were produced by NOAH Technologies Corporation, the supplier of simulant and feed samples used in previous testing on the DM100 and DM1200 melter systems.

SECTION 3.0
GLASS FORMULATION STUDIES OF CAUSE OF FOAMING AND METHODS OF SUPPRESSION

3.1 Introduction

As part of the overall effort to better understand the foaming behavior during canister centerline cooling of glasses developed for the Bi-limited waste stream previously specified by ORP [1], the small-scale work reported in this section was focused on preparation and characterization of crucible melts designed to determine the underlying causes of the foaming behavior as well as to assess potential mitigation strategies.

Foaming was reported for the Bi-limited glass HLW-E-Bi6 when it was subjected to canister centerline cooling [1]. Such foaming, during or after filling of HLW canisters, would be a serious operational issue if it was to occur during waste processing at the WTP. As discussed in Sections 4 and 5, large-scale prototypic tests performed on the DM1200 melter system with the same glass formulation clearly show that this is a very real possibility. Development of a robust mitigation strategy requires an improved understanding of the underlying foaming mechanism in Bi-rich glass melts. Given the scope of this work, the small-scale work was designed to collect data that would aid the characterization of the foaming process and identification of the key glass components that could be used to formulate glasses to mitigate foaming. Since the properties and behavior of glass melts are closely related to the local structure or speciation of elements in addition to the chemical composition, Raman spectroscopy was used for characterization of short range order of the representative glass/melt samples. The association of foaming events and the short range order by Raman spectra could potentially provide useful information to identify chemical species that are responsible for foaming.

A secondary objective of the glass formulation work was to improve the melt rate of the high bismuth glass formulation, which was lower than desirable in vertical gradient furnace VGF) tests [19], DM100 melter tests [1], and in DM1200 tests performed in the present study (Section 4).

Therefore, the small-scale studies were conducted in four inter-related areas:

- Investigation of the underlying cause of foaming upon CCC;
- Investigation of the effect of waste loading and glass forming components on foaming upon CCC;
- Feed conversion tests (VGF) on the selected glass formulation with different glass forming additives;
- Characterization of the short range order of glass samples by Raman spectroscopy.

The HLW-E-Bi6 glass formulation [1], which was developed previously for the high-bismuth HLW stream specified by ORP and which was tested previously on the DM100 system was used as the starting point for the small-scale investigation. Ten new glasses at the same or higher waste loadings as compared to HLW-E-Bi6 were formulated and tested to examine the effects of waste loading and other glass components on foaming behavior during canister centerline cooling (CCC). A further ten glass samples, eight of which were newly formulated for this work, were chosen to investigate the underlying causes of the foaming behavior and the conditions under which foaming occurs. As part of the integrated effort for identifying the process that is responsible for the observed foaming, 16 newly formulated glasses and HLW-E-Bi6 were analyzed by Raman spectroscopy to investigate their characteristic short range order.

Feed conversion behavior was evaluated using VGF tests under standard conditions [19]. Seven melter feed samples were tested for their feed conversion behavior. These high-bismuth HLW glasses employed different waste loadings and used different combinations of glass former additives.

3.2 Experimental Methods

3.2.1 Waste Simulant

The waste stream compositions previously provided by ORP are given in Table 2.1 on an oxide basis [1]. The work described in this report focused exclusively on the bismuth limited waste stream in response to the foaming observed at crucible scale during CCC [1].

3.2.2 Glass Sample Preparation

Glass samples were prepared according to VSL standard operating procedures. Chemicals were batched and mixed before being fused at 1200°C. The glass was melted in a Pt/Au crucible and was homogenized by continuous mechanical stirring at 1200°C for 1.5 hours and quenched by pouring directly into a graphite mold at ambient temperature. The glass compositions were confirmed by XRF analysis. Selected glasses were further analyzed by DCP-AES for confirmation of their Li_2O and B_2O_3 concentrations.

3.2.3 Characterization of Glass Samples

3.2.3.1 Glass Foaming on CCC Heat Treatment

Glass samples were subjected to CCC [27] heat treatment to determine their foaming tendency. All CCC heat treatments were performed in large Pt/Au crucibles holding ~45 grams of glass in order to provide sufficient volume to contain the sample in case of foaming. Glass

samples after CCC were first inspected visually and then cross-sectioned to prepare petrographic thin sections.

Depending on sample condition, if possible, the whole cross-section of the CCC glass sample was preserved in the petrographic thin section. After polishing, thin sections of the CCC glass samples were optically scanned in reflection mode and the acquired images were reviewed on a computer monitor for signs of development of gas bubbles during CCC heat treatment.

A few glass samples were tested using a "*truncated* CCC profile" in order to capture the onset of the foaming event. A truncated CCC follows the standard CCC profile down to the truncation point at which time the experiment is terminated by rapidly quenching the glass sample in cold water. The glass samples thus collected (usually fragmented due to the rapid quench) were inspected visually and prepared as thin sections for further examination.

3.2.3.2 Glass Crystallinity

Secondary phases in the glass samples after 70-hour heat treatments (at 950, 900, 850 and 800°C) were determined by scanning electron microscopy coupled with energy dispersive x-ray spectroscopy (SEM-EDS). The volume percentage of crystals in the glass samples were estimated by performing image analysis on the SEM images.

3.2.4 Vertical Gradient Furnace Tests

The temperature gradient inside the VGF is maintained by two separate sets of heating elements, both of which are arranged in cylindrical form and aligned along their axis (Figure 3.1). The inner heater is set at 1150°C, which is the nominal temperature of the glass pool, and the ambient heater is set at 600°C, which is similar to the melter plenum temperature. A ceramic crucible (4 inches tall) was used to contain the reacting feed blend. The temperature gradient in the furnace is shown in Figure 3.2. For a typical feed conversion test, a dried feed sample was introduced into the ceramic crucible, which was already loaded with about 10 grams of glass of identical composition and preheated in the inner heater. Feed reactions under the controlled temperature gradient were allowed to continue for the designated test duration (typically 30 minutes) and then stopped by rapid cooling in room temperature air. The top surface of the reacted feed blends were then inspected and photographed for assessment before being cross-sectioned to reveal the conversion progress of the feed pile. The images of the cross sectioned feed pile inside the crucible were optically scanned and stored as image files.

3.3 Investigation of Foaming Mechanism

3.3.1 Basic Considerations and General Approach

Foaming can occur in commercial and waste glass melters as a result of physical or chemical processes that involve generation and release of gases. Most commonly for waste glass

melters, this is the result of release of oxygen gas produced via reduction of multivalent metal oxides at elevated temperatures. Gases other than oxygen dissolved in glass melts can also be released due to reduced solubility with increasing temperature. In both cases, the so-called *reboiling* phenomenon results in gas generation and foaming as the temperature is increased, with typically greater tendency for foaming with more rapid heating. In this context, the foaming behavior observed for glass HLW-E-Bi6 is unusual in that a large amount of gas bubbles formed and accumulated inside the melt during a controlled and relatively slow *cooling* process. As noted above, such behavior in a HLW canister during or after filling could have serious consequences.

As listed in Table 2.3, the Bi-limited HLW waste contains several groups of elements that can contribute to gas formation: 1) Multivalent Bi that can be trivalent or reduce to Bi metal in a borosilicate glass; 2) Volatile elements F and S; 3) Considerable amounts of multivalent elements Cr and Fe that could be sensitive to the redox environment; 4) The high concentration of P_2O_5 (~5 wt% P_2O_5 in the glass at 50 wt% waste loading) is also noteworthy. SEM/EDS analysis of a sample of HLW-E-Bi6 glass after standard CCC showed the presence of dentritic sodium and calcium phosphates with bismuth.

The general approach adopted in the present study was to identify the roles of the selected key constituents experimentally from a series of glasses that deviated from a central composition by removal or addition of one or two key components of interest. To the extent that these constituents are involved in the foaming mechanism, foaming will be enhanced or suppressed when the components responsible for foaming are added or removed entirely from the glass formulation.

Table 3.1 lists a total of ten glass compositions prepared to investigate the foaming mechanism. Besides the starting composition HLW-E-Bi6 and its melter-discharged equivalent, eight other glasses were newly formulated around the center glass composition HLW-Bi-F2, with Bi, P, F, or Cr removed or added, individually or jointly. The results from this study are presented below.

3.3.2 Baseline Glass HLW-E-Bi6 and HLW-Bi-F2

The three glasses that were tested initially for foaming included the crucible glass HLW-E-Bi6 that was developed previously and tested in the DM100 melter [1], its melter-discharged equivalent (BLL-G-46A), and a lower-viscosity variation (HLW-Bi-F2).

In an effort to capture the foaming progress, all samples in this group were subjected to shorter (truncated) CCC profiles (2 hours to 6 hours) as well as the standard CCC. As explained in Section 3.2.3.1, the truncated CCC tests captured the higher temperature part of the CCC and were terminated after 2 to 6 hours from the point at which the samples reached 1050°C during the cooling process. Because the melt viscosity increases rapidly with decreasing temperature, at low enough temperatures, foaming will be inhibited due to restrictively high viscosity. As a result, it was hypothesized that foaming was most likely to occur at a relatively high temperature where the melt is fluid enough to allow formation of gas bubbles but not so fluid as to allow them to

rise and dissipate. As listed in Table 3.2, CCC tests for this group were truncated after 2, 4 and 6 hours for HLW-E-Bi6, after 2 and 6 hours for the re-melted glass HLW-E-Bi6r, its melter-discharged equivalent BLL-G-46A, and its low-viscosity variation HLW-Bi-F2.

Foaming was observed in **HLW-E-Bi6**, its re-melt HLW-E-Bi6r, and its lower viscosity variation HLW-Bi-F2 when subjected to the full CCC. In addition, these samples showed extensive crystallization of predominantly spinel crystals present as clusters or swirls indicative of possible flow patterns when the melt viscosity is sufficiently low. Gas bubbles were widely distributed and tended to concentrate near the top half of the samples after full CCC treatment, with majority of the bubbles ranging in sizes between around 100 microns to several hundred microns. Gas bubbles apparently started to form within the HLW-E-Bi6 melt as early as two hours into controlled cooling and became more extensive as cooling continued into the 4th hour and 6th hour. It appears that the formation of gas bubbles continued beyond 6 hours into the CCC because more gas bubbles were observed on the images of thin sections of samples subjected to the full CCC profile (Figures 3.3a, b and 3.4a-f).

Glass **HLW-Bi-F2** after truncated CCC for two hours displayed bands of spinel crystals without any sign of gas bubble formation. However, after 6 hours truncated CCC, gas bubbles ranging in size from around 100 microns to several hundred microns were observed. Along with the gas bubbles, clusters of spinel crystals were observed. As shown in Figures 3.3a and 3.4h, i, it is apparent that more gas bubbles formed in glass HLW-Bi-F2 even though it is less viscous than HLW-E-Bi6.

No gas bubbles formed in **BLL-G-41A** after CCC (Figures 3.3d and 3.4j-l). As listed in Table 3.1, analysis of HLW-E-Bi6 and BLL-G-41A show that they are virtually identical in terms of concentrations of major components. However, the two glass samples have major differences in their thermal history. The implication of the two different thermal histories will be discussed later in this report, but at this point, it suffices to point out that it is evident that something other than chemical composition also contributed to the foaming event. In addition to the absent gas bubbles in the CCC samples, the morphology and distribution of crystalline phases appeared considerably different in the melter discharged glass sample as compared to the crucible samples. Overall, no flow pattern is present in the scanned image of the thin sections; rather, the glass contains densely populated crystals and more or less uniformly dispersed lighter-colored spheres of around 100 microns or larger. Under an optical microscope using transmitted light, these lighter colored spheres contain skeletal opaque crystals of acicular nature. It is likely that these acicular crystals are a Cr-rich phase and the formation and growth of this phase depleted the chromium concentration surrounding the center, which is manifested by a light-colored spherical volume. Moreover, the linear dimensions of the skeletal crystals are usually 100 to 200 microns, which is roughly 10 times larger than those observed in HLW-E-Bi6 or HLW-Bi-F2. The crystals in samples subjected to truncated CCC tests are less densely populated and the light-colored spheres are absent. Generally, however, crystalline phases are distributed more or less uniformly after 2 hours or 6 hours truncated CCC, with substantially larger crystals, especially in 6-hour samples, as compared to the crucible glass samples (Figures 3.3d and 3.4j-l).

3.3.3 HLW-Bi-F2 without Bi, P and F

HLW-Bi-F2 was initially formulated as a lower viscosity variation of the foaming-prone HLW-E-Bi6 in order to investigate if a melt of lower viscosity would facilitate the release of gas bubbles from the glass melt. However, more gas bubbles are present in the CCC sample of HLW-Bi-F2 than HLW-E-Bi6. Nevertheless, HLW-Bi-F2 was used in this work as a worst case example in the search for waste constituents that are likely to be responsible for foaming during CCC. As stated earlier (Table 2.3), the Bi-limited waste stream is rich in Bi, P and F. Three variations of HLW-Bi-F2 glass were formulated removing one of the three elements individually. The resultant glass compositions are listed in Table 3.1. The ratios between all other glass components remain the same after removal of each component and renormalization.

The cross section of **HLW-Bi-Bi0** (without Bi_2O_3) after CCC looks very much like that of HLW-Bi-F2 and both are similarly populated with gas bubbles. The F-free version **HLW-Bi-F0** also appears similar but with smaller gas bubbles than in HLW-Bi-F2. The crystals in the two CCC samples are small spinel crystals in the translucent glass matrix (Figures 3.3e and 3.4m, n). In contrast, no gas bubbles were observed in the P-free **HLW-Bi-P0** melt. Moreover, the cross section of the CCC sample is dominated by dark-brown streaks intertwined with black streaks comprised mostly of spinel crystals. Under an optical microscope, opaque acicular crystals are seen forming radiating star-shaped centers inside lighter colored spheres that are dispersed within a thick matrix of dark brown glass. Overall, the texture in the dark brown portion is similar to that observed in the melter discharged glass BLL-G-46A (Figures 3.3e and 3.4o, p).

Based on the above observations, both F and Bi can be ruled out as primary causes of the observed foaming. P, on the other hand, evidently plays an important role in the formation of gas bubbles. As the data show, waste glasses of otherwise identical compositions and thermal history will or will not generate gas bubbles under the same cooling condition depending on the presence or absence of phosphorus in the glass.

Both Bi and P were removed from HLW-Bi-F2 in the formulation of **HLW-Bi-BiP0**. Visual inspection of the cross section of the CCC sample suggests that the CCC sample of HLW-Bi-BiP0 is very similar to that of the Bi-free glass HLW-Bi-Bi0 except for very small amounts of gas bubbles of smaller size. It is clear that the population of gas bubbles diminishes to a very low level in the P-Bi-free glass melt but does not disappear completely, even without P_2O_5 in HLW-BI-BiP0. It is interesting to note that the dark brown colored streaks are no longer present in this P-Bi-free glass sample (Figures 3.3e and 3.4p).

In summary, it is apparent that formation of gas bubbles during CCC is the result of a complex process that involves phosphorus and possibly other waste/glass component(s) to be identified. In view of its stable valence state, it is very unlikely that pentavalent phosphorus could be reduced during the cooling process. Therefore, one or more other elements must have participated, and likely became reduced during cooling, which ultimately resulted in the development of gas bubbles under CCC conditions. Consequently, it is necessary to identify those other elements and their mode of interaction with phosphorus.

3.3.4 HLW-Bi-F2 with Additional Bi and/or P

The presence of phosphorus in the Bi-limited HLW glasses apparently plays a critical role in the formation of gas bubbles under CCC conditions. It is thus of interest to investigate the effect of phosphorus at different concentrations for the same base glass system. Two glasses were formulated as variations of HLW-Bi-F2 with **HLW-Bi-2P** containing 60% more P_2O_5 than HLW-Bi-F2, while **HLW-Bi-2Bi**, has about 60% more Bi_2O_3 than HLW-Bi-F2. Since HLW-Bi-F2 contains similar amounts (in wt %) of Bi_2O_3 and P_2O_5, the glass components other than P_2O_5 and Bi_2O_3 are therefore similar after renormalization.

The development of gas bubbles in the above two glasses and HLW-Bi-F2 can be directly compared in Figure 3.3f from the scanned images and in Figure 3.4q, r on a microscopic scale. Overall, the higher Bi glass HLW-Bi-2Bi appears very similar to HLW-Bi-F2 with swirls of crystals and abundant gas bubbles throughout the whole sample volume. However, a higher concentration of P_2O_5 in HLW-Bi-2P results in considerably more gas bubbles and less dark brown streaks. Based solely on empirical observation, it can be concluded that bismuth, in spite of its high concentration in the Bi-limited waste stream, did not play an essential role in the formation of gas bubbles. In contrast, phosphorus at a similar concentration level (wt%) proved critical in the generation of gas bubbles. It is further evident that more bubbles were generated at a higher P_2O_5 concentration under similar conditions.

3.3.5 HLW-Bi-F2 with Additional P and without Cr

One of the scenarios that would involve phosphate and gas generation is via participation of another multivalent element that would assume a high valence state in the presence of phosphate in a borosilicate glass, but would later prefer a more reduced form at a lower temperature as triggered by other events or merely by temperature change as the melt cools according to the CCC curve. An inspection of the Bi-limited waste composition suggests SO_3 and Cr_2O_3 as the most likely candidates to investigate. Both S and Cr can exist in multiple valence states in borosilicate glass melts. S can exist as S^{6+} (as sulfate), S^{4+} (as sulfite) and even as S^{2-} (as sulfide); and Cr as Cr^{6+} (as chromate) or as Cr^{3+} (in simple oxide form or as spinel). Although there is lack of a reaction product between sodium phosphate and sodium sulfate, these two salts mix completely as melts within their binaries [28]. However, S^{4+} is not stable in typical borosilicate melts in equilibrium with ambient atmosphere [29]. Without a stable species to host S^{4+} within the molten glass, it is unlikely for sulfate to be reduced as temperature decreases according to the CCC curve.

Chromium can exist as trivalent Cr^{3+} and hexavalent Cr^{6+} in typical borosilicate melts under ambient conditions [30]. Complex phosphate/chromate forms as a reaction product between phosphate and hexavalent chromium salts [31]. Sodium chromate melt can mix completely with sodium phosphate. Sodium chromate/phosphate crystallizes at 916°C with the stoichiometric composition ($Na_4P_2O_7 \cdot 4Na_2CrO_4$) and at much lower temperature moving away from this thermal ridge, down to 833°C (eutectic with phosphate) or to 765°C (eutectic with chromate). Moreover, it has been reported that chromophosphate more polymerized than

pyrophosphate (dimer) can form with one PO_4^{3-} shared with up to four CrO_4^{2-}. It is conceivable then that part of the chromium from the Bi-limited waste will exist as chromate residing within phosphate-rich domains, given the high concentration of P_2O_5 in the glass (5 wt% at 50 wt% waste loading), and later be reduced as a result of competition from structurally more favorable spinel as the melt cools below the spinel liquidus along the CCC curve.

HLW-Bi-2P, the CCC sample of which developed the most gas bubbles, was chosen to check the possible effect of removing 0.5 wt% Cr_2O_3 from the glass formulation. As shown in Figure 3.3g, Cr-free glass **HLW-Bi-2P0Cr** is free of gas bubbles after CCC heat treatment, with a nearly uniform-looking dark red interior. In comparison to the CCC sample of glass HLW-Bi-2P, it is striking that the absence of merely 0.5 wt% Cr_2O_3 has resulted in such a large difference in behavior.

The inspection and comparison of the CCC samples of the Bi-limited HLW glasses clearly indicate that phosphorus plays a critical role in the formation of gas bubbles under CCC condition. However, P alone is not sufficient for the development of pervasive foaming. The other ingredient that is necessary for foaming development is apparently chromium. Interestingly, bismuth, in spite of its rather high concentration in the waste stream, is apparently not responsible for the foaming observed during the CCC process.

3.3.6 Mechanism of Foaming During CCC and Proposed Mitigation Strategy

The discussion in this section is based on the empirical data collected in this work supplemented by additional information from the literature and Raman spectroscopic analysis of air-quenched samples of the glasses (see Section 3.5). A total of ten crucible melts were prepared and characterized to support this effort.

The apparently synergetic effect between P and Cr in gas generation is believed to be due to the chemical affinity between Cr^{6+} and P^{5+}. As documented by Wells [32], phosphorus and chromium form poly ions containing both P and Cr that are closely related to the pyrophosphate and linear polyphosphate ions with P and Cr both in tetrahedral coordination. In this group of phosphochromates, one, two, three, or four of the O atoms of a PO_4 group can be shared with tetrahedral CrO_4 groups. Therefore, formation of the phosphochromate species in the P-rich HLW glass would probably stabilize Cr^{6+} and result in a higher Cr^{6+}/Cr^{3+} ratio. In a simple homogeneous system, the redox equilibrium will normally shift towards the more reduced direction with *increasing* temperature. Thus, something else must be involved in the overall reactions that create a superficial reversal of the trend in order to cause the observed foaming during cooling. The available phase equilibrium data and experimental data suggest that two factors that involve heterogeneous reactions could have determined the final outcome: 1) the solubilities of chromate within phosphate and phosphate within borosilicate; and 2) the competition for chromium between phosphochromate and spinel. As shown in the binary phase diagram of sodium chromate and pyrophosphate [31], sodium pyrophosphate will crystallize from P-rich molten salt at a temperature at or below 999°C (assuming that the additional silicate in the glass would not affect the phase boundary significantly). As a result, the salt species will become progressively enriched in chromate content. Below the 833°C eutectic, both sodium

pyrophosphate and phosphochromate will crystallize. Meanwhile, spinel would start to crystallize around or below 950ºC from the Bi-limited HLW waste glasses, as shown in the heat treated glass sample [1]. Considering the strong affinity of trivalent chromium for the spinel lattice [33], it is not surprising that phosphochromate, after, and possibly even before, being separated from phosphate-rich domains would be reduced to Cr^{3+} in order to be accommodated by the more favorable spinel structure. The likely reactions can be expressed in two steps (to facilitate analysis):

$$\text{P-rich chromophosphoric species } (m) \rightarrow Na_4P_2O_7\ (xl) + Na_3[PCrO_7]\ (m) \qquad (1)$$

$$Na_3[PCrO_7]\ (m) + \tfrac{1}{2}\ NiO\ (m) \rightarrow Na_3PO_4\ (xl) + \tfrac{1}{2}\ NiCr_2O_4\ (Sp) + \tfrac{3}{4}\ O_2\ (g) \qquad (2)$$

where *m* indicates a melt phase, *xl* a crystalline phase, *Sp* a spinel crystal, and *g* a gas phase.

A simple dimer type of phosphochromate is chosen to represent the proposed Cr and P poly ions in both reactions. Sodium pyrophosphate is chosen in the first reaction to match the same dimer configuration. In the second reaction, as Cr^{6+} is reduced to Cr^{3+}, it is assumed that all sodium atoms associated with this phosphochromate remain with phosphate to form a less polymerized orthophosphate. Cr^{3+} will then react with appropriate available divalent cations (such as Ni^{2+}) to form spinel crystals. Stoichiometrically, each mole of Cr_2O_3 generated will be accompanied by 1.5 moles of O_2. A simple estimation shows that for a glass with a density of 2.6 g/cm^3 at 1100 K (833°C), 0.5 wt% Cr_2O_3 in the glass will release an amount of gas equal to approximately 10 times the melt volume. Even under the assumption that only 10% of the Cr exists as phosphochromate at high temperature (before CCC cooling), the gas volume released will equal that of the glass melt.

The impact of spinel crystallization on foaming provides a possible explanation as to why no gas bubbles developed in the melter-discharged glass, which was identical to HLW-E-Bi6 in its chemical composition. Very likely, spinel crystals that had nucleated and grown during the particular cooling conditions for glass discharged from the DM100 melter had effectively depleted the Cr^{6+} before the CCC heat treatment. The premelting step for the standard CCC test (1200ºC for one hour before cooling) does not appear to have been adequate to reverse the reactions. It is not clear why no foaming was apparent during DM100 melter processing of the HLW-E-Bi6 feed but the difference may be due to much faster cooling based on the size of the pours and the discharge container. However, no data are available for the actual cooling history of the glass discharged from the DM100 melter.

It should be pointed out that the ratio of Cr^{6+} to Cr^{3+} can be also be influenced by glass components other than phosphates. It has been reported that more hexavalent chromium will form as the optical basicity of a glass melt increases [34]. In that sense, a high sodium glass would likely contain more Cr as sodium chromate species at the glass melting temperature. Indeed, the Raman bands of discrete alkaline chromate are present in higher sodium glasses, as represented by HLW-Bi-F2 (see Section 3.5). However, Raman bands of the alkaline chromate species are most intense in P-free HLW-Bi-P0 and HLW-Bi-BiP0 in which, no or very few gas

vesicles formed after CCC. It is, therefore, highly unlikely that Cr^{6+} as predominantly sodium chromate will significantly impact the observed foaming. Rather, the combined effect of both P and Cr is suspected to be responsible for the foaming observed during the CCC process. It is not clear how the proposed phosphochromate species behave differently from sodium chromate. It is, however, likely that the reduction reaction from Cr^{6+} to Cr^{3+} will need to occur in the appropriate temperature range in order to match the liquidus of spinel and the necessary range of melt viscosities for retention of gas bubbles to cause foaming.

The above discussion captures what appears to be the essential features of the foaming mechanism. However, a glass melt being subjected to CCC would evolve as an interrelated system. For example, the liquidus of the spinel phase will likely be influenced by the stability of Cr^{6+} in phosphochromate. As more Cr^{3+} becomes available, the spinel liquidus will move to a higher temperature in response. Nevertheless, the same general behavior would be expected.

Based on these results, several possible methods for mitigating the foaming observed on CCC are evident:

- Suppression of Cr^{6+} with a reductant or glass chemistry.
- Reduction of glass melt viscosity to facilitate release of gas bubbles.
- Formation of other competing phosphate species.

Suppression of Cr^{6+} will reduce the amount of oxygen gas that would be generated due to reduction of hexavalent chromium. In principle, this could be accomplished through the use of reductants or by decreasing the optical basicity of the host glass melt by, for example, decreasing the levels of alkalis such as sodium or potassium. However, this approach may cause unfavorable crystallization and high viscosities due to lack of flux.

A glass melt of considerably lower viscosity, especially at temperatures where the reduction reaction takes place, would possibly facilitate the escape of oxygen gas bubbles. However, considering the steep temperature dependence of melt viscosity and the adverse effects of very low melt viscosity on melter refractory corrosion, this route may have limited practical value.

The third option is aimed at creating direct competition with Cr^{6+} for the available phosphorus in the waste glass. The strategy is then to tie up the phosphorus that could otherwise interact with Cr^{6+} to form detrimental phosphochromate species. The chemical additives that can effectively bond to phosphorus may also act to suppress Cr^{6+} in glass. This approach for mitigation of foaming was emphasized in the work described in the next section.

3.4 Development of Formulations to Suppress Foaming During CCC

3.4.1 Basic Considerations and Formulation Strategy

Glass composition development and foaming mitigation studies were based on the same HLW Bi-limited waste compositions used in the investigation of the foaming mechanism. The HLW-E-Bi6 glass formulation [1] was used as the starting point for the small scale investigation. Ten new crucible melts at the same or higher waste loading as compared to HLW-E-Bi6 were formulated and tested to examine the effects of waste loading and the effects of other glass components on foaming behavior during CCC heat treatment.

In addition to foaming mitigation, the current formulations were designed to improve the processing rate of the melter feed. As reported previously [1], the melt rate attained during processing the Bi-limited HLW feed was not as high as that for some other high waste loading HLW glasses developed for ORP. In agreement with the melter test results, the simulated feed conversion experiments with the HLW-E-Bi6 feed using the vertical gradient furnace (VGF) showed a rather persistent dome-like structure [19] in the early stage of feed conversion. As a result, the heat transfer from the glass melt to the cold-dap was hampered, which consequently slowed the melting of the feed. In addition to its negative impact on the melt rate during melter processing, a dome-like structure indicates that substantial degassing occurs during feed conversion in such a way that the gas phase is trapped within a dome structure. At a larger scale, the phenomenon may appear as a foaming process near the cold cap region. In that sense, the feed conversion tests of the new glass formulations may be useful in developing a strategy to mitigate such foaming. For these reasons, as part of the new glass formulation work, the slurry feeds of seven formulations were prepared and tested in the VGF to assess their feed conversion behavior.

It should be noted that, in view of the schedule for this work, the development of new glass formulations was carried out in parallel with the foaming mechanism investigation work. The results from each of these activities were used to advance both efforts to the extent possible. A stepwise iteration process was used in the development of the new formulations, where results from the previous tests were used to refine the glass formulations for the following tests.

3.4.2 Results and Discussion

A total of ten new formulations were tested for their foaming tendency during CCC. In addition, six melter feed samples based on selected new formulations were tested for their feed conversion behavior by using the VGF. The formulations that passed the screening test for foaming were characterized for their properties relevant to processing and product quality. The experimental results are presented below in three separate groups. Section 3.4.2.1 evaluates the starting glass formulation HLW-E-Bi6 on the basis of the data reported before and the experimental results from this work. Results from a group of six glass formulations are reported in Section 3.4.2.2 followed by Section 3.4.2.3 in which results from a group of four glass formulations are discussed. The new glass formulations recommended for the Bi-limited HLW also are discussed below.

3.4.2.1 Reassessment of HLW-E-Bi6

HLW-E-Bi6 was developed to treat the Bi-limited HLW at high waste loadings [1]. This formulation is not atypical regarding major glass forming chemical components. However, the Bi-limited waste is unique in its unusually high contents of Bi_2O_3 and P_2O_5 together with relatively abundant minor components such as Cr_2O_3, NiO, SO_3 and F. As a result, a Bi-limited glass at 50 wt% waste loading tends to display some levels of spinel crystallization in the quenched glass samples and additional crystallization of phosphates after heat treatment at lower temperatures [1]. Among the processing properties measured for this formulation, the melt viscosity of 96 poise at 1150°C is within acceptable limits but is notably higher than that for typical WTP waste glasses. It is likely that this relatively high value would exacerbate the effects of foaming and sluggish melt rate and, therefore, a somewhat lower viscosity would be desirable.

As reported earlier, a dome-like structure [19] developed in the early stage of feed reaction and the overall feed melt rate appeared lower than the average melt rates obtained from a group of a dozen representative HLW melter feeds. The feed sample of this formulation was tested again in the present work by the VGF method and similar results were obtained (Figure 3.5a).

3.4.2.2 Formulations with Higher Sodium Concentration

A total of six new glass formulations at similar or higher sodium contents than the HLW-E-Bi6 glass were prepared and tested for their foaming tendency during CCC. As given in Table 3.3, three glasses were formulated at 50 wt% waste loading, two at 55 wt% waste loading, and one at 60 wt% loading.

HLW-Bi-F1 and **HLW-Bi-F2** were formulated as the lower viscosity variations of HLW-E-Bi6. HLW-Bi-F2, with higher B_2O_3 and lower SiO_2, was melted and quenched into a clear glass. However, HLW-Bi-F1 with the same amount of B_2O_3 and molar substitution of Li_2O for 3 wt% Na_2O resulted in a glass that crystallized partially. Therefore, only HLW-Bi-F2 was tested for its foaming tendency during CCC. As shown in Figures 3.3c and 3.6a, substantial amounts of gas bubbles developed during CCC heat treatment.

HLW-Bi-F3, with 3 wt% more Na_2O and less B_2O_3 than HLW-Bi-F2, was melted to form a clear glass and was free of gas bubbles after CCC heat treatment. However, the feed materials for HLW-Bi-F3 and HLW-Bi-F2 reacted in different ways in 30 and 60 minute VGF experiments. Feed of HLW-Bi-F2 melted reasonably fast with only slight residue on the side wall of the test crucible. In contrast, feed of HLW-Bi-F3 reacted considerably slower due to the development of a rather thick dome structure (Figure 3.5b).

Two formulations were prepared at 55 wt% waste loading (**HLW-Bi-F5** and **HLW-Bi-F8**) and one at 60 wt% loading (**HLW-Bi-F7**). HLW-Bi-F5 with more Al_2O_3 and B_2O_3 and less SiO_2 showed small amounts of gas bubbles after CCC (Figures 3.6b and 3.7d, e); the formation of gas bubbles was reduced to occurring only sporadically near the crucible wall for HLW-Bi-F8 (Figures 3.6c and 3.7f). At 60 wt% waste loading, large gas bubbles formed during

CCC heat treatment of HLW-Bi-F7. A dome-like structure developed after 30-minute VGF tests for both HLW-Bi-F5 and HLW-Bi-F8. No feed tests were conducted using HLW-Bi-F7 because of the foaming observed on CCC.

Overall, judging by the development of gas bubbles during CCC, HLW-Bi-F3 at 50 wt% and HLW-Bi-F8 at 55 wt% waste loading are considered acceptable with no or minimum tendency for foaming during CCC. However, the VGF feed test results for both formulations suggest a relatively poor processing rate based on the dome-like structure that emerged during the first 30 minutes of the feed conversion experiments. The processing and leaching properties of these two glasses are summarized in Section 3.4.2.4.

3.4.2.3 Formulations with Higher Alumina Concentration

A total of four new glass formulations at considerably higher alumina content than HLW-E-Bi6 glass were tested for their foaming tendency during CCC heat treatment. As listed in Table 3.3, three glasses were formulated at 50 wt% waste loading (**HLW-Bi-F4**, **HLW-Bi-F6** and **HLW-Bi-F9**) and one was formulated at 55 wt% waste loading (**HLW-Bi-F10**). **HLW-Bi-F4** was derived from HLW-Bi-F2 with 5 wt% more Al_2O_3 and 3 wt% more Li_2O for SiO_2 and Na_2O, respectively. No foaming was observed in the HLW-Bi-F4 glass after CCC heat treatment (Figures 3.6a and 3.7c). However, the as-melted glass showed some level of crystallization. No feed conversion experiment was conducted using this formulation. HLW-Bi-F6 is a higher CaO version of HLW-Bi-F4 with reduced Al_2O_3 and SiO_2 (Table 3.3). However, 3 wt% CaO was not effective in suppressing spinel crystallization, although no gas bubbles formed during CCC in both glasses. HLW-Bi-F9 (50 wt% waste loading) and HLW-Bi-F10 (55 wt% waste loading) were formulated as the lower sodium/higher lithium variations of HLW-Bi-F4 with additional boron. A small degree of crystallization is present in the as-melted glasses. No gas bubbles formed during CCC heat treatment of the two glasses and the feed samples of both formulations showed normal feed conversion after 30 minutes, with only slight residue on the wall of the test crucible (Figure 3.6c).

Overall, judging by the glass quality and the absence of gas bubbles during CCC, HLW-Bi-F9 at 50 wt% waste loading and HLW-Bi-F10 at 55 wt% waste loading are considered acceptable improvements over HLW-E-Bi6. Moreover, the VGF feed test results for both formulations suggest much improved processing rate as compared to the higher sodium alternatives. The processing and leaching properties of these two glasses are summarized in Section 3.4.2.4.

3.4.2.4 Characterization of Candidate Glasses

As discussed in Sections 3.4.2.2 and 3.4.2.3, two glasses at a waste loading of 50 wt% and two glasses at a waste loading of 55 wt% were identified as potential candidates for further characterization of their processing and leaching performance. The measurement results are given in Table 3.4 for crystallinity after isothermal heat treatment, Table 3.5 for melt viscosity and electrical conductivity, and Table 3.6 for leaching performance of glass samples by PCT and

TCLP. All four glasses meet the PCT and TCLP release limits. Among the four glasses, HLW-Bi-F3 (50 wt% loading) and HLW-Bi-F8 (55 wt% loading) displayed considerably better leaching resistance by PCT, normal viscosity, and lower crystallinity than HLW-Bi-F9 (50 wt%) and HLW-Bi-F10 (55 wt%) at similar waste loadings. Although the measured viscosity values for HLW-Bi-F9 and HLW-Bi-F10 are within the normal operating window, the considerably higher crystallinity after heat treatment could potentially be problematic, especially for HLW-Bi-F10. As shown in Figure 3.8, at 50 wt% waste loading, HLW-Bi-F9 contains about 2 vol% of crystalline phases at 950°C in comparison to 1 vol% in HLW-Bi-F3. At 55 wt% waste loading, more than 3 vol% crystals are observed in the glass HLW-Bi-F10 heat treated at 950°C while about 2.5 vol% crystals are observed in HLW-Bi-F8. However, the relatively lower crystallinity in the two high sodium glasses is offset by their apparently slower feed conversion rate as indicated by the VGF test results. In that respect, the two high alumina formulations outperform considerably judged by the VGF results.

In summary, **HLW-Bi-F3** at 50 wt% waste loading is considered the overall best formulation with low crystallinity, acceptable viscosity and electrical conductivity, and good leaching resistance. More importantly, no foaming was observed in the CCC sample of this glass. The main reservation for this formulation is its slow feed conversion rate. As an alternate, HLW-Bi-F9 performs considerably better in the feed conversion test and is free of gas bubbles after CCC heat treatment but shows somewhat higher crystallization.

At 55 wt% waste loading (5 wt% above HLW-E-Bi6), HLW-Bi-F8 and HLW-Bi-F10 have one or two properties that are less than optimum. Both glasses show more than 2 vol% crystalline phase after isothermal heat treatment at 950°C. HLW-Bi-F8, the one with better leaching resistance and less crystallization, showed very minor amounts of foaming near the interface between the glass melt and the crucible wall and tends to melt slowly. HLW-Bi-F10, with faster feed conversion rate and no sign of gas bubble generation after CCC heat treatment, crystallized more readily at 950°C and showed higher PCT leaching. Accordingly, while these formulations should provide a good basis for further formulation optimization work, neither of these glasses is recommended for future melter testing.

3.4.3 Summary and Recommendations

Two glass formulations at 50 wt% waste loading are recommended for further tests to support vitrification of the Bi-limited HLW. HLW-Bi-F3 shows the best properties overall but may exhibit a relatively slower melt rate than the alternate HLW-Bi-F9, while HLW-Bi-F9 shows even less tendency for foaming during CCC but somewhat greater crystallization on heat treatment.

3.5 Structural Analysis of Bi-Limited Glasses by Raman Spectroscopy

3.5.1 Introduction

Structural information obtained from Raman spectroscopic measurements on Bi-containing HLW glasses may provide insights into the atomic structural causes behind the observed melt foaming phenomena. Bi acts as a silicate network modifier in crystalline silicates [35, 36, 37], and a similar role in borosilicate glass structure would be anticipated. Raman spectroscopy may be able to provide additional information about chromate, phosphate, and sulfate anions in these glasses and how any changes in these environments may be linked to the melt foaming issues. Observations from SEM analyses of standard CCC samples identified micron-scale Bi-containing phosphate phases. Raman spectroscopy may also detect Bi-phosphate domains in the glasses. Structural findings from these studies can be useful in guiding adjustments in glass chemistry that can reduce or eliminate foaming on CCC.

Several structural investigations concerning binary Bi-silicate glasses have been published [38, 39, 40], where Bi_2O_3 concentrations vary near 50 mol%. A spectroscopic study of $x(Bi_2O_3)$-$(100-x)(SiO_2)$ glasses [38] indicated separate Bi-O-Bi and Si-O-Si environments that form Bi_2O_3 layers and silicate chains cross-linking the layers. X-ray absorption spectroscopy (XAS) and Raman studies of binary Bi-silicate glasses exposed to hydrogen indicate that Bi^{3+} in the initial glasses changes to metallic Bi [39, 40]. XAS studies of similarly processed Bi-silicate glasses [39] showed that Bi-O correlations diminish, while Bi-Bi correlations increase with more hydrogen exposure. The original glass had Bi within environments similar to those in crystalline Bi_2O_3, while Bi-metal domains were observed in any sample subjected to hydrogen reduction. Raman spectra of the Bi-silicate binary glasses [40] show a peak near 132 cm^{-1} assigned to Bi-O stretch motions; this feature decreases in intensity with increasing hydrogen exposure time. Another narrow peak near 81 cm^{-1} (claimed to be an artifact [40]) appears in the Raman spectra of the reduced glass. Considering the results of the XAS study [39], this mode may be due to Bi-Bi motions in Bi metal within an amorphous silica matrix.

The borosilicate glasses investigated here are more chemically complex and have considerably lower Bi_2O_3 concentrations (approximately 6 wt%) than the glasses discussed above. The waste loading in the Bi-limited HLW glasses developed in this work varied from 50 to 60 wt% for the series HLW-Bi-F2 to HLW-Bi-F10 synthesized for this study. Not surprisingly, from initial Raman and SEM observations, Bi behavior in these waste glasses is different from that observed for the binary Bi-silicates. In light of the Bi-to-phosphate correlation found in some of the equivalent CCC samples and the possible correlation of these elements to foaming, two additional glass series were made where Bi_2O_3- and P_2O_5-content were varied independently; a P_2O_5- and Bi_2O_3-free glass (HLW-Bi-BiP0) was also synthesized. Raman spectra were also collected for the crystalline Bi-silicate, eulytite $Bi_4Si_3O_{12}$ and $BiPO_4$, (Figure 3.9), where SiO_4 and PO_4 tetrahedra, respectively, are isolated from each other by Bi^{3+} [35, 41].

The HLW glasses investigated here contain chromate, phosphate, and sulfate anions, all of which have large Raman cross-sections. Raman studies of phosphate and sulfate modes in the spectra of silicate glasses [42-45] assign P-O and S-O stretch modes to Raman features near 950 and 985 cm^{-1}, respectively. The Raman spectra of chromate in solution [46] have two Cr-O

stretch modes at 847 and 884 cm^{-1}, and less prominent O-Cr-O bending modes at 348 and 368 cm^{-1}. Chromate modes are observed at similar frequencies for Cr-containing oxide and silicate minerals [46]. To more clearly assign the chromate, phosphate, and sulfate modes in the Raman spectra of the glasses, spectra for Na_2SO_4, (Na,K)-chromate, as well as $BiPO_4$, are compared with the Raman spectrum of a representative Bi-waste glass, HLW-Bi-F3 (Figure 3.10). These contributions include two Cr-O, one P-O, and one S-O stretch modes near 850, 880, 950, and 985 cm^{-1}, respectively, and are plotted with the Raman spectra of the three glass series investigated (Figures 3.11 – 3.13). Cr-O stretch modes are clearly seen when comparing the spectrum of a Cr-containing glass (HLW-Bi-2P) with that for the Cr-free glass (HLW-Bi-2P0Cr) (Figure 3.13).

3.5.2 Experimental Procedure

The crystalline samples used in this study were polycrystalline powders. Phase identifications of the crystalline standards were verified by powder x-ray diffraction (XRD). These crystalline samples include: eulytite (NMNH# R170518 from Schneeberg, Germany), and chemical reagents: Na_2SO_4 and $BiPO_4$ from Alfa-Aesar. The crystalline (Na,K)-chromate yellow phase was found as layers on waste glass HLW-E-Cr-1 that was investigated earlier [1]; XRF analysis of this sample indicates Cr, Na, K, and S as major elements, where chromate and sulfate phases are mostly segregated, as indicated by Raman spectroscopy. The three Bi-containing HLW glass series were synthesized from reagent grade chemicals; some samples are either completely amorphous or have spinel crystals suspended in a glass matrix, as determined by Raman spectroscopy and SEM. The bulk glass fragments were taken from the quenched glass samples that were as homogeneous as possible.

High temperature Raman spectra were collected on one HLW glass while simulating the HLW CCC cooling conditions (Figure 3.14). The samples were placed in a 1 cm diameter Pt crucible that was heated in a Linkam TS1500 heating stage. Temperatures were rapidly increased from room temperature to 580°C at 100°C per minute, and then to 1200°C at 50°C per minute. The sample was then quickly cooled at 100°C per minute to 1050°C, and then slowly cooled to 500°C at 2°C per minute. During the cooling part of the run, Raman spectra were gathered every 100°C to monitor any changes.

A single grating spectrograph – notch filter micro-Raman system [47] was used to gather the spectra presented here. A Melles-Griot Model 45 Ar^+ laser provided the 5145 Å wavelength incident light that was directed through a broad band polarization rotator (Newport Model PR-550) to the laser microscope which guided the laser light down to the sample surface through a long working distance Mitutoyo 10× microscope objective. The laser light was focused to a 10 μm diameter spot on each sample. The laser light power was approximately 25 mW at the sample. Polarized spectra were gathered in back-scattering geometry. The scattered light was directed through an analyzer polarizer in the microscope column that was set to one orientation for all polarized spectra collected. After the analyzer, the scattered light proceeded through a 150 μm aperture to reduce Rayleigh scattering intensity at low frequencies and then to holographic notch and super-notch filters (Kaiser Optical Systems), which reduced the Rayleigh scattered light intensity by ten optical densities. The notch filters were oriented in the scattered

light path so that the filter cut-off frequency was minimized to near 70 cm^{-1} from the laser line. The spectrograph used a 1200 gr/mm grating (Richardson Grating Laboratory) that was set to disperse the Stokes scattered light from the sample on to a 2048 x 512 element Peltier cooled CCD detector (Model DU440BV, Andor Technology). The incident slits of the JY-Horiba HR460 spectrograph were set to 6 cm^{-1} resolution to collect spectra from 50 to 1600 cm^{-1}. The spectrograph was frequency calibrated using CCl_4, so that the recorded frequencies are accurate to within ±1 cm^{-1}. Parallel-polarized (VV) or cross-polarized (HV) spectra were collected, where the incident laser light was vertically or horizontally polarized, respectively, as it entered the microscope. Each crystalline and glass Raman spectrum is an average of 10 exposures and 30 exposures, respectively, collected at 10 seconds each.

3.5.3 Discussion

Relatively narrow chromate-, phosphate-, and sulfate-related peaks are found superimposed on the Si-O stretch Q-species envelope in the Raman spectra between 800 and 1150 cm^{-1} [48] (where Q^0 = isolated SiO_4 tetrahedron to Q^4 = fully polymerized SiO_4 tetrahedron linked to four other tetrahedra). The Raman data collected for the glasses investigated do not have any low frequency features that can be correlated to Bi (Figures 3.11 – 3.14), such as the peaks near 132 and 81 cm^{-1} observed for Bi-silicate binary glasses [40]. Prominent peaks at frequencies ≤ 210 cm^{-1} appear in the spectra of eulytite and $BiPO_4$ (Figure 3.9). Due to the lack of low frequency Bi-related modes, Bi ions in the glasses must be far enough apart from each other so that no spectral features associated with Bi-Bi or Bi-O-Bi environments are possible; this is expected considering the relatively low Bi_2O_3 concentrations in these glasses compared with the binary Bi-silicate glasses [40].

3.5.3.1 High Temperature Raman Spectra of HLW-Bi-F2 Glass

Two heating runs were performed on HLW-Bi-F2, a glass formulation that showed significant foaming problems. In both runs, the glass initially changed as the temperature increased through 550°C. The spectrum collected at 580°C showed a relatively large peak near 680 cm^{-1}, in addition to the broad glass bands near 450 and 1000 cm^{-1}. At temperatures above 900°C, black body radiation dominates the data such that Raman features could not be observed. Spectra collected during the cooling part of the run (as the temperature was dropped from 900°C) have the broad silicate glass bands, as well as the peak near 680 cm^{-1} (Figure 3.14). As the sample cooled to room temperature, spectral features generally sharpened and shifted to higher frequencies. There was no sign of sample foaming during either run; at the end of each experiment a re-melted bead was found that comprised of Cr, Fe, and Ni spinel crystals within a glass matrix, as determined from SEM and XRD. The Raman peaks near 680 and 550 cm^{-1} have similar frequencies and relative intensities to those observed for $MgCr_2O_4$ spinel [49] (Figure 3.15); therefore, these two peaks can be attributed to (Cr,Fe,Ni)-spinel crystals.

The re-melted HLW-Bi-F2 glass spectra are different as compared to those from the original glass for both runs (Figure 3.15). The Si-O-Si bend envelope near 480 cm^{-1} sharpens and shifts to higher frequency, indicating changes to a narrower distribution of smaller silicate rings

or smaller Si-O-Si bond angles [48]. The features between 800 and 1150 cm^{-1} for the re-melted sample show only the relatively broad Si-O stretch envelope and the narrow P-O stretch phosphate mode near 965 cm^{-1} for one point (Figure 3.15), with no evidence of the 850 and 885 cm^{-1} chromate modes, or the 990 cm^{-1} sulfate mode. Due to the superposition of Cr-O, S-O, and P-O stretch modes on the Si-O stretch bands for the original glass, it is difficult to interpret from these spectra any redistribution of silicate Q-species populations during heating. Spinel crystallization is correlated to the disappearance of the 850 and 885 cm^{-1} chromate modes for the re-melted sample. SEM analyses of the heating run products indicate no evidence of Cr in the glass. Therefore, the data indicate that during heating experiments, Cr in the original glass was consumed by spinel crystallization.

3.5.3.2 New Bi-Limited HLW Glasses

This series includes samples HLW-Bi-F2 to HLW-Bi-F10 (Figure 3.11). The higher Na_2O content for HLW-Bi-F3 versus HLW-Bi-F2 likely enhances the intensity of chromate modes near 325, 850, and 880 cm^{-1} in the Raman spectrum of this sample. The HLW-Bi-F5r glass has higher waste loading than HLW-Bi-F3, while HLW-Bi-F7 has the highest waste loading of all glasses in the series. The major changes in the Raman spectra are observed for the spinel peak near 680 cm^{-1} and chromate modes near 850 and 880 cm^{-1}, similar to that observed for the heating experiment. In general, samples that appear to be completely or mostly amorphous have the largest intensity chromate modes, while samples that have prominent spinel peaks either have weak or no chromate peaks. Melt foaming was minimal for HLW-Bi-F3 and HLW-Bi-F8 formulations, which are the samples with the largest intensity chromate modes and no observed spinel features (Figure 3.11). Sample formulation HLW-Bi-F5r exhibited small amounts of foaming and the spectrum of the equivalent crucible glass has less prominent chromate modes with no spinel peaks.

Half of the samples in this series, HLW-Bi-F4, HLW-Bi-F6, HLW-Bi-F7, HLW-Bi-F9, and HLW-Bi-F10, are not homogeneous, where interior portions contain spinel crystals within the glass and only the exterior may be glass (as in HLW-Bi-F7). For these samples, HLW-Bi-F7 showed extensive foaming, while the others showed no evidence of foaming. For HLW-Bi-F6, HLW-Bi-F9, and HLW-Bi-F10, a narrow peak near 947 cm^{-1} is observed that is not correlated to the spinel features; this is likely due to another crystalline phase. The spectra for HLW-Bi-F6 are complicated: the spinel peak near 690 cm^{-1} is frequently observed, while chromate modes near 325, 850, and 880 cm^{-1} can be seen at many points, independent of the spinel peaks. HLW-Bi-F6 also has narrow peaks near 914 and 961 cm^{-1} that indicate other crystalline phases.

3.5.3.3 Bi-Series Glasses

Raman data for this series of glasses (Figure 3.12) indicate that as Bi_2O_3 increases from 0 to approximately 10 wt%, intensities generally decrease for the borosilicate network features: the Si-O-Si bend envelope near 450 cm^{-1}, the Si-O stretch Q-species bands between 800 and 1200 cm^{-1}, and the B-O stretch modes (in BO_3 groups) near 1370 cm^{-1}. The peak centered near 980 cm^{-1} appears to have two components: a S-O stretch mode near 990 cm^{-1} from sulfate in the

glass [44] and a mode near 970 cm^{-1} that is correlated to phosphate. This 970 cm^{-1} mode is at a similar frequency to the 965 cm^{-1} peak for $BiPO_4$ (Figure 3.12) and is likely due to a P-O stretch mode in isolated PO_4 tetrahedra. This is the best explanation for this mode as the P-O stretch mode frequencies of other plausible crystalline compounds (e.g. Na_3PO_4 and $Na_4P_2O_7$) and solutions [42, 50] that may model phosphate environments in these samples are not close to 970 cm^{-1}. However, this feature appears to not be dependent on Bi-content because it is present in the spectra of HLW-Bi-Bi0 glass, which contains P but no Bi (Figure 3.13). Comparing the spectra of HLW-Bi-BiP0 with HLW-Bi-P0 shows that the 850 and 885 cm^{-1} chromate modes reverse their relative intensities as the Bi-content increases. Adding more Bi to the glass in the presence of P decreases the intensities of the borosilicate network features, as well as Cr-O, P-O, and S-O modes, while broad bands near 600 and 1050 cm^{-1} become more prominent. The 990 cm^{-1} S-O stretch mode frequency does not appear to change throughout this series and indicates that Na^+ is a likely a nearest-neighbor to SO_4 tetrahedra [44], which is consistent with Na being the most common network-modifying cation in these glasses.

3.5.3.4 P-Series Glasses

As P_2O_5 is added to the phosphate-free HLW-Bi-BiP0 glass composition, the P-O stretch in phosphate modes appears near 970 cm^{-1} (Figure 3.13). Earlier studies [42, 43, 45] show that significant effects on silicate tetrahedral networks can take place as P_2O_5 is added, even in small amounts, such as phosphate segregation and P-O-P modes. With increasing P_2O_5 content, Raman intensities increase for features near 1050 and 600 cm^{-1}, which may be due to vibrations similar to those in crystalline $BiPO_4$ that have mode frequencies at 1035, 970, 595, and 551 cm^{-1}. These trends may indicate Bi-phosphate domains in HLW-Bi-F2 and HLW-Bi-2P glasses. Na-silicate glass studies [45] found that phosphate domains can attract network-modifying Na^+. The Raman observations here may indicate Bi attraction to phosphate-rich regions in the glass that contain isolated PO_4 tetrahedra. Phosphate domains in some of these borosilicate glasses may be reasonable in light of earlier findings [43, 45] where silicate glasses, even with low P_2O_5 concentrations, can have phosphate segregation from the silicate network.

Phosphate addition to the glass also changes the Cr-O stretch chromate modes (Figure 3.13). The 850 cm^{-1} mode intensity decreases, while the 880 cm^{-1} mode intensity remains the same or increases slightly when comparing the spectra of HLW-Bi-BiP0 (0 wt% Bi_2O_3 and P_2O_5) with HLW-Bi-Bi0 (0 wt% Bi_2O_3). As more P is added to the glass, especially from HLW-Bi-F2 to HLW-Bi-P2, both chromate modes become weaker, indicating reduced isolated chromate populations. Phosphate and chromate tetrahedra are known to polymerize with each other in some crystalline compounds [32]. As phosphate content is increased in the glass structure, this polymerization may be creating phospho-chromate domains, while consuming isolated CrO_4 tetrahedra and decreasing the Raman intensities of the associated modes. Like sulfate, unpolymerized chromate environments in the glass are also likely to be surrounded by Na. Raman intensities are expected to be larger from isolated chromate environments (more ionic Na-O and more covalent Cr-O bonds), than from polymerized phospho-chromate environments (more covalent P-O and Cr-O bonds).

The glass formulation containing the largest concentration of phosphate (HLW-Bi-2P) showed the worst foaming problems. Eliminating P or Cr from this glass eliminated foaming, as seen for HLW-Bi-2P0Cr and HLW-Bi-P0. Therefore, the sensitivity of chromate modes to phosphate content may indirectly suggest some phosphate-chromate affinity in the glass structure that could be linked to foaming. Unfortunately, phospho-chromate modes cannot be clearly identified in the Raman spectra.

3.5.4 Conclusions

Raman spectra of quenched samples of the Bi-limited HLW glasses provide structural information on certain chemical components that may be directly related to the CCC foaming issues. Raman spectra show no evidence of Bi-Bi or Bi-O-Bi modes or Bi-rich domains in the samples investigated that can be related to the observed foaming event. Raman trends for these samples indicate relationships between chromate and spinel crystallization, as well as chromate and phosphate. Phosphate-dependent features seen in the Raman spectra suggest the presence of Bi-phosphate domains in these glasses. Addition of phosphate to the glass may replace isolated chromate groups with polymerized phospho-chromate domains in some of the samples investigated. Higher P_2O_5 concentrations in these glasses can also be linked to increased melt foaming.

Chromate modes are clearly seen for spinel-free glass samples and are weak or absent when samples contain spinel crystals. Significant concentrations of (Fe,Cr,Ni)-spinel crystals are observed in about half the samples measured. Glass formulations, such as HLW-Bi-F3, HLW-Bi-F8, HLW-Bi-BiP0, and HLW-Bi-P0, exhibit minimal foaming while having prominent chromate modes and no spinel crystals. The reverse is true for some (HLW-Bi-F4 and HLW-Bi-F7) but not for all formulations that experienced spinel crystallization. Formulation HLW-Bi-F2 had the worst foaming characteristics of the Bi-limited glasses, while the Raman spectra of the glass sample show no spinel features and moderately strong chromate modes. Raman and SEM evidence from the quenched glasses show that the process of spinel crystallization consumes chromate in the melt to the point where Cr can be completely eliminated from the glassy part of the sample. Heating experiments on HLW-Bi-F2 glass (a formulation with foaming issues) caused spinel crystallization that consequently removed Cr from the glass, with no evidence of foaming in the resulting sample.

In summary, the results from the Raman studies provide some support for the proposed foaming mechanism. However, additional studies using X-ray absorption spectroscopy would be useful to further elucidate the interactions between chromium and phosphorus that appear to underlie the observed foaming behavior.

SECTION 4.0
DM1200 OPERATIONS

Testing with the high bismuth HLW simulant and the HLW-E-Bi-6 glass composition was conducted between 10/20/09 and 10/30/09, producing over six metric tons of glass. It should be noted that the tests were conducted with the original formulation that showed foaming in crucible tests during CCC heat treatment. However, the same formulation did not show foaming during DM100 melter tests. Consequently, the primary objective of the DM1200 tests was to determine whether or not the behavior observed in the crucible tests would occur under prototypical conditions at large scale. Clearly, such an occurrence during cooling of actual HLW canisters would be highly undesirable and it was important to ascertain whether the potential for such behavior in the WTP was real or simply an artifact of the crucible scale tests. Large scale testing on the DM1200 under near prototypical conditions provided the most definitive method of addressing this issue.

In the present work, a total of fourteen canister cooling experiments were performed with the high bismuth formulation on the DM1200. The total testing duration, including the time for water feeding and cold-cap burn-off, was 193 hours, during which over seventeen metric tons of feed was processed. For scheduling convenience, testing was conducted over two intervals, from 10/20/09 to 10/23/09 and from 10/26/09 to 10/30/09. A summary of the test conditions and results is provided in Table 4.1. The tests were conducted primarily to support large scale canister cooling tests over a range of glass compositions and secondarily to determine glass production rates for a high bismuth waste. The tests employed double-outlet prototypical bubblers, a glass pool temperature of 1150°C, and bubbling adjusted to maximize glass production rates.

4.1 Melter Operations

The DM1200 melter tests employed a single feed tube in the center of the melter and a side-to-side electrode firing pattern. Two double-ported bubblers (see Figure 1.3) positioned in a manner to mimic the WTP HLW melter bubbler configuration (see Figure 1.4) were used throughout testing. In each test, the cold-cap-limited production rate was estimated by visual observations of the cold cap and confirmed by the plenum temperature. Determination of steady state production rates was complicated by the high glass discharge rates and amounts required for the canister cooling tests. A summary of operational events is provided in Table 4.2. Operators observed the cold cap through view ports on the side of the melter on average every 20 minutes to guide melter operation, particularly the adjustment of bubbler air flow and feed rate. These observations are listed in Table 4.3.

The majority of the feed was processed with the prototypical ADS feed system. Near the end of the tests feeding was switched to the backup AOD system to remove the maximum amount of feed from the feed tank while testing. The heel for the ADS feed system is over a

thousand kilograms of feed, whereas the residual feed from AOD system is only about a hundred kilograms. No feed line or pump blockages occurred during the tests. The feed tube clogged twice during testing, resulting in five to seven minute feeding interruptions to allow for manual clearing of the feed tube.

Feeding was interrupted sixteen times for a total of thirty nine hours during testing. Brief interruptions of less than ten minutes occurred for routine activities such as taking feed samples and clearing the feed tube. Feeding hiatuses of less than an hour were required to change to the AOD pumping system and to remove occlusions in the film cooler region. On nine occasions, feeding interruptions of 1 to 4 hours were necessary to allow the cold cap and feed deposits in the melter to be incorporated into the glass pool in order to maintain a stable cold cap. The feed used in these tests formed cold caps that often formed mounds and ridges and incorporated relatively slowly into the glass melt. Also, the large volume of glass in each discharge required for the canister cooling tests in order to match the full-scale WTP discharge rate resulted in the melt pool level decreasing by about three inches, which would leave feed deposits attached to the melter walls. These deposits or "shelves" were no longer in contact with the molten glass pool and therefore melted slowly. Another negative consequence of "shelving" is that these deposits often fall into the melt pool once partially melted causing pressure spikes. Once large mounds and shelves were incorporated into the glass pool, the melt surface was mostly bare, necessitating a brief period of water feeding prior to resuming slurry feeding. Ridges or mounds forming in the center of the melt pool often made direct observation of the melt surface opposite the view ports impossible. In these instances, the amount of cold cap was estimated by the amount of light visible as a result of openings in the cold cap. The configuration of the cold cap was constantly in flux throughout the tests, ranging from the desired state of a relatively flat surface with aqueous feed observed boiling on the top, to an irregular surface with large feed deposits preventing the feed from spreading out across the melt pool surface. Plenum pressure spikes occur from the sudden release of pooled aqueous feed within ridges onto a bare melt surface and therefore feeding was slowed or paused when large ridges were observed. The visual observations of the DM1200 melt pool is a key operational aspect of current DM1200 testing. In contrast to the operation of the LAW Pilot Melter, use of non-visual data, such as plenum temperature, have not been developed as reliable indicators of cold-cap conditions while processing HLW feeds [53]. In fact, high plenum temperatures can result from a high mound over a portion of the melt surface preventing feed from spreading across the melt surface and creating an opening on the glass surface. Without the visual evidence, an operator may conclude that feed rates should be increased, which could exacerbate the problem.

The glass production rates achieved during testing are provided in Table 4.1; these are illustrated in Figure 4.1 and are compared to rates achieved with other HLW feeds using the DM1200 with the optimized bubbling configuration in Table 4.4. Steady state production rates were difficult to obtain due to the large discharge volumes required for the canister cooling experiments and the tendency of the feed to form mounds and ridges on the glass surface. Average production rates decreased from 815 $kg/m^2/day$ to 558 $kg/m^2/day$ as the glass pool approached the target composition. Both these rates are the lowest production rates achieved with this configuration at nominal processing conditions. This is despite the high feed solids content of 500 g glass per liter, as compared to 340 to 430 g glass per liter used in many of the previous tests, and the higher bubbling rate used in the tests with the bismuth feed. The lower

rates are a result of the observed poor cold cap conditions, the large discharge volumes required for the canister cooling tests, and the high viscosity of the target bismuth glass (96 poise at 1150ºC, see Table 2.3). Testing on the DM100 with HLW wastes has shown that glass production rate exhibits a general decreasing tendency with increasing glass viscosity [19, 20, 54, 55]. A production rate of 830 kg/m^2/day was achieved on the DM100 while processing the same high bismuth composition at 1150ºC; the bubbling rate in that test was held constant and was lower per unit melt surface area than that used in the DM1200 tests. This suggests that the lower production rates from the DM1200 test are attributable in part to the manner in which glass was discharged during the current tests. A steady state rate for the high bismuth composition under nominal discharging conditions therefore is probably closer to the high average of 815 kg/m^2/day obtained in these tests. It should be noted that even the higher rate obtained while processing the high bismuth composition is lower than all of the rates achieved on the DM1200 with other HLW compositions.

A variety of operational measurements recorded during these tests, including temperatures throughout the melter system, are given in Table 4.5. Data are collected and electronically logged every two minutes, and data and observations are also recorded manually throughout the tests. The 1150ºC glass temperature was targeted and successfully maintained for most of the glass pool throughout the testing, as illustrated in Figure 4.2. Glass temperatures near the surface of the glass pool (27" from the floor) were lower due to the thermocouples being in or near the cold cap. Bulk glass temperatures were relatively constant throughout the glass pool. Average glass temperatures measured on the east side were up to 17°C higher than those on the west side of the melter. Plenum temperatures, given in Figure 4.3, spanned a larger range during the testing, 350 to 950°C, than the 450 to 550°C target given in the Test Plan. Average plenum temperatures were above this range due to the lack of uniform cold cap coverage across the melt pool surface and the feeding interruptions. Higher plenum temperatures were observed at the beginning of each testing sequence, as the cold cap was being formed, and as the thermowell and bare thermocouple were exposed to openings in the cold cap. Plenum temperatures also rose during feeding interruptions, most notably between 102 and 117 hours run time, as shown in Figure 4.3. The side electrode temperatures averaged about 5 to 50°C below the glass temperatures, with the east being up to 50°C higher than the west electrode, as illustrated in Figure 4.4. The bottom electrode, which was not powered during these tests, was 50 to 100ºC lower than the side electrodes. The discharge chamber and riser temperatures were largely maintained above 950ºC throughout the tests. (The riser thermocouple is located about 4 inches above the bottom of the riser pipe, which is about 7.5 inches above the melter floor.) Gas temperatures at the outlet of the film-cooler were 100 - 200ºC lower than the measured plenum temperature as a result of film-cooler and control-air dilution and depending on the position of the thermocouple in the plenum with respect to the cold cap. The film cooler was rinsed by a water spray every 12 hours during testing, resulting in a short-duration reduction to about 75ºC in the film cooler outlet temperature.

Conditions in the glass pool are illustrated for electrical properties in Figure 4.5, level and density in Figure 4.6, and bubbling in Figure 4.7. Power supplied to the electrodes averaged 158 and 136 kW for the two testing intervals; however, power supplied during feeding was higher due to the lower power demand during idling periods. This level of power usage is comparable to

that used to process a high aluminum waste at a higher production rate (1050 kg/m^2/day) [19, 21], further indicating the relative difficulty in processing the high bismuth feed formulation.

Average glass pool resistance for the two testing intervals was 0.09 and 0.095 ohms, with fluctuations due to changes in bubbling rate and power associated with idling periods, startup, and cold cap burn-off at the end of each interval. Glass pool depth varied from 27 to nearly 40 inches in response to the large glass discharge volumes required for the canister cooling tests. Typically during melter testing, the level varies between 29 to 33 inches in response to continuous feeding and glass discharge [19, 21]. The average glass density during the first testing interval, 2.21 g/cc, was within the average range observed in the previous tests of 2.20 to 2.23 g/cc [21]. Conversely, the average value for the second testing interval of 2.07 g/cc, with many values below 2.0 g/cc, is significantly below normal operations, suggesting that gas was entrained in the glass as a result of foaming. This decrease in density also coincides with the approach of the glass composition to the target composition and, specifically, the higher phosphate and bismuth concentrations (see Section 5.2). Foaming was not observed on the glass surface through the view ports; however, foamy glass was observed in the discharge trough. Water was fed onto the melt surface at about 135 hours run time to reduce the foaming discerned from the density readings; however, the feeding of water had no effect on the low measured density values. The highest measured density values coincide with the lowest power, lowest glass resistance, and lowest applied melt pool bubbling at the beginning and end of each testing sequence and during an extended feeding hiatus for the repair of the emergency off-gas valve. This is in keeping with previous tests which show the lowest glass pool resistance and highest glass density at lowest bubbling rates [19, 21]. Lance bubbling rates ranged from 7 to 222 lpm over the course of testing with an overall average bubbling rate of 126 lpm. The average bubbling rate from these tests is higher than all but one of the steady state rates used to achieve significantly higher production rates with other HLW feeds, as shown in Table 4.4, further illustrating the difficulty in processing the high bismuth waste. Frequent changes to the bubbling rate as well as the distribution of bubbler air between the double ported lances were made in an attempt to create an even cold-cap across the melt pool surface.

Both of the Inconel 690 bubblers employed for these tests experienced localized but severe corrosion at their tips. This behavior is atypical and appears to be associated with certain constituents in this waste stream, including phosphorus, sulfur, and bismuth. The observed corrosion behavior and results from analysis of the corroded bubbler materials are presented in Section 5.4.

4.2 Canister Cooling Tests

Fourteen canister cooling experiments were conducted over the course of the tests, each mimicking cooling rates measured on the prototypical HLW canisters filled at the Energy*Solutions* LAW pilot facility. Temperatures were measured at the center of the drum, 3" from the center, 9" from the center, at the exterior of the drum, and of the air flowing through the cooling system. Glass temperatures during canister cooling tests are shown in Figures 4.8 and 4.9. Approximately 150 kg of glass is discharged, causing an abrupt increase in temperature to about 550°C, followed by decreasing temperature over the next approximately two hours. The

level of the poured glass is below the thermowell and serves as an insulator for the test pour. Approximately 250 kg of glass is then poured at the full-scale WTP rate to a level six inches above the thermowell. This glass level was achieved by viewing a 6" vertical pipe welded to the top of the thermowell, once the pipe was no longer visible the glass discharge was stopped. The initial temperature of the glass was the same as the discharge glass, 1050 - 1100ºC. The drum inside the insulated enclosure was then cooled at the prototypical rate [25] to less than 800ºC. The last drum was only half way filled and therefore did not cool at the managed rate.

4.3 Off-Gas System Performance

Tests on the DM1200 system at VSL have been used extensively to evaluate the performance of a pilot scale off-gas system that is prototypical of that designed for the WTP by BNI engineering [5, 11-21]. In the current test, data objectives primarily related to the detection of foaming under prototypical canister cooling conditions and secondarily to determine achievable glass production rates for a high-bismuth HLW feed composition. However, data for each of the off-gas system components and samples of solutions from the off gas system were collected and evaluated and are provided in this report. Data are collected and electronically logged every two minutes and data and observations are also recorded manually throughout the tests. The average, minimum, and maximum values of the measured off-gas system parameters are given in Table 4.6. Target operational conditions for the system components such as sump temperatures, unit spray rates, and sump pH values that were not specified were adapted from previous tests conducted on the DM1200 [5]. The catalytic unit was in place, but ammonia was not added during these tests in light of the low concentrations of nitrogen oxides in the feed. Plots of the typical sequence of gas temperatures through the DM1200 off-gas system at various locations are given in Figures 4.10.a and 4.10.b for the fist and second intervals of testing, respectively. In summary, plenum gas from the melter is cooled by dilution with film cooler air to about 250°C, drops another 100°C by control air dilution and heat loss along the transition line, is quenched to 44°C in the SBS, and reheated to about 71°C to prevent condensation in the HEPA filtration unit. The exhaust is heated by another 15°C to 17°C by the Paxton blowers, and then further heated to about 360°C prior to entering the thermal catalytic units. Temperatures drop about 100°C across the catalyst unit by air dilution and heat loss from the duct up to the PBS where the exhaust stream is further quenched to 32°C to 37°C.

The initial portion of feed processing occurred up to 77.9 hours run time; the cold cap was then consumed between 77.9 and 82.1 hours of operations, the melter was placed on standby and the off gas system was shut down prior to resuming testing approximately three days latter. In many of the depictions of the off-gas system data, a major change in the data trends is readily apparent at the end of the initial portion of the test.

4.3.1 Melter Pressure

A vacuum on the melter of three to three and half inches of water was targeted and maintained throughout the tests. This is achieved by setting blower speeds and using a control air

system which constantly monitors the vacuum on the melter and injects sufficient air into the transition line immediately downstream of the film cooler to maintain a relatively constant vacuum on the melter. The computer-logged melter pressures measured at the instrument port and calculated control air flow rates for the test is plotted in Figures 4.11. The range of control air flow rates of up to 72 scfm reflect the changes of melter exhaust volume in response to changes in the cold cap and feed rate, including pulsing of the feed (due to the ADS pump) throughout the tests. There were five occasions of instantaneous positive pressure spikes in the electronic data during testing, the last two of which occurred at about 126 and 135 hours run time during a hiatus in feeding required for maintenance activities or to allow portions of the cold cap to be assimilated into the glass pool. In response to the brief positive pressure spikes observed in the initial portion of the test, the amount of control air used in the second portion of the test was almost doubled to accommodate larger variation in plenum pressure. The mound and ridge formation in the cold cap combined with the exaggerated glass discharge volumes created a greater challenge for maintaining negative pressure on the melter plenum than in previous melter tests. Ultimately, these cold cap conditions led to reduction of the processing rate over the course of the test to maintain consistent negative pressure on the melter plenum.

The differential pressure across the film cooler and transition line is shown in Figure 4.12. The typical film cooler and transition line differential pressures ranged between one and a half and two inches water column and two and a half and three and a half inches water column, respectively. Measured values outside these ranges resulted from either manual or spray cleaning of the film cooler, clogged sensor lines, opening of ports in the transition line and melter lid for sampling activities, and small pressure surges resulting from either the pulsed nature of feeding or changing conditions in the cold cap. Transient spikes in differential pressure occurred every 12 hours when the film cooler was rinsed with 5 liters of water. The film cooler was fully occluded at 173.3 hours of operations, necessitating a pause in feeding to manually rod out the occlusion. In response to the cleaning, the differential pressure across the film cooler dropped from 10 inches W.C to about 1 inches W.C.

4.3.2 SBS

The SBS quenches the melter exhaust, condenses much of the water from the melter feed, and removes the majority of the particulate in the exhaust stream. Many parameters of the SBS were recorded during testing, including inlet and outlet gas temperatures, pressures, and flow rates, pressure drops, sump temperature, heat exchanger inlet and outlet water temperatures, and flow rates. The amounts of heat removed by the SBS jacket, and the SBS inner cooling coil were calculated from the measured data using the hourly averaged cooling water temperature increases (outlet temperature minus supply temperature) across the SBS inner cooling coil and cooling jacket multiplied by the same time-averaged water flow rate through each.

The SBS inlet and outlet gas temperatures are plotted in Figure 4.13. The average SBS inlet and outlet gas temperatures were 299°C and 42.4°C and 280°C and 42.6°C during the first and second portions of the test, respectively.

SBS inlet, outlet, and differential pressures are plotted in Figures 4.14. During the first part of testing, the inlet gas pressure averaged -7.4 inches W.C., the outlet pressure averaged -40.4 in. W.C. and the pressure drop across the SBS averaged 34 inches W.C. During the latter portion of the test, the inlet gas pressure averaged -7.6 in. W.C., the outlet pressure averaged -39.7 in. W.C. and the pressure drop across the SBS averaged about 33.5 inches W.C. The SBS down-comer annulus pressures are given in Figure 4.15. The SBS off-gas temperatures in the down-comer measured at various depths (from 3 to 53 inches) and the SBS sump water temperature are given in Figures 4.16. The average SBS sump temperatures were 36.5°C and 36.8 °C, which are about 6°C less than the SBS outlet gas temperature during the two portions of the test. The measured off-gas temperatures decrease as the depth from the SBS lid increases due to cooling of the gas in the down-comer pipe by the surrounding SBS liquid.

Water temperatures at the SBS inner cooling coil inlet, inner cooling coil, outlet/jacket inlet, and jacket outlet are given in Figure 4.17. The average water temperature differences were 15.0°C and 16.8°C across the SBS inner cooling coil and 3.2°C and 3.2°C across the jacket during the first and second testing portions. The SBS cooling coil and SBS jacket water flow rates are plotted in Figure 4.18 and averaged 18.3 gal/min and 13.1 gal/min for the first and second portions of the test, respectively. The corresponding amounts of heat removed by the SBS inner coil and jacket are shown in Figure 4.19. During the first part of the test, heat removal averaged 59.2 kW by the SBS inner cooling coil and 13.2 kW by the cooling jacket. This corresponds to about 82.8 % of the heat load to the SBS being removed by the inner cooling coil and about 17.2% by the cooling jacket. During the second part of the test, heat removal averaged 46.7 kW by the SBS inner cooling coil and 9.4 kW by the cooling jacket. This corresponds to about 83.2 % of the heat load to the SBS being removed by the inner cooling coil and about 16.8% by the cooling jacket.

One of the functions of the SBS is to condense water that originated in the waste feed. Figure 4.20 compares the amount of water fed to the total volumetric accumulations in the SBS during testing. The difference between the amounts of water coming from the feed and the amounts blown down from the SBS sump represent the amount of water carried out in the off-gas stream as a result of it being saturated at the SBS sump temperature, as well as a small amount of entrained droplets. This amount is largely determined by the SBS sump water temperature. In the current tests, of the 2721 gal of water entering the SBS as part of the exhaust stream, 1863 gal or 68.5% was condensed in the SBS.

4.3.3 WESP

The primary function of the WESP is to remove fine, often water soluble particles from the exhaust stream that are not efficiently removed by the SBS. The inlet and outlet gas temperatures, differential pressure across the WESP, and the WESP current and voltage were measured and recorded by the computer data acquisition system. The WESP inlet and outlet gas temperatures for the test are plotted in Figure 4.21. A temperature increase of 1.2°C is observed in the exhaust temperature as gas passes through the WESP. The periodic downward spikes in the WESP outlet temperature are a result of the daily deluge of the WESP to wash collected deposits off the electrodes and into the WESP sump. The WESP differential pressures and outlet gas flow rates are plotted in Figures 4.22 for the test. Pressure drops of 5.5 and 7.6 inches W.C. across the WESP were observed during the first and second portions of test. The typical wet gas flow rate exiting the WESP was between 250 and 260 scfm.

The amount of liquid accumulated in the WESP (not including the deluge volume) is plotted as a function of run time in Figure 4.23 where it is compared with the amount of fresh water sprayed into the WESP during the test. The inlet spray water was targeted at 2.0 ± 0.2 gph; however, the actual spray water flow rate was ≈ 1.7 gph because of the limitations of the spray nozzle. As evident from both figures, spray water accounts for the majority of the liquid accumulation in the WESP. The difference between accumulated liquid and fresh water sprayed is equal to the amount of liquid removed from the off-gas, which is also plotted in Figure 4.23. The WESP electrodes were deluged daily, as planned, with water at a nominal rate of 12 gpm for 3.33 minutes.

The WESP voltage and current are plotted as functions of run time in Figure 4.24. During the initial portion of the test, the voltage averaged 30.2 kV and the current averaged 14.8 mA. During the second portion, the voltage averaged 30.4 kV and the current averaged 14.5 mA. The power stabilized immediately after the daily deluges.

4.3.4 Secondary Off-gas System

A HEME filtration unit (HEME 1) follows the WESP in the off-gas system to remove water droplets that may be present in water-saturated gas exiting the WESP. The outlet gas temperature and differential pressure are plotted in Figure 4.25. The typical pressure drop across HEME 1 during testing was about 1.6 in W.C.

The HEME is followed in the off-gas system by a heater, a HEPA filter (HEPA 1), and a Paxton blower (Blower 1). The purpose of the heater is to ensure that water-saturated gas exiting HEME 1 is heated above its dew point before passing through the HEPA filter in order to prevent moisture condensation in the HEPA filter. The outlet gas temperature and the pressure differential across the HEPA filter are the two parameters monitored by the off-gas data acquisition system; these are shown in Figure 4.26. The typical pressure drop across the HEPA filter was 0.6 inch water column throughout testing.

A vacuum is maintained on the melter by a pair of redundant Paxton blowers (Blowers 701 and 702) immediately downstream of the HEPA filtration unit and a blower (Blower 801) downstream of the packed bed scrubber.

Downstream of the HEPA filter and Paxton blowers in the off-gas train is the thermal catalytic oxidizer (TCO) and selective catalytic reduction unit (SCR). The TCO/SCR unit consists of a heater, a Thermal Catalytic Oxidizer and a Selective Catalytic Reduction Unit with an ammonia injection system. After the off-gas is heated in the TCO/SCR heater the organics are catalytically oxidized in the TCO. The off-gas is then mixed with ammonia before entering the SCR unit where NO_x is reduced to nitrogen; however, in this test ammonia was not used.

The TCO/SCR heater gas inlet temperatures are plotted in Figure 4.27. The heater gas inlet temperatures averaged 89°C. The TCO inlet and mid-bed, SCR inlet and outlet, and post SCR temperatures are plotted in Figure 4.28. The average TCO inlet and mid-bed temperatures were 357°C and 355°C during the first part of the test and 364°C and 366°C during the second part of the test. During the first portion of the test, the average SCR outlet temperatures were 328°C and 304°C, respectively, at two locations, one foot apart at the outlet of SCR. The corresponding temperatures were 330°C and 310°C during the second portion of the test. The differential pressures across the TCO/SCR are plotted in Figure 4.29. The TCO and SCR differential pressures were 3.9 and 2.5 inches W.C., and 4.3 inches W.C. and 2.8 inches W.C, during the fist and second portions of the test, respectively.

Downstream of the TCO/SCR is the packed bed caustic scrubber (PBS) to remove acid gases from the off-gas stream. The PBS sump solution is derived from process water; caustic solution (25% NaOH) is added to control the solids content and pH of the scrubber liquid. The PBS inlet gas temperature and pressure drop across are shown in Figure 4.30. The average pressure drops across the PBS were 3.2 inches W.C. and 3.4 inches W.C. during first and second portions of the test, respectively. The average inlet gas temperature at about 262°C and 278°C was quenched to about 33.5°C and 32.8°C in the PBS during the first and second portions of the test, respectively. The PBS sump temperature and pH are shown in Figure 4.31. The saw tooth appearance of the measured pH values around 9 and 10 results from the automated additions of NaOH solution to maintain the relatively constant pH.

4.3.5 SBS, WESP, HEME, and PBS Process Fluids

Throughout the tests liquid is removed from the SBS, WESP, PBS, and HEME sumps to maintain a constant volume in each of these reservoirs. The total amount removed from each is given in Table 4.7. As expected, the removed volume mostly decreases down stream along the off-gas system from the SBS to WESP to PBS. The amount of solution removed from the first (immediately downstream of the WESP) HEME during testing is primarily attributable to added process water. The HEME unit was continuously sprayed at ~0.2 gal/hr, resulting in the addition of about 40 gallons of water during testing. The liquid volume accumulated during testing was about ten gallons greater than the amount sprayed as a result of condensation. The SBS and PBS

were blown down as required to maintain constant volume. The WESP is typically blown down around each deluge – prior to and after introducing 40 gallons of water to wash the elements. One-liter samples were collected from the SBS, WESP, first HEME, and PBS sumps at the end of testing. Samples were subjected to total dissolved solids (TDS) and total suspended solids (TSS) determinations by gravimetric analysis of filtered material and the evaporated filtrate. An additional sample was filtered to generate solids and filtrate for complete chemical analysis, which included pH determination, direct current plasma atomic emission spectroscopy (DCP-AES) analysis for metals, and ion chromatography (IC) for anions; the dried filtered solids underwent microwave-assisted acid dissolution prior to chemical analysis. The analyzed chemical compositions for samples taken at or near the end of each test are provided in Table 4.8. The sample names are coded as follows: the first letter in the sample name is "S", "W", "H1", and "P" for the SBS, WESP, first HEME, and PBS samples, respectively. The "A" and "B" suffixes in the name of the WESP samples correspond to samplings immediately before and after the 40-gallon deluge.

The pH of sump solutions is affected by constituents removed from the exhaust by each component and the amount of process water or sodium hydroxide added. Feed processed in the current tests contains relatively high concentrations of fluoride and sulfate as compared to other HLW feeds previously processed [5, 11-13, 15, 16, 18]. As a result, the pH in the primary off-gas system effluents were significantly more acidic than in previous tests on DM1200 with HLW feeds. The pH values of less than 2 are more similar to values measured while processing some LAW wastes than to those for HLW wastes, which typically result in near-neutral solution pH values. Similarly low pH values were obtained while processing a HLW waste with high concentrations of nitrates [21]. The pH of the post deluge WESP solution was higher due to dilution with the deluge tap water than is the solution sampled from the WESP prior to the deluge. The solution from the HEME that follows the WESP has a similar pH to that of the WESP solution. The PBS sump is maintained around a pH of 9 during testing by the addition of 25% sodium hydroxide solution, which is reflected by measured pH values near 9 in the PBS solutions.

The chemical composition as well as the distribution between dissolved and suspended solids fractions was measured on sump solutions from the end of testing and is provided in Table 4.8. Most of the chemical species measured in off-gas system solutions were dissolved due to the efficiency of the SBS at removing coarse particles, which are often insoluble, and the acidic conditions in the primary off-gas system components. As expected, the most abundant constituents in the SBS solution were soluble species such as halogens, boron, alkali metals, nitrate, and sulfate. These species are readily volatilized from the glass and cold cap in the melter as soluble salts. Similar results were obtained from analysis of SBS solutions in tests with other HLW simulants [5, 11-21]. Dissolved chlorine and iodine were observed in significant proportions, even though chlorine and iodine were not targeted as a result of the ubiquity of chlorine as a feed contaminant and iodine remaining in the off-gas system from previous tests [19, 21]. In contrast to previous tests with HLW simulants [5, 11-18] but similar to tests with the high aluminum waste [19, 21] that was run prior to the present tests, aluminum was also abundant in these solutions as a dissolved species due to the relatively high concentration in the feed and the acidic conditions in the sump solution. The WESP solutions contain mainly volatile salts (alkali halides, borates, and sulfates) carried over from the SBS, and contaminants from

previous tests. Impurities in the feed and tap water are major constituents in the WESP solutions. The concentration of suspended solids in the WESP post-deluge sample is about fives times higher than for pre-deluge solutions; this material was presumably dislodged from the electrodes. Conversely, the dissolved solids concentration in the post-deluge sample is about two and a half times less than the pre-deluge sample due to dilution by the deluge water. The chemical analysis of the solids dislodged by the deluge suggests that the material coating the internal WESP elements consists mainly of the metals Bi, Cr, Fe, Ni, and Pb. The chemical analysis of the fluid from the first HEME indicates that it is essentially diluted WESP solution, which is consistent with the HEME collecting mist carried over from the WESP. The nitrate concentration is higher in the HEME solutions than the contemporaneous WESP solutions, suggesting that the HEME is more efficient at removing nitrogen oxides from the exhaust stream, as observed in the preceding DM1200 test [21]. The relatively high concentrations of sodium, halides, nitrogen oxides, and sulfate in the PBS indicate that the PBS is functioning as intended. Also of note, is the higher concentration of nitrite than nitrate, consistent with the caustic solution selectively removing NO_2 from the exhaust stream. Since many of the components include tap water sprays or are initially charged with tap water, elements common in tap water, such as calcium, are over represented in the solutions as compared to the amounts in the target feed composition.

SECTION 5.0
FEED SAMPLE AND GLASS PRODUCT ANALYSIS

5.1 Analysis of Feed Samples

5.1.1 General Properties

Feed samples from day of testing were analyzed to confirm physical properties and chemical composition. Samples were taken during melter testing from an inline sampling port. Sample names, sampling dates, and measured properties are given in Table 5.1. A sample was also taken from the as-received feed to confirm the oxide composition and solids content. Density, pH, water content, glass conversion ratio, and oxide composition by XRF were measured on all samples; in addition, three selected samples were dissolved and analyzed by DCP-AES. The measured glass conversion ratios for all feed samples were within six percent of the target on a weight per weight basis, validating the use of the target conversion ratio for calculating glass production rates. The measured values from the melter feed samples taken during the test varied within narrow ranges: pH from 10.34 to 10.72, density from 1.36 to 1.40 g/ml, and water content 58.52 to 61.90 percent. Taken together, the data show the consistency of the feed processed during the test. As expected, the undiluted, as-received feed had higher measured solids content and higher density with lower water content.

5.1.2 Chemical Composition

The methods used for analysis of feed sample chemical compositions are described in Section 1.5. The boron, fluorine, and lithium oxide target values were used for normalizing the XRF data since their concentrations were not determined by XRF. These results, compared to the target composition in Table 5.2 corroborate the consistency of the feed compositions and show excellent agreement with the target composition for the major elements. All oxides with target concentrations greater than one percent deviated by less than three and third percent from target for feed samples. Additional analysis using DCP on solutions of acid-dissolved glass was performed on select glasses; the results are compared to the XRF analysis in Table 5.3. Values for all the major oxides compare favorably with the XRF analysis and target composition except for sodium, which often exhibits a low bias using this procedure [56]. Low biases were also observed for chromium and nickel. In previous tests with a range of waste compositions, low biases for chromium and nickel using the DCP method were observed [1, 19]; however, this bias was not observed in various LAW and HLW waste glasses [56], suggesting that the low bias is matrix dependant with respect to the sample preparation currently being used. Consequently, the XRF values are to be preferred. The closeness of the DCP boron and lithium analyses to the target (deviations of less than 5% for boron and lithium oxide) validates the use of the target boron and lithium concentrations for normalizing the XRF data. The composition of these feeds is further corroborated by comparison to the product glasses (see Section 5.2.1), which also shows that all oxides with concentrations greater than 1 wt% in the target composition deviate by less than 10% from the target.

Low concentrations of manganese in feed samples were measured, even though manganese was not included in the target composition. Also, common elements such as magnesium, calcium, zirconium, and barium, when targeted at low concentrations, were typically above these targets. These positive deviations are often observed in melter feeds due to their ubiquity in the raw materials used to make up the simulants and in the glass forming additives. Analyzed sulfur concentrations are below target concentrations due to volatilization during sample preparation.

5.2 Discharge Glass

Over six metric tons of glass was discharged from the DM1200 into 55 gallon drums using an airlift system. The glass was poured into fifteen drums, which were cooled using air to create a cooling rate replicating that expected in WTP HLW waste canisters. Product glass masses, discharge date, analysis performed, observations during discharge, and observations of foam on the surface of the discharged glass are given in Table 5.4. Once the glass had cooled sufficiently, the drum was dismounted from the discharge chamber, photographed, weighed, and sampled by removing sufficient glass from the top of the drum for total inorganic analysis. Photographs of the glass discharged from each drum are provided in Figures 5.1 – 5.15.

Foaming increased in the discharge product over the course of testing. No foaming was observed in the first three discharge cans, either in the discharge trough or on the surface of the discharged glass. In the subsequent five discharges, foamy glass was observed on the surface of the discharged glass but no foaming was observed in glass passing through the discharge chamber and no major auto discharges[1] were observed. However, in the remainder of the glass discharges, auto discharges were frequent and foamy glass was often observed in the discharge chamber and foamy glass was observed on the surface of the discharged glass. Examples of auto discharged glass on the surface of the drums can be observed in Figures 5.11.a – 5.14. Also observed in some drums were large cavities in the poured glass, as shown in Figure 5.6. Typical porosity in the discharge glasses is readily observed in Figure 5.11.b, with most pores being about 1 mm in diameter and ranging to over 1 cm in diameter. Opaque streaks in the glass were typical in the discharge glass, particularly on the surface of glass discharged into the drums.

5.2.1 Compositional Analysis of Discharge Glasses

All discharge glass samples were crushed and analyzed directly by XRF. The target values for boron and lithium oxides, which are not determined by XRF, were used for normalizing the XRF data to 100 wt%. Fluorine analysis by XRF required a polished monolith as opposed to the standard ground glass preparation used for the other elements. Every second or third discharged glass sample was directly analyzed for fluorine; fluorine concentrations of other glasses were then interpolated in between the measured values. The XRF analyzed compositions

[1] "Auto discharge" refers to the unintentional discharge of glass that occurs even though the air flow to the air-lift lance is secured.

of discharged glass samples are provided in Table 5.5. The XRF analysis results compared very favorably to their corresponding target values and feed sample analyses (see Section 5.1.2). Oxides with a target concentration greater than one weight percent deviated less than 8% from the target values in glass discharged at the end of the test. Similar to the feed sample analyses, common elements such as magnesium, zirconium, and calcium targeted at low concentrations were above their respective targets. Also, manganese was again observed as a minor contaminant. Sulfur and fluorine are below target for almost all glasses due to volatilization from the glass pool and cold cap.

Compositional trends for selected constituents shown in Figures 5.16.a - 5.16.f illustrate the closeness to the target composition at the end of DM1200 testing. Exceptions include volatile species such as sulfur and fluorine, which remain significantly below their target concentrations as a result of release to the melter exhaust. Over the course of testing, the concentrations of bismuth, phosphorus, silicon, sodium, and nickel increase at the expense of aluminum, boron (not shown), calcium, and zirconium. These changes were expected as the glass transitions from the high aluminum (24.6 wt % Al_2O_3), high boron (19.2 wt % B_2O_3) glass remaining in the melter from the previous tests [21] to the high bismuth, high phosphorus target glass composition. The increase in bismuth and phosphorus shown in Figure 5.16.a correlates with increase in foaming over the course of testing (see Sections 5.2 and 5.2.2).

5.2.2 Internal Analysis of Discharge Glass Drums

An internal inspection was performed on the twelve drums that showed evidence of foaming during discharge and upon cooling. Each of these drums was cut in half with a diamond tipped, water cooled circular saw. Pictures of the drum cutting rig are provided in Figures 5.17.a – 5.17.e. Once each drum was cut in half from top to bottom, photographs were taken, the height of the glass was measured at five locations (1" from each wall, 6" from each wall, and the center), the glass was inspected for secondary phases and porosity, and samples were taken at various horizons in the drum. A complete log of drum inspections including pictures is provided in Appendix A.

Generally, all drums contained glass with vesicles resulting from foaming. The highest concentrations of vesicles were on the glass surface and around the outside of the drums. Glass from the earlier portions of the test had smaller layers of foamy glass than later portions of the test, corroborating observations of the glass surface prior to cutting the drum and while pouring the glass. Bands of brownish red opaque glass were also observed on the glass surface and drum edges as well as the interface between the initial, and test glass pour. The vesicles in the glass were typically one or two mm in diameter. Large cavities in the center of the drum, typically adjacent to the thermowell, were observed in seven of the drums. These irregular voids ranged from about 100 to 4000 cm^3 in size. Voids were also observed in the last drum poured, which did not have a thermowell and was not cooled at the prototypical rate. Suspect metallic phases were observed in small quantities in two drums; samples were taken for further analysis. Samples were also taken to further document the size and nature of the porosity in the glass as well as to determine the phases creating the opaque bands in glass.

5.2.3 Microscopy Analysis of Discharge Glass

Select discharge glass samples were analyzed by SEM-EDS to document the presence of secondary phases and porosity. A summary of glasses inspected by SEM-EDS is provided in Table 5.6. Examples of vesicles observed in glass are provided in Figures 5.18 – 5.23. Estimates of porosity in the samples ranged from 10 to 33 volume percent. These values are higher than for the average respective discharge glasses as a result of selecting samples with higher suspected secondary phases, which often also contained higher concentrations of vesicles than much of the glass in the drums. The size of the vesicles appeared to range between 0.2 to 2 mm in diameter. Examples of secondary phases observed in the glass are provided in Figures 5.24 – 5.29. Estimates of crystallinity in the samples ranged from 1.7 to 5.8 volume percent, with about half the crystals being spinel and half apatite. Again, many of these samples were taken from areas in the drum with opaque streaks and therefore they are likely to have a higher concentration of crystalline phases. It is worth noting that the glass composition melted in a crucible was observed to contain only trace amounts of crystals and a sample heat treated for 72 hours at 950°C contained 1.8 volume percent of crystals (see Table 2.3). The higher degree of crystallinity in the melter test samples is either due to sampling variation in heterogeneous discharge, differences in the glass composition as the melt pool reaches the target composition, or the differences in the cooling history. Samples G-12O-150A-4 and G-12P-32A-1 were analyzed primarily to determine the content and source of the suspect metal content observed during visual inspection. One of the samples, G-12P-32A-1, contained flakes of metal derived from the Inconel thermowell during sawing of the drum. The other sample, G-12O-150A-4, contained small amounts of bismuth metal in the form of droplets ranging from about 5 to 50 microns in diameter. Given that metallic bismuth was observed in only one sample as a localized phenomenon, it would appear that this form of bismuth is uncommon in the discharged glass; however, its presence does illustrate the potential for its formation during the vitrification process.

5.3 Void Fraction from Bulk Density

The bulk density of glass that was poured into the twelve bisected 55-gallon drums was calculated from the measured glass mass and the estimated bulk volume of the glass in the drum, with the results shown in Table 5.7. A perfect cylinder was assumed for the bulk volume calculations. This assumption neglects the small volume contribution from the two externally protruding strengthening rings located one third and two thirds from the base of the drum and the slightly internally protruding drum bottom. The glass volume was calculated as:

$$\text{Glass volume } (\text{cm}^3) = (D/2)^2 \times 3.1416 \times H \times 16.3872\ \text{cm}^3/\text{inch}^3.$$

where D = Drum diameter (inches)
H = Average height of glass in drum (inches)

The bulk glass density was then calculated using this volume and the glass mass. Also included in Table 5.7 is the measured density of glass removed from the surface of the drums prior to the internal inspection. Glass density was measured using a pycnometric water displacement

procedure (ASTM D854-83). These calculated and measured densities were compared to a small bubble-free shard of glass discharged at the end of testing on the DM100 using the same glass composition [1]. No glass foaming was observed in these DM100 tests and therefore the density of 2.6878 g/cm^3 was used as the intrinsic, porosity-free glass density for the target composition. This intrinsic density measurement is compared with the bulk and surface glass density measurements in Table 5.7. The percentage void volume was then calculated as:

$$\text{Void \%} = 100 \times (1/\rho_B - 1/\rho_G) \times \rho_B$$

where ρ_B = Bulk or surface glass density
ρ_G = Intrinsic glass density, 2.6878 g/cm^3.

The void percentage calculated using the bulk density and measured density of glass from the surface of the drum is given as the calculated bulk and micro porosity in Table 5.7, respectively. The bulk porosity averages both the smaller vesicles observed on the surfaces of the drum with the larger voids over the entire mass of the drum, whereas the micro porosity extrapolates the measured porosity in the surface samples over the entire drum. Higher calculated bulk porosity results from larger voids contributing more to the overall porosity, while higher calculated porosity based on measurements of surface glass indicates that the glass at the drum surface is more porous than that in the bulk of the drum. These porosities are plotted against the measured glass bismuth and phosphorus concentrations in Figures 5.30 and 5.31. Porosity calculated by both methods generally increase over the course of testing as bismuth and phosphorus increase toward their target concentrations. At bismuth and phosphorus oxide concentrations of 5.5 and 4.5 weight percent, void space in the drums range from 12 to 20 volume percent.

In a similar study with a HLW AZ-101 composition, the void volume calculated from the average bulk density of glass poured from the DM1200 and average intrinsic glass density was 2.77% [57]. Unlike the current tests with the high bismuth waste, no foaming was observed and therefore low bulk porosity was anticipated.

5.4 Analysis of Corroded Bubblers

Components from the DM1200 melter and off-gas are visually inspected after each test series for indications of wear and corrosion; key components, such as bubblers, are also routinely subjected to "before" and "after" dimensional measurements. Of the components inspected in the present tests, the glass bubblers used to deliver air to the bottom of the glass pool for melt pool mixing showed significant corrosion despite the short duration of the tests. These observations prompted further detailed analysis of the bubblers.

The exposure history of the bubblers that were used while processing the high bismuth composition is provided in Table 5.8. After the previous DM1200 test [21], the bubblers were removed, inspected, and deemed satisfactory for subsequent use. The bubblers were reinstalled approximately one week prior to the tests with the high bismuth composition. The bubblers were then exposed for 383 hours to a high bismuth glass composition: 193 hours while processing the

high bismuth composition, 157 hours of idling, and 30.5 hours while processing a bismuth-free feed [20] to turn over the glass pool. The bubblers were removed and inspected within a few hours after the turnover was completed. The amount of bismuth-free feed available was only sufficient for one melt pool turnover and therefore although the concentration of bismuth was significantly reduced in the melt pool, bismuth and other waste components were not fully removed.

5.4.1 Visual Inspection of Bubblers

Visual inspection of the bubblers removed after processing the bismuth-rich feed showed significant corrosion of the bubblers, primarily at the tip at the terminal nozzle and on the foot which rests on the melt pool floor. Photographs of the bubbler tips prior to testing are shown in Figures 5.32 and 5.33; the condition after testing is shown in Figures 5.34 and 5.35, which clearly illustrate the extent of the damage. Figure 5.36 shows the corrosion of the bubbler tip in the context of the entire bubbler. In addition to visual observations, measurements were made of the bubbler tube diameter at several locations before and after testing; the results are provided in Table 5.9. Interestingly, the data indicate minimal corrosion loss for the majority of the bubbler but substantial damage near the tip of the bubbler and of the foot which rests on the melt pool floor. Up to about an inch from the end of the approximately 1-inch diameter bubbler, and the majority of the foot was lost. This is in stark contrast to the side bubbling outlet, located 8 inches up the bubbler from the corroded tip, which shows little sign of corrosion.

5.4.2 SEM Analysis of Corroded Bubblers

Sections were taken from the remaining material on the corroded tips of the two bubblers and mounted for examination in the SEM. These samples were designated O-12Q-31B and O-12Q-31C. Mapping and spectral acquisition were used to characterize the microstructure of the corroded areas. Figure 5.37 shows a low magnification SEM electron backscatter micrograph and EDS spectra at selected points of a representative reaction interface of the Inconel with the melter glass in O-12Q-31B. Spectrum 1 is taken from the lighter grey outer layer, which is a complex spinel containing Fe, Cr, Mn, Zn, and a little Al. Spectrum 2 is from the dark grey crystals in the layer beneath the spinel and is an oxide of chromium incorporating also small amounts of Ti and Al. By comparing Line Spectrum 1 with Line Spectrum 2, one can see the severe depletion of chromium in the Inconel near the reaction interface with the glass. The brighter regions within the chromium oxide layer are metallic corrosion products; these were characterized by EDS X-ray mapping of a portion of the area shown in Figure 5.37. The maps and the area are shown in Figure 5.38. Examination of the maps reveals that there are several areas where sulfur and phosphorus are concentrated in association with other elements and areas where bismuth is present either as a metal or associated with sulfur and phosphorus. A small nodule in the upper right of Figure 5.38 is shown in greater detail together with selected area spectra in Figure 5.39. Spectrum 4 is primarily nickel phosphide, Spectrum 5 is a nickel-iron-chromium alloy, and Spectrum 6 shows nickel and bismuth associated with both phosphorus and sulfur.

Most of the corrosion features in O-12Q-31C were similar but a few new types were evident. Figure 5.40 shows a micrograph and X-ray maps of a detached nodule that was found in the corrosion interface. The metal in the nodule is primarily nickel containing very small amounts of iron and chromium. There are mixed phosphates of iron, nickel, chromium, and aluminum, and regions of nearly pure silica. Another area of interest in O-12Q-31C is shown with some typical local spectra in Figure 5.41. There are some unusual phases present here, as well as evidence of penetration of bismuth, silica, and sulfur to a depth of a few hundred microns into the Inconel (Spectra 1, 2, 8, and 9). The interface layer appears to contain a chromium silicate (Spectrum 3) and a mixed nickel-chromium sulfide or sulfate (Spectrum 5).

Although the process of formation of the observed phases remains unclear, many of the phases observed would seem to require reducing conditions, at least locally, for their formation.

5.4.3 Sampling of Melt Pool Floor

The localized nature of the corrosion and its apparent confinement to the lowest points on the bubblers (the foot and the bottommost part of the tip) are suggestive of partial immersion in a corrosive phase that might have been present on the melter floor. To evaluate the potential of this mechanism, a suction sample was taken from the melt pool floor and analyzed for possible corrosive secondary phases. This type of sampling is conducted by lowering a ceramic tube to the melt floor while maintaining a small positive pressure in the gas flow to the tube. Once the tube is in the sampling location, the pressure supply is switched over to a vacuum supply using a three-way valve, which then draws glass and any other materials into the suction tube. The tube is then pulled from the melter to allow the glass to freeze. Glass is then removed from the tube for visual inspection and subsequent analysis by SEM and XRF. The glass sample taken from the melter floor showed no visual signs of secondary or metallic phases. More detailed analysis for secondary phases by SEM revealed only trace amounts of spinels, which are typical of HLW glasses. The results from chemical analysis of the glass discharged at the end of the turnover period and the suction sample show them to be virtually identical. This sample therefore provides no indication of significant segregation of select glass components onto the melt pool floor. It should be noted, however, that such sampling could miss localized accumulations of material and could be limited with respect to the ability to pull and retain low viscosity molten metal phases into the sampling tube.

Another phenomenon that could be preferentially localized to the tips of the bubblers might be electrochemical corrosion as a result of current flows along the bubbler tubes and then from the tip of one bubbler to the other, perhaps via the bottom electrode (which is not powered).

While the cause of the observed corrosion is uncertain at this time, this is clearly a phenomenon of potentially significant impact for processing waste streams of this type at the WTP.

SECTION 6.0
MONITORED OFF-GAS EMISSIONS

6.1 Particulate Sampling

The melter exhaust was sampled for metals/particles according to 40-CFR-60 Methods 3, 5, and 29 at steady-state operating conditions during each test segment. The concentrations of off-gas species that are present as particulates and gaseous species that are collected in impinger solutions were derived from laboratory data on solutions extracted from air samples (filters and various solutions) together with measurements of the volume of air sampled. Particulate collection required isokinetic sampling, which entails removing gas from the exhaust at the same velocity that the air is flowing in the duct (40-CFR-60, Methods 1-5). Typically, a sample size of 30 dscf was taken at a rate of between 0.5 and 0.75 dscfm. Total particulate loading was determined by combining gravimetric analysis of the standard particle filter and chemical analysis of probe rinse solutions. An additional impinger containing 2 N NaOH was added to the sampling train to ensure complete scrubbing of all acid gases. The collected materials were analyzed using direct current plasma atomic emission spectroscopy for the majority of the constituents and ion chromatography (IC) for anions. Melter emission fluxes are compared to feed fluxes in Table 6.1. Notice the distinction that is made between constituents sampled as particles and as "gas". The "gaseous" constituents are operationally defined as those species that are scrubbed in the impinger solutions after the air stream has passed through a 0.3 μm heated filter. All samples are well within the 90 – 110% limits for isokinetic sampling.

Particulate emissions from the melter constituted 0.25, 0.23, and 0.98 percent of feed solids for the three sampling periods. Two of these results are below but similar to the 0.27 and 0.41 percent of feed solids emitted from the DM100 while processing the same waste and glass composition [1]. The higher of the three solids carryover values was measured near the end of testing while the cold cap was less extensive (65% vs. 90% coverage) and glass was being discharged, which created increased opportunity for emissions directly from the well agitated melt pool. Carryover measured during the first two sampling periods was higher than that for the previously processed HLW high aluminum composition [1, 19, 21] but lower than that for most of the HLW high iron compositions [5, 11-18, 53] due mainly to the relative amounts of volatile components such as halides and sulfates in the respective wastes. In addition, bubbling rates were high during the sampling periods of the current tests as compared to most of the tests with the high iron wastes (152 – 162 lpm vs 65 lpm), which would result in higher particulate carryover with feed of the same composition [5, 13-15]; however, the compositional differences between the waste streams appears to have a greater effect on total carryover than bubbling.

As expected, the feed elements emitted at the lowest melter decontamination factor (DF) were clearly fluorine and sulfur. Other elements exhibiting some volatile behavior were boron and potassium. The relative volatility of barium and lithium are difficult to evaluate due to the low target concentrations in the feed. Also, higher than actual carryover was calculated for common elements such as magnesium, zirconium, and calcium, which were targeted at low

concentrations with measured feed concentrations above their respective targets. Bismuth carryover ranged from 0.42 to 1.5 percent and was 1.5 to 2 times higher than the aggregate particulate. Boron, sulfur, and fluorine were the only elements detected in the impinger solutions collected downstream of the heated particle filter in the sampling train, which constitutes the "gas" fraction of the melter emissions. A greater proportion of fluorine and sulfur were measured as gaseous rather than particulate emissions. Of the fluorine captured in the impinger solutions, fluorine was measured only in the acidic impinger solutions, indicating that fluorine was present as HF. These emissions trends are consistent with previous tests on the DM100 and DM1200 while processing various simulated HLW streams [1, 5, 10-21].

6.2 Gases Monitored by FTIR

Melter emissions were monitored in each test for a variety of gaseous components, most notably CO and nitrogen species, by Fourier Transform Infra-Red Spectroscopy (FTIR). The exhaust stream was sampled at the outlets of several prototypical components (melter, SBS, WESP, and PBS) to discern the effect these components have on the volatiles in the exhaust stream. It should be noted, however, that the off-gas system component most responsible for the removal of nitrogen oxide and volatile organics, the TCO-SCR catalyst unit, was not active in all the tests. Also, a single FTIR unit was used for all of the measurements and, therefore, the various locations were sampled sequentially and not simultaneously.

A summary of the average concentrations of gaseous species monitored during the DM1200 tests is provided in Table 6.2. The concentrations of five of the most abundant monitored species are plotted in Figures 6.1 - 6.5. The analytes listed in Table 6.2 are those that were thought likely to be observed during the tests based on previous work; no other species were detected in the off-gas stream by FTIR. Generally, emissions from the melter were relatively low as a result of the low concentrations of nitrogen, organic carbon, ammonia, and halogens in the feed. The most abundant nitrogen species monitored was NO, which is in keeping with previous melter tests with both HLW and LAW feeds. Little nitrogen was detected as other species, except for NO_2, which was about 8 times lower in concentration than NO in the exhaust upstream of the catalyst unit. About half of the NO in the exhaust stream was converted to NO_2 within the catalyst unit (note that ammonia was not introduced into the SCR during these tests). Very low concentrations of nitric and hydrochloric acids were measured in the exhaust, the latter as a result of the use of tap water to dilute feed and rinse feed lines. Consistent with the gaseous fluorine concentrations observed using the Method 5-type sampling (see Section 6.1), HF was observed throughout the testing by FTIR. Also consistent with the Method 5-type results, low sulfur dioxide concentrations were monitored during testing; however, gaseous sulfur emissions can also be present in forms other than sulfur dioxide that are not monitored by the FTIR, such as sulfuric acid. Measured concentrations for most constituents through the DM1200 exhaust system were very similar. This confirms the expectation that the SBS, WESP, HEME, and PBS do not remove significant proportions of nitrogen and carbon oxides. Conversely, moisture and some minor components such as HF and SO_2 are greatly reduced in concentration by removal in the SBS. These trends can be readily discerned by comparing NO concentrations in Figure 6.1, which do not show significant differences at the various sampling localities, and HF concentrations in Figures 6.5, which are noticeably higher in the melter

exhaust. The variability of many of the analyte concentrations at each sampling location is attributable to the dynamic conditions in the cold cap and is in keeping with previous melter tests.

SECTION 7.0
SUMMARY AND CONCLUSIONS

A series of tests was conducted at the crucible scale and on the HLW pilot melter (DM1200) to determine the nature, cause, and extent of glass foaming while processing a high bismuth waste stream. This HLW composition was one of several previously specified by ORP for which a glass composition was developed that achieved high waste loading and acceptable glass properties and was processed on the DM100 under a variety of test conditions [1]. This glass formulation exhibited foaming during heat treatment simulating WTP HLW canister centerline cooling (CCC) conditions. Conversely, foaming was not evident during the DM100 melter tests where the cooling rate for the poured glass was faster than that for the WTP HLW CCC. Clearly, foaming during pouring or cooling of actual HLW canisters would be highly undesirable. Accordingly, the present work involved a program of larger-scale testing to determine whether this effect occurs under conditions more prototypical of those at the WTP. In addition, crucible-scale tests were used to determine the likely causes for the observed foaming behavior and to develop potential methods to mitigate that behavior. A significant finding of the present work is that foaming can indeed occur during prototypic cooling of simulated HLW canisters that are filled at prototypic WTP HLW rates with a glass formulation with a high loading of the high bismuth waste. Consequently, this phenomenon represents a real risk that must be recognized and appropriately mitigated. The results from the crucible-scale tests provide insight into the causes of the observed foaming behavior and strategies to prevent such behavior while retaining high waste loadings.

7.1 Crucible Scale Testing

Crucible scale tests were conducted to determine the cause of foaming in the Bi-limited glasses on canister center line cooling. In addition, the test examined methods to mitigate the foaming, improve waste loadings, and improve processing characteristics.

The base glass HLW-E-Bi6 showed both foaming and crystallization of Cr-containing spinel on CCC heat treatment. However, a DM100 melter discharged glass sample with the same target composition as HLW-E-Bi6 did not show any foaming on CCC indicating that, in addition to composition, the thermal history of the sample is an important factor in the foaming mechanism observed on CCC. A lower viscosity version of HLW-E-Bi6 also foamed on CCC, demonstrating that the observed foaming is not solely due to a higher viscosity glass retaining gas bubbles generated during CCC. Variations of HLW-E-Bi6 glass prepared without Bi or F and subjected to CCC showed similar amounts of bubbles as HLW-E-Bi6 on CCC. In contrast, variations of HLW-E-Bi6 glass prepared without phosphorous showed a marked decrease in the amount of bubbles in CCC samples, identifying phosphorous as a contributor to the observed foaming. However, since it was unlikely that the oxidation state of phosphorus could be changing, it was suspected that the mechanism must involve other multivalent components that interact with phosphorous in some way to become reduced during CCC, thus releasing gas

bubbles. A review of phase diagrams relevant to the HLW-E-Bi6 glass composition showed that reactions between P and Cr could potentially result in the reduction of Cr from Cr^{6+} to Cr^{3+} under CCC conditions, releasing gas bubbles that would cause the observed foaming. Preparation and CCC heat treatment of a variation of HLW-E-Bi6 without Cr did not show any gas bubbles in the CCC samples, confirming this hypothesis. The results show that P and Cr are contributors to the foaming observed on CCC whereas Bi, which is a major glass component plays no major role. Based on these observations, a potential mechanism for the observed foaming may involve the following illustrative reactions:

P-rich chromophosphoric species (*m*) → $Na_4P_2O_7$ (*xl*) + $Na_3[PCrO_7]$ (*m*)
$Na_3[PCrO_7]$ (*m*) + ½ NiO (*m*) → Na_3PO_4 (*xl*) + ½ $NiCr_2O_4$ (*Sp*) + ¾ O_2 (*g*)

where *m* indicates a melt phase, *xl* a crystalline phase, *Sp* a spinel crystal, and *g* a gas phase.

The impact of spinel crystallization on foaming provides a possible explanation as to why no gas bubbles developed in the melter-discharged glass, which was identical to HLW-E-Bi6 in its chemical composition. Very likely, spinel crystals that had nucleated and grown during the particular cooling conditions for glass discharged from the DM100 melter had effectively depleted the Cr^{6+} before the CCC heat treatment. The premelting step for the standard CCC test (1200ºC for one hour before cooling) does not appear to have been adequate to reverse the reactions.

Based on these results, several possible methods for mitigating the foaming observed on CCC are evident:

- Suppression of Cr^{6+} with a reductant or glass chemistry.
- Reduction of glass melt viscosity to facilitate release of gas bubbles.
- Formation of other competing phosphate species.

For a number of reasons, the foaming mitigation work was based primarily on the last of these methods. This part of the work concentrated on formulations containing higher concentrations of sodium or aluminum. In addition to mitigation of foaming, the new formulations were designed to improve waste loading and processing characteristics. Glass formulations at 50, 55 and 60 wt% waste loading were prepared and characterized to identify compositions with high waste loading, good processing characteristics and no foaming on CCC. The formulations at 55 and 60 wt% waste loading showed some level of crystallization or small amounts of foaming. Two formulations at 50 wt% waste loading showed acceptable properties. One of them, HLW-Bi-F3, with 3 wt% more Na_2O and less B_2O_3 than HLW-E-Bi6 eliminates foaming but may show slow processing rate based on VGF test results. The other candidate, HLW-Bi-F9, with higher Li_2O and B_2O_3 and less Na_2O, shows small amounts of crystallization in the as-melted glass but otherwise has acceptable properties, including no foaming on CCC and good processing characteristics based on the VGF test.

Raman spectroscopic studies were conducted on several Bi-limited glasses and included the collection of high temperature data under CCC conditions. These studies of the structure of the Bi-limited glasses generally were in agreement with the conclusions from the crucible scale

studies regarding the mechanism that causes foaming in these glasses on CCC. However, additional studies using X-ray absorption spectroscopy would be useful to further elucidate the interactions between chromium and phosphorus that appear to underlie the observed foaming behavior.

7.2 HLW Pilot Scale Testing

Over seventeen metric tons of feed containing the high bismuth HLW simulant was processed on the HLW Pilot Melter (DM1200) producing over six metric tons of glass. In the present work, a total of fourteen canister cooling experiments were performed with the high bismuth formulation on the DM1200. The melter tests were conducted primarily to determine whether foaming during canister cooling occurs under conditions more prototypical of those at the WTP and secondarily to determine glass production rates for a high bismuth waste. The tests employed double-outlet prototypical bubblers, a glass pool temperature held of 1150°C, and bubbling adjusted to maximize glass production rates. Glass production rates were between 500 and 1000 kg/m^2/day at 1150°C melt pool temperature and decreased as the target glass pool composition was approached. The WTP bench mark production rate of 1050 kg/m^2/day was not obtained despite an optimized bubbler configuration and high levels of melt pool bubbling. Extensive operational data was collected on the one-third scale WTP HLW Pilot Melter system and prototypical off-gas treatment train throughout the tests. Observations of melt pool surface, discharge glass, and cooled glass product were made throughout testing to document the extent of melt pool foaming. Extensive analysis of the glass product, including thorough internal analysis of the drum contents, SEM analysis, and porosity determination were also conducted.

Both of the Inconel 690 bubblers employed for these tests experienced localized but severe corrosion at their tips. This behavior is atypical and appears to be associated with certain constituents in this waste stream, including phosphorus, sulfur, and bismuth. While the cause of the observed corrosion is uncertain at this time, this is clearly a phenomenon of potentially significant impact for processing waste streams of this type at the WTP.

The melter exhaust was sampled for particulate and gaseous species to determine the effect of the variations in feed composition and glass temperature on emissions. Total particulate carryover constituted 0.25, 0.23, and 0.98 percent of feed solids for the three sampling periods; two of these results are below but similar to the 0.27 and 0.41 percent of feed solids emitted from the DM100 while processing the same waste and glass composition [1]. The higher of the three solids carryover values was measured near the end of testing while the cold cap was less extensive (65% vs. 90% coverage) and glass was being discharged, which increased the opportunity for emissions directly from the well agitated melt pool. Melter DFs were determined for most elements in the feed for all three sampling periods. The most volatile species were sulfur and fluorine, which is typical. Gaseous emissions of nitrogen oxides and byproducts of incomplete combustion, such as carbon monoxide and ammonia, were very low due to the lack of nitrates and organic carbon in the feed.

7.3 Foaming During Pilot Scale Processing and Canister Cooling

Observations made during testing with the high bismuth waste on the DM1200 using prototypical canister cooling can be summarized as follows:

- No visual signs of melt pool foaming were evident through the melter view port.
- No foaming of glass out of the discharge drums occurred.
- The melt pool density decreased as the target glass pool composition (Bi_2O_3 6.71, P_2O_5 4.99 wt%) was approached.
- Foamy glass was observed on the surface once the glass was only partially turned over (Bi_2O_3 4.4, P_2O_5 3.7 wt%).
- Frequent auto discharge[2] of foamy glass was observed once the glass was partially turned over (Bi_2O_3 5.7, P_2O_5 4.6 wt%).
- Foamy glass was observed in the discharge trough once the glass was only partially turned over (Bi_2O_3 5.7, P_2O_5 4.6 wt%).
- Internal inspection of drums revealed a foamy layer of glass on the top and around the sides of drums once the glass was only partially turned over (Bi_2O_3 4.4, P_2O_5 3.7 wt%). The foamy layer became more extensive in subsequent discharges, although it never extended to the entire contents of the drum.
- Large cavities of up to three and half liters were observed in the center of the drums. This is in contrast to the 0.2 – 2 mm in diameter vesicles present in the foamy layer.
- The overall void space in drums increased to between 12 and 20 volume percent once the glass composition contained greater than 5.5 wt % Bi_2O_3 and 4.5 wt % P_2O_5.
- Secondary phases, primarily spinel and apatite, at one to six volume percent were observed concentrated in bands often associated with foamy layers. Isolated bismuth metal droplets were observed in samples from only one drum.

Taken together these results confirm that the foaming behavior observed in crucible scale tests with this composition also occurs at larger scale under conditions more prototypical of those at the WTP and raises concerns with respect to processing this composition on the full scale melter. The decrease in melt pool density and foamy glass in the discharge glass suggests that gas is evolving from the glass at or near melt pool temperatures. The foaming in the discharge and into the glass drum is consistent with the foaming during cooling observed in the crucible scale tests. Much of the evolved gas is trapped in the glass in regions were the glass cools rapidly. The large cavities observed in the center of many of the drums may result from the coalescence of evolved gas. The calculated void volume and the observations of foamy glass illustrate the relationship between glass composition and foaming tendency: the closer the glass composition approached the target (the higher the bismuth and phosphorus), the greater was the degree of foam in the glass product. Although no glass was observed to foam out of the drum, auto discharges of foamy glass have the potential to clog the discharge system. The high void

[2] "Auto discharge" refers to the unintentional discharge of glass that occurs even though the air flow to the air-lift lance is secured.

space in the discharged glass would result in the production of up to twenty percent more canisters for this waste stream, substantially increasing overall waste vitrification costs.

7.4 Recommendations for Future Work

The results of the testing presented herein clearly demonstrate a compositional dependence of foaming for glasses formulated with a high bismuth waste stream. A significant finding of the present work is that foaming can indeed occur during prototypic cooling of simulated HLW canisters that are filled at prototypic WTP HLW rates with a glass formulation with a high loading of the high bismuth waste. The results also indicate that under prototypical canister filling and subsequent cooling, up to twenty percent void space can be created, inflating the number of canisters produced for the high bismuth waste stream. In addition, atypical localized but severe corrosion was observed at the tips of the bubblers, which appears to be associated with certain constituents in this waste stream, including phosphorus, sulfur, and bismuth.

New glass formulation development performed in the present work has identified the causes of the observed melt pool foaming and identified methods to decrease the likelihood of foaming under actual processing and cooling conditions. The glass formulation work also indentified glasses with increased waste loading and increased melting rates that avoid foaming. These results have the potential for significant risk mitigation and enormous savings in cost and schedule. As a result, it is recommended that testing and evaluation of these strategies be continued in order to provide a solid basis for their broad implementation in order to maximize the cost and schedule benefits while minimizing technical risk. Some of the elements of such a program are summarized below with respect to high bismuth waste streams.

- *Throughput*: A key risk area addressed in the present work relates to the strong dependence of glass production rates on waste composition. The extent of this variation across the full spectrum of HLW waste types needs to be quantified in order to accurately project waste treatment rates. The vast majority of the previous testing for the WTP has been performed on iron-limited wastes and those results have formed the basis for vitrification system capacity projections. The original glass formulation for the high bismuth waste stream processed below the WTP benchmark of 1050 $kg/m^2/day$ at 1150°C melt pool temperature on both the DM100 and HLW Pilot Melter scale. New formulations that have been developed have the potential to exceed the minimum required production rate; however, melter testing needs to be performed to determine actual production rates.

- *Scale-Up Testing*: The new bismuth waste glass compositions developed in this work should be processed on the DM100 and the larger-scale DM1200 melter system in order to address potential risks associated with scale-up, particularly with respect to processing rates and glass foaming. Optimization of bubbling rate at the DM1200 WTP HLW Pilot Melter scale ($1.2\ m^2$) is a critical variable and therefore testing with bubblers in the prototypical orientation at larger scale is required to confirm achievable production rates. Canister cooling rates differ at various melter scales such that foaming with the bismuth

waste glass was not observed on the DM100 melter but was on HLW Pilot Melter making testing at scale under prototypical cooling conditions critical to verifying the lack of foam in the discharged product.

- *Integrated System Testing*: Testing on the DM1200 WTP HLW Pilot Melter system provides data from a one-third scale system with a prototypical feed delivery system and off-gas treatment train. Such testing is necessary to evaluate potential interactive effects on system operation arising from implementation of the enhancement strategies and to provide data on the performance of each unit operation, input for flow-sheet models and regulatory requirements, and information on recycle streams.

- *Longer-Duration Testing*: After validation at larger scale, the duration of testing should be extended in order to address and quantify any chronic issues, such as the slow accumulation of crystals in the melter cavity, refractory and bubbler corrosion, any degradation in the ability to discharge glass, and effects on off-gas line plugging.

- *Bubbler Corrosion*: Testing is necessary to determine the cause of the observed severe localized bubbler corrosion that was observed in these tests that appears to be associated with the high levels of certain constituents in this waste stream. The observed behavior is clearly of potentially significant impact for processing waste streams of this type at the WTP.

Finally, it is likely that the maximum production rate for each set of test conditions would have been significantly impacted for most of the tests if the cold cap conditions were not monitored visually. Consequently, it is recommended that the ability to maintain production rates without use of visual information be evaluated, if that is the planned WTP operating mode.

SECTION 8.0
REFERENCES

[1] "High Level Waste Vitrification System Improvements," K.S. Matlack, H. Gan, W. Gong, I.L. Pegg, C.C. Chapman and I. Joseph, VSL-07R1010-1, Rev. 0, Vitreous State Laboratory, The Catholic University of America, Washington, DC, 4/16/07.

[2] "Tests with High-Bismuth HLW Glasses," K.S. Matlack, W.K. Kot, R.K. Mohr, and I.L. Pegg, Test Plan, VSL-09T1780-1, Rev. 0, Vitreous State Laboratory, The Catholic University of America, Washington, DC, 8/26/09.

[3] "Bismuth Glass Testing (HLW)," Contract Number DE-AC27-07RV14884, Mod. A006, US Department of Energy, Office of River Protection, Richland, WA, 2009.

[4] "Test and Evaluate High Level Waste (HLW) Vitrification System Improvements," Contract Number DE-AC27-06RV14790, US Department of Energy, Office of River Protection, Richland, WA, April, 2006.

[5] "Integrated DM1200 Melter Testing of Bubbler Configurations Using HLW AZ-101 Simulants," K.S. Matlack, W. Gong, T. Bardakci, N. D'Angelo, W. Lutze, R. A. Callow, M. Brandys, W.K. Kot, and I.L. Pegg, VSL-04R4800-4, Rev. 0, Vitreous State Laboratory, The Catholic University of America, Washington, DC, 10/5/04.

[6] "Glass Formulation and Testing with RPP-WTP HLW Simulants," W.K. Kot, and I.L. Pegg, VSL-01R2540-2, Rev. 0, Vitreous State Laboratory, The Catholic University of America, Washington, DC, 2/16/01.

[7] "Glass Formulation to Support Melter Runs with HLW Simulants," Final Report, W.K. Kot, K. Klatt, and I.L. Pegg, VSL-03R3760-2, Rev. 0, Vitreous State Laboratory, The Catholic University of America, Washington, DC, 8/8/03.

[8] "HLW Glass Formulation to Support C-106/AY-102 Actual Waste Testing," W.K. Kot and I.L. Pegg, VSL-04R4770-1, Rev. 0, Vitreous State Laboratory, The Catholic University of America, Washington, DC, 8/12/04.

[9] "Melter Tests with AZ-101 HLW Simulant Using a DuraMelter 100 Vitrification System," K.S. Matlack, W.K. Kot, and I.L. Pegg, VSL-01R10N0-1, Rev. 1, Vitreous State Laboratory, The Catholic University of America, Washington, DC, 2/25/01.

[10] "DuraMelter 100 HLW Simulant Validation Tests with C-106/AY-102 Feeds," K.S. Matlack, W. Gong and I.L. Pegg, VSL-05R5710-1, Rev. 0, Vitreous State Laboratory, The Catholic University of America, Washington, DC, 6/2/05.

[11] "Integrated DM1200 Melter Testing of HLW C-106/AY-102 Composition Using Bubblers," K.S. Matlack, W. Gong, T. Bardakci, N. D'Angelo, W. Kot and I.L. Pegg, VSL-03R3800-1, Rev. 0, Vitreous State Laboratory, The Catholic University of America, Washington, DC, 9/15/03.

[12] "Integrated DM1200 Melter Testing of HLW C-104/AY-101 Compositions Using Bubblers," K.S. Matlack, W. Gong, T. Bardakci, N. D'Angelo, W. Kot and I.L. Pegg, VSL-03R3800-3, Rev. 0, Vitreous State Laboratory, The Catholic University of America, Washington, DC, 11/24/03.

[13] "DM1200 Tests with AZ-101 HLW Simulants," K.S. Matlack, W. Gong, T. Bardakci, N. D'Angelo, W.K. Kot, and I.L. Pegg, VSL-03R3800-4, Rev. 0, Vitreous State Laboratory, The Catholic University of America, Washington, DC, 2/17/04.

[14] "Start-Up and Commissioning Tests on the DM1200 HLW Pilot Melter System Using AZ-101 Waste Simulants," K.S. Matlack, M. Brandys, and I.L. Pegg, VSL-01R0100-2, Rev. 1, Vitreous State Laboratory, The Catholic University of America, Washington, DC, 10/31/01.

[15] "Tests on the DuraMelter 1200 HLW Pilot Melter System Using AZ-101 HLW Simulants," K.S. Matlack, W.K. Kot, T. Bardakci, T.R. Schatz, W. Gong, and I.L. Pegg, VSL-02R0100-2, Rev. 0, Vitreous State Laboratory, The Catholic University of America, Washington, DC, 6/11/02.

[16] "Integrated DM1200 Melter Testing of HLW AZ-102 Compositions Using Bubblers," K.S. Matlack, W. Gong, T. Bardakci, N. D'Angelo, W. Kot and I.L. Pegg, VSL-03R3800-2, Rev. 0, Vitreous State Laboratory, The Catholic University of America, Washington, DC, 9/24/03.

[17] "Integrated DM1200 Melter Testing of Redox Effects Using HLW AZ-101 and C-106/AY-102 Simulants," K.S. Matlack, W. Gong, T. Bardakci, N. D'Angelo, W. Lutze, P. M. Bizot, R. A. Callow, M. Brandys, W.K. Kot, and I.L. Pegg, VSL-04R4800-1, Rev. 0, Vitreous State Laboratory, The Catholic University of America, Washington, DC, 5/6/04.

[18] "Integrated DM1200 Melter Testing Using AZ-102 and C-106/AY-102 HLW Simulants: HLW Simulant Verification," K.S. Matlack, W. Gong, T. Bardakci, N. D'Angelo, M. Brandys, W.K. Kot, and I.L. Pegg, VSL-05R5800-1, Rev. 0, Vitreous State Laboratory, The Catholic University of America, Washington, DC, 6/27/05.

[19] "Melt Rate Enhancement for High Aluminum HLW Glass Formulations," K.S. Matlack, H. Gan, M. Chaudhuri, W.K Kot, W. Gong, T. Bardakci, I. Joseph, and I.L. Pegg, Final Report, VSL-08R1360-1, Rev. 0, Vitreous State Laboratory, The Catholic University of America, Washington, DC, 12/19/08.

[20] "Regulatory Off-Gas Emissions Testing on the DM1200 Melter System Using HLW and LAW Simulants," K.S. Matlack, W. Gong, T. Bardakci, N. D'Angelo, M. Brandys, W. Kot, and I.L. Pegg, Final Report VSL-05R5830-1, Rev. 0, Vitreous State Laboratory, The Catholic University of America, Washington, DC, 10/31/05.

[21] "DM100 and DM1200 Melter Testing with High Waste Loading Glass Formulations for Hanford High-Aluminum HLW Streams," K.S. Matlack, H. Gan, M. Chaudhuri, W.K. Kot, W. Gong, T. Bardakci, I.L. Pegg, and I. Joseph, Final Report, VSL-10R1690-1, Rev. 0, Vitreous State Laboratory, The Catholic University of America, Washington, DC, 8/16/10.

[22] "Quality Assurance Project Plan for ORP Support Activities Conducted by VSL," Vitreous State Laboratory, VSL-QAPP-ORP, Rev. 2, Vitreous State Laboratory, The Catholic University of America, Washington, DC, 2/2/10.

[23] "Master List of Controlled VSL Manuals and Standard Operating Procedures in Use," QA-MLCP, Rev. 56, Vitreous State Laboratory, The Catholic University of America, Washington, DC, 11/5/10.

[24] "High-Level Waste Melter Alternate Bubbler Configuration Testing," R.K Mohr, C.C. Chapman and I.L. Pegg, Final Report, VSL-04R4800-3, Rev. 0, 6/18/04.

[25] "RPP-WTP Pilot Melter Prototypic LAW Container and HLW Canister Glass Fill Test Results Report," TRR-PLT-080, Rev.0, Duratek, Inc., Columbia, MD, 4/27/04.

[26] "Round Robin Testing of a Reference Glass for Low-Activity Waste Forms," W.L. Ebert and S.F. Wolf, Department of Energy report ANL-99/22, Argonne National Laboratory, Argonne, IL, 1999.

[27] "Container Centerline Cooling Data, Revision 1" RPP-WTP Memorandum, L. Petkus to C. Musick, CCN# 074851, 10/29/03.

[28] *Russ. J. Inorg. Chem. (Engl. Transl.)*, A. G. Bergman and V. A. Matrosova, **14** [6], 875-876 (1969).

[29] "Determination of Sulfur Environments in Borosilicate Waste Glasses Using X-Ray Absorption Near Edge Spectroscopy", D. A. Mckeown, I. S. Muller, H. Gan, I. L. Pegg, and W. C. Stolte, Journal of Non-Crystalline Solids, 333, 74-84 (2004)

[30] "Cr^{3+}-Cr^{6+} Equilibrium in Binary Alkali Silicate Glasses", P. Nath and R. W. Douglas, Physics and Chemistry of Glasses, 6, No. 6, 197-202, (1965)

[31] *Zhur. Obshchei. Khim.,* A. G. Bergman and M. L. Sholokhovich, 24, 596 (1954).

[32] *Structural Inorganic Chemistry*, A. F. Wells, 5th ed., Oxford University Press, 1984.

[33] "Spinel Crystallization in HLW Glass Melts: Cation Exchange Systematics and the Role of Rh_2O_3 in Spinel Formation," S. Annamalai, H. Gan, M. Chaudhuri, W. Kot and I. L. Pegg, *Environmental Issues and Waste Management Technologies* IX, pp 279-288 (2003).

[34] "Effect of Basicity on Redox Equilibria in Sodium Silicate Melts: An In Situ Electrochemical Investigation," J.-Y. Tilquin, P. Duveiller, J. Glibert, and P. Claes, *Journal of Non-Crystalline Solids*, 211, pp95-104 (1997).

[35] H. Liu and C. Kuo, "Crystal Structure of Bismuth (III) Silicate, $Bi_4(SiO_4)_3$," *Zeitschrift fur Kristallographie* v. 212, p. 48 (1997).

[36] J. Ketterer and V. Kramer, "Crystal Structure of Bismuth Silicate Bi_2SiO_5", *Neues Jahrbuch fur Mineralogie Monatschefte.*, v. 1986 H1, p. 13-18 (1986).

[37] A.P. Zukhlistov and B.B. Zvjagin, "Crystal structure of Bismutoferrite ($BiFe_2Si_2O_8OH$)", *Kristallografiya.*, v. 22, p. 731-738 (1977).

[38] T. Nanbi, H. Tabuchi, and Y. Miura, "Structure of Bi_2O_3-SiO_2 Glasses," Thesis, Okayama University (2004).

[39] A. Witkowska, J. Rybicki, and A. DiCicco, "EXAFS Analysis of Bismuth Atom Neighborhood in Reduced Bismuth Silicate Glass," *Physics and Chemistry of Glasses*, v. 43C, p. 124 (2002).

[40] Z. Pan, D.O. Henderson, and S.H. Morgan, "Vibrational Spectra of Bismuth Silicate Glasses and Hydrogen-Related Reduction Effects," *Journal of Non-Crystalline Solids,* v. 171, p. 134 (1994).

[41] B. Romero, S. Bruque, M.A.G. Aranda, and J.E. Iglesias, "Syntheses, Crystal Structures, and Characterization of Bismuth Phosphate," *Inorganic Chemistry,* v. 33, p. 1869 (1994).

[42] H. Gan and P.C. Hess, "Phosphate Speciation in Potassium Aluminosilicate Glasses," *American Mineralogist*, v. 77, p. 495 (1992).

[43] H. Gan, P.C. Hess, and R.J. Kirkpatrick, "Phosphorus and Boron Speciation in K_2O-B_2O_3-SiO_2-P_2O_5 Glasses," *Geochimica et Cosmochimica Acta*, v. 58, p. 4633-4647 (1994).

[44] D.A. McKeown, I.S. Muller, H. Gan, I.L. Pegg, and Christopher A. Kendziora, "Raman Studies of Sulfur in Borosilicate Waste Glasses: Sulfate Environments," *Journal Non-Crystalline Solids*, v. 288, p. 191-199 (2001).

[45] C. Nelson and D.R. Tallant, "Raman Studies of Sodium Silicate Glasses with Low Phosphate Contents", *Physics and Chemistry of Glasses*, v. 25, p. 31-38 (1984).

[46] R.L. Frost, "Raman Microscopy of Selected Chromate Minerals," *Journal of Raman Spectroscopy*, v. 35, p. 153-158 (2004).

[47] A. Goncharov and V. V. Struzhkin, "Raman Spectroscopy of Metals, High-Temperature Superconductors and Related Materials Under High Pressure," *Journal of Raman Spectroscopy*, v.34, p. 532-548 (2003).

[48] P. McMillan, "Structural Studies of Silicate Glasses and Melts – Applications and Limitations of Raman Spectroscopy," *American Mineralogist* v. 69, p. 622-644 (1984).

[49] R.T. Downs (2006), "The RRUFF Project: An Integrated Study of the Chemistry, Crystallography, Raman, and Infrared Spectroscopy of Minerals." Program and Abstracts, 19th General Meeting of the International Mineralogical Association in Kobe, Japan. O03-13.

[50] A. Ghule, N. Baskaran, R. Murugan, H. Chang, "Phase Transformation Studies of Na_3PO_4 by Thermo-Raman and Conductivity Measurements," Solid State Ionics, v. 161, p. 291-299 (2003).

[51] W.W. Rudolph and G. Irmer, "Raman and IR Spectroscopic Investigations of Aqueous Alkali-Metal Phosphate (PO_4^{3-}) Solutions", Applied Spectroscopy, v. 61, p. 1312-1327 (2007).

[52] G. Malmros, "The Crystal Structure of α-Bi_2O_3", *Acta Chemica Scandinavica*, v. 24, p.384-396 (1970).

[53] "Summary of DM1200 Operation at VSL," K.S. Matlack, G. Diener, T. Bardakci, and I.L. Pegg, Final Report, VSL-06R6710-2, Rev. 0, Vitreous State Laboratory, The Catholic University of America, Washington, DC, 9/7/06.

[54] "Small Scale Melter Testing of HLW Algorithm Glasses: Matrix 1 Tests," K.S. Matlack, W.K. Kot, W. Gong and I.L. Pegg, Final Report, VSL-07R1220-1, Rev. 0, Vitreous State Laboratory, The Catholic University of America, Washington, DC, 11/12/07.

[55] "Small Scale Melter Testing of HLW Algorithm Glasses: Matrix 2 Tests," K.S. Matlack, W.K. Kot, W. Gong and I.L. Pegg, Final Report, VSL-08R1220-1, Rev. 0, Vitreous State Laboratory, The Catholic University of America, Washington, DC, 6/27/08.

[56] "Review of Properties of Simulated Feeds Used for Melter Testing," K.S. Matlack, W. Gong, and I.L. Pegg, Final Report, VSL-06R6410-1, Rev. 0, Vitreous State Laboratory, The Catholic University of America, Washington, DC, Washington, DC, 8/16/06.

[57] "Gas Bubbles in DM1200 Glass Produced From AZ-101 HLW Simulants," W. Gong, K.S. Matlack, and I.L. Pegg, Final Report, VSL-03L3800-1, Rev. 0, Vitreous State Laboratory, The Catholic University of America, Washington, DC, 8/16/06.

Table 2.1. Oxide Composition of Limiting Waste Streams.

Waste Component	Bi Limited Glass	Cr Limited Glass	Al Limited Glass	Al and Na Limited Glass
Al_2O_3	22.45%	25.53%	49.21%	43.30%
B_2O_3	0.58%	0.53%	0.39%	0.74%
CaO	1.61%	2.47%	2.21%	1.47%
Fe_2O_3	13.40%	13.13%	12.11%	5.71%
Li_2O	0.31%	0.36%	0.35%	0.15%
MgO	0.82%	0.16%	0.24%	0.44%
Na_2O	12.97%	20.09%	7.35%	25.79%
SiO_2	12.04%	10.56%	10.05%	6.22%
TiO_2	0.30%	0.01%	0.02%	0.35%
ZnO	0.31%	0.25%	0.17%	0.36%
ZrO_2	0.40%	0.11%	0.81%	0.25%
SO_3	0.91%	1.52%	0.41%	0.44%
Bi_2O_3	12.91%	7.29%	2.35%	2.35%
ThO_2	0.25%	0.04%	0.37%	0.04%
Cr_2O_3	1.00%	3.07%	1.07%	1.44%
K_2O	0.89%	0.37%	0.29%	1.34%
U_3O_8	3.48%	7.59%	7.25%	4.58%
BaO	0.02%	0.03%	0.11%	0.06%
CdO	0.00%	0.01%	0.05%	0.02%
NiO	3.71%	1.06%	0.82%	0.20%
PbO	0.48%	0.48%	0.84%	0.18%
P_2O_5	9.60%	3.34%	2.16%	4.10%
F-	1.58%	2.00%	1.37%	0.46%
Total	100.0%	100.0%	100.0%	100.0%

Table 2.2. Compositions of the Bi-Limited Waste (Oxide Basis) and the HLW Waste Simulant to Produce 100 kg of Waste Oxides (20 wt% suspended solids).

Bi-Limited Waste Composition		Bi-Limited HLW Waste Simulant	
Waste Oxide	**Wt%**	**Starting Materials**	**Target Weight (kg)[1]**
Al_2O_3	22.45%	Al_2O_3	22.677
B_2O_3	0.58%	H_3BO_3	1.041
CaO	1.61%	CaO	1.643
Fe_2O_3	13.40%	$Fe(OH)_3$ (13% Slurry)	26.752
Li_2O	0.31%	Li_2CO_3	0.786
MgO	0.82%	MgO	0.863
Na_2O	12.97%	NaOH	11.108
SiO_2	12.04%	SiO_2	12.162
TiO_2	0.30%	TiO_2	0.303
ZnO	0.31%	ZnO	0.313
ZrO_2	0.40%	$Zr(OH)_4 \cdot xH_2O$	1.034
SO_3	0.91%	Na_2SO_4	1.632
Bi_2O_3	12.91%	Bi_2O_3	13.040
ThO_2	0.25%	Omitted	
Cr_2O_3	1.00%	$Cr_2O_3 \cdot 1.5H_2O$	1.190
K_2O	0.89%	KNO_3	1.940
U_3O_8	3.48%	Omitted	
BaO	0.02%	$BaCO_3$	0.026
CdO	0.00%	CdO	0.000
NiO	3.71%	$Ni(OH)_2$	4.771
PbO	0.48%	PbO	0.485
P_2O_5	9.60%	$FePO_4 \cdot xH_2O$	25.501
F	1.58%	NaF	3.510
Carbonate	1.20[2]	Na_2CO_3	1.011
Nitrite	0.50	$NaNO_2$	0.769
Nitrate	2.00	$NaNO_3$	1.141
Organic Carbon	0.05	$H_2C_2O_4 \cdot 2H_2O$	0.264
—	—	Water	353.500
TOTAL	100.0%	TOTAL	487.463

[1]Target weights adjusted for assay information of starting materials
[2]—Unit for volatile components is g/100 g of waste oxide
— Empty data field

Table 2.3. Composition and Properties of Bismuth Limited Waste and Glass Formulation at 50% Waste Loading Used in Melter Tests (wt%).

-	Bi-Limited Waste*	Waste in Glass	Glass Forming Additives	Target Glass HLW-E-Bi-6
Al_2O_3	23.31	11.66	-	11.66
B_2O_3	0.60	0.30	11.00	11.30
BaO	0.02	0.01	-	0.01
Bi_2O_3	13.41	6.71	-	6.71
CaO	1.67	0.84	-	0.84
Cr_2O_3	1.04	0.52	-	0.52
F	1.64	0.82	-	0.82
Fe_2O_3	13.92	6.96	-	6.96
K_2O	0.92	0.46	-	0.46
Li_2O	0.32	0.16	-	0.16
MgO	0.85	0.43	-	0.43
Na_2O	13.47	6.74	9.00	15.74
NiO	3.85	1.93	-	1.93
P_2O_5	9.97	4.99	-	4.99
PbO	0.50	0.25	-	0.25
SiO_2	12.51	6.26	30.00	36.26
TiO_2	0.31	0.16	-	0.16
SO_3	0.95	0.48	-	0.48
ZnO	0.32	0.16	-	0.16
ZrO_2	0.42	0.21	-	0.21
Sum	100	50	50	100

* Renormalized from Ref. [3] after removal of radioactive components

Viscosity @1150°C, P			96
Conductivity @1150°C, S/cm			0.47
Crystal Content, As Melted			Trace
Crystal Content, 72 hr at 950°C			~1.8vol%
TCLP			Pass
PCT, g/L	-	DWPF-EA	HLW-E-Bi-6
	B	16.7	0.49
	Li	9.6	0.18
	Na	13.3	0.53

- Empty data field

Table 2.4. Compositions of Melter Feed to Produce 100 kg of Target Glass HLW-E-Bi-6 (Glass Yield = 500 g/L Feed) from the Bi-Limited Waste Simulant.

Bi-Limited HLW Simulant		Glass-Forming Additives	
Starting Materials	**Target Weight (kg)[1]**	**Starting Materials**	**Target Weight (kg)[1]**
Al_2O_3	11.773		
H_3BO_3	0.538	$Na_2B_4O_7.10H_2O$	30.433
$BaCO_3$	0.013		
Bi_2O_3	6.773		
CaO	0.852		
Cr_2O_3	0.531		
NaF	1.822		
$Fe(OH)_3$ (13% Slurry)	13.913		
KNO_3	1.003		
Li_2CO_3	0.406		
MgO	0.438		
NaOH	5.828	Na_2CO_3	7.088
$Ni(OH)_2$	2.476		
$FePO_4 \cdot xH_2O$	13.242		
PbO	0.253		
Na_2SO_4	0.852		
SiO_2	6.318	SiO_2	30.303
TiO_2	0.157		
ZnO	0.162		
$Zr(OH)_4 \cdot xH_2O$	0.543		
Na_2CO_3	0.488		
$NaNO_2$	0.385		
$NaNO_3$	0.544		
$H_2C_2O_4 \cdot 2H_2O$	0.132		
H_2O	142.206		
Simulant TOTAL	211.65	Additives TOTAL	67.82
		Feed TOTAL	279.47

[1] Target weights adjusted for assay information of starting materials.

Table 3.1. Glass Compositions for Investigation of Foaming Mechanism.

Oxides (wt%)	HLW-E-Bi6			BLL-G-46A		HLW-Bi-F2		HLW-Bi-Bi0		HLW-Bi-P0		HLW-Bi-F0		HLW-Bi-BiP0		HLW-Bi-2Bi		HLW-Bi-2P	
Data Type	Target	HLW-E-Bi-6r (XRF)	HLW-E-Bi-6r2 (XRF)	Target	XRF	Target	XRF	Target	XRF	Target	XRF	Target	XRF	Target	XRF	Target	XRF	Target	XRF
Al_2O_3	11.66	11.14	11.07	11.66	11.83	11.66	10.91	12.49	11.78	12.27	11.26	11.75	10.79	13.20	12.89	11.22	10.31	11.28	10.43
B_2O_3	11.30	11.30	11.30	11.30	11.29	14.30	14.30	15.33	15.33	15.05	15.05	14.42	14.42	16.19	16.19	13.76	13.76	13.84	13.84
BaO	0.01	0.01	0.01	0.01	0.02	0.01	0.01	0.01	0.01	0.01	0.02	0.01	0.02	0.01	0.02	0.01	0.01	0.01	0.01
Bi_2O_3*	6.71	7.39	7.64	6.71	5.93	6.71	8.13	0.00	--	--	8.35	6.76	7.27	0.00	--	10.20	11.12	6.49	7.10
CaO	0.84	0.89	0.91	0.84	0.83	0.84	0.94	0.90	0.94	0.88	0.97	0.84	0.89	0.95	1.01	0.80	0.85	0.81	0.87
Cr_2O_3	0.52	0.72	0.73	0.52	0.45	0.52	0.77	0.56	0.70	0.55	0.77	0.52	0.70	0.59	0.77	0.50	0.71	0.50	0.69
F	0.82	--	--	0.82	0.48	0.82	--	0.88	--	0.86	--	0.00	--	0.93	--	0.79	--	0.79	--
Fe_2O_3	6.96	7.44	7.65	6.96	6.65	6.96	8.00	7.46	7.44	7.33	8.46	7.02	7.59	7.88	8.41	6.70	7.32	6.74	7.35
K_2O	0.46	0.46	0.46	0.46	0.49	0.46	0.46	0.49	0.49	0.48	0.49	0.46	0.45	0.52	0.52	0.44	0.42	0.45	0.43
La_2O_3	0.00	0.01	0.01	0.00	--	0.00	--	0.00	--	0.00	--	0.00	--	0.00	--	0.00	--	0.00	--
Li_2O*	0.16	0.16	0.16	0.16	0.19	0.16	0.16	0.17	0.17	0.17	0.17	0.16	0.16	0.18	0.18	0.15	0.15	0.15	0.16
MgO	0.43	0.41	0.34	0.43	0.47	0.43	0.43	0.46	0.48	0.45	0.38	0.43	0.40	0.48	0.50	0.41	0.38	0.41	0.41
MnO	0.00	--	--	0.00	0.14	0.00	--	0.00	--	0.00	--	0.00	--	0.00	--	0.00	--	0.00	--
Na_2O	15.74	15.11	15.25	15.74	16.15	15.74	14.79	16.87	18.13	16.56	16.19	15.87	16.12	17.82	18.62	15.15	15.34	15.23	15.22
Nd_2O_3	0.00	--	--	0.00	0.05	0.00	--	0.00	0.01	0.00	--	0.00	--	0.00	--	0.00	0.01	0.00	--
NiO	1.93	2.04	2.11	1.93	1.46	1.93	2.24	2.06	1.95	2.03	2.28	1.94	2.01	2.18	2.28	1.85	1.95	1.86	1.95
P_2O_5	4.99	5.45	5.36	4.99	5.23	4.99	5.35	5.34	5.78	0.00	--	5.03	5.31	0.00	0.01	4.80	5.12	8.03	8.67
PbO	0.25	0.25	0.25	0.25	0.27	0.25	0.27	0.27	0.24	0.26	0.28	0.25	0.25	0.28	0.28	0.24	0.24	0.24	0.24
SiO_2	36.26	36.17	35.69	36.26	36.85	33.26	32.11	35.64	35.61	35.00	34.26	33.53	32.75	37.66	37.27	32.01	31.42	32.19	31.70
SrO	0.00	--	--	0.00	0.02	0.00	--	0.00	--	0.00	--	0.00	--	0.00	--	0.00	--	0.00	--
TiO_2	0.16	0.18	0.18	0.16	0.17	0.16	0.19	0.17	0.18	0.16	0.20	0.16	0.18	0.18	0.19	0.15	0.18	0.15	0.17
SO_3	0.48	0.40	0.40	0.48	0.44	0.48	0.40	0.51	0.34	0.50	0.36	0.48	0.27	0.54	0.37	0.46	0.30	0.46	0.31
ZnO	0.16	0.18	0.18	0.16	0.18	0.16	0.21	0.17	0.18	0.17	0.20	0.16	0.17	0.18	0.19	0.15	0.17	0.15	0.17
ZrO_2	0.21	0.21	0.22	0.21	0.36	0.21	0.24	0.23	0.20	0.22	0.25	0.21	0.21	0.24	0.24	0.20	0.20	0.20	0.21
Sum	100.00	99.91	99.93	100.00	99.95	100.00	99.90	100.00	99.96	100.00	99.94	100.00	99.95	100.00	99.94	100.00	99.95	100.00	99.93

"--" Empty data field
*Target, not analyzed by XRF.

Table 3.2. Summary of Standard CCC and Truncated CCC for Foaming Mechanism Investigation.

Glass ID	History	Character	Origin	CCC	CCC (2h)	CCC (4h)	CCC (6h)
HLW-E-Bi6	Crucible	Starting Point	Starting point	√	√	√	√
HLW-E-Bi6r	Crucible	Starting Point	Remelt of HLW-E-Bi6		√		√
BLL-G-46A	Melter	Starting Point	Melter glass of HLW-E-Bi6	√	√		√
HLW-Bi-F2	Crucible	Lower Viscosity	Lower viscosity variation of HLW-E-Bi6	√	√		√
HLW-Bi-Bi0	Crucible	Bi-free	Variation of HLW-Bi-F2	√			
HLW-Bi-P0	Crucible	P-free	Variation of HLW-Bi-F2	√			
HLW-Bi-F0	Crucible	F-free	Variation of HLW-Bi-F2	√			
HLW-Bi-BiP0	Crucible	Bi-, P-free	Variation of HLW-Bi-F2	√			
HLW-Bi-2Bi	Crucible	Higher Bi	Variation of HLW-Bi-F2	√			
HLW-Bi-2P	Crucible	Higher P	Variation of HLW-Bi-F2	√			
HLW-Bi-2P0Cr	Crucible	Higher P and Cr-free	Variation of HLW-Bi-F2	√			

Table 3.3. Composition of New Bi-limited HLW Glasses.

Glass ID	HLW-E-Bi6			HLW-Bi-F1		HLW-Bi-F2		HLW-Bi-F3				HLW-Bi-F4		HLW-Bi-F5		
Waste Loading (wt%)	50 wt%			50 wt%		50 wt%		50 wt%				50 wt%		55 wt%		
Data Type	Target	HLW-E-Bi-6r(XRF)	HLW-E-Bi-6r2(XRF)	Target	XRF	Target	XRF	Target	XRF	HLW-Bi-F3r(XRF)	DCP	Target	XRF	Target	XRF	HLW-Bi-F5r(XRF)
Al_2O_3	11.66	11.14	11.07	11.66	11.25	11.66	10.91	11.66	10.66	10.69	10.98	16.66	15.46	13.82	12.79	12.66
B_2O_3	11.30	11.30	11.30	14.30	14.30	14.30	14.30	10.30	10.30	10.30	11.29	14.30	14.30	11.33	11.33	11.33
BaO	0.01	0.01	0.01	0.01	0.02	0.01	0.01	0.01	0.01	0.02	0.01	0.01	0.01	0.01	0.01	0.01
Bi_2O_3*	6.71	7.39	7.64	6.71	7.59	6.71	8.13	6.71	7.76	7.60	7.38	6.71	7.22	7.38	8.10	8.13
CaO	0.84	0.89	0.91	0.84	0.89	0.84	0.94	0.84	0.92	0.92	0.92	0.84	0.89	0.92	0.98	1.01
Cr_2O_3	0.52	0.72	0.73	0.52	0.72	0.52	0.77	0.52	0.73	0.72	0.53	0.52	0.67	0.57	0.77	0.77
F	0.82	--	--	0.82	--	0.82	--	0.82	--	--	--	0.82	--	0.90	--	--
Fe_2O_3	6.96	7.44	7.65	6.96	7.58	6.96	8.00	6.96	7.93	7.75	7.31	6.96	7.45	7.66	8.32	8.34
K_2O	0.46	0.46	0.46	0.46	0.49	0.46	0.46	0.46	0.45	0.45	0.54	0.46	0.45	0.51	0.47	0.50
La_2O_3	0.00	0.01	0.01	0.00	0.01	0.00	--	0.00	0.01	--	--	0.00	0.01	0.00	--	0.01
Li_2O*	0.16	0.16	0.16	1.66	1.66	0.16	0.16	0.16	0.16	0.16	0.20	3.16	3.16	0.18	0.18	0.18
MgO	0.43	0.41	0.34	0.43	0.38	0.43	0.43	0.43	0.38	0.34	0.41	0.43	0.40	0.47	0.40	0.38
MnO	0.00	--	--	0.00	--	0.00	--	0.00	--	--	--	0.00	--	0.00	--	--
Na_2O	15.74	15.11	15.25	12.74	12.54	15.74	14.79	18.74	18.51	18.74	16.26	10.74	11.49	17.41	17.81	17.63
Nd_2O_3	0.00	--	--	0.00	--	0.00	--	0.00	--	--	--	0.00	--	0.00	--	--
NiO	1.93	2.04	2.11	1.93	2.07	1.93	2.24	1.93	2.11	2.08	1.76	1.93	1.90	2.12	2.19	2.19
P_2O_5	4.99	5.45	5.36	4.99	5.40	4.99	5.35	4.99	5.33	5.36	4.97	4.99	5.38	5.48	5.87	5.97
PbO	0.25	0.25	0.25	0.25	0.25	0.25	0.27	0.25	0.26	0.25	0.30	0.25	0.24	0.28	0.27	0.28
SiO_2	36.26	36.17	35.69	34.76	33.77	33.26	32.11	34.26	33.44	33.63	34.31	30.26	29.99	29.88	29.41	29.50
SrO	0.00	--	--	0.00	0.01	0.00	--	0.00	--	--	--	0.00	--	0.00	--	--
TiO_2	0.16	0.18	0.18	0.16	0.20	0.16	0.19	0.16	0.19	0.18	0.17	0.16	0.18	0.17	0.20	0.20
SO_3	0.48	0.40	0.40	0.48	0.40	0.48	0.40	0.48	0.37	0.36	NA	0.48	0.36	0.52	0.39	0.40
ZnO	0.16	0.18	0.18	0.16	0.20	0.16	0.21	0.16	0.17	0.17	0.15	0.16	0.17	0.18	0.19	0.19
ZrO_2	0.21	0.21	0.22	0.21	0.17	0.21	0.24	0.21	0.22	0.23	0.21	0.21	0.21	0.23	0.24	0.24
Sum	100.00	99.91	99.93	100.00	99.90	100.00	99.90	100.00	99.91	99.94	97.70	100.00	99.94	100.00	99.92	99.91

"--" Empty data field
*Target, not analyzed by XRF.

Table 3.3. Composition of New Bi-limited HLW Glasses (continued).

Glass ID	HLW-Bi-F6		HLW-Bi-F7		HLW-Bi-F8			HLW-Bi-F9			HLW-Bi-F10		
Waste Loading (wt%)	50 wt%		60 wt%		55 wt%			50 wt%			55 wt%		
Data Type	Target	XRF	Target	XRF	Target	XRF	DCP	Target	XRF	DCP	Target	XRF	DCP
Al_2O_3	15.66	14.54	13.99	12.89	12.82	11.80	12.09	16.66	14.78	15.06	15.82	13.95	14.13
B_2O_3	14.30	14.30	11.36	11.36	10.33	10.33	9.88	16.30	16.30	16.69	15.33	15.33	15.58
BaO	0.01	0.01	0.01	0.01	0.01	0.01	0.01	0.01	--	0.01	0.01	0.02	0.01
Bi_2O_3*	6.71	7.17	8.05	8.68	7.38	8.22	7.93	6.71	6.90	7.05	7.38	7.61	7.61
CaO	3.84	3.95	1.00	1.06	0.92	1.00	1.09	0.84	0.92	0.99	0.92	0.99	1.08
Cr_2O_3	0.52	0.68	0.62	0.82	0.57	0.76	0.57	0.52	0.62	0.25	0.57	0.70	0.18
F	0.82	--	0.98	--	0.90	--	--	0.82	--	--	0.90	--	--
Fe_2O_3	6.96	7.47	8.35	8.90	7.66	8.41	7.26	6.96	7.01	6.56	7.66	7.77	6.89
K_2O	0.46	0.43	0.55	0.53	0.51	0.49	0.59	0.46	0.45	0.50	0.51	0.51	0.53
La_2O_3	0.00	--	0.00	--	0.00	0.01	--	0.00	--	--	0.00	--	--
Li_2O*	3.16	3.16	0.19	0.19	0.18	0.18	0.23	5.16	5.16	5.19	5.18	5.18	5.15
MgO	0.43	0.36	0.51	0.39	0.47	0.40	0.49	0.43	0.35	0.41	0.47	0.40	0.43
MnO	0.00	--	0.00	--	0.00	--	--	0.00	--	0.01	0.00	--	--
Na_2O	10.74	11.55	16.58	17.15	18.41	18.58	16.00	7.74	8.64	7.56	7.41	8.90	7.51
Nd_2O_3	0.00	--	0.00	--	0.00	--	--	0.00	--	--	0.00	--	--
NiO	1.93	1.95	2.31	2.30	2.12	2.24	1.96	1.93	1.78	1.47	2.12	1.94	1.48
P_2O_5	4.99	5.36	5.98	6.47	5.48	5.82	5.87	4.99	5.54	5.36	5.48	6.07	5.40
PbO	0.25	0.25	0.30	0.30	0.28	0.28	0.28	0.25	0.23	0.26	0.28	0.26	0.28
SiO_2	28.26	27.86	28.01	27.74	30.88	30.40	32.20	29.26	30.28	30.74	28.88	29.34	30.47
SrO	0.00	--	0.00	--	0.00	--	--	0.00	--	--	0.00	--	--
TiO_2	0.16	0.17	0.19	0.21	0.17	0.20	0.20	0.16	0.18	0.18	0.17	0.20	0.19
SO_3	0.48	0.35	0.57	0.45	0.52	0.36	NA	0.48	0.38	NA	0.52	0.36	NA
ZnO	0.16	0.17	0.19	0.20	0.18	0.19	0.17	0.16	0.16	0.16	0.18	0.18	0.17
ZrO_2	0.21	0.21	0.25	0.25	0.23	0.24	0.26	0.21	0.20	0.23	0.23	0.22	0.25
Sum	100.00	99.93	100.00	99.90	100.00	99.92	97.08	100.00	99.88	98.68	100.00	99.91	97.34

"--" Empty data field
*Target, not analyzed by XRF.

Table 3.4. Crystallinity (vol%) after 70 Hours Isothermal Heat Treatment (by SEM/EDS).

Temperature (°C)	HLW-Bi-F10		HLW-Bi-F9		HLW-Bi-F8		HLW-Bi-F3	
	Xl Vol%	Major Xl Phase	Xl Vol%	Major Xl Phase	Xl Vol%	Major Xl Phase	Xl Vol%	Major Xl Phase
950	3.2	Fe-Cr-Ni Spinel	2.2	Fe-Cr-Ni Spinel	2.5	Fe-Cr-Ni Spinel and Phosphate	1.0	Fe-Cr-Ni Spinel
900	3.4	Fe-Cr-Ni Spinel	2.1	Fe-Cr-Ni Spinel	2.8	Fe-Cr-Ni Spinel and Phosphate	1.0	Fe-Cr-Ni Spinel and Phosphate
850	5.4	Fe-Cr-Ni Spinel and Phosphate	4.5	Fe-Cr-Ni Spinel and Phosphate	4.1	Fe-Cr-Ni Spinel and Phosphate	2.6	Fe-Cr-Ni Spinel and Phosphate
800	7.5	Fe-Cr-Ni Spinel and Phosphate	6.3	Fe-Cr-Ni Spinel and Phosphate	5.6	Fe-Cr-Ni Spinel and Phosphate	--	--

"--" Empty data field

Table 3.5. Viscosity and Electrical Conductivity of Candidate Glass Melts.

Temperature (°C)	HLW-Bi-F3		HLW-Bi-F8		HLW-Bi-F9		HLW-Bi-F10	
	Viscosity (Poise)	Conductivity (S/cm)	Viscosity (Poise)	Conductivity (S/cm)	Viscosity (Poise)	Conductivity (S/cm)	Viscosity (Poise)	Conductivity (S/cm)
1250	21.98	0.55	17.73	0.59	8.76	0.53	8.68	0.56
1150	47.36	0.43	38.02	0.45	18.52	0.39	20.35	0.43
1050	121.03	0.32	97.59	0.34	45.98	0.28	56.97	0.31
950	391.09	0.23	322.08	0.24	142.17	0.19	202.58	0.22

Table 3.6. Leaching Results of Candidate Glasses by PCT and TCLP.

Property	Element	Limit (DWPF-EA)	HLW-Bi-F10	HLW-Bi-F9	HLW-Bi-F8	HLW-Bi-F3
Normalized PCT (g/L)	B	16.7	2.571	3.112	0.780	0.917
	Li	9.6	1.625	1.901	0.191	0.323
	Na	13.3	1.116	1.309	0.740	0.812
Property	**Element**	**Delisting Limit**	**HLW-Bi-F10**	**HLW-Bi-F9**	**HLW-Bi-F8**	**HLW-Bi-F3**
TCLP (ppm)	Ba	100	0.10	0.10	1.23	0.07
	Bi	N/A	1.12	0.99	1.04	0.71
	Cd	0.48	NA	NA	NA	NA
	Cr	4.95	<0.01	<0.01	0.08	0.08
	Ni	22.6	<0.04	0.06	0.57	0.44
	Pb	5	<0.1	<0.1	<0.1	<0.1
	Zn	225	0.08	0.08	0.09	NA

Table 4.1. Summary of DM1200 Test Conditions and Results.

Time	Feed Start	10/20/09 10:40	10/26/09 8:45
	Feed End	10/23/09 16:36	10/30/09 17:00
	Interval	77.9 hr	104.3 hr
Initial Water Feeding for Cold Cap		50 min	60 min
Slurry Feeding		77.1 hr	103.3 hr
Feeding Interruptions		13.1 hr	26.0 hr
Cold cap burn		4.2 hr	2.7 hr
Average Total Bubbling		126 lpm	126 lpm
Average Glass Temperature, East		1156°C	1152°C
Average Glass Temperature, West		1149°C	1149°C
Average Plenum Temperature		381°C	443°C
Average Electrode Power		138 kW	193 kW
Feed	Used	8881 kg	8124 kg
	Average Rate	115.2 kg/hr	78.6 kg/hr
Glass	Number of CCC Tests	7	8
	Poured	2970 kg	3097 kg
	Average Rate$	770 kg/m^2/day	600 kg/m^2/day
	Average Rate*	815 kg/m^2/day	558 kg/m^2/day

$ - Rates calculated from glass poured.
*- Rates calculated from feed data.
Note: Rates do not take into account the time for water feeding and cold cap burn-off.
NA: Not applicable.

Table 4.2. Summary of Operational Events.

Date	Time	Run Time (hours)	Notes
10/20/2009	7:35	-	Canister cooling (CCC) drum is installed under discharge chamber.
10/20/2009	4:01	-	Transferred feed to mix tank. Net mass transferred is 4,056.0 kg (35.0 kg water is included).
	7:30	-	Transferred feed to feed tank. Net mass transferred is 3,961.0 kg (includes 736.0 kg water).
	10:40	0.0	Started water feeding at 10/20/2009 10:40 at 1 liter water/min.
	11:00	0.3	Water flow rate was raised to 2 liter/min.
	11:20	0.7	Water flow rate was raised to 3 liter/min.
	11:30	0.8	Started slurry feeding. Start of Test 1, secured water.
	11:31	0.8	Turned on SBS booster pump.
	12:10	1.5	Secured SBS booster pump.
	12:45	2.1	Restarted SBS booster pump.
	13:44	3.1	SBS outlet temperature 42-43°C, increased control set point to 42°C.
	16:46	6.1	Increased SBS outlet temperature control set point to 44°C
	17:04	6.4	Feed transferred to the mix tank. Net mass transferred is 3,304.0 kg (25 kg flush water is included).
	18:42	8.0	CCC blower is set to 16 hz. Discharged glass @3 scfh 3 minutes, @5 scfh 3 minutes, @7 scfh 3 minutes, @3 scfh 2 minutes. . Starting level is 32.8", ending level is 31.1".
	18:56	8.3	Pressure spike in Melter plenum due to a chunk of cold cap falling into the glass pool.
	20:25	9.7	Discharged glass @7scfh 9 minutes, @9 scfh 1 minutes, @15 scfh 2 minutes, @20 scfh 3 minutes, @10 scfh 4 minutes, @15 scfh 1 minute, @20 scfh 5 minutes, @12 scfh 4 minutes. CCC blower increased to 40 hz before discharge. Glass starting level is 30.6", ending level is 27.9".
	21:27	10.8	Reduced CCC blower from 40 hz to 25 hz. Start of temperatures dropping.
	22:06	11.4	Reduced CCC blower from 25 to 16 hz.
	22:15	11.6	Turned off CCC blower, cooling was occurring too quickly..
10/21/2009	0:45	14.1	Liquid is splashing onto build up by center view port, close to the top of brick, stopped feeding.
	1:19	14.6	Transferred feed to the feed tank. Net mass transferred is 1938 kg (includes 362 kg water).
	3:00	16.3	Resumed feeding.
	4:47	18.1	CCC blower is turned on at 16 hz. Discharge glass @11 scfh for 1 minute, @8 scfh 5minutes, @6 scfh 8 minutes.
	6:08	19.5	Transferred 390 gallons from neutralization tank to effluent storage tank.
	6:15	19.6	LabVIEW was lost and had to reboot and reset blowers. Cold cap collapsed and melter was tripped into Emergency Off Gas (EOG).

Table 4.2. Summary of Operational Events (continued).

Date	Time	Run Time (hours)	Notes
10/21/2009	6:36	19.9	Discharge glass @5 scfh for 7 minute, @6 scfh 11minutes, @7 scfh 4 minutes, @9 scfh 1 minute, @10 scfh 3 minutes, @12 scfh 1minute, @14 scfh 3 minutes, @18scfh 2 minutes, @20scfh 5 minutes. Increased CCC blower speed to 40hz.
	7:13	20.5	Secured glass discharge.
	7:33	20.9	Reduced CCC blower from 40 to 25 hz.
	7:53	21.2	Performed film cooler rinse.
	10:37	23.9	Transferred feed to mix tank. Net mass transferred is 1284.5 kg (25 kg flush water is included).
	11:45	25.1	Reduced CCC blower speed from 25 to 20 hz.
	12:02	25.4	Reduced CCC blower speed from 20 to 16 hz.
	12:14	25.6	Secured CCC blower.
	13:38	27.0	Paused feeding for feed sample.
	13:43	27.0	Resumed feeding.
	13:49	27.1	Secured feeding.
	14:15	27.6	Performed WESP deluge, pre-blow down and post blow down.
	15:18	28.6	Energized CCC blower to 16 hz. Discharge glass @15 scfh for 4 minute, @10 scfh 5 minutes, @7 scfh 3 minutes, @10 scfh 1 minute. Glass starting level is 34.5", ending level is 32.1".
	15:37	28.9	Started feeding again.
	17:18	30.6	Discharged glass @10 scfh for 15 minute, @15 scfh 6 minutes, @17 scfh 8 minutes, @20 scfh 1 minute. Glass starting level is 31.1", ending level is 26.7".
	17:55	31.2	Increased CCC blower speed to from 16 hz to 40hz.
	18:26	31.8	Reduced CCC blower speed from 40 hz to 25 hz.
	18:55	32.2	Reduced CCC blower speed from 25 hz to 20 hz.
	19:55	33.2	Reduced CCC blower speed from 20 hz to 16 hz.
	20:01	33.3	Performed film cooler rinse.
	21:10	34.5	Secured CCC blower and opened breaker.
	21:12	34.5	Transferred feed from mix tank to feed tank. Net mass transferred is 2219.5 kg (414 kg water is included)
10/22/2009	2:15	39.6	CCC blower speed is set to 16 hz. Discharged glass @9 scfh for 5 minute, @8 scfh 5 minutes, @5 scfh 3 minutes, @3 scfh 1 minute. Glass starting level is 31.5" glass density is 1.52 g/cc.
	4:02	41.4	Observing auto discharge, causing temperatures to increase slightly. CCC blower will be set to 40 hz.
	4:06	41.4	Discharged glass @12 scfh for 3 minutes, @7 scfh 14 minutes, @12 scfh 4 minutes, @20 scfh 10 minute. Glass starting level is 30.7", ending level is 26.9".

Table 4.2. Summary of Operational Events (continued).

Date	Time	Run Time (hours)	Notes
10/22/2009	5:01	42.3	Stopped feeding. Massive amount of shelf is left after glass discharge.
	5:23	42.7	CCC blower speed is reduced from 40 hz to 25 hz.
	7:20	44.7	Resumed feeding.
	7:39	45.0	Performed film cooler rinse.
	9:09	46.5	Reduced CCC blower speed from 25 to 20 hz.
	9:25	46.7	Reduced CCC blower speed from 20 to 16 hz.
	9:45	47.1	Secured CCC blower.
	13:08	50.5	Feed transferred to the feed tank. Net mass transferred is 1086.5 kg (202 kg water included)
	13:38	51.0	CCC blower speed is set to 16 hz. Discharged glass @4 - 8 scfh for 17 minutes. Glass starting level is 33.0", ending level is 29.5".
	14:06	51.4	Performed WESP deluge, pre-blow down and post blow down.
	15:32	52.9	Paused feeding so cold cap can melt before the next discharge.
	15:40	53.0	Increased CCC blower speed from 16 to 40 hz.
	15:42	53.0	Discharged glass @10 scfh for 12 minutes, @12 scfh 12 minutes, @10 scfh 7 minutes. Glass starting level is 31.7", ending level is 27.9".
	17:01	54.3	Resumed feeding.
	17:31	54.8	Decreased CCC blower speed from 40 hz to 25hz.
	18:02	55.4	Increased CCC blower speed from 25 to 30 hz.
	18:29	55.8	Increased CCC blower speed from 30 to 35 hz.
	19:30	56.8	Secured CCC blower and opened the breaker.
	19:39	57.0	Performed film cooler rinse.
	19:42	57.0	200 gallons of liquid was sent from neutralization tank to effluent tank. Effluent tank is full.
	20:09	57.5	East side electrode alarm sounded.
	20:25	57.7	Increased east electrode high temperature alarm form 1165°C to 1175°C.
	20:52	58.2	Transferred feed from mix tank to feed tank. Net mass transferred is 1424.0 kg (266.0 kg water is included)
	22:10	59.5	Collected a feed sample.
	22:56	60.3	Turned CCC blower on and set to 16hz.
	23:01	60.3	Discharge glass @5 scfh for 16 minutes. Glass starting level is 32.1", ending level is 30.0".
	23:15	60.6	Stopped feeing due to liquid level at the middle view port.
10/23/2009	0:15	61.6	Resumed feeding.
	0:47	62.1	CCC BB-TR-01 thermocouple is reading 288°C to 326°C. Looking in discharge view port shows a slight drip of molten glass which is the cause. Glass level is at 30.9". Discharge difference is at 420 kg. Will stay on 90 minutes course prior to main discharge as BB-TR-01 is cooling down again.

Table 4.2. Summary of Operational Events (continued).

Date	Time	Run Time (hours)	Notes
10/23/09	1:02	62.4	Increased CCC blower to 40 hz.
	1:05	62.4	Discharged glass @11 scfh for 20 minutes, @8 scfh 7 minutes, @10 scfh 3 minutes, @20 scfh 2 minute. Glass starting level is 30.9", ending level 26.6".
	1:37	62.9	Increased CCC blower speed from 16 hz to 40 hz.
	4:08	65.5	Due to incorrect temperature data input, CCC blower was wrongly adjusted to 25 hz for about 3 minutes then brought back to 40 hz.
	5:14	66.6	Decreased CCC blower speed from 40 hz to 25 hz.
	6:17	67.6	Decreased CCC blower speed to 16 hz.
	6:30	67.8	CCC blower is turned off.
	7:25	68.7	Performed film cooler rinse.
	8:49	70.1	CCC blower speed is set to 16 hz. Discharged glass @5 scfh for 16 minutes. Glass starting level is 33.5", ending level is 29.7".
	10:38	72.0	CCC blower speed is switched to 40hz. Discharged glass @4 – 12 scfh 35 minutes. Glass starting level 31.7", ending level is 27.0".
	11:15	72.6	Stop feeding
	12:01	73.3	Performed WESP deluge, pre-blow down and post blow down.
	12:14	73.6	Increased CCC blower speed from 40 hz to 50 hz.
	13:13	74.5	Reduced CCC blower speed from 50 hz to 40 hz.
	13:48	75.1	Began filling the feed tank. Net mass transferred is 1885.0 kg (including 355.5 kg water)
	14:43	76.0	Increased CCC blower speed to 45 hz.
	15:00	76.3	Resumed feeding slurry.
	15:03	76.4	Stopped feeding due to a lack of E.O.G closure.
	15:13	76.5	Decreased CCC blower speed from 45 hz to 40 hz.
	15:21	76.7	E.O.G. valve closed, start up water will be used at 1500 ml/min.
	15:30	76.8	Resumed feeding, water rate is reduced to 500 ml/min.
	15:32	76.9	Reduced CCC blower speed from 40 hz to 25hz.
	15:40	77.0	Stopped feeding water.
	15:45	77.1	Turned off CCC blower.
	16:24	77.7	Due to off gas sampling, melter went positive, causing E.O.G. to trip, knife-gate on E.O.G. is stuck open not able to get it closed.
	16:36	77.9	Stopped feeding.
	18:09	79.5	Put feed in recycle in feed tank, mass of the tank is at 3644.0 kg (ending mass)
	20:46	82.1	Cold cap is gone. Started melter & off gas shut down

Table 4.2. Summary of Operational Events (continued).

Date	Time	Run Time (hours)	Notes
10/23/2009	23:15	-	All shut downs are completed.
10/26/2009	8:45	82.1	Started feeding water at 1000 ml/min.
	9:05	82.4	Increased water flow rate to 2000 ml/min
	9:20	82.7	Increased water flow rate to 3000 ml/min
	9:45	83.1	Begin feeding HWI-EBi-6 to melter.
	13:43	87.1	CCC blower speed is set to 16 hz. Discharge glass @10 – 20 scfh 17 minutes. Glass starting level is 33.3", ending level is 30.1".
	14:30	87.9	Started off gas testing.
	15:36	89.0	Increased CCC blower speed from 16 hz to 40 hz. Discharged glass @10 scfh for 10 minutes, @12 scfh 7 minutes, @15 scfh 5 minutes, @10 scfh 8 minutes.
	17:07	90.5	Increased CCC blower speed from 40 to 50hz.
	17:30	90.9	Transferred feed to mix tank. Net mass transferred is 3787.5 kg (including 25.0 kg water)
	17:44	91.1	Stop feeding due to too much build up in the cold cap.
	17:55	91.3	Just had a major shift in the melter, liquid feed rushed into the melt pool causing the melter to trip E.O.G.
	18:16	91.6	labVIEW down for a minute.
	18:40	92.0	Increased CCC blower speed from 50 to 55 hz.
	19:06	92.5	Reduced CCC blower speed from 55 to 40 hz.
	19:48	93.2	Started feeding water at 1500 ml/min. Performed film cooler rinse.
	20:02	93.4	Reduced water to 500 ml/min. Resumed feeding slurry.
	20:29	93.8	Secured water flow to feed tube.
	20:36	94.0	Secured CCC blower and opened breaker.
	20:48	94.2	Paused feeding to collect feed sample.
10/27/2009	1:30	98.9	Turned on CCC blower and set to 16 hz.
	1:35	98.9	Discharged glass @12 scfh for 15 minutes, @5 scfh 1.5 minutes. Glass starting level is 32.1".
	3:40	101.0	CC blower speed is increased to 45 hz. Discharged glass @12 scfh for 29 minutes, @5 scfh 1.5 minutes. Glass starting level is 31.0" ending level is 27.7", glass density is 2.03 g/cc.
	4:10	101.5	Feed transferred from mix tank to feed tank. Net mass transferred is 2152.5 kg (including 402.5 kg water) Increased CCC blower speed from 16 to 45 hz.
	5:00	102.4	Stopped feeding due to massive shelf cold cap ~80%.
	5:13	102.6	Increased CCC blower speed from 45 to 50hz.
	7:21	104.7	Performed film cooler rinse.

Table 4.2. Summary of Operational Events (continued).

Date	Time	Run Time (hours)	Notes
10/27/2009	7:40	105.0	Secured SBS cold water booster pump. SBS outlet temperature is 31°C. Decreased the CCC blower speed to 45 hz.
	8:40	106.0	Decreased the CCC blower speed from 45 to 16 hz.
	9:10	106.5	Secured CCC blower.
	9:41	107.0	Started feeding water at 1000 ml/min.
	10:01	107.4	Started SBS cold water booster pump. SBS outlet temperature is 46°C.
	10:42	108.1	Secured water feed to melter.
	10:50	108.2	Restarted water feed to melter at 1000 ml/min.
	11:04	108.4	Reduced water flow rate to 500 ml/min.
	11:43	109.1	Secured SBS cold water booster pump. SBS outlet temperature is 39°C.
	11:52	109.2	Reduced water flow rate to 250 ml/min.
	12:07	109.5	Secured water feed to melter.
	12:20	109.7	Discharge chamber is clogged.
	14:39	112.0	Glass is removed from the discharge chamber.
	15:58	113.3	Currently repairing E.O.G. valve that is stuck ½ open. Reassembling discharge knife gate and chamber.
	16:37	114.0	Reinstalled slide gate on discharge chamber, discharge chamber is unclogged.
	19:13	116.6	Added 20 gallons to SBS. It was 60 gallons.
	19:19	116.7	E.O.G. valve not working; removed, cleaned and straightened knife gate valve and then lubed, replaced and cycled 5 times. All is satisfactory.
	19:30	116.9	Started feeding water at 1500 ml/min.
	19:36	117.0	Performed WESP deluge, pre-blow down and post blow down.
	20:00	117.4	Resumed feeding slurry. Reduced water flow rate to 500 ml/min.
	20:06	117.5	Started SBS cold water booster pump. SBS outlet temperature is 51°C.
	21:47	119.1	Collected a feed sample.
	23:27	120.8	Performed film cooler rinse.
	23:36	121.0	Film cooler rinse did not stop automatically. 7 extra liters of water flowed through.
10/28/2009	1:32	122.9	Turned on CCC blower , set to 16 hz
	1:35	122.9	Discharged glass @10 scfh for 15 minutes, @5 scfh 2 minutes. Glass starting level is 33.8" ending level is 29.2".
	3:36	125.0	Increased CCC blower speed 50 hz.
	3:39	125.0	Discharged glass @12 scfh for 16 minutes, @15 scfh 4 minutes, @20 scfh 2 minutes. Glass starting level is 31.0" ending level is 25.7". Glass density is 2.10 g/cc.
	4:13	125.6	Increased CCC blower speed from 16 to 50 hz.
	4:15	125.6	Paused feeding.

Table 4.2. Summary of Operational Events (continued).

Date	Time	Run Time (hours)	Notes
	5:49	127.2	**Start feeding water at 1000 ml/min.**
	6:05	127.4	Reducing water flow rate to 500 ml/min.
	6:12	127.6	Stopped feeding water.
	6:32	127.9	Reduced CCC blower speed from 50 hz to 40 hz
	6:46	128.1	Secured SBS cold water booster pump. SBS outlet is 34°C. Reduced CCC blower speed from 40 hz to 25 hz.
	7:13	128.6	Reduced CCC blower speed from 25 hz to 16 hz.
	7:39	129.0	Started feeding water at 500 ml/min.
	7:43	129.1	Secured CCC blower.
	7:45	129.1	Resumed feeding.
	7:53	129.2	Paused feeding to rod feed tube. Feed was spraying out of bottom of tube.
	7:58	129.3	Resumed feeding.
	8:01	129.4	Started SBS cold water booster pump. SBS outlet is 44°C.
	8:02	129.4	Secured water feed to melter.
	9:37	131.0	Set CCC blower speed to 16 hz. Discharged glass @5-15 scfh for 23 minutes. Glass starting level is 30.9" ending level is 26.8".
	11:50	133.2	Off gas testing started and ended 60 minutes later.
	12:55	134.3	Paused/stopped feeding to allow cold cap to melt.
	13:05	134.4	Transferred feed from mix tank to feed tank. Net mass transferred is 1845.0 kg (including 345.0 kg water)
	13:25	134.8	Performed film cooler rinse.
	13:45	135.1	Started feeding water at 1000 ml/min to reduce foaming in glass.
	13:50	135.2	Stopped water; no indication it was flowing into melt pool.
	14:19	135.7	Resumed feeding water at 1000 ml/min.
	14:39	136.0	Stopped feeding water, it did not help.
	15:14	136.6	Resumed feeding water at 1500 ml/min.
	15:37	137.0	Reduced water flow rate to 500 ml/min.
	16:04	137.4	Secured feeding water.
	16:30	137.9	Resumed feeding slurry. Net target is 500/kg/m^2/day production rate.
	18:27	139.8	Collected a feed sample.
	19:56	141.3	Performed WESP deluge, pre-blow down and post blow down.
	21:03	142.4	Lowered can and removed glass hanging in discharge chamber.

Table 4.2. Summary of Operational Events (continued).

Date	Time	Run Time (hours)	Notes
10/28/2009	21:05	142.4	CCC blower speed is set to 45 hz. Discharged glass @10 scfh 16 minutes, @8scfh 9 minutes. Glass starting level is 31.3" ending level is 28.0". During the last 9 minutes CCC blower speed was at 40hz.
	21:30	142.9	Stopped discharge which looks like it coned from center.
	21:35	142.9	CCC blower speed was reduced from 40 to 35hz.
	21:40	143.0	Cold cap ~70%, after glass discharge. Massive build up in the center is left behind. Not able to see the east side due to the ridge on that side.
	21:55	143.3	Cold cap ~70%, no visible changes at this observation
	22:45	144.1	Lowered CCC blower speed from 35 hz to 30hz. Also started to observe auto discharge. Glass level is 28.1", glass density is 2.02 g/cc.
	23:19	144.7	Still observing auto discharge, may have to pull can early.
	23:41	145.0	One of the CCC blower hose connections loose on overpack can, reconnected.
	23:45	145.1	Still observing slight auto discharge. Glass level is 28.4", density is 2.02 g/cc.
	23:58	145.3	Auto discharge continues.
10/29/2009	0:30	145.9	Lowered discharge can to knock down auto discharge, build up is only moderate amount, will not abort canister cooling at this time.
	0:36	146.0	Still have a slight auto discharge.
	0:55	146.3	Observing more feed flowing over ridge and into west opening, causing slight pressure spikes.
	1:05	146.4	Still have auto discharge taking place. Glass level is 29.4", density is 2.01 g/cc.
	1:36	147.0	Lowered discharge can to clear auto discharge, fairly substantial build up.
	1:52	147.2	Changed CCC blower speed from 25 to 16 hz.
	1:53	147.2	Auto discharge continues.
	2:04	147.4	Turned CCC blower is turned off.
	2:35	147.9	Secured neutralization tank at 500 gallons.
	3:07	148.5	Turned on CC blower and set to 16 hz.
	3:14	148.6	Discharged glass @10 scfh for 4 minutes, @8 scfh 14 minutes. Glass starting level is 30.4" ending level is 28.0".
	3:48	149.2	Pumped liquid from neutralization tank to effluent tank.
	3:50	149.2	No sign of auto discharge at this time. Glass level is 28.7", density is 1.94 g/cc.
	4:19	149.7	No auto discharge present.
	4:37	150.0	Slight auto discharge exists.
	4:51	150.2	Slight foamy discharge exits.
	5:06	150.5	Slight foamy auto discharge exists.
	5:34	150.9	Slight foamy auto discharge exists, same as before. Glass level is 29.7", density is 1.93 g/cc.

Table 4.2. Summary of Operational Events (continued).

Date	Time	Run Time (hours)	Notes
10/29/2009	5:35	150.9	Transferred feed from mix tank to feed tank. Net mass transferred is 605.0 kg (including 113.0 kg water).
	5:48	151.2	Still auto discharging, glass level is 29.8", density is 1.93 g/cc.
	6:18	151.7	Slight foamy auto discharge exists. Glass level is 29.9", density is 1.96 g/cc.
	9:48	155.2	Paused feeding to rod feed tube.
	9:55	155.3	Resumed feeding.
	10:48	156.2	Increased CCC blower speed from 16 to 40hz. Discharged glass @5-10 scfh for 20 minutes. Glass starting level is 31.2" ending level is 28.6". Glass density is 1.97 g/cc, resistance is 0.103 Ω.
	11:45	157.1	Off gas sampling completed, started at 10:45.
	12:24	157.8	Performed film cooler rinse.
	12:40	158.0	Reduced CCC blower speed from 40 to 35 hz.
	15:11	160.5	CCC blower setting is decreased from 35 to 16 hz.
	15:27	160.8	Secured CCC blower.
	15:42	161.1	Stopped canister cooling.
	16:47	162.1	Collected a feed sample.
	18:02	163.4	Started off-gas testing.
	18:48	164.2	CCC blower is set to 16 hz. Discharged glass @8 scfh 6 minutes, @5 scfh 8 minutes, Glass starting level is 31.6", ending level is 29.9".
	20:55	166.3	Auto discharging.
	21:19	166.7	Lowered can to clear away auto discharge from discharge chamber.
	21:25	166.8	Still auto discharging.
	21:40	167.0	Still auto discharging.
	22:06	167.5	Lowered discharge can to clear mound from auto discharge.
	23:21	168.7	Performed film cooler rinse.
	23:39	169.0	Center connection on CCC hose loose, reconnected.
10/30/2009	0:10	169.5	CCC blower speed is increased form 16 to 45 hz.
	0:12	169.6	Discharged glass @12scfh 2 minutes, @10 scfh 9 minutes, @5 scfh 7 minutes. Glass starting level is 32.4", ending level is 29.6".
	0:58	170.3	No auto discharge observed.
	1:32	170.9	E.O.G. tripped. Film cooler differential pressure is 6.5 in. W.C.
	2:11	171.5	Turned on SBS cold water booster pump.
	2:30	171.9	Paused feeding to switch to AOD feed system.
	2:32	171.9	CCC blower secured.
	2:58	172.3	Replaced discharge can due to massive auto discharge.
	3:11	172.5	Resumed feeding.

Table 4.2. Summary of Operational Events (continued).

Date	Time	Run Time (hours)	Notes
10/30/2009	3:14	172.6	Stopped feeding.
	3:27	172.8	E.O.G. tripped. Film cooler differential pressure is 6.4 in. W.C.
	3:28	172.8	Start feeding water at 1000 ml/min.
	3:41	173.0	Melter continues to trip to E.O.G. Film cooler differential pressure is 10.0 in. W.C.
	3:55	173.3	Completed unclogging of film cooler. Film cooler was 100% clogged at the inlet section. Film cooler differential pressure went from 10.7 in. W.C. to 2.1 in. W.C..
	4:00	173.4	Resumed feeding slurry with AOD system, secured water feeding.
	4:11		Minimal auto discharge observed.
	4:33	173.9	Slight auto discharge.
	5:08	174.5	Turned on CCC blower at 16 hz.
	5:12	174.6	Discharged glass @5 scfh 16 minutes. Glass starting level is 30.6", ending level is 28.7". Glass density is 2.02 g/cc.
	6:57	176.3	Auto discharge observed.
	7:15	176.6	Discharged glass @7 -20 scfh 30 minutes. Glass starting level is 29.7", ending level is 26.3". Glass density is 2.10 g/cc, glass resistance is 0.103 Ω
	7:45	177.1	Increased CCC blower speed from 16 to 40 hz
	10:05	179.4	Auto discharge has started.
	10:50	180.2	Auto discharge continues which requires occasional lowering of the can clearing discharge outlet.
	11:00	180.4	Increased CCC blower speed to 50 hz.
	11:35	180.9	Auto discharge continues which requires occasional lowering of the can clearing discharge outlet.
	11:45	181.1	Increased CCC blower speed from 50 to 60 hz.
	11:47	181.1	Performed film cooler rinse.
	12:48	182.2	Reduced CCC blower speed to 25 hz.
	13:03	182.4	Reduced CCC blower speed from 25 to 16 hz.
	13:30	182.9	Secured CCC blower.
	14:02	183.4	Mixer blade is completely out of feed. Stopped mixer.
	14:53	184.2	Discharged glass for demonstration @5 scfh 3 minutes. Glass starting level is 29.2", ending level is 29.1".
	15:22	184.7	Paused feeding momentarily due to collapse of cold cap and resulting steam surge.
	17:00	186.4	Stopped feeding. End of the ORP Hi Bi Foaming Test.
	17:20	186.7	Removed feed from the feed tank. Net mass removed is 130.6 kg. Feed sample taken.

Table 4.2. Summary of Operational Events (continued).

Date	Time	Run Time (hours)	Notes
10/30/2009	17:27	186.8	Collected a dip sample.
	17:36	187.0	Discharged glass @5scfh 28 minutes, glass starting level is 30.3", ending level is 27.1".
	17:51	187.2	Opened melter port to take pictures.
	18:25	187.8	Secured SBS cold water booster pump.
	19:47	189.1	Cold cap is gone.
	20:05	189.4	Started melter off-gas shut downs.
	20:30	189.9	SBS is blown down and a sample taken S-12P-117A.
	22:11	191.5	Foam has subsided still some build up is melting down.
	22:31	191.9	Performing WESP deluge, pre-blow down and post blow down. Samples W-12P-117A and W-12P-117B (after deluge) were taken.
10/31/2009	0:40	194.0	Performed PBS blow down. Sample P-12P-118A is taken.
	0:45	194.1	Performed a HEME#1 blow down. Sample H1-12P-118A is taken.
	0:50	194.2	Performed a HEME#2 blow down. Sample H2-12P-118A is taken.
	0:51	194.2	All shut downs are completed.

Table 4.3. Operator Observations of Cold Cap (CC).

Date	Time	Run Time (hours)	Cold Cap Observations
10/20/2009	10:40	0.0	Started feeding water at 1000 mL/min.
	11:30	0.8	Started slurry feeding for Test 1.
	12:05	1.4	CC ~80%, CC is flat, feed is flowing into the openings on east and west sides with feed boiling on top of CC.
	12:20	1.7	CC ~80%, ridges are forming around the openings, feed is flowing into the glass, CC is floating.
	12:35	1.9	CC ~90%, openings are smaller.
	12:50	2.2	CC ~90%, ridges are getting thicker.
	13:05	2.4	CC ~90%, ridges look larger, CC is no longer floating, feed is flowing into glass during feed shot.
	13:20	2.7	CC ~85%, openings are slightly larger.
	13:35	2.9	CC ~85%, same as previous observation.
	13:50	3.2	CC ~85%, ridges look slightly larger.
	14:05	3.4	CC ~80%, opening are bigger, ridges are the same size.
	14:20	3.7	CC ~85%, openings are slightly smaller.
	14:35	3.9	CC ~85%, openings are the same, ridges are slightly thicker.
	14:55	4.2	CC ~85%, mostly flat surface, feed is boiling between feed shots.
	15:10	4.5	CC ~85%, there are ridges on east side of both openings. They are starting to grow in size.
	15:20	4.7	CC ~85%, more feed is flowing into the openings.
	15:35	4.9	CC ~85%, ridges are larger, and have enclosed the openings.
	15:55	5.2	CC ~85%, same as before.
	16:10	5.5	CC ~90%, large openings on east and west sides.
	16:25	5.7	CC ~85%, feed is boiling most of the times, no change in ridges.
	16:40	6.0	CC ~85%, some feed is boiling on top of CC and large openings on east and west sides.
	16:55	6.2	CC ~85%, some feed is boiling on top of CC, good size large opening on east and west sides.
	17:10	6.5	CC ~85%, ridges look the same.
	17:25	6.7	CC ~85%, ridges have melted down some, openings are the same.
	17:40	7.0	CC ~85%, no visible changes at this time.
	17:55	7.2	CC ~85%, CC is thick, large openings are at the east and west sides.
	18:10	7.5	CC ~85%, large openings are at the west and east sides. Feed is boiling on top of CC.
	18:25	7.7	CC ~85%, CC is thick, no feed is boiling on top. Openings exist on both east and west sides.
	18:39	8.0	CC ~85%, west side opening is getting larger, east side opening smaller.
	18:56	8.3	CC ~90%, a fair amount of build up exits, small openings in east and west sides. Melter pressure went positive due to probably a chunk of CC falling into the glass pool.

Table 4.3. Operator Observations of Cold Cap (CC) (continued).

Date	Time	Run Time (hours)	Cold Cap Observations
10/20/2009	19:10	8.5	CC ~90%, the openings are slowly opening back. Feed is boiling all the time.
	19:25	8.7	CC ~85%, no visible changes at this time.
	19:40	9.0	CC ~85%, ridges are slowly growing.
	19:55	9.2	CC ~85%, large amount of liquid is boiling on the surface.
	20:10	9.5	CC ~85%, ridges are little higher, liquid feed is flowing into the melt pool.
	20:25	9.7	CC ~85%, small opening exists in east side, large opening exists on west side, lots of build up, huge ridge in the middle of CC which is very thick.
	20:40	10.0	CC ~85%, CC conditions are the same as last reading, ridge on the west side is stopping feed flowing into the melt pool, lots of liquid is boiling on top of CC.
	20:55	10.2	CC ~85%, is very thick, large opening exist in east side and a huge ridge exists in the center of west side.
	21:10	10.5	CC ~85%, large ridges exist around the openings.
	21:25	10.7	CC ~85%, conditions are the same as previous observation. CC is ~8" thick.
	21:40	11.0	CC ~85%, a tall ridge exits in the center of the melt pool. Other conditions are the same as previous reading.
	21:55	11.2	CC ~85%, the conditions are the same as previous reading.
	22:10	11.5	CC ~85%, giant ridge is still in the center of the melt pool, there are very large openings on east and west sides. Feed is boiling on top of the CC.
	22:25	11.7	CC ~85%, is thick and openings exist on both east and west sides, feed is boiling between the openings.
	23:00	12.3	CC ~85%, large glazed ridges exist around openings, large solids are built up on west wall near the center view port and liquid level is several inches below the solids.
	23:15	12.6	CC ~80-85%, the conditions are the same as previous observation.
	23:28	12.8	CC ~80%, ridge exits at the opening and heavy boiling is observed in the middle of CC.
	23:45	13.1	CC ~85%, unchanged conditions.
10/21/2009	0:00	13.3	CC ~80-85%, the ridge on west side seems less glazed, but is still high.
	0:15	13.6	CC ~80%, east side is no longer visible, there is ridge near Lance Bubbler #2.
	0:30	13.8	CC ~80%, is thick and fresh build up is seen on top of CC.
	0:45	14.1	Liquid is splashing onto build up by center view port, it is close to the top of brick, will stop feeding.
	1:00	14.3	CC ~85%, no light is visible via center view port, a ridge is visible near Lance Bubbler #2.
	1:40	15.0	Electrode high temperature alarm is sounded, average glass temperature is 1184°C. This high temperature alarm is repeated at 1185°C, 1175°C and 1166°C at 1:52, 1:55 and 2:01 respectively.
	2:15	15.6	CC ~60%, thin and floating, still dark in the center view port.
	2:30	15.8	CC ~60%, same as the last observation.
	2:45	16.1	CC ~60%, thin and floating.

Table 4.3. Operator Observations of Cold Cap (CC) (continued).

Date	Time	Run Time (hours)	Cold Cap Observations
10/21/20009	**3:00**	16.3	**Resumed feeding**
	3:15	16.6	CC ~80-85%, flat with feed vigorously boiling on melt surface. Build up still is visible in the center view port.
	3:30	16.8	CC ~85%.
	3:45	17.1	CC ~85%, unchanged conditions.
	4:03	17.4	CC ~85%, unchanged conditions.
	4:16	17.6	CC ~90%, thin feed is pooling on top of the CC.
	4:33	17.9	CC ~90%, unchanged conditions.
	4:56	18.3	CC ~95%, feed is pooling on top of CC and flowing into the melt pool.
	5:15	18.6	CC ~95%, feed is pooling on top of CC.
	5:32	18.9	CC ~98%, feed is pooling on top of CC.
	5:47	19.1	CC ~95%, feed is pooling on top CC.
	6:00	19.3	CC ~98%, opening near Lance Bubbler #2 is crusted over, east side can not be seen but light is visible.
	6:15	19.6	CC ~98%, labVIEW lost and had to reboot and reset blowers. CC is collapsed and melter tripped into Emergency Off Gas (EOG).
	6:27	19.8	Very little light is visible on the east side of the melter.
	7:05	20.4	CC ~99%, no openings are directly visible, light can be seen in north and south view ports.
	7:20	20.7	CC ~98%, small opening is visible on west side, large thick ridge is around the opening, more glow is visible on the east side.
	7:35	20.9	CC ~97%, east opening is slightly larger.
	7:50	21.2	CC ~97%, unchanged CC conditions.
	8:05	21.4	CC ~95%, west opening is little larger at the shape of elongated oval running almost north to south slightly toward the melter center. Ridges on either side of this slot are large and thick.
	8:20	21.7	CC ~95%, the ridges are larger.
	8:32	21.9	Trying to break down very large ridge on the west side.
	8:35	21.9	CC ~95%, CC looks unchanged.
	8:50	22.2	CC ~90%, is ~10-12" thick, small openings exist on east and west sides.
	9:20	22.7	CC ~85-90%, opening on west side looks larger, the top of ridge can not be seen, more light is visible on the east side.
	9:35	22.9	CC ~85%, west side opening is larger, glass pool can now be seen, the ridge is still large but its base looks to be eroding away.
	9:50	23.2	CC ~80-85%, opening looks large, more of the glass pool can be seen, ridge looks the same, there may be a small stalactite but it can not be seen clearly due to build up of mossy looking substance.
	10:05	23.4	CC ~80%, west side opening looks about the same size, ridge looks slightly smaller and a glimpse of the east side glass pool can be seen.
	10:20	23.7	CC ~80%, west side opening is the same, more of the east side opening can be seen, and ridge is smaller.

Table 4.3. Operator Observations of Cold Cap (CC) (continued).

Date	Time	Run Time (hours)	Cold Cap Observations
10/21/2009	10:35	23.9	CC ~80-85%, openings exist on east and west sides, ridge has continued to become smaller, feed is entering directly to the melt pool.
	10:50	24.2	CC ~80%, looks the same, small stalactite can be seen but it is not affecting the feed shot.
	11:05	24.4	CC ~80%, ridge is slightly smaller, boiling feed can now be seen on CC surface, it flows into the glass pool during feed shot.
	11:20	24.7	CC ~80-85%, still have visible ridge, boiling feed on CC with large opening.
	11:35	24.9	CC ~80-85%, openings on west and east sides are visible, west side opening with a ridge is smaller. Feed is boiling on top of CC.
	11:50	25.2	CC ~80-85%, still have ridge on west side, both west and east side openings are visible with feed flowing to openings.
	12:05	25.4	CC ~80-85%, west side opening is a little smaller and it still has ridge.
	12:20	25.7	CC ~85%, west opening is smaller, east opening can not be seen, feed is boiling and splashing behind the ridge which runs north to south slightly toward the center, stalactite is larger but still not affecting the feed shot.
	12:35	25.9	CC ~80%, west opening looks larger, cap along the west wall is thin and floating as seen through the middle view port. Feed is still boiling and splashing on the other side of the ridge.
	12:50	26.2	CC ~80-85%, with a large ridge from north-east corner to south-west corner. Opening is visible on west side with light visible from south-east corner.
	13:05	26.4	CC ~80%, CC conditions are not changed.
	13:20	26.7	CC ~80%, with large ridge down at the center along north-east corner to south-west corner, opening is visible on west side, with light visible on east side.
	13:38	27.0	Paused feeding for feed sample.
	13:40	27.0	CC ~80%, conditions are same as the previous observation.
	13:43	27.0	Resumed feeding.
	13:49	27.1	Secured feeding. CC is at the bottom edge of center view port. CC ~80% with ridge in the center from northeast to southwest corner.
	14:05	27.4	CC ~80% is ~8-10" thick with opening on west side and light is visible from the east side. Ridge is in the middle running from north-east to south-west corners.
	14:25	27.7	CC is unchanged from previous observation.
	14:55	28.2	CC ~80%, center view port has softened up. North view port still has a large mound that can be seen.
	15:10	28.5	CC ~40%, CC is only at the center of the melt pool, still thick but glowing hot.
	15:25	28.7	CC ~40%, huge wall in the center of the melt pool, CC is so tall, unable to see the back of the melter.
	15:37	28.9	Started feeding again.
	15:40	29.0	CC ~30%, inside the mound on the west side can be seen, a little foam is visible, no stalactites.
	15:55	29.2	CC ~60%, it is thick, there is a huge ridge in the center of the melt pool.
	16:10	29.5	CC ~80%, the liquid is hitting the ridge in the center on every shot. This is spraying the feed all over.

Table 4.3. Operator Observations of Cold Cap (CC) (continued).

Date	Time	Run Time (hours)	Cold Cap Observations
10/21/2009	16:25	29.7	CC ~85%, has closed up. Feed is still spraying all over, a second ridge has formed on the west side.
	16:40	30.0	CC ~85%, conditions are the same as the previous reading.
	16:55	30.2	CC ~85%, is a very thick wall in the center of the melt pool, wall is too thick to view the top of the cap or pool behind it .
	17:10	30.5	CC ~90%, is very thick and east side can not be seen.
	17:25	30.7	CC ~90%, is very thick, is more of a shelf now, ~2"above the melt pool. Only one opening on the west side is visible.
	17:40	31.0	CC ~90%, is ~6" thick, the top is visible again, it is ~4" above the glass pool, boiling liquid feed is on top of CC.
	17:55	31.2	CC ~90%, many layers of the CC. Large amount of liquid exists on surface.
	18:10	31.5	CC ~90%, is very thick, liquid is boiling on top of the CC surface.
	18:25	31.7	CC ~90%, is ~6" thick, and a few inches above the melt pool, only one opening is visible in the west side.
	18:40	32.0	CC ~85%, multiple layers, there is a dome shaped opening over the west side opening, east side is not visible.
	18:56	32.3	CC ~85%, no visible changes for this observation.
	19:05	32.4	CC ~85%, liquid feed is slowly flowing into the melt pool, no other changes observed.
	19:20	32.7	CC ~85%, is very thick, east side can not be seen, liquid boiling feed is on top of the CC surface.
	19:35	32.9	CC ~85%, is very thick and tall.
	19:50	33.2	CC ~85%, is very thick and tall. One large opening exists in the west side that is all visible.
	20:05	33.4	CC ~85%, more light is seen through the east and south view ports.
	20:20	33.7	CC ~85%, opening is getting wider, not as much liquid feed pooling on surface as before.
	20:35	33.9	CC ~80%, is still thick starting to open up little more, opening in the west is getting larger and now is visible in the center of the melt pool.
	20:50	34.2	CC ~80%, opening in the west is getting larger.
	21:05	34.4	CC ~80%, same as the last observation.
	21:20	34.7	CC ~80%, east side has opened up little more.
	21:35	34.9	CC 80%, one visible opening exits, still opening more, liquid boiling feed on the CC surface, a small stalactite has formed.
	21:50	35.2	CC ~90%, opening is still growing, liquid feed is now pooling up on the ridge around the opening preventing it from flowing into the melt pool.
	21:51	35.2	Removed stalactite from the feed tube by tapping on the top of the feed tube.
	22:05	35.4	CC ~75%, still opening up, liquid feed is blocked by a ridge from flowing into the melt pool, and is pooling on the surface.
	22:20	35.7	CC ~80%, conditions are the same as last observation.
	22:35	35.9	CC ~75%, one large opening, still very thick, liquid feed is pooling on the surface.

Table 4.3. Operator Observations of Cold Cap (CC) (continued).

Date	Time	Run Time (hours)	Cold Cap Observations
10/21/2009	22:50	36.2	CC ~75%, very massive ridge is visible via north view port, nothing is visible via east side of the melter.
	23:05	36.4	CC ~75-80% , no change since light is visible on east side via south view port.
	23:20	36.7	CC ~75-80%, wall of cold cap at west opening is not visible from south view port.
	23:40	37.0	CC ~75-80%, same as last observation.
	23:57	37.3	CC ~80%, same as above.
10/22/2009	0:13	37.5	CC ~80%, east wall of the melter is not visible.
	0:28	37.8	CC ~75-80%, huge ridge still visible in north view port. Light is seen along the east wall.
	0:43	38.0	CC conditions are not changed.
	0:58	38.3	CC conditions are not changed.
	1:13	38.5	CC ~80%, unchanged CC conditions.
	1:52	39.2	CC ~75-80%, unchanged CC conditions.
	2:09	39.5	CC ~75-80%, large opening on the west side.
	2:34	39.9	CC ~75-80%, slight opening on the wall CC revealing another opening at the center.
	2:49	40.1	CC ~75%, no change in CC from the last observation.
	3:06	40.4	CC ~75%, no change in CC from the last observation.
	3:20	40.7	CC ~75%, still small opening formed in ridge, visible in north view port.
	3:35	40.9	CC ~75%.
	4:35	41.9	CC ~70%, is now separated from the melt pool.
	4:50	42.2	CC ~70%, no change from the last observation.
	5:01	42.3	Stopped feeding. Large amount of shelf is left after glass discharge.
	5:16	42.6	CC ~60%.
	5:39	43.0	CC ~60%, is not on top of melt pool.
	6:10	43.5	CC ~65%, a large amount of shelf has melted, still large chunks are floating along the west wall.
	6:40	44.0	CC is same as last observation, chunks along the west wall are breaking down somewhat.
	7:20	44.7	Resumed feeding. CC ~50%, is soft and floating, there is a moderate size mound in the center of glass pool.
	7:35	44.9	CC ~65%, mound in the center is getting larger and is still floating. Feed is boiling on the CC surface and flowing into the glass melt during feed shots.
	7:50	45.2	CC ~65-70%, is floating. The ridge is not floating and runs diagonally from north-east to south-west corner through the center of the melter. The feed is boiling on the CC surface.
	8:05	45.4	CC ~75%, ridges are bordering both openings, the feed is boiling between the ridges as well as the CC surface which is now fixed.
	8:20	45.7	CC ~75%, ridges are slightly taller, otherwise looks mostly the same.
	8:35	45.9	CC ~75%, ridges are continuing to grow.

Table 4.3. Operator Observations of Cold Cap (CC) (continued).

Date	Time	Run Time (hours)	Cold Cap Observations
10/22/2009	8:50	46.2	CC ~75-80%, openings are slightly smaller and ridges are slightly larger.
	9:05	46.4	CC ~80%, opening is visible through view port, smaller ridge exists on the west side with boiling feed on CC.
	9:20	46.7	CC ~80%, still have a small ridge on west side. East side is still visible, boiling feed is on top of CC.
	9:35	46.9	CC ~80-85%, small ridge on the west side look flat with boiling feed flowing into the melt pool.
	9:50	47.2	CC ~85%, still have boiling feed on CC, at this time boiling feed is not flowing into the melt pool.
	10:05	47.4	CC ~85%, west ridge continues to be taller.
	10:20	47.7	CC ~80-85%, looks the same except the feed splashes into the melt pool during the feed shots.
	10:35	47.9	CC ~85%, is thick with ridge on west side remaining tall, lots of vigorously boiling feed on CC surface.
	10:50	48.2	CC ~80%, looks mostly the same as last observation. Removed stalactite which was causing feed shot to go directly into the glass pool.
	11:05	48.4	CC ~80%, openings look about the same, west ridge look slightly smaller.
	11:20	48.7	CC ~80%, still has ridge boiling feed on CC is flowing into the melt pool.
	11:35	48.9	CC ~80%, feed is flowing into the melt pool and ridge on the west side is still present.
	11:50	49.2	CC ~80%, ridge on the west side still visible, openings east and west sides are the same size.
	12:05	49.4	CC ~80%, west side opening looks a little bigger, the ridge on the east side is still visible.
	12:14	49.6	West ridge is higher and prevents feed from flowing into the west side glass pool, all feed is flowing to east side pool.
	12:20	49.7	CC ~80%, ridge is beginning to show signs of breaking down. Some feed is flowing into the glass pool during feed shots.
	12:35	49.9	CC %75-80%, ridge continues to erode but very slowly, east opening can just barely be seen.
	12:50	50.2	CC ~75%, appears to be the same.
	13:05	50.4	CC ~75%, no visible chances.
	13:18	50.6	West side is opened up considerably.
	13:20	50.7	CC ~75%, the ridge is smaller and opening is larger.
	13:50	51.2	CC ~75%, west ridge is bigger.
	14:05	51.4	CC ~75%, base of the large west side ridge has a hole and continues to erode.
	14:20	51.7	CC ~75%, the hole in the west side ridge now allows east side glass pool to be seen, the ridge is still too tall to see over.
	14:35	51.9	CC ~70-75%, the hole in the west side ridge is much larger, still can not see over. The feed is boiling on the surface of the rest of the CC.
	14:50	52.2	CC ~80%, there is a very large mound around the west side opening and feed is flowing into the melt pool.
	15:16	52.6	CC ~80%, only change is that liquid feed is up to the bottom of the middle view port.

Table 4.3. Operator Observations of Cold Cap (CC) (continued).

Date	Time	Run Time (hours)	Cold Cap Observations
10/22/2009	15:30	52.8	CC ~75%, feed is no longer pooling on the CC surface, now flowing into melt pool, also stalactite has formed on the feed tube.
	15:32	52.9	Paused feeding so CC can melt down before the next discharge.
	15:45	53.1	CC ~60%, is very thick and a large opening exists on the west side.
	16:00	53.3	CC ~40%, conditions are the same as previous observation.
	16:15	53.6	CC ~35%, moderate amount of liquid build up exists.
	16:25	53.7	CC ~80%, able to see inside from the north view port, the build up is melting down.
	16:42	54.0	CC ~80%, build up is still melting down.
	16:57	54.3	CC ~20%, CC is loose and floating.
	17:01	54.3	Resumed feeding. CC is mostly gone.
	17:10	54.5	CC ~30%, material is just under the walls and right underneath the feed tube.
	17:25	54.7	CC ~40%, center has grown.
	17:40	55.0	CC ~50%, is in the center of the melt pool, small mound exists at this time.
	17:55	55.2	CC ~55%, gaining in height, now formed a ridge at the center of melt pool.
	18:10	55.5	CC ~60%, the ridge at the center of the pool is getting taller, openings are visible in east and west, liquid feed is on top of CC.
	18:25	55.7	CC ~70%, the openings are slowly closing up.
	18:40	56.0	CC ~75%, is getting thicker, and ridges around the openings are getting taller.
	18:55	56.2	CC ~75%, is thick, large ridge is through the center of the pool, openings exist on west and east sides.
	19:10	56.5	CC ~75%, more liquid is pooling on CC surface and ridges are growing.
	19:25	56.7	CC ~75%, no visible changes from last observation.
	19:40	57.0	CC ~70%, east side has opened up some, the ridge on west side is little taller.
	19:55	57.2	CC ~70%, the ridge is high, almost blocking the view of the east side.
	20:19	57.6	CC ~70%, wide opening on east-west side is closed with ridge build up around it. The feed is boiling on ridge on west side.
	20:35	57.9	CC ~70%, very little to no change in CC conditions.
	20:50	58.2	CC ~70%, there is strip in the center underneath the feed tube and most of the south side liquid is boiling on CC surface.
	21:05	58.4	CC ~70%, there are openings on east and west sides and a large ridge dividing the openings in the center of the pool containing a lot of liquid boiling feed.
	21:20	58.7	CC ~70%, west side opening is closing up, still able to see east side.
	21:33	58.9	CC ~70%, is ~4" thick, east is open more than the west side, both openings are visible, the feed is boiling on top of CC.
	21:50	59.2	CC ~75%, is flat and getting thicker, liquid boiling feed is on top of CC which is 2" below center view port.
	22:05	59.4	CC ~75%, large openings exist on east and west sides, flat ridge exits between them. Feed is boiling on ridge.
	22:25	59.7	CC ~75%, there is a large opening between east and west sides, and a thick ridge on the south side. Feed is boiling on the ridge.

Table 4.3. Operator Observations of Cold Cap (CC) (continued).

Date	Time	Run Time (hours)	Cold Cap Observations
10/22/2009	23:15	60.6	Stopped feeding due to liquid level at the middle view port.
	23:33	60.9	CC ~75-80%, there are 2 large openings near the Lance Bubblers but with ridges around them blocking feed from easily flowing into melt pool. Liquid has receded a couple of inches below the middle view port.
	23:48	61.1	CC ~70%, most of the liquid is dried on surface, ridges are still in place around the openings.
10/23/2009	0:13	61.5	CC ~50-60%. The ridges have melted down and middle view port is not in jeopardy of having feed flow into it. It looks safe to resume feeding.
	0:15	61.6	Resumed feeding.
	0:27	61.8	CC ~70-75%, feed shot is spraying as it hits CC surface.
	1:09	62.5	CC ~70%, opening are near both Lance Bubblers.
	1:40	63.0	CC ~75%, is tiered in two layers, top is slightly separated, bottom cap is with boiling feed on the surface. Both east and west openings are visible.
	1:56	63.3	CC ~75%, same conditions as last observation.
	2:15	63.6	CC ~75%, with glass level much lower, upper CC is now farther apart from the bottom, this shelf is also visible from the mid view port.
	2:32	63.9	CC ~75%, bottom cap appears to be thinner.
	2:48	64.1	CC ~75%, no changes.
	3:07	64.4	CC ~70-75%, large opening exist near Lance Bubblers with shelf build up from west wall into center of the melter.
	3:14	64.6	Thermo well #2 is encased in shelf.
	3:35	64.9	CC ~70%, same conditions as before.
	4:02	65.4	CC ~70%, thick chunks and big openings exist.
	4:14	65.6	Large growth exists from west wall out into center of the melter.
	4:44	66.1	CC ~70%, large chunks and large opening exist.
	5:13	66.5	CC ~70%, same as the last observation.
	5:50	67.2	CC ~70-75%, west side opening looks to have filled in some, east side still has a large opening.
	6:08	67.5	CC ~70%, shelf no longer exists, east and west openings are visible.
	6:50	68.2	CC ~70%, is thick and surface is very irregular, appears to be located in south and west areas of the melter. Most of the north side is open.
	7:05	68.4	CC ~70%, mostly the same as last observation; feed is flowing into north side of the glass pool.
	7:20	68.7	CC ~70%, same as last observation.
	7:35	68.9	CC ~70-75%, CC is slowly moving to the north side.
	7:50	69.2	CC ~75-80%, is in the center and along the west wall moving north.
	8:05	69.4	CC ~75%, west side opening continues to close slowly, CC now is beginning to divide east and west openings.
	8:20	69.7	CC ~75%, north side is still closing slowly. East side is barely visible as ridge in the center moves north.

Table 4.3. Operator Observations of Cold Cap (CC) (continued).

Date	Time	Run Time (hours)	Cold Cap Observations
10/23/2009	8:35	69.9	CC ~75%.
	8:50	70.2	CC ~75%, ridge looks thicker and taller.
	9:05	70.4	CC ~75%, continues to thicken.
	9:20	70.7	CC ~80%, opening is visible on west side, large thick ridge exits on the west side.
	9:35	70.9	CC ~80%, opening on west side is visible with a large ridge.
	9:50	71.2	CC ~80%, opening on the west side is still visible, ridge is still present.
	10:05	71.4	CC ~75-80%, west side opening is still visible with visible light on the east side, still large ridge exists on the west side.
	10:20	71.7	CC ~75-80%, west side is still visible and is flowing to melt pool, the ridge is smaller.
	10:35	71.9	CC ~75%, same as last observation.
	10:50	72.2	CC ~75%, opening on west side seems to have gotten a little bigger, east side is visible.
	11:15	72.6	Stopped feeding.
	11:40	73.0	CC ~70%, still have opening on west side with large ridge, east side opening is not visible but has visible light.
	12:40	74.0	CC ~40%, consists of a large shelf on west-center to west-south sides.
	13:15	74.6	CC ~30%, with shelf hanging off west side, not in contact with melt pool.
	13:32	74.9	Still have large amount of solids, ~ 1"thick, attached to west wall and thermo well #2.
	14:05	75.4	CC ~5-10%, is foamy.
	15:00	76.3	Resumed feeding slurry.
	15:03	76.4	Stopped feeding due to E.O.G will not close.
	15:15	76.6	Foam is floating on the surface of the pool, is very thin with lots of hot spots.
	15:30	76.8	Resumed feeding, water rate is reduced to 500 ml/min.
	15:37	76.9	CC ~40%, is building, opening is in the center of the melter.
	15:56	77.3	CC ~75%, is getting thick, liquid feed is boiling in the center of CC contained by a ridge and openings in east and west sides.
	16:18	77.6	CC ~85%, the opening on the east side is small, on west side is larger.
	16:36	77.9	Stopped feeding.
	20:46	82.1	Started melter & off gas shut down.
	23:15	-	All shut downs are completed.
10/26/2009	8:45	82.1	Started feeding water at 1000 ml/min.
	9:39	83.0	CC ~90%.
	9:45	83.1	Began feeding HWI-EBi-6 to melter.
	9:50	83.2	CC ~70%.

Table 4.3. Operator Observations of Cold Cap (CC) (continued).

Date	Time	Run Time (hours)	Cold Cap Observations
10/26/2009	10:05	83.4	CC ~80%, ridges are beginning to form around the openings.
	10:20	83.7	CC ~75%, small ridges are present, feed is boiling on surface of CC and flowing onto the glass pool.
	10:35	83.9	CC ~75%, ridges are slightly larger, west side is floating and east side is not.
	10:50	84.2	CC ~75%, CC conditions are the same as last observation.
	11:20	84.7	CC ~80%, ridges are slightly larger, west opening is smaller then the east opening, west side is floating and east side is rigid, feed is flowing between the ridges.
	11:35	84.9	CC ~80%, same as previous observation.
	11:50	85.2	CC ~80%, ridges continue to grow.
	12:05	85.4	CC ~75%m west opening is larger, ridges are a little large, and west side still floating.
	12:20	85.7	CC ~75%, west side is no longer floating however east side is floating now. Openings are ridging up and CC is getting thicker.
	12:35	85.9	CC ~75% is similar to previous observations.
	12:50	86.2	CC ~75-80%, its surface is covered with boiling feed. East side is still floating, west side is not. Ridge appears to have reduced in size/height.
	13:05	86.4	CC ~75%, looks flat with large openings on both east and west sides. Pool of boiling feed is visible on west side with a small ridge at opening.
	13:20	86.7	CC ~75%, there is still a small ridge on west side opening, boiling of feed on CC.
	13:50	87.2	CC ~75%, openings are visible on east and west sides. West side has a ridge.
	14:05	87.4	CC ~75%, large ridge exist on west side after discharge, still have boiling feed on CC.
	14:20	87.7	CC ~75-80%, large opening exist on both sides, west side has large ridge with boiling feed on CC.
	14:52	88.2	CC ~75%, is ~5-6" thick, large openings exists on both east and west sides with liquid boiling on CC.
	15:10	88.5	CC ~75%, Large amount of liquid on CC surface boiling all the time. The ridge on west side is growing.
	15:54	89.3	CC ~80%, is tall ridge, cannot see over it, one opening exist on the east side.
	16:12	89.6	CC ~85%, huge ridge exist in the center of the melt pool, CC is so thick west side can not be seen, large opening exists on the east side.
	16:24	89.8	CC ~85%, CC is higher than center view port.
	16:44	90.1	CC ~85%, east side can not be seen, west side ridge is over 12" high.
	17:02	90.4	CC ~80%, is very thick with huge ridge in the center of CC, east side can not be seen.
	17:17	90.6	CC ~85%, no visible changes at this time.
	17:32	90.9	CC ~85%, east side must be opening up, more light is visible from that side.
	17:44	91.1	Stopped feeding due to too muck build up in the CC that is not melting.
	17:55	91.3	CC ~90%, major shift in the melter, liquid feed was rushed into the melt pool causing the melter to trip E.O.G.

Table 4.3. Operator Observations of Cold Cap (CC) (continued).

Date	Time	Run Time (hours)	Cold Cap Observations
10/26/2009	18:10	91.5	CC ~90%, is very thick, large opening exist in west side, east side is not visible and still huge ridge exist in the center of pool.
	18:28	91.8	CC ~85%, CC conditions are same as the previous observation.
	18:48	92.2	CC ~60%, melted down a lot, ridge in the center is only 5" high, also west and east sides are seen, large opening exists in east side, still unable to see through center view port.
	18:54	92.3	Unable to see through center view port, massive build up, rodded view port.
	19:00	92.4	CC ~35%, a ridge exists in the center of pool but it is much smaller. Lots of build up preventing much view through the center port.
	19:24	92.8	CC ~15%, is melting down in front of the center view port, there is still build up which prevent from seeing. Very small ridge exist in the center of pool.
	19:48	93.2	Started feeding water at 1500 ml/min.
	19:57	93.3	CC ~40%, flat and thin, large openings in east and west.
	20:02	93.4	Reduced water to 500 ml/min. Resumed feeding slurry.
	20:11	93.5	CC ~55%, is a long but thin CC in the center of the melt pool.
	20:30	93.9	CC ~85%, is ~8" thick, large openings are visible in east and west sides.
	20:45	94.1	CC ~75%, west side has a ridge that is growing and is ~4-5" thick. East side opening can be seen.
	21:03	94.4	CC ~80%, west side has closed up some.
	21:15	94.6	CC ~80%, east side ridge is too high to see the opening. No visible changes exist in the west side.
	21:45	95.1	CC ~80%, west side ridge is little higher, barely see the opening on the east side.
	21:58	95.3	CC ~80%, can barely see over the west ridge.
	22:22	95.7	CC ~80%, conditions are the same as last observation.
	22:36	96.0	CC ~85%, CC is getting higher, no longer able to see opening in east, glass level has raised on CC.
	22:55	96.3	CC ~80-85%, fairly large openings exists on east and west sides. Glazed ride is visible on west side opening.
	23:13	96.6	CC ~80%, liquid feed is starting to get near middle view port. Bubbling will be reduced to see if liquid recedes from near center view port.
	23:22	96.7	CC ~80%, liquid seems to have receded slightly from middle view port.
	23:22	96.7	CC ~80%.
	23:20	96.7	CC ~80%, liquid level is getting close to bottom of middle view port, bubbling increased to try to break down ridges around the openings and allow liquid to flow to melt pool away from the middle view port.
10/27/2009	0:10	97.5	CC ~80%, is thick and feed is boiling on top of CC.
	0:25	97.8	Liquid has fully receded from middle view port however large build up of solids is adhered to west wall directly under middle view port.
	0:35	97.9	CC ~80-85%, losing the view of east side, although plenty of light is visible via south view port.
	0:48	98.2	CC ~80%, only west opening is visible, ridge around the opening exist.

Table 4.3. Operator Observations of Cold Cap (CC) (continued).

Date	Time	Run Time (hours)	Cold Cap Observations
10/27/2009	1:05	98.4	CC ~80%, almost flat now, ridges have been reduced dramatically, no view of the west side of the melter.
	1:22	98.7	Liquid feed again approaching center view port.
	1:56	99.3	CC ~80%, is thick and feed pooling on top of CC.
	2:14	99.6	CC ~80%, same as above.
	2:27	99.8	CC ~80%, still same as the previous observation.
	2:41	100.0	CC ~80%, still same as the previous observation.
	2:52	100.2	Decreased bubbling on Lance Bubbler #2 so the feed flows freely into melt pool.
	2:57	100.3	CC ~80%, is thick and feed is pooling on top of CC.
	3:15	100.6	CC ~80%, is still thick and feed is pooling on top of CC.
	3:32	100.9	CC ~80%, ridge exists at west side opening, liquid flow from north side is visible.
	4:02	101.4	CC ~80%, same as previous observations.
	4:16	101.6	CC ~80%, glass is currently separated from CC.
	4:30	101.9	CC ~80% is thick.
	4:45	102.1	CC ~80% is thick.
	5:00	102.4	Stopped feeding due to large shelf CC ~80%.
	5:18	102.7	CC ~80%, large shelf still in place.
	5:34	102.9	CC ~70% is thick and chunky.
	5:49	103.2	CC ~70% is thick and chunky.
	6:03	103.4	CC ~70-75%, just slightly separated, soft cap is present under shelving. West opening extend visibility at the middle view port.
	6:20	103.7	Large sections of ridge/wall cap have been dissolved. East side is opening and is now partially visible. CC is ~6.5-7" thick.
	6:30	103.9	CC ~70-75%, shelf is still melting down.
	6:50	104.2	CC ~30%, ridge is almost completely gone, CC is only seen in north-west corner and along west wall.
	7:05	104.4	CC ~25%, ridge is gone, CC in north-west corner and along west wall is slightly smaller.
	7:20	104.7	CC ~20%, north-west corner and west side CC is dissolving.
	7:35	104.9	CC ~10% is mostly gone.
	7:50	105.2	CC ~<10%.
	8:35	105.9	CC ~<5%, floating and appears to be soft and thin.
	9:41	107.0	Started feeding water at 1000 ml/min.
	10:42	108.1	Secured water feed to melter.
	10:50	108.2	Restarted water feed to melter at 1000 ml/min.

Table 4.3. Operator Observations of Cold Cap (CC) (continued).

Date	Time	Run Time (hours)	Cold Cap Observations
10/27/2009	12:07	109.5	Secured water feed to melter.
	12:20	109.7	CC ~99%. Discharge chamber is clogged.
	19:30	116.9	Started feeding water at 1500 ml/min.
	19:48	117.2	CC ~30%, is thin.
	20:00	117.4	Resumed feeding slurry.
	20:05	117.4	CC ~40%, is thin, large opening on east side, smaller opening exist on west side.
	20:25	117.8	CC ~85%, small openings on east and west sides, feed is boiling on top of CC.
	20:40	118.0	CC ~85%, very thin opening exists in east and west sides.
	20:55	118.3	CC ~85%, is getting thicker, openings in east and west are larger.
	21:10	118.5	CC ~ 85%, openings are the same as previous reading, CC is a little thicker, liquid feed is boiling on top of CC.
	21:25	118.8	CC ~90%, is much thicker ~4", and both openings are larger, ridge in the center is starting to form.
	21:40	119.0	CC ~90%, openings in east and west still look larger, CC is covered with liquid boiling feed.
	21:55	119.3	CC ~75%, is opened up, small ridge exists around the west side opening.
	22:12	119.6	CC ~80%, both openings are surrounded by a ridge along CC edge, liquid boiling feed is splashing around the CC.
	22:50	120.2	CC ~80-85%, flat and even.
	23:05	120.4	CC ~75-8-%, large openings exist near Lance Bubblers.
	23:20	120.7	CC is unchanged since previous observation.
	23:35	120.9	CC ~80%, slightly more coverage than previous observation, however it is still flat.
	23:50	121.2	CC ~80%, unchanged since last observation.
10/28/2009	0:05	121.4	CC ~80%, unchanged since last observation.
	0:25	121.8	CC ~80-85%, east opening is not visible, heavy boiling is taking place at the CC surface, the size of the ridge at west side opening is starting to increase.
	0:40	122.0	CC ~80-85%, similar to the last observation, liquid is overflowing from CC surface to the opening.
	1:03	122.4	CC ~80%, starting to lose view of east side, large opening still exists on west side with a slight ridge starting to grow around it.
	1:20	122.7	CC ~80-85%, not able to see east opening due to glass level at 33". Sizeable opening on west side, CC is mostly flat with liquid boiling moderately at the surface.
	1:49	123.2	CC ~80%, thick and flat, feed is boiling on CC surface.
	1:55	123.3	CC ~80-85%, glass discharge revealed a very thick ridge near west opening.
	2:07	123.5	Large ridge is visible via north view port.
	2:40	124.0	CC ~80%, thick and flat.
	2:55	124.3	CC ~80%, ridge on the west opening blocks the visibility to the east side.

Table 4.3. Operator Observations of Cold Cap (CC) (continued).

Date	Time	Run Time (hours)	Cold Cap Observations
10/28/2009	3:05	124.4	CC is unchanged, massive ridge is still seen in north view port.
	3:33	124.9	CC ~80%, unchanged since last observation.
	3:58	125.3	CC ~80%, west opening extends pass Lance Bubbler #2 as seen in the middle view port, ridge/wall covers the visibility to the east side.
	4:15	125.6	CC ~80%, ridge/wall is seen at the north view port, opening is visible in the middle view port, ridge/wall is not yet seen in the south view port. Paused feeding.
	4:30	125.9	Massive ridge exits in center of melter and unable to see east side.
	4:55	126.3	CC ~80-85%, shelf was slightly reduced but is still in place, there is no sign of foam.
	5:25	126.8	CC ~80%, ridge is still blocking view of the east side, glass is away from middle view port.
	5:40	127.0	CC is unchanged.
	5:45	127.1	Observing some slight foamy glass discharge moving down.
	5:49	127.2	Started feeding water at 1000 ml/min.
	5:58	127.3	CC ~90%, liquid is boiling on the bottom of CC, ridge/wall partially dissolved at the bottom making it available to see east opening partially,
	6:08	127.5	CC ~95%.
	6:12	127.6	Stopped feeding water.
	7:20	128.7	CC ~90%, surface is irregular with ridges and some high mounds.
	7:35	128.9	CC ~80%, ridges and mound mostly are gone,
	7:39	129.0	Started feeding water at 500 ml/min.
	7:45	129.1	Resumed feeding.
	7:50	129.2	CC ~70%, small ridge in the center looks a little hot and soft, build up around thermo well #2 is still moderate in size rest of the CC is floating
	7:53	129.2	Paused feeding to rod feed tube. Feed was spraying out of bottom of tube.
	7:58	129.3	Resumed feeding.
	8:02	129.4	Secured water feed to melter.
	8:05	129.4	CC ~75%, ridge in the center is wider and slightly taller. Feed is boiling on CC surface, feed is shooting straight down into melter, and mound is still visible along west wall south of middle view port.
	8:20	129.7	CC ~80%, ridge has separated and is beginning to grow around each opening.
	8:36	130.0	CC ~80%, lots of boiling feed exists, ridges are similar around the east and west openings.
	8:55	130.3	CC ~80%, melt pool is splashing more vigorously while CC surface has boiling feed on its surface.
	9:05	130.4	CC ~80%, both openings are smaller, each has a small ridge, lots of boiling feed exist on CC surface, mound along west wall is much smaller.
	9:20	130.7	CC ~80%, ridges are getting slightly larger.
	9:50	131.2	CC ~80%, openings on both sides are visible, west side has visible ridge.

Table 4.3. Operator Observations of Cold Cap (CC) (continued).

Date	Time	Run Time (hours)	Cold Cap Observations
10/28/2009	10:20	131.7	CC ~80%, opening on west side and east side CC is very thick, small ridge exists on west side.
	10:50	132.2	CC ~85%, Since ridges are grown east side opening is no longer visible.
	11:05	132.4	CC ~85%, west opening looks slightly smaller, ridge is slightly higher, feed can be seen boiling on CC surface just beyond the top of the ridge.
	11:26	132.8	CC and ridges continue to grow, glass level is not increasing due to the ridges.
	11:35	132.9	CC ~85-90%, same as previous observation.
	11:48	133.2	CC ~90%, opening exist on west side, light is visible on east side, large shelf is 14-15" thick running from north-east to south-west corner.
	12:05	133.4	CC ~90%, opening on west side is visible, on east side has a large shelf is ~14-15" thick running from north-east to south-east corner.
	12:25	133.8	CC ~85-90%, large openings exist on west side with light visible on east side, large shelf/CC extending from north-east to south-west corner. Shelf/CC Is ~14-15" thick, feed is collecting on CC surface and boiling.
	14:40	136.0	CC ~85-90%, same as last observation.
	12:55	134.3	Paused/stopped feeding to allow CC to melt.
	13:20	134.7	CC ~85%, opening exists on west side with light visible on east side. Ridge is ~14-15" thick extending from north-east to south-west corner.
	13:37	135.0	Glass pool does not appear to be excessively foamy.
	13:45	135.1	Started feeding water at 1000 ml/min to reduce foaming in glass.
	13:50	135.2	Stopped water, there were no indication it was flowing into melt pool. CC ~80%, ridge has decreased in size, opening exists on west side with light visible on east side.
	14:05	135.4	CC ~80%, west and east sides are visible. East side has a ridge.
	14:19	135.7	Resumed feeding water at 1000 ml/min. CC ~80%, ridge is still present on west side.
	14:39	136.0	Stopped feeding water, it did not help.
	15:00	136.4	There is a large ridge which is not allowing seeing the east side.
	15:09	136.5	Able to see east side now.
	15:14	136.6	Resumed feeding water at 1500 ml/min.
	15:52	137.2	CC ~80%, the center mound has built back up.
	16:04	137.4	Secured feeding water.
	16:20	137.7	CC ~50%, most of the mound in the center has melted.
	16:30	137.9	Resumed feeding slurry.
	16:40	138.0	CC ~50%, glass pool starting to look less foamy.
	16:55	138.3	CC ~80%, center ridge has formed, not able to see the east side.
	17:10	138.5	CC ~75%, able to see east side opening.
	17:25	138.8	CC ~75%, the ridge on west side is higher, feed is flowing over into the melt pool.
	17:40	139.0	CC ~75%, no visible changes at this observation.

Table 4.3. Operator Observations of Cold Cap (CC) (continued).

Date	Time	Run Time (hours)	Cold Cap Observations
10/28/2009	17:55	139.3	CC ~75%, large openings exist on both east and west sides. The CC is thick, feed is boiling on top on ridge between the openings.
	18:10	139.5	CC ~75%, is thick, east and west sides are wide open. Feed is boiling on ridge between the openings.
	18:25	139.8	CC ~75%, able to see the glass pool from center view port. The ridge around the west side pool is about 6-7" tall.
	18:40	140.0	CC ~75%, west side ridge is starting to look like a dome. Sill able to see east side opening.
	18:55	140.3	CC ~75%, no visible changes from last observation.
	19:10	140.5	CC ~75%, no visible changes from last observation.
	19:25	140.8	CC ~75%, still able to see east side opening, west side ridge is slowly coming down.
	19:40	141.0	CC ~75%, no visible changes.
	19:55	141.3	CC ~75%, west side ridge is taller, no visible changes on the east side.
	20:10	141.5	CC ~75%, liquid feed is flowing over west side ridge.
	20:25	141.8	CC ~70%, both openings have opened up some, west side ridge is not as high from previous observation.
	20:40	142.0	CC ~70%, no visible changes from last observation.
	20:55	142.3	CC ~70%, ridge on west side is higher, feed is flowing over CC.
	21:10	142.5	CC ~70%, is thick, large openings exists on both east and west sides. Feed is flowing into melt pool.
	21:25	142.8	CC ~70%, is ~12" thick, wide open on east and west sides, feed is flowing into the melt pool.
	22:10	143.5	CC ~70%, large ridge exists in the center, west side is wide open.
	22:53	144.2	Large ridge exist in the center of melter, have seen liquid flow over ridge into opening on west side.
	23:23	144.7	Glow of feed is seen over shelf and into west side opening.
	23:45	145.1	CC ~75%, ridge is still blocking east side view. Glass does not appear foaming in melt pool, but glass trickling down the glass chamber through definitely foamy.
10/29/2009	0:20	145.7	CC ~75%, large opening exists on the west side, light is seen on the east from south view port.
	0:36	146.0	CC is unchanged.
	0:42	146.1	Observing a moderate amount of feed spilling over ridge right after feed shot. CC is unchanged; glass is not near middle view port.
	0:55	146.3	Observing more feed flowing over ridge and into west opening, causing slight pressure spikes.
	1:05	146.4	Can now see east opening, melter seems divided by a long relatively thin ridge, feed is continuing to spill over into west opening.
	1:36	147.0	CC ~70% same as before, ridge is still dividing melter, east side is still visible.
	1:53	147.2	CC ~70%, ridge is much lower than before but it is still present.
	2:20	147.7	CC ~70% is thick and flat.
	2:34	147.9	CC ~70 same as previous observation.

Table 4.3. Operator Observations of Cold Cap (CC) (continued).

Date	Time	Run Time (hours)	Cold Cap Observations
10/29/2009	3:02	148.4	CC ~70%, thick and flat, feed is boiling on top of CC.
	3:27	148.8	CC ~70%, same as above observations.
	3:34	148.9	CC ~65-70%, after glass discharge massive shelf was revealed starting at north side of melter running down to center. A slight view of the east opening is now visible.
	3:50	149.2	CC ~60%, ridge is only a couple of inches above the melt pool and appears to be on the verge of total collapse. It still appears to be thicker, a piece is jutting out from north-west corner of melter.
	4:05	149.4	CC ~60%, is thick and flat with 2 large holes. Feed is boiling on top of CC.
	4:19	149.7	CC ~60%, still the same as the previous observation.
	4:37	150.0	CC ~60%, is thick and flat, 2 large holes exist. Feed is boiling on top of CC.
	4:51	150.2	CC ~60%, still the same as the previous observation, slight foamy discharge.
	5:06	150.5	CC ~69%, same as before, a slight foamy discharge is observed.
	5:21	150.7	CC ~60%, is thick and flat, 2 large holes exist, feed is boiling on top of CC.
	5:34	150.9	CC ~65%, same as before, a slight foamy discharge is observed.
	5:48	151.2	CC ~60%, most of the CC is in north-central portion of the melter.
	6:18	151.7	CC ~60% is thicker and flat with 2 large holes. Feed is boiling into the west hole.
	6:37	152.0	CC ~60%, majority of CC is in north-central part of the melter.
	7:00	152.4	CC ~70%, openings are on west and east sides, small ridge extending from north wall to south wall with feed collecting on top of CC and running into opening.
	7:35	152.9	CC ~75%, looks thick, there is large build up around the Lance Bubbler #2 , and area along west wall is thin and floating.
	7:50	153.2	CC ~75%, mostly the same as before except that build up around the Lance Bubbler #2 is not as large as before.
	8:05	153.4	CC ~70%, both openings look longer to the north, CC along west wall looks thicker and is still floating.
	8:20	153.7	CC ~70%, mostly the same as before.
	8:38	154.0	CC ~70%, west side continues to float, east side is also open with little noticeable change.
	8:55	154.3	CC ~70%, opening on east and west sides are separated by small ridge ~4" thick, feed is boiling on top of ridge and flowing into openings.
	9:08	154.5	CC ~65-70%, openings on east and west sides are separated by a ridge ~4-6" thick. Feed is pooling on ridge, boiling and flowing into openings.
	9:20	154.7	CC ~70%, in addition to the above, cap portion along west wall is still floating.
	9:35	154.9	CC ~70%, unchanged.
	9:48	155.2	Paused feeding to rod feed tube.
	9:55	155.3	Resumed feeding.
	10:05	155.4	CC ~65-70%, unchanged.

Table 4.3. Operator Observations of Cold Cap (CC) (continued).

Date	Time	Run Time (hours)	Cold Cap Observations
10/29/2009	10:20	155.7	CC ~65%, both opening look larger, visible portion of the cap along west wall is soft and floating. Ridges look a little taller.
	10:35	155.9	CC ~70%, openings exist on both west and east sides, ridge on west side is small, pool of the feed is in between both openings.
	11:04	156.4	CC ~65-70%, east and west sides have openings, ridge is located around west side. Between openings feed is boiling with glass (molten) splash vigorously.
	11:20	156.7	CC ~65%, ridge is much smaller, ridge and cap are floating.
	11:35	156.9	CC ~60-65%, mostly the same.
	11:50	157.2	CC ~65-70%, small ridge is separating openings on east and west side. Ridge is ~5-6" thick and floating on melt pool. Feed is boiling on surface and flowing into openings.
	12:08	157.5	CC ~70%, east side cap is floating, west side is thicker, a fair amount of boiling feed is on CC surface.
	12:50	158.2	CC ~65%, CC and ridge are floating, feed is boiling and flowing into the glass melt.
	13:05	158.4	CC ~65%, mostly unchanged CC conditions.
	13:20	158.7	CC ~65%, ridge is no longer floating, east side is floating, west side is fixed.
	13:36	159.0	CC ~65%, glass pool violently splashing, boiling liquid is on CC surface, east and west sides are opening.
	13:50	159.2	Ridge continues to be taller.
	14:05	159.4	CC ~65%, ridge is still growing.
	14:20	159.7	CC ~65%, conditions are the same.
	14:35	159.9	CC ~65%, ridge is slightly larger.
	14:52	160.2	CC ~60%, large and tall ridge is in the center of melt pool, east side and west sides are open.
	15:05	160.4	CC ~60%, still a tall and narrow ridge is in the center of the glass pool.
	15:08	160.5	East and west sides are open.
	15:20	160.7	CC ~60%, same as last observation.
	15:34	160.9	CC ~70%, ridge is not as tall but wider, looks like glass level is rising and west side is closing up.
	15:50	161.2	CC ~70%, ridge is larger, west side is closing up and east side has a larger opening.
	16:05	161.4	CC ~75%, the ridge in the center is almost too tall to see behind it, east side continues to close up.
	16:20	161.7	CC ~75%, CC conditions are the same as the previous observation.
	16:35	161.9	CC ~65%, feed is pooling in the center, than boils over mostly to the east side, the ridge on the west holds some of it back.
	16:50	162.2	CC ~65%, no visible changes for this observation.
	17:05	162.4	CC ~65%, ridge in the center is a little taller.
	17:20	162.7	CC ~65%, east side view is almost blocked by west side ridge, feed is flowing a little heavier to the west.
	17:35	162.9	CC ~65%, little to no change for this observation.
	17:50	163.2	CC ~60%, build up is mostly in the center.

Table 4.3. Operator Observations of Cold Cap (CC) (continued).

Date	Time	Run Time (hours)	Cold Cap Observations
10/29/2009	18:10	163.5	CC ~70%, large ridge is in the center of pool, so tall that barely able to see east side, CC is thin, and floating on west opening.
	18:25	163.8	CC ~75%, ridge is a little taller otherwise conditions are the same.
	18:48	164.2	CC ~80%, can no longer see the ridge in the center of the pool, CC is thin and floating on the west side.
	19:04	164.4	C ~80%, conditions are same as the last observation.
	19:25	164.8	CC ~65%, able to see east side opening, ridge has broken down some, both opening are wide open.
	19:40	165.0	CC ~65%, same as before.
	19:55	165.3	CC ~65% is thick, large openings exists on east and west sides. The ridge is running the middle.
	20:10	165.5	CC ~70%, is thick, large opening exist on west and east sides. Feed is flowing into the east side.
	20:25	165.8	CC ~70%, large opening on west side, east side is hard to see behind the ridge.
	20:40	166.0	CC ~75%, opening exist on west side, thick ridge is blocking view of east side.
	20:55	166.3	CC ~75%, west side is open, view of east side ridge is blocked by ridge.
	21:25	166.8	CC ~70%, west side is open, cannot see east side over large ridge in the middle of the melter.
	21:40	167.0	CC ~70%, west side is open, large ridge exists in the middle of the melter.
	21:54	167.3	CC ~75%, ridge in the center is so tall that you cannot see over it. Large opening exists in west side.
	22:10	167.5	CC ~75%, west side has closed up more.
	22:51	168.2	CC ~7075%, only west side opening is visible due to the wall/mound at the mid section of the CC.
	23:10	168.5	CC ~60-65%, glass level is high, east ca not be seen, large opening exits on west side.
	23:52	169.2	CC ~75%, cannot see east side, cold cap is thick and flat, slight foamy discharge.
10/30/2009	0:18	169.7	CC ~65%, is thick and flat.
	0:39	170.0	CC ~70%, large opening exists on west side, ridge is blocking the view of east side, glass level look fairly high.
	0:58	170.3	CC conditions are the same.
	1:15	170.6	CC ~70%, unchanged CC conditions.
	1:35	170.9	CC ~70%, is thick and flat also small ridge exists on the opening, feed pooling on that ridge.
	1:49	171.2	CC ~70%, same as last observation.
	2:23	171.7	CC ~75%, is thick and flat.
	2:30	171.9	Paused feeding to switch to AOD feed system.
	3:07	172.5	CC ~50%.
	3:11	172.5	Resumed feeding.

Table 4.3. Operator Observations of Cold Cap (CC) (continued).

Date	Time	Run Time (hours)	Cold Cap Observations
10/30/2009	3:14	172.6	Stopped feeding.
	3:22	172.7	CC ~20%.
	3:28	172.8	Started feeding water at 1000 ml/min.
	3:37	173.0	Reduced water flow rate to 500 ml/min.
	4:00	173.4	Resumed feeding slurry with AOD system, secured water feeding.
	4:04	173.4	CC ~90%, is flat and even.
	4:33	173.9	CC ~70-75%, is flat, there are large openings on east and west sides.
	4:55	174.3	CC ~70%, evenly flat with boiling feed on the CC surface, both east and west openings are visible.
	5:32	174.9	CC ~80%, is flat with 2 openings, feed is boiling on top.
	5:51	175.2	CC ~80%, same as above conditions.
	6:06	175.5	CC ~80%, 2 openings, large pool of feed boiling on top of CC.
	6:32	175.9	CC ~70-75%, heavy boiling is taking place on the surface, both Lance Bubbler openings have slight ridges.
	6:50	176.2	CC ~75%, moderate ridges exist around both openings, feed continues to boil on surface.
	7:05	176.4	CC ~75%, unchanged CC conditions.
	7:20	176.7	CC ~70%, west opening looks larger.
	7:37	177.0	CC ~65-70%, east side cap is floating, ridge is running down center, west side is opened as well.
	7:50	177.2	CC ~70%, west side is closing slightly.
	8:06	177.5	CC ~65-70%, west side is opening slightly and is more visible, ridges are about the same size, and glass looks foamier.
	8:20	177.7	CC ~65-70%, looks unchanged.
	8:32	177.9	CC ~65-70%, east cap remains soft and floating, both east and west sides are opening.
	8:48	178.2	CC ~65-70%, cap appears unchanged.
	9:05	178.4	CC ~70%, ridges look a little larger.
	9:20	178.7	CC ~75%, east opening is slightly smaller.
	9:35	178.9	CC ~75-80%, both openings are hardly visible.
	9:50	179.2	CC ~75%, both opening are now clearly visible, ridge is about the same size and floating.
	10:05	179.4	CC ~75%, mostly unchanged.
	10:20	179.7	CC ~75%, unchanged.
	10:35	179.9	CC ~75%, ridge look taller.
	10:50	180.2	CC ~75%, cap is floating, so are ridges, vigorously boiling feed is between the ridges.
	11:09	180.5	CC ~70-75%, both openings look a little bigger but the ridges are the same.
	11:20	180.7	CC ~70-75%, ridges are slightly smaller, cap is still floating, melter shots are causing slightly positive pressure spikes.
	11:35	180.9	CC ~70%, looks the same as previous observation.

Table 4.3. Operator Observations of Cold Cap (CC) (continued).

Date	Time	Run Time (hours)	Cold Cap Observations
10/30/2009	11:50	181.2	CC ~75%, ridges are higher.
	12:05	181.4	CC ~75-80%, both openings are smaller, mound is growing between ridges, ridge and cap are no longer floating.
	12:20	181.7	CC ~80%, with openings on both east and west sides, ridge formed around the west opening with feed boiling on cap between east and west openings, feed is flowing into east side.
	12:36	182.0	CC ~75-80%, openings exist on east and west sides.
	12:50	182.2	CC ~80%, unchanged conditions.
	13:07	182.5	CC ~80%, ridges look like they are growing together especially near melter center.
	13:20	182.7	CC ~80%, unchanged conditions.
	13:35	182.9	CC ~80%, ridge in center appears to be narrowing; cap looks thick and has boiling feed on surface.
	13:50	183.2	CC ~80%, ridge is slowly growing.
	14:05	183.4	CC ~80%, unchanged conditions.
	14:49	184.2	CC ~75%, east side is open, west side is blocked by thick ridge. Feed is flowing into east side opening.
	15:05	184.4	CC ~80%; cap is very thick, large ridge in the center of the melter, unable to see the east, small opening in the west.
	15:22	184.7	Paused feeding due to collapse of cap. Opened view port due to rush of air, cold cap collapsed and massive steam surge occurred.
	15:26	184.8	CC ~85%, massive amounts of build up, ridge is still very tall, very small opening in west, unable to see east side.
	15:44	185.1	CC ~80%, still a huge ridge and massive amounts of build up exists.
	16:01	185.4	CC ~75%, cap is starting to open up, still small opening in west and east is now visible over the ridge.
	16:15	185.6	CC ~80%, west side is open more than the eastside. Thick ridge exists in middle of pool. Feed is boiling on top of ridge.
	16:30	185.9	CC ~80%, both east and west sides are wide open. Feed is boiling on the ridge.
	16:45	186.1	CC ~75%, ridge is getting smaller, east and west are opening up wider. Feed is flowing into the east side.
	17:00	186.4	Stopped feeding. End of the ORP Hi Bi Foaming Test.
	19:07	188.5	Cold cap is mostly foam.
	19:47	189.1	Cold cap is gone. There is a foamy cap ~3" thick. There is moderate amount of build up on the walls.
	20:05	189.4	Start melter off-gas shut downs.

Table 4.4. DM1200 Tests Performed with Final HLW Bubbler Configuration, Glass Temperature of 1150ºC, and Optimized Bubbling /Production Rates.

Test	Feed	Glass Yield	Duration	Bubbling Rate	Glass Production Rate
Current Tests	High Bismuth	500 g/l	77.1 hr	126 lpm	815 kg/m^2/d
	High Bismuth	500 g/l	103.3 hr	126 lpm	558 kg/m^2/d
High Waste Loading Glass Formulations for Hanford High-Aluminum HLW Streams VSL-10R1690-1 [21]	Al-Limited Waste with LAW stream as sodium source, sugar	500 g/l	54 hrs	62 lpm	1050 kg/m^2/d
High Waste Loading Glass Formulations for Hanford High-Aluminum HLW Streams VSL-10R1690-1 [21]	Al-Limited Waste with LAW stream as sodium source, sugar	500 g/l	51 hrs	101 lpm	1450 kg/m^2/d
High Waste Loading Glass Formulations for Hanford High-Aluminum HLW Streams VSL-10R1690-1 [21]	Al-Limited Waste with LAW stream as sodium source, sugar	400 g/l	48 hrs	85 lpm	1150 kg/m^2/d
High Waste Loading Glass Formulations for Hanford High-Aluminum HLW Streams VSL-10R1690-1 [21]	Al-Limited Waste with LAW stream as sodium source, cellulose	500 g/l	50 hrs	81 lpm	1050 kg/m^2/d
Melt Rate Enhancement for High Aluminum HLW Glass Formulations VSL-08R1360-1 [19]	Al-Limited Waste	500 g/l	48 hrs	124 lpm	1500 kg/m^2/d
Melt Rate Enhancement for High Aluminum HLW Glass Formulations VSL-08R1360-1 [19]	Al-Limited Waste	500 g/l	48 hrs	71 lpm	1050 kg/m^2/d
Configuration Test 9A VSL-04R4800-4 [5]	AZ-101	400 g/l	145 hrs	64 lpm	1050 kg/m^2/d
Configuration Test 9B VSL-04R4800-4 [5]	AZ-101	400 g/l	72 hrs	134 lpm	1400 kg/m^2/d
Test 1B VSL-05R5800-1 [18]	AZ-102	340 g/l	114 hrs	65 lpm	900 kg/m^2/d
Test 2B VSL-05R5800-1 [18]	C-106/AY-102, High Waste Loading	340 g/l	105 hrs	90 lpm	1050 kg/m^2/d

Table 4.5. Measured DM1200 Melter System Parameters.

Tests			10/20-23/2009			10/26-30/2009		
			avg	min	max	avg	min	max
TEMPERATURE (°C)	Glass	13" from floor E	1144	1069	1197	1154	1093	1208
		15.5" from floor E	1162	1121	1210	1162	1110	1231
		18" from floor E	1161	1105	1211	1163	1091	1229
		27" from floor E	1051	407	1183	1119	523	1199
		13" from floor W	1148	1090	1200	1145	1092	1186
		15.5" from floor W	1148	1083	1204	1145	1078	1191
		18" from floor W	1150	1085	1204	1148	1065	1206
		27" from floor W	1050	355	1202	1122	567	1203
	Plenum	8" below ceiling	611	400	907	651	418	912
		17" below ceiling	567	354	835	640	425	910
		Exposed	671	384	951	675	333	925
	Discharge	TC 1	982	901	1054	1015	924	1130
		TC 2	1013	939	1072	1062	987	1136
		Air Flow	280	237	299	261	47	304
		Riser	1091	931	1170	1067	890	1160
	Electrode	East	1145	994	1182	1126	1046	1162
		West	1125	1059	1148	1101	1036	1137
		Bottom	1047	967	1111	1021	919	1067
	Film Cooler	Added Air	171	58	306	177	58	263
		Outlet	388	75	563	404	62	584
Glass	Density (g/cc)		2.21	1.35	2.52	2.07	1.53	2.60
	Level (" from floor)		30.96	25.16	43.29	31.82	26.65	41.26
	Resistance (ohms)		0.090	0.071	0.110	0.095	0.067	0.116
Electrodes	Current (A)		761	640	942	847	692	1083
	Voltage (V)		118	83	145	113	69	141
	Power (kW)		158	88	201	136	70	192
Lance Bubblers	1	Rate (lpm)	62.2	2.7	111.0	62.4	6.2	101.5
	2	Rate (lpm)	62.5	2.6	120.5	62.3	5.9	111.6
Total Lance Bubbling (lpm)			125.9	6.5	222.2	125.9	13.3	214.3

Table 4.6. Measured DM1200 Off-Gas System Parameters.

		10/20-23/2009			10/26-30/2009		
		Avg.	Min.	Max.	Avg.	Min.	Max.
Melter	Pressure at Level Detector Port ("water)	-2.4	-6.3	1.4	-2.5	-5.2	2.2
	Pressure at Instrument Port ("water)	-2.7	-6.8	1.5	-2.8	-5.7	2.5
	Control Air Flow Rate (scfm)	19.7	11.2	65.1	37.0	11.1	72.0
Film Cooler Differential Pressure ("water)		1.98	0.47	10.05	1.47	0.36	10.05
Transition Line Differential Pressure ("water)		3.2	0.0	14.0	3.7	2.2	16.2
SBS	Differential Pressure ("water)	34.0	13.5	55.1	33.5	27.3	40.8
	Inlet gas pressure ("water)	-7.4	-24.0	-1.1	-7.6	-25.1	-3.6
	Outlet gas pressure ("water)	-40.4	-58.5	-20.8	-39.7	-62.0	-23.4
	Downcomer Annulus Pressure (psia)	14.2	9.3	14.5	14.3	13.4	14.5
	Inlet gas Temp. (°C)	299	151	484	280	125	393
	Outlet gas Temp. (°C)	42.4	27.8	55.2	42.6	25.7	53.3
	C. Coil W. Inlet Temp (°C)	19.4	13.8	23.9	18.4	13.5	22.3
	C. Coil W. Outlet Temp (°C)	34.4	20.7	47.8	35.2	20.7	47.3
	Jacket W. Outlet Temp (°C)	37.6	23.9	50.1	38.4	22.0	49.2
	Sump Temp. (°C)	36.5	21.9	49.9	36.9	21.8	48.9
	Off-gas Downcomer Temp @3" (°C)	234	145	378	218	134	297
	Off-gas Downcomer Temp @8" (°C)	248	157	398	231	142	316
	Off-gas Downcomer Temp @13" (°C)	255	164	402	237	149	325
	Off-gas Downcomer Temp @18" (°C)	245	157	392	227	143	312
	Off-gas Downcomer Temp @28" (°C)	230	145	368	213	135	294
	Off-gas Downcomer Temp @33" (°C)	222	134	359	207	133	285
	Off-gas Downcomer Temp @38" (°C)	202	107	351	191	122	275
	Off-gas Downcomer Temp @48" (°C)	109	60.0	333	89.5	63.8	176
	Off-gas Downcomer Temp @53" (°C)	78.1	42.6	280	65.5	44.4	92.2
	C. Coil/Jacket W. Flow Rate (gal/min)	18.3	4.6	30.1	13.1	2.3	29.8
	Recirc. pump discharge Temp (°C)	42.9	28.2	53.0	43.1	25.9	49.6
	Recirc. pump discharge Pressure (psi)	38.8	0.1	41.2	40.4	27.1	46.1
WESP	Differential Pressure ("water)	5.5	0.5	10.1	7.6	1.1	10.1
	Inlet gas Temp. (°C)	42.5	29.9	54.8	42.6	26.0	53.0
	Outlet gas Temp. (°C)	44.0	26.1	53.2	44.0	26.1	51.0
	Wet Gas Flow Rate (scfm)	250	67.1	288	259	114	313
	Voltage (kV)	30.2	0.0	32.4	30.4	0.1	31.7
	Current (mA)	14.8	0.0	17.0	14.5	0.0	18.3
HEME #1	Differential Pressure ("water)	1.6	0.5	2.0	1.6	0.3	2.6
	Outlet Gas Temp. (°C)	43.0	32.9	51.6	43.0	28.9	49.1
HEPA 1	Differential Pressure ("water)	0.6	-1.2	0.9	0.5	0.2	0.8
	Outlet Gas Temp. (°C)	70.6	37.8	74.9	71.1	66.8	74.2
TCO/SCR Heater Inlet Gas Temp. (°C)		89.1	50.6	91.9	89.3	85.6	93.7
TCO	Inlet Gas Temp. (°C)	357	118	370	364	356	374
	Mid-bed Temp. (°C)	355	87.0	374	366	332	373
	Differential Pressure ("water)	3.9	0.9	4.7	4.3	1.9	5.9
SCR	Inlet Gas Temp. (°C)	338	108	347	338	328	345
	Outlet Gas Temp. Right (°C)	328	122	335	330	310	334
	Outlet Gas Temp. Left (°C)	304	122	315	310	285	315
	Differential Pressure ("water)	2.5	0.6	3.1	2.8	1.3	3.8
	Post Outlet Gas Temp. (°C)	273	122	293	289	257	293
PBS	Inlet Gas Temp. (°C)	262	130	283	278	239	282
	PBS Sump Temp. (°C)	32.7	20.2	37.1	32.3	23.7	35.6
	Differential Pressure ("water)	3.2	-0.3	5.2	3.4	0.6	7.1
HEME #2	Differential Pressure ("water)	4.8	2.2	5.8	4.8	2.0	6.8
	Inlet Gas Temp. (°C)	33.6	24.0	37.3	33.1	25.1	36.2
	Outlet Gas Temp. (°C)	34.2	24.6	37.8	33.8	28.8	37.4
Exhaust Stack Absolute Pressure ("water)		-9.2	-9.7	-6.4	-9.4	-9.8	-8.9

Table 4.7. Off-Gas Solution Volumes.

Type of Sample	Date	Sample ID for last Blow-down	Number of Blow-downs	Total Blow-down Volume (gal)
SBS	10/30/2009	S-12-P-117A	47	1863.4
WESP	10/30/2009	W-12P-117A	11	638.9
		W-12P-117B		
HEME 1	10/30/2009	H1-12P-118A	2	51.0
PBS	10/30/2009	P-12P-118A	16	570.8

Table 4.8. Analytical Results for Solutions from the DM1200 Off-Gas System Sampled at End of Testing (mg/L).

Sample ID	S-12P-117A			W-12P-117A			W-12P-117B		
Deluge	No			Before Deluge			After Deluge		
pH	1.93			2.69			3.08		
-	Sus*	Dis.#	Total	Sus*	Dis.#	Total	Sus*	Dis.#	Total
Solid	2407	7531	9938	5	1868	1873	26	750	776
Al	26.98	351.88	378.86	NA	2.83	2.83	0.06	0.93	0.99
B	1.21	788.85	790.06	NA	47.92	47.92	<0.20	15.37	15.57
Ba	0.11	1.33	1.44	NA	0.06	0.06	<0.00	0.04	0.04
Bi	114.60	5.45	120.05	NA	4.62	4.62	7.15	0.79	7.94
Ca	4.23	44.25	48.48	NA	41.21	41.21	0.02	38.53	38.55
Cd	0.05	0.49	0.54	NA	0.16	0.16	<0.03	0.09	0.09
Cr	3.62	19.28	22.9	NA	19.08	19.08	1.17	7.75	8.92
Cs	<0.11	0.29	0.29	NA	0.31	0.31	<0.11	0.28	0.28
Fe	69.24	39.53	108.77	NA	1.98	1.98	0.94	1.23	2.17
K	0.58	73.68	74.26	NA	48.23	48.23	<0.08	22.61	22.61
Li	0.24	22.66	22.9	NA	6.17	6.17	<0.05	2.37	2.37
Mg	0.48	34.24	34.72	NA	8.70	8.70	<0.01	8.74	8.74
Mn	0.11	1.51	1.62	NA	<0.04	<0.04	<0.04	<0.04	<0.04
Na	3.51	1338.00	1341.51	NA	389.52	389.52	0.11	130.35	130.46
Ni	29.54	24.05	53.59	NA	0.51	0.51	0.61	0.47	1.08
P	24.53	104.31	128.84	NA	5.18	5.18	<0.60	1.58	1.58
Pb	3.39	11.13	14.52	NA	6.18	6.18	0.24	2.11	2.35
Si	174.72	277.78	452.5	NA	6.95	6.95	0.25	5.21	5.46
Sr	0.04	0.80	0.84	NA	0.28	0.28	<0.00	0.23	0.23
Ti	2.78	4.77	7.55	NA	0.04	0.04	<0.02	<0.02	<0.02
Zn	0.31	7.35	7.66	NA	0.28	0.28	<0.02	0.10	0.10
Zr	2.33	4.87	7.2	NA	<0.02	<0.02	<0.02	<0.02	<0.02
F	NA	2915.75	2915.75	NA	117.05	117.05	NA	37.55	NC
Cl	NA	98.03	98.03	NA	41.38	41.38	NA	40.33	NC
I	NA	101.17	101.17	NA	<0.1	<0.1	NA	0.79	NC
Nitrate	NA	349.61	349.61	NA	55.11	55.11	NA	28.76	NC
Nitrite	NA	<0.1	<0.1	NA	0.54	0.54	NA	<0.1	NC
Sulfate	NA	1734.71	1734.71	NA	1214.93	1214.93	NA	492.22	NC

NA – Not analyzed; NC - Not calculated
*. – Suspended solid; # - Dissolved solid

Table 4.8. Analytical Results for Solutions from the DM1200 Off-Gas System Sampled at End of Testing (mg/L) (continued).

Sample Type	HEME 1		PBS	
Sample I.D.	H1-12P-118A		P-12P-118A	
pH	2.28		9.29	
Solid	Sus*	Dis.#	Sus*	Dis.#
Total	2	513	8	4206
Al	NA	0.69	NA	0.46
B	NA	16.53	NA	4.06
Ba	NA	0.04	NA	0.00
Bi	NA	0.77	NA	<0.25
Ca	NA	36.55	NA	<0.00
Cd	NA	0.62	NA	<0.03
Cr	NA	2.68	NA	0.06
Cs	NA	0.61	NA	0.22
Fe	NA	2.73	NA	<0.05
K	NA	18.82	NA	3.08
Li	NA	3.35	NA	<0.05
Mg	NA	9.56	NA	0.16
Mn	NA	<0.04	NA	<0.04
Na	NA	51.52	NA	1233.70
Ni	NA	0.31	NA	<0.04
P	NA	0.87	NA	<0.06
Pb	NA	0.74	NA	<0.10
Si	NA	2.49	NA	<0.04
Sr	NA	0.25	NA	0.05
Ti	NA	<0.02	NA	<0.02
Zn	NA	3.26	NA	<0.02
Zr	NA	0.04	NA	<0.02
F	NA	40.68	NA	23.66
Cl	NA	46.14	NA	12.29
I	NA	4.51	NA	40.74
Nitrate	NA	357.72	NA	128.07
Nitrite	NA	0.45	NA	1159.86
Sulfate	NA	376.81	NA	327.91

NA – Not analyzed*. – Suspended solid; # - Dissolved solid

Table 5.1. Characteristics of Melter Feed Samples from DM1200 Tests.

Formulation	Date	Name	% Water	pH	Density (g/ml)	Glass Yield			
						(g/l)	Measured (kg/kg)	Target (kg/kg)	%Dev.
As Received	10/19/09	F-12N-121A	50.17	10.63	1.56	711	0.456	0.435	4.73
Melter feed	10/20/09	F-12N-145A	58.52	10.34	1.39	519	0.374	0.354	5.56
	10/21/09	F-12O-32A	59.45	10.40	1.38	491	0.356	0.354	0.54
	10/22/09	F-12O-74A	61.90	10.57	1.37	485	0.354	0.354	0.00
	10/26/09	F-12O-136A	60.87	10.38	1.36	472	0.347	0.354	-2.01
	10/27/09	F-12P-20A	61.10	10.48	1.37	481	0.351	0.354	-0.79
	10/28/09	F-12P-51A	59.84	10.68	1.40	508	0.363	0.354	2.57
	10/29/09	F-12P-83A	60.59	10.40	1.38	494	0.358	0.354	1.05
	10/30/09	F-12P-116A	59.60	10.72	1.40	519	0.370	0.354	4.63
	Average		60.23	10.50	1.38	496	0.359	0.354	1.44

Table 5.2. XRF Analyzed Compositions of Vitrified DM1200 Melter Feed Samples (wt%).

Constituent	Target	F-12N-121A	F-12N-145A	F-12O-32A	F-12O-74A	F-12O-136A	F-12P-20A	F-12P-51A	F-12P-83A	F-12P-116A	Avg.	%Dev.
Al_2O_3	11.66	11.50	10.89	11.42	11.81	11.96	12.17	11.76	11.90	11.45	11.65	-0.02
B_2O_3*	11.3	11.30	11.30	11.30	11.30	11.30	11.30	11.30	11.30	11.30	11.30	NC
BaO	0.01	0.02	0.01	0.01	0.03	0.02	0.02	0.02	0.02	0.02	0.02	NC
Bi_2O_3	6.71	6.80	6.64	6.69	6.47	6.09	6.19	6.26	6.11	7.14	6.49	-3.27
CaO	0.84	1.00	0.85	0.88	0.84	0.83	0.88	0.89	0.91	0.93	0.89	NC
Cr_2O_3	0.52	0.70	0.67	0.68	0.69	0.63	0.67	0.62	0.68	0.71	0.67	NC
F*	0.82	0.82	0.82	0.82	0.82	0.82	0.82	0.82	0.82	0.82	0.82	NC
Fe_2O_3	6.96	7.31	7.04	7.19	7.04	6.70	6.69	6.81	6.73	7.59	7.01	0.70
K_2O	0.46	0.49	0.45	0.46	0.48	0.44	0.49	0.47	0.48	0.47	0.47	NC
Li_2O*	0.16	0.16	0.16	0.16	0.16	0.16	0.16	0.16	0.16	0.16	0.16	NC
MgO	0.43	0.58	0.58	0.57	0.58	0.58	0.61	0.59	0.55	0.57	0.58	NC
MnO	§	0.04	0.03	0.03	0.02	0.02	0.03	0.03	0.03	0.04	0.03	NC
Na_2O	15.74	14.72	16.78	15.41	15.44	15.92	15.28	16.22	16.01	15.03	15.65	-0.56
NiO	1.93	2.02	1.91	1.99	1.97	1.82	1.91	1.83	1.95	1.94	1.93	0.19
P_2O_5	4.99	5.18	4.98	5.05	5.18	5.02	5.31	5.09	5.28	5.14	5.14	3.06
PbO	0.25	0.24	0.24	0.24	0.22	0.21	0.21	0.22	0.21	0.25	0.23	NC
SiO_2	36.26	36.09	35.70	36.07	35.93	36.49	36.21	35.90	35.83	35.42	35.96	-0.81
SO_3	0.48	0.44	0.35	0.40	0.43	0.42	0.47	0.44	0.44	0.41	0.42	NC
TiO_2	0.16	0.18	0.16	0.17	0.17	0.17	0.18	0.17	0.17	0.17	0.17	NC
ZnO	0.16	0.17	0.17	0.17	0.16	0.15	0.15	0.15	0.15	0.17	0.16	NC
ZrO_2	0.21	0.27	0.27	0.28	0.27	0.25	0.26	0.26	0.26	0.27	0.26	NC
Sum	100.00	100.000	100.000	100.000	100.000	100.000	100.000	100.000	100.000	100.000	100.000	NC

* Target values; § - Not a target constituent
NA – Not analyzed

Table 5.3. Comparison of XRF and DCP Analyzed Compositions of Select Vitrified DM1200 Melter Feed Samples and Discharged Melter Glass.

Sample Type	Target	Vitrified Melter Feed						Glass	
Sample I.D.		F-12N-121A		F-12O-32A		F-12P-116A		G-12P-116A	
Constituent		XRF	DCP	XRF	DCP	XRF	DCP	XRF	DCP
Al_2O_3	11.66	11.50	11.43	11.42	11.38	11.45	11.52	12.10	11.98
B_2O_3	11.30	11.30*	11.24	11.30*	11.52	11.30*	10.54	11.66*	11.82
BaO	0.01	0.02	0.03	0.01	0.02	0.02	0.02	0.02	0.02
Bi_2O_3	6.71	6.80	6.65	6.69	6.88	7.14	6.90	6.29	6.76
CaO	0.84	1.00	1.09	0.88	0.97	0.93	1.04	1.08	1.20
Cr_2O_3	0.52	0.70	0.33	0.68	0.31	0.71	0.28	0.65	0.23
F	0.82	0.82*	NA	0.82*	NA	0.82*	NA	0.43**	NA
Fe_2O_3	6.96	7.31	6.30	7.19	6.14	7.59	6.41	7.06	5.84
K_2O	0.46	0.49	0.57	0.46	0.56	0.47	0.57	0.47	0.55
Li_2O	0.16	0.16*	0.33	0.16*	0.27	0.16*	0.33	0.31*	0.50
MgO	0.43	0.58	0.64	0.57	0.65	0.57	0.63	0.50	0.64
MnO	§	0.04	0.04	0.03	0.03	0.04	0.04	0.03	0.04
Na_2O	15.74	14.72	13.47	15.41	13.41	15.03	13.38	15.90	13.42
NiO	1.93	2.02	1.56	1.99	1.54	1.94	1.48	1.78	1.35
P_2O5	4.99	5.18	5.33	5.05	4.91	5.14	5.40	5.00	5.10
PbO	0.25	0.24	0.25	0.24	0.25	0.25	0.27	0.24	0.25
SiO_2	36.26	36.09	36.83	36.07	38.19	35.42	37.97	35.61	37.73
SO3	0.48	0.44	NA	0.40	NA	0.41	NA	0.27	NA
TiO_2	0.16	0.18	0.19	0.17	0.18	0.17	0.18	0.17	0.18
ZnO	0.16	0.17	0.15	0.17	0.15	0.17	0.15	0.16	0.14
ZrO_2	0.21	0.27	0.30	0.28	0.30	0.27	0.30	0.28	0.32
Sum	100.00	100.00	96.73	100.00	97.66	100.00	97.41	100.00	98.07

§ - Not a target constituent;
NA - Not analyzed
* - Target values for XRF-analyzed compositions
** - Determined by XRF on the polished sample surface

Table 5.4. List of Glass Discharged, Masses, and Analysis Performed during DM1200 Tests.

Date	Name	Analysis Performed	Observations Of Glass in Discharge Trough	Mass (kg)	Cumulative Mass (kg)	Foamy Glass Observed on Surface
10/20/2009	G-12N-150A	-	-	431.0	431.0	No
	G-12N-151A	XRF, DCP, F	-			
10/21/2009	G-12O-18A	-	-	425.5	856.5	No
	G-12O-20A	XRF	-			
	G-12O-35A	-	-	428.0	1284.5	No
	G-12O-37A	XRF. F	-			
10/22/2009	G-12O-37B	-	-	423.5	1708.0	Yes
	G-12O-53A	XRF, Internal Inspection	Minor Auto Discharge			
	G-12O-67A	-	-	424.0	2132.0	Yes
	G-12O-69A	XRF, F, Internal Inspection	-			
	G-12O-75A	-	-	413.5	2545.5	Yes
10/23/2009	G-12O-85A	XRF, Internal Inspection	-			
	G-12O-99A	-	-	424.5	2970.0	Yes
	G-12O-101A	XRF, F, Internal Inspection	-			
10/26/2009	G-12O-131A	-	-	405.0	3375.0	Yes
	G-12O-133A	XRF, Internal Inspection	-			
10/27/2009	G-12O-149A	-	-	413.5	3788.5	Yes
	G-12O-150A	XRF, F, Internal Inspection, SEM	Auto Discharge			
10/28/2009	G-12P-31A	-	Auto Discharge, Foamy Glass	385.5	4174.0	Yes
	G-12P-32A	XRF, Internal Inspection, SEM	Auto Discharge, Foamy Glass			
	G-12P-37A	-	Foamy Glass	416.5	4590.5	Yes
	G-12P-53A	XRF, Internal Inspection, SEM	Auto Discharge, Foamy Glass			
10/29/2009	G-12P-66A	-	Auto Discharge, Foamy Glass	404.5	4995.0	Yes
	G-12P-72A	XRF, F, Internal Inspection, SEM	Auto Discharge, Foamy Glass			
	G-12P-85A	-	-	407.5	5402.5	Yes
10/30/2009	G-12P-88A	XRF, Internal Inspection, SEM	Auto Discharge, Foamy Glass			
	G-12P-100A	-	Auto Discharge, Foamy Glass	413.0	5815.5	Yes
	G-12P-101A	XRF, Internal Inspection, SEM	Auto Discharge, Foamy Glass			
	G-12P-115A	-	Auto Discharge, Foamy Glass	251.0	6066.5	Yes
	G-12P-116A	XRF, DCP, F, Internal Inspection	-			

"-" empty data field

Table 5.5. XRF Analyzed Composition for Glass Discharged During DM1200 Melter Tests (wt%).

Glass (kg)	Target	431.0	856.5	1284.5	1708.0	2132.0	2545.5	2970.0	3375.0	3788.5
Constituent		G-12N-151A	G-12O-20A	G-12O-37A	G-12O-53A	G-12O-69A	G-12O-85A	G-12O-101A	G-12O-133A	G-12O-150A
Al_2O_3	11.66	21.34	19.08	17.48	16.41	15.25	14.64	14.25	13.88	13.44
B_2O_3*	11.30	17.95	16.63	15.57	14.73	14.05	13.52	13.08	12.75	12.47
BaO	0.01	0.05	0.04	0.03	0.03	0.03	0.03	0.02	0.02	0.02
Bi_2O_3	6.71	2.21	3.12	3.85	4.37	5.01	5.32	5.02	5.64	5.70
CaO	0.84	3.96	3.19	2.72	2.38	2.13	1.91	1.56	1.53	1.38
Cr_2O_3	0.52	0.54	0.56	0.53	0.59	0.62	0.66	0.61	0.61	0.61
F	0.82	0.27#	0.33	0.40#	0.39	0.37#	0.37	0.38#	0.36	0.34#
Fe_2O_3	6.96	6.20	6.24	6.29	6.59	6.89	6.98	6.45	6.85	6.80
K_2O	0.46	0.23	0.28	0.31	0.36	0.37	0.39	0.39	0.41	0.42
Li_2O*	0.16	3.00	2.44	1.98	1.63	1.34	1.11	0.92	0.78	0.66
MgO	0.43	0.25	0.34	0.36	0.42	0.42	0.50	0.51	0.50	0.52
MnO	§	0.05	0.04	0.04	0.04	0.04	0.04	0.03	0.03	0.03
Na_2O	15.74	11.05	11.91	12.76	12.66	13.75	13.53	15.08	13.98	14.82
NiO	1.93	0.51	0.73	0.82	1.08	1.30	1.38	1.34	1.45	1.47
P_2O_5	4.99	1.93	2.69	3.32	3.68	3.84	4.16	4.36	4.54	4.61
PbO	0.25	0.39	0.35	0.33	0.31	0.32	0.30	0.26	0.27	0.25
SiO_2	36.26	29.26	31.18	32.33	33.44	33.37	34.26	34.92	35.53	35.61
SO_3	0.48	0.17	0.21	0.23	0.25	0.24	0.25	0.26	0.24	0.25
TiO_2	0.16	0.10	0.11	0.13	0.13	0.14	0.15	0.14	0.15	0.15
ZnO	0.16	0.11	0.12	0.13	0.14	0.15	0.16	0.14	0.16	0.15
ZrO_2	0.21	0.45	0.40	0.37	0.36	0.36	0.34	0.28	0.31	0.30
Sum	100.00	100.00	100.00	100.00	100.00	100.00	100.00	100.00	100.00	100.00

§ - Not a target constituent
* - Target values calculated using simple well-stirred tank model
# - Fluorine was measured by XRF on polished samples, values for other samples calculated by interpolation

Table 5.5. XRF Analyzed Composition for Glass Discharged During DM1200 Melter Test (wt%) (continued).

Glass (kg)	Target	4174.0	4590.5	4995.0	5402.5	5815.5	6066.5	
Constituent		G-12P-32A	G-12P-53A	G-12P-72A	G-12P-88A	G-12P-101A	G-12P-116A	%Dev.
Al2O3	11.66	13.37	12.79	12.49	12.53	12.22	12.10	3.79
B_2O_3*	11.30	12.26	12.07	11.92	11.81	11.71	11.66	NC
BaO	0.01	0.02	0.02	0.02	0.02	0.01	0.02	NC
Bi_2O_3	6.71	5.61	6.07	6.29	5.96	6.53	6.29	-6.21
CaO	0.84	1.30	1.23	1.22	1.10	1.16	1.08	NC
Cr_2O_3	0.52	0.61	0.62	0.60	0.59	0.66	0.65	NC
F	0.82	0.34	0.34	0.34#	0.37	0.41	0.43#	NC
Fe_2O_3	6.96	6.66	6.93	7.07	6.73	7.28	7.06	1.41
K_2O	0.46	0.42	0.44	0.45	0.43	0.46	0.47	NC
Li_2O*	0.16	0.57	0.49	0.43	0.38	0.33	0.31	NC
MgO	0.43	0.51	0.51	0.54	0.54	0.51	0.50	NC
MnO	§	0.03	0.03	0.03	0.03	0.04	0.03	NC
Na_2O	15.74	14.71	15.17	15.15	16.39	15.40	15.90	1.02
NiO	1.93	1.46	1.56	1.61	1.60	1.75	1.78	-7.55
P_2O_5	4.99	4.78	4.78	4.88	4.86	4.92	5.00	0.28
PbO	0.25	0.24	0.25	0.25	0.23	0.26	0.24	NC
SiO_2	36.26	36.31	35.83	35.84	35.60	35.45	35.61	-1.77
SO_3	0.48	0.23	0.25	0.25	0.26	0.26	0.27	NC
TiO_2	0.16	0.16	0.16	0.16	0.16	0.17	0.17	NC
ZnO	0.16	0.15	0.16	0.17	0.16	0.17	0.16	NC
ZrO_2	0.21	0.28	0.29	0.30	0.27	0.30	0.28	NC
Sum	100.00	100.00	100.00	100.00	100.00	100.00	100.00	NC

§ - Not a target constituent.
* - Target values calculated using simple well-stirred tank model.
# - Fluorine was measured by XRF on polished samples, values for other samples calculated by interpolation.
NC – Not calculated

Table 5.6. SEM Results on Selected Glass Samples Discharged During DM1200 Testing.

Sampling Date	Sample I.D.	Sample Location	Crystallinity (vol.%)	SEM Observations	Estimated Porosity (vol.%)
10/27/09	G-12O-150A	Drum Surface	4.9	Sample contains secondary phases and large vesicles. The secondary phases consist of about 45 to 50% spinel and 50-55% apatite. Very fine particles (about 300 nm) rich in phosphorus	ND
10/27/09	G-12O-150A-4	Right half of drum, glazed area of glass near center	4.9	Sample contains secondary phases and large vesicles. The secondary phases consist of about 40 to 45% spinel and 55-60% apatite. Probably metallic Bi spheres/droplets appear locally, containing several percent of fluorine.	11.2
10/28/09	G-12P-32A-1	Left half of drum, near thermowell, includes suspect metal contamination	ND	Thin metallic flake in the glass matrix. Metallic Fe with trace of Cr and Si. Small amount of glass adhered with high content of Bi some spinel and apatite. The spinel crystals are rich in Cr.	ND
10/28/09	G-12P-32A-3	Left half of drum suspect secondary phase	4.8	Sample contains secondary phases and many large vesicles. The secondary phases consist of about 45 to 50% spinel, 50-55% apatite. Very tiny particles of about 300 nm may be indicative of early apatite nucleation.	10-25
10/28/09	G-12P-53A	Drum Surface	1.7	Only spinel was observed.	32.7
10/29/09	G-12P-72A-1	Left half of drum around thermowell	4.4	The glass contains 1.75% spinel and 2.6% apatite needle like crystals.	25.8
10/30/09	G-12P-88A-1	Center of drum, left half	5.8	The glass contains 2.53% spinel and 3.3% apatite. Apatite appears as short cylinders and dendrite. Large spinel crystals (>10μm) are Cr-rich and the small ones (<10 μm) Cr-poor.	19.0
10/30/09	G-12P-101A-1	Left half of drum, near thermowell	3.1	The glass contains 2.0% spinel and 1.1% apatite. Larger spinel crystals are rich in Cr with Fe and Ni. The smaller crystals (<10 μm) are depleted in Cr. Apatite is present as short cylinders and dendrites of smaller particles.	12.3

ND – Not Determined.

Table 5.7. Calculated Glass Density and Porosity.

Name	Mass (kg)	Volume (liters)	Calculated Bulk Density (g/cc)	Measured Density of Glass from the Surface of Drum (g/cc)	Calculated Micro-porosity (Vol. %)	Calculated Bulk porosity (Vol. %)
G-12O-37B	423.5	171.9	2.46	2.6258	2.31	8.48
G-12O-53A						
G-12O-67A	424.0	170.3	2.46	2.6485	1.46	8.48
G-12O-69A						
G-12O-75A	413.5	170.7	2.40	2.5902	3.63	10.71
G-12O-85A						
G-12O-99A	424.5	174.3	2.44	2.4394	9.24	9.22
G-12O-101A						
G-12O-131A	405.0	169.0	2.35	2.1992	18.18	12.57
G-12O-133A						
G-12O-149A	413.5	176.1	2.32	2.3307	13.29	13.68
G-12O-150A						
G-12P-31A	385.5	170.5	2.26	2.3005	14.41	15.92
G-12P-32A						
G-12P-37A	416.5	177.9	2.34	2.3404	12.93	12.94
G-12P-53A						
G-12P-66A	404.5	171.9	2.35	2.2433	16.54	12.57
G-12P-72A						
G-12P-85A	407.5	179.9	2.27	2.1944	18.36	15.54
G-12P-88A						
G-12P-100A	413.0	170.3	2.34	2.2371	16.77	12.94
G-12P-101A						
G-12P-115A	251.0	115.1	2.17	2.3631	12.08	19.26
G-12P-116A						

Table 5.8. Chronology of Bubbler Use while Processing High Bismuth Feeds.

Double-Ported Bubblers Used	DB-3 in Port A3*
	DB-4 in Port D1
Installation	9/24/09 12:30
Operating duration with high-bismuth feed	193 hours
Idling time between the two high-bismuth feeding periods	60 hours
Idling time prior to melt pool turnover after completion of high-bismuth tests	97 hours
Operation time for turnover with bismuth-free feed	30.5 hours
Removal and inspection	11/5/09 09:30
Total time immersed in bismuth rich glass	383 hours
Original dimensions of foot on bubbler bottom	Inconel 690, 1.75" x 1.5" x 0.5"#
Original distance between the end of foot to the bubbler tip	1.5"

* - See Figure 1.4 for port locations.
# - See Figure 1.3

Table 5.9. Caliper Readings (Inches) of Bubbler Dimensions Before and After Exposure to High Bismuth Feeds.

Location	DB-3		DB-4	
	Before	After	Before	After
48" from bottom	1.050	1.048	1.050	1.050
36" from bottom	1.053	1.048	1.052	1.047
24" from bottom	1.052	1.045	1.056	1.045
18" from bottom	1.055	1.046	1.048	1.046
12" from bottom	1.047	1.047	1.052	1.044
6" from bottom	1.051	1.044	1.057	1.046
12" from tip	1.041	1.037	1.040	1.038
6" from tip	1.050	1.045	1.055	1.045
Average loss during testing, inches	0.005		0.006	
Visually estimated loss of original foot	60%	95%	0%	75%
Visually estimated loss of material between the foot and end of bubbler	0%	70%	0%	50%

Table 6.1. Results from DM1200 Off-Gas Emission Samples.

		10/26/2009 14:29 – 15:29 21.9% Moisture; 104% Isokinetic				10/28/2009 11:50 – 12:50 19.5% Moisture; 95.4% Isokinetic			
		Feed[#] (mg/min)	Output (mg/min)	% Emitted	DF	Feed[#] (mg/min)	Output (mg/min)	% Emitted	DF
Particulate	Total[$]	903857	2293	0.25	394	682504	1566	0.23	436
	Al	50375	38.7	0.08	1302	38038	26.80	0.07	1419.2
	Bi	24577	108	0.44	228	18558	78.47	0.42	236.5
	B	28640	94.4	0.33	303	21626	58.97	0.27	366.7
	Ba	73	0.37	0.51	197	55	0.14	0.25	404.5
	Ca	4903	12.5	0.25	393	3703	6.57	0.18	563.3
	Cr	2906	13.2	0.45	221	2194	16.86	0.77	130.2
	F*	6697	14.0	< 0.01	478	5057	23.2	0.46	218
	Fe	39745	69.7	0.18	571	30012	39.95	0.13	751.2
	K	3119	22.4	0.72	139	2355	19.29	0.82	122.1
	Li	607	7.03	1.16	86.4	458	4.96	1.08	92.4
	Mg	2117	8.51	0.40	249	1599	4.43	0.28	360.6
	Na	95371	329	0.35	290	72015	540.84	0.75	133.2
	Ni	12386	27.2	0.22	456	9352	14.21	0.15	658.2
	P	17793	48.98	0.28	363.3	13436	26.73	0.20	502.7
	Pb	1895	8.30	0.44	229	1431	6.64	0.46	215.5
	S*	1571	25.8	1.64	60.9	1186	55.6	4.69	21.3
	Si	138427	188	0.14	735	104527	108.49	0.10	963.5
	Ti	783	2.97	0.38	264	592	1.62	0.27	364.4
	Zn	1050	2.01	0.19	522	793	1.12	0.14	709.9
	Zr	1270	2.07	0.16	613	959	0.79	0.08	1215.5
Gas	B	28640	197	0.69	145	21626	154.76	0.72	139.7
	F	6697	944	14.1	7.1	5057	1000	19.78	5.1
	S	1571	291	18.5	5.4	1186	292	24.61	4.1

[$] - From gravimetric analysis of filters and particulate nitric acid rinses
[#] - Feed rate calculated from target composition and steady state production rate
* - Calculated from analysis of filter particulate by water dissolution

Table 6.1. Results from DM1200 Off-Gas Emission Samples (continued).

		10/29/2009 10:45 – 11:45 18.7% Moisture; 102% Isokinetic			
		Feed[#] (mg/min)	Output (mg/min)	% Emitted	DF
Particulate	Total[$]	627166	6160	0.98	102
	Al	34954	92.85	0.27	376.5
	Bi	17053	255.37	1.50	66.8
	B	19872	287.22	1.45	69.2
	Ba	51	0.92	1.81	55.2
	Ca	3402	36.21	1.06	94.0
	Cr	2016	16.84	0.84	119.7
	F*	4647	41.07	0.88	113
	Fe	27578	213.02	0.77	129.5
	K	2164	50.42	2.33	42.9
	Li	421	11.92	2.83	35.3
	Mg	1469	25.69	1.75	57.2
	Na	66176	842.91	1.27	78.5
	Ni	8594	83.24	0.97	103.3
	P	12346	133.46	1.08	92.5
	Pb	1315	15.09	1.15	87.2
	S*	1090	22.68	2.08	48.1
	Si	96052	644.08	0.67	149.1
	Ti	544	8.54	1.57	63.7
	Zn	728	5.62	0.77	129.5
	Zr	881	6.57	0.75	134.0
Gas	B	19872	132.24	0.67	150.3
	F	4647	534.15	11.50	8.7
	S	1090	209.57	19.23	5.2

[$] - From gravimetric analysis of filters and particulate nitric acid rinses
[#] - Feed rate calculated from target composition and steady state production rate
* - Calculated from analysis of filter particulate by water dissolution

Table 6.2. Average Concentrations [ppmv] of Selected Species in DM1200 Exhaust Measured by FTIR Spectroscopy.

	Melter outlet			SBS outlet			WESP outlet			SCR outlet		
	Aver.	Min.	Max.	Aver.	Min.	Max.	Aver.	Min.	Max.	Aver.	Min.	Max.
N_2O	<1.0	<1.0	2.1	<1.0	<1.0	7.7	<1.0	<1.0	2.3	<1.0	<1.0	16.3
NO	283	4.0	654	322	15.7	2005	280	49.0	822	261	<1.0	2870
NO_2	31.2	<1.0	83.5	38.5	<1.0	641	37.3	<1.0	171	162	<1.0	1590
NH_3	<1.0	<1.0	1.9	<1.0	<1.0	2.5	1.3	<1.0	8.9	<1.0	<1.0	3.8
H_2O%	20.5	10.3	35.6	8.4	4.3	12.0	8.7	5.1	15.9	8.4	1.4	10.7
CO_2 %	0.20	0.04	0.40	0.19	0.05	1.29	0.17	0.03	0.48	0.23	0.01	2.38
Nitrous Acid	<1.0	<1.0	<1.0	<1.0	<1.0	5.5	<1.0	<1.0	3.3	<1.0	<1.0	13.4
Nitric Acid	3.6	<1.0	27.2	<1.0	<1.0	7.7	<1.0	<1.0	2.2	<1.0	<1.0	9.7
HCN	<1.0	<1.0	<1.0	1.0	<1.0	<1.0	<1.0	<1.0	<1.0	<1.0	<1.0	<1.0
SO_2	23.0	9.4	42.8	6.0	<1.0	20.2	2.2	<1.0	8.4	1.8	<1.0	14.1
CO	<1.0	<1.0	1.7	<1.0	<1.0	6.8	<1.0	<1.0	3.3	1.9	<1.0	8.5
HCl	2.2	<1.0	23.3	<1.0	<1.0	5.7	<1.0	<1.0	<1.0	<1.0	<1.0	8.2
HF	21.1	4.1	45.2	10.8	4.6	27.0	3.1	1.4	19.0	5.1	1.4	13.3

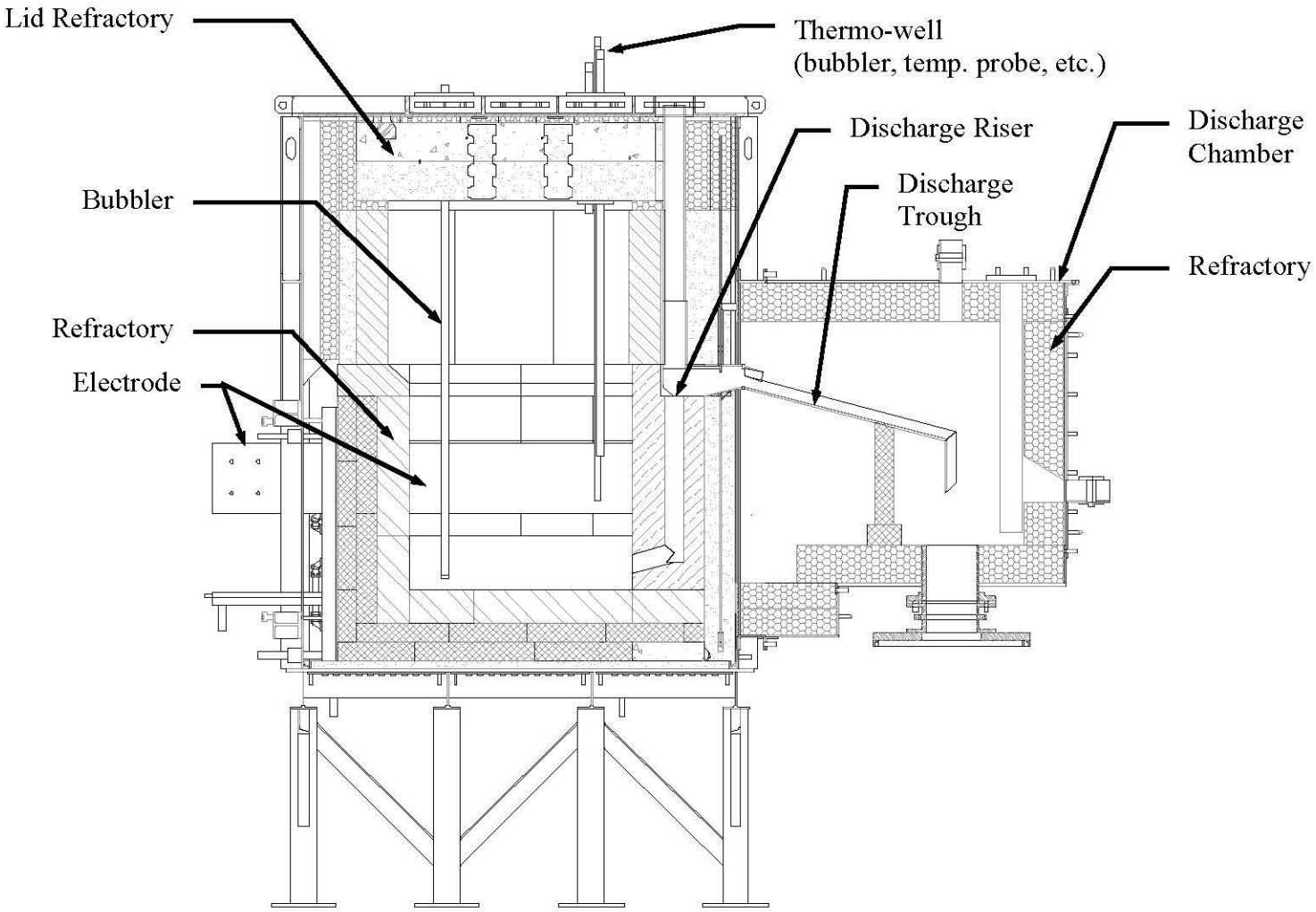

Figure 1.1. Cross-section of the DM1200 melter through the discharge chamber.

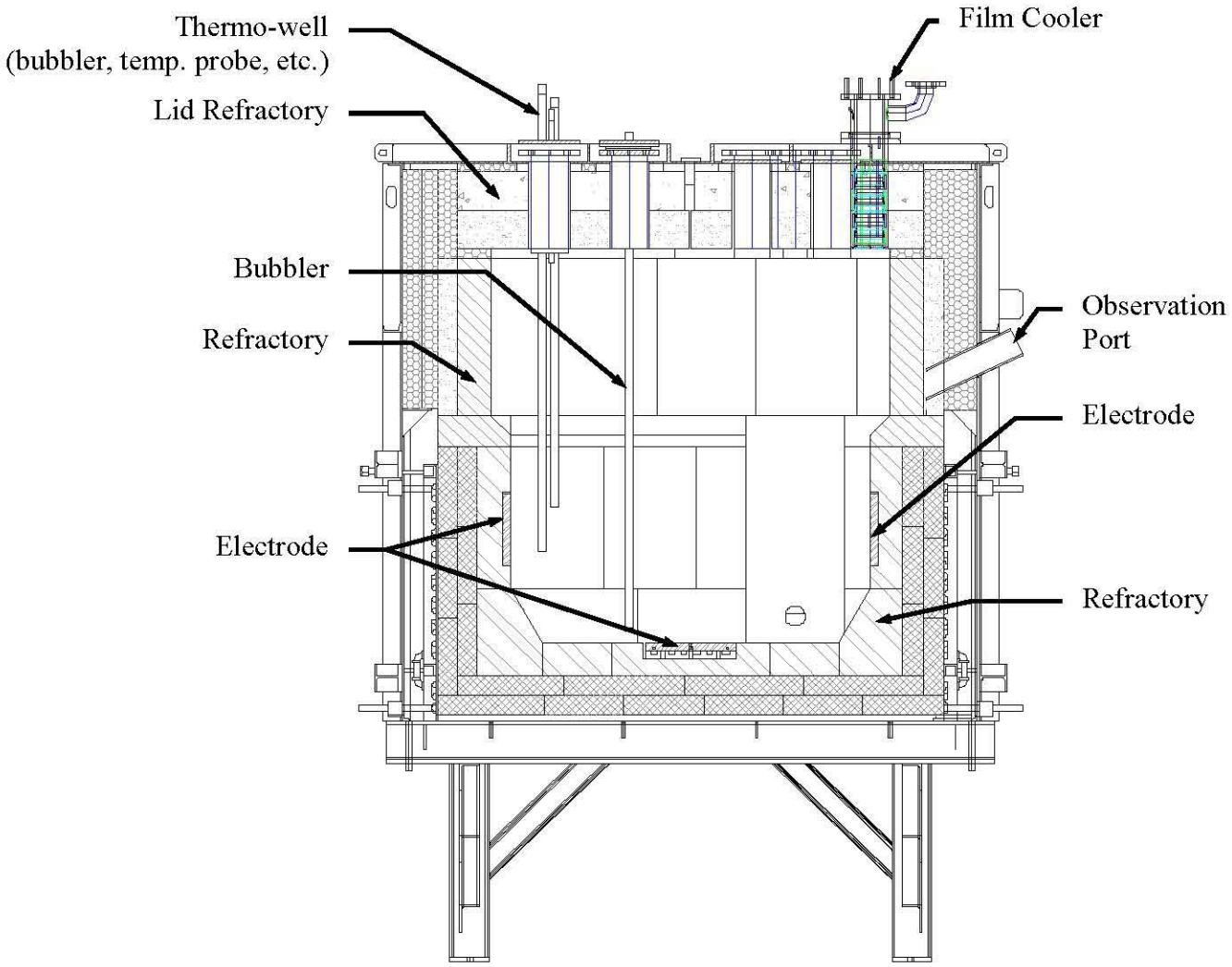

Figure 1.2. Cross-section through the DM1200 melter showing electrodes.

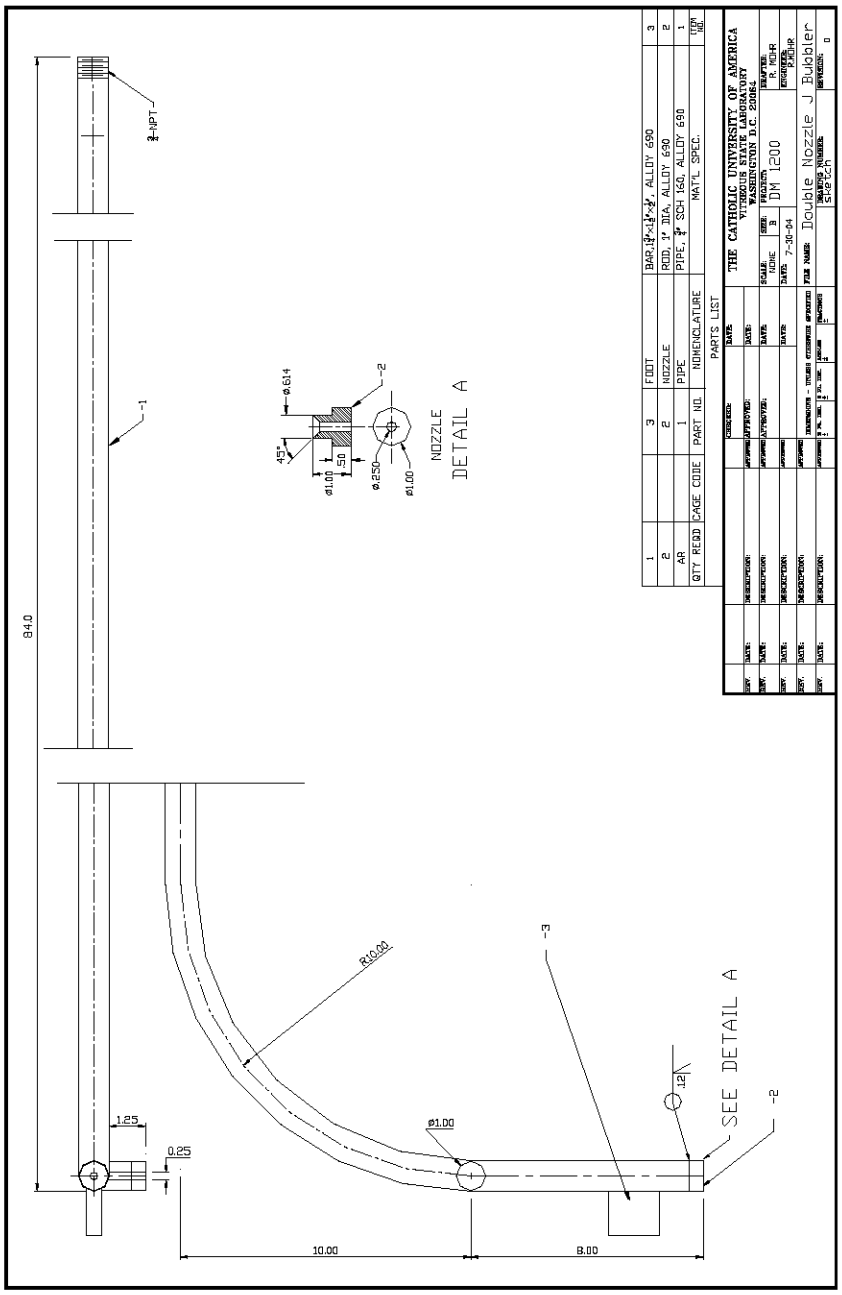

Figure 1.3. Specifications of Double Outlet "J" Bubbler.

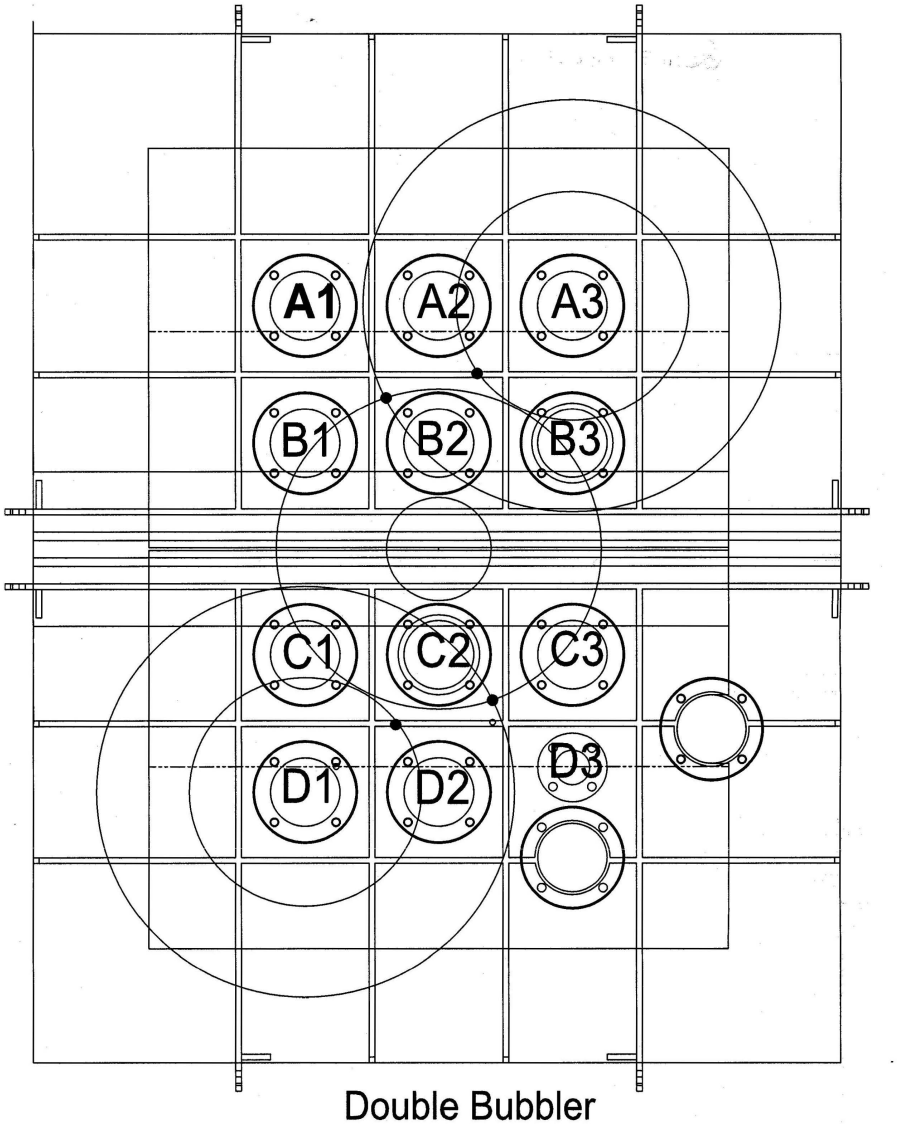

Figure 1.4. Placement of double outlet bubblers. Note: solid circles represent location of bubbler outlet.

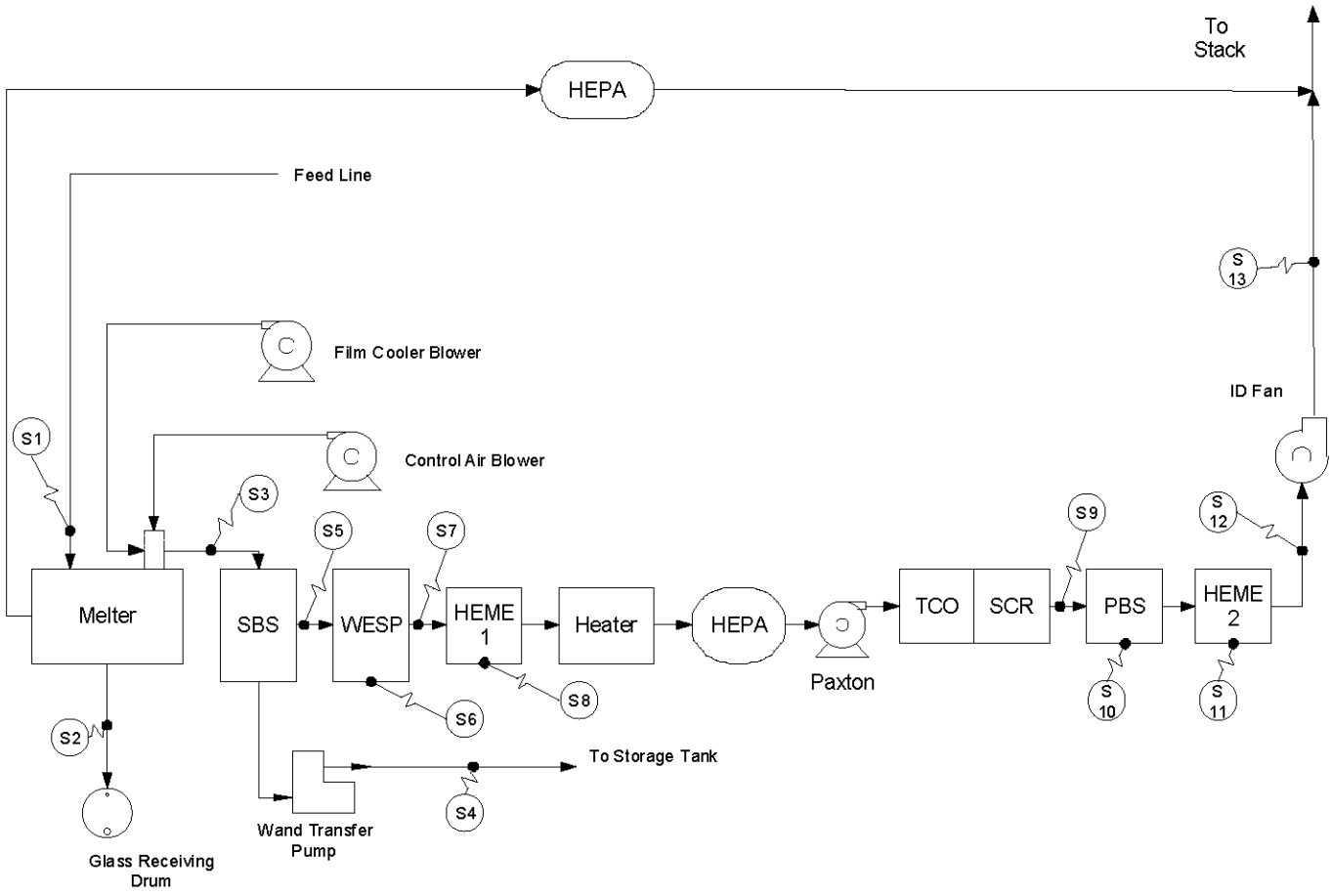

Figure 1.5. Schematic diagram of DM1200 off-gas system. "Sx" indicates sampling point.

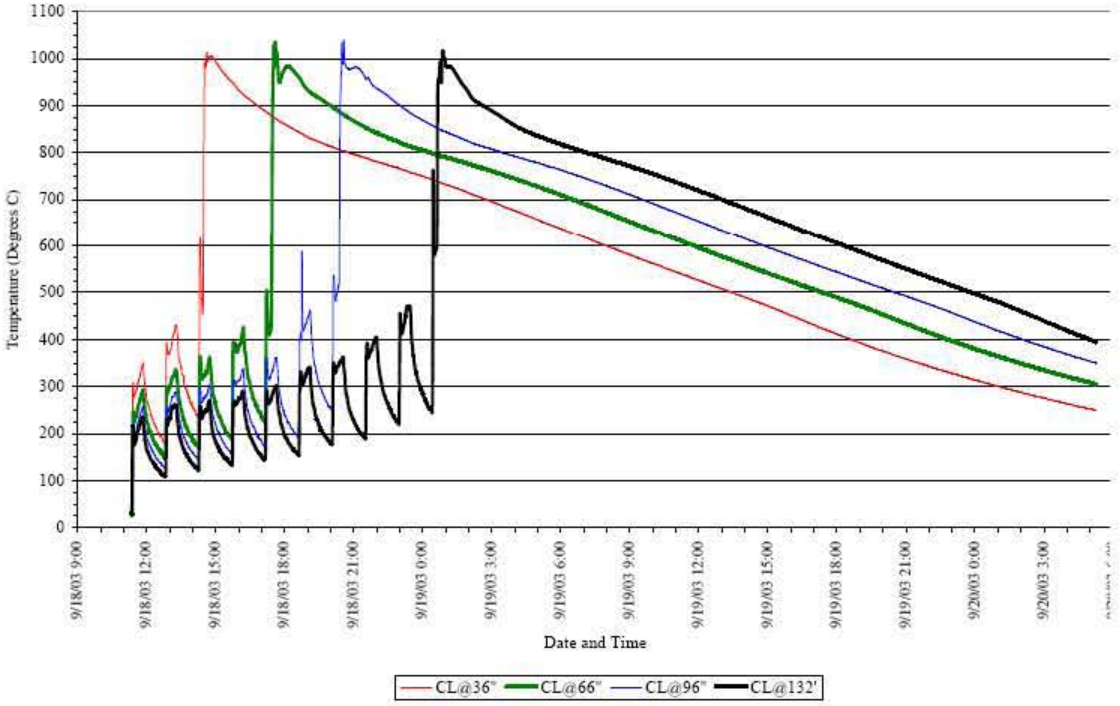

Figure 1.6. Glass Temperature Profile of HLW Canisters filled by the Energy*Solutions* LAW Pilot Melter.

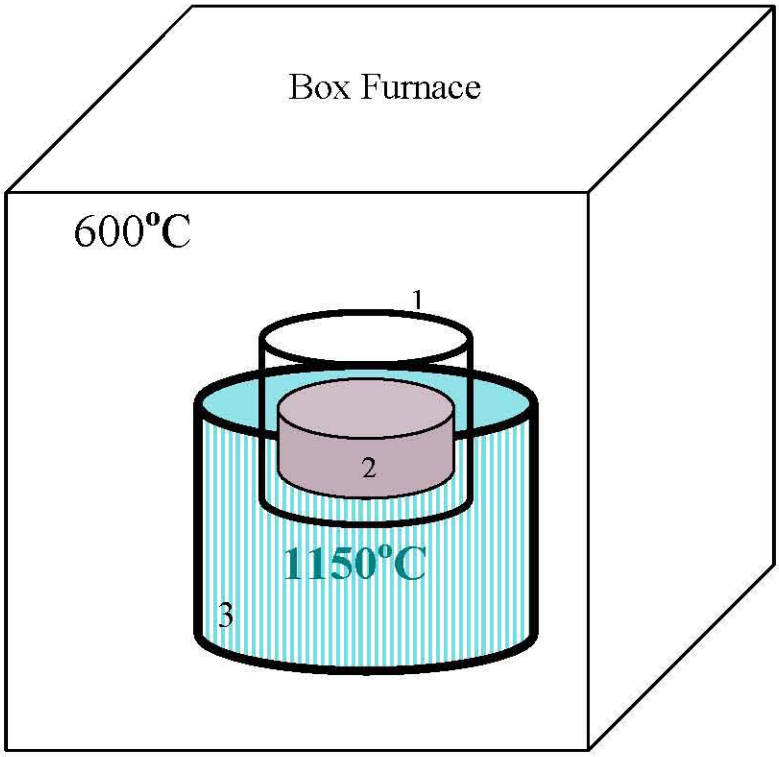

Figure 3.1. Schematic drawing of vertical gradient furnace (VGF) for feed conversion test (1=ceramic crucible half inside the local heater; 2=feed for 20 gram glass; 3=local heater at 1150°C).

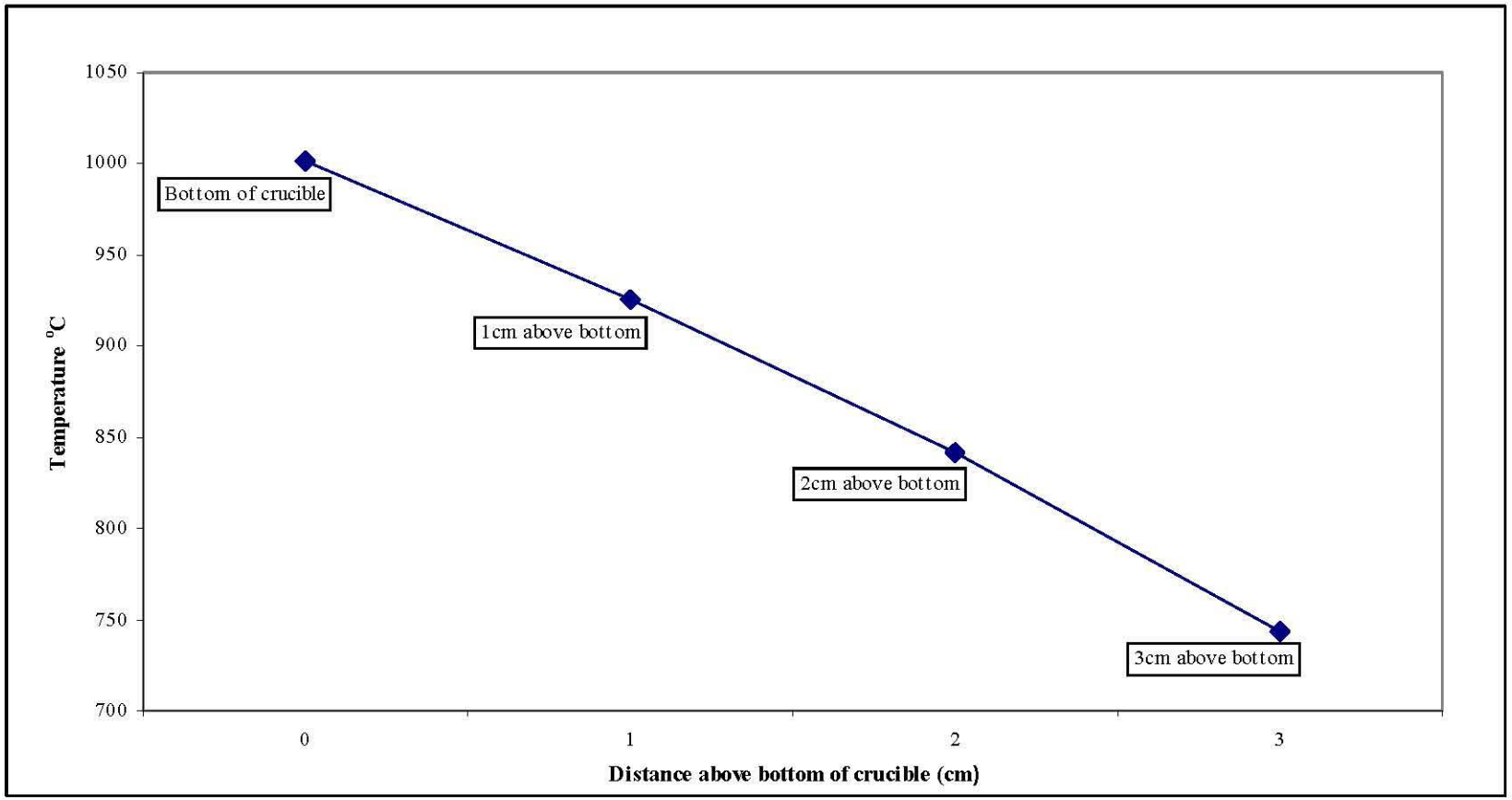

Figure 3.2. Temperature gradient (inside the loaded ceramic crucible) of the Vertical Gradient Furnace (VGF).

1)

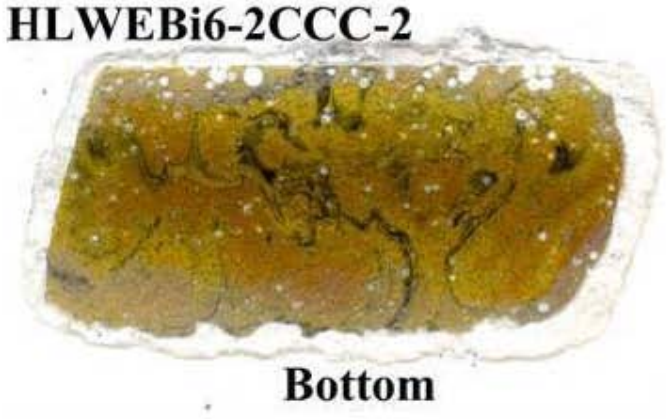

2)

3)

4)

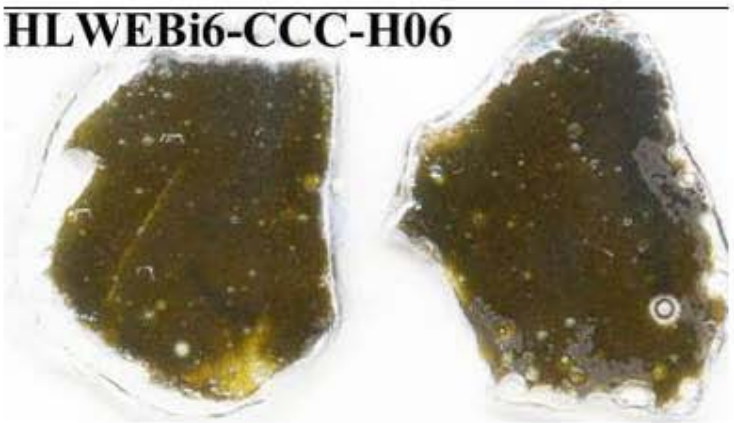

Figure 3.3a. 1) Scanned image of thin sections of HLW-E-Bi6 after CCC. "Bottom" indicates the sample orientation during CCC; 2)-4) Scanned images of the thin sections of HLW-E-Bi6 after 2, 4 and 6 hours of truncated CCC.

1)

2)

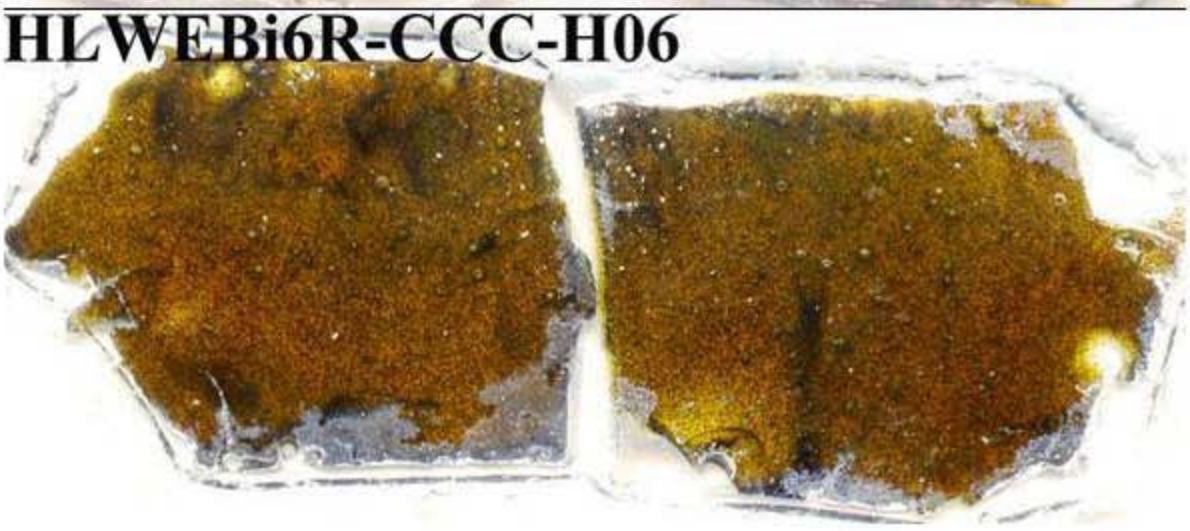

Figure 3.3b. (1)- (2) Scanned images of the thin sections of HLW-E-Bi6r after 2 and 6 hours of truncated CCC.

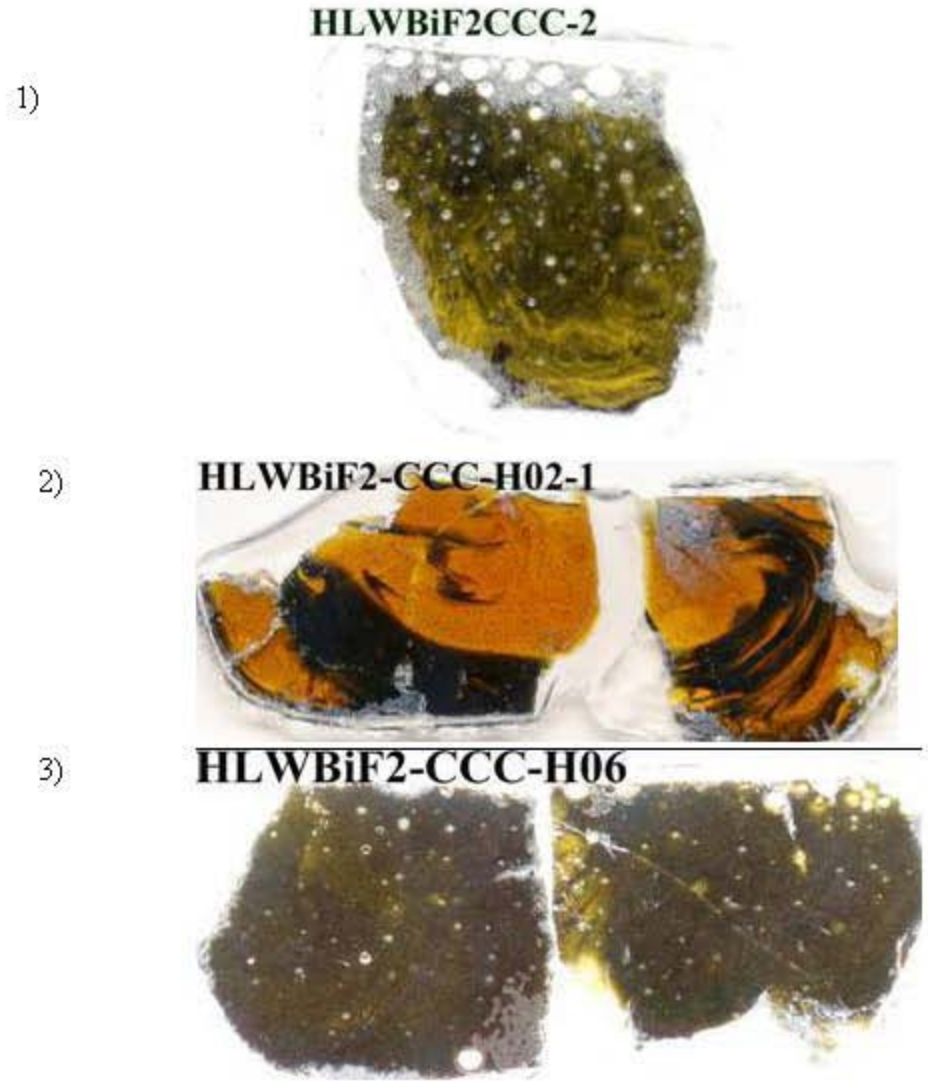

Figure 3.3c. 1) Scanned image of thin sections of HLW-Bi-F2 after CCC; 2)-3) Scanned images of the thin sections of HLW-Bi-F2 after 2 and 6 hours of truncated CCC.

1)

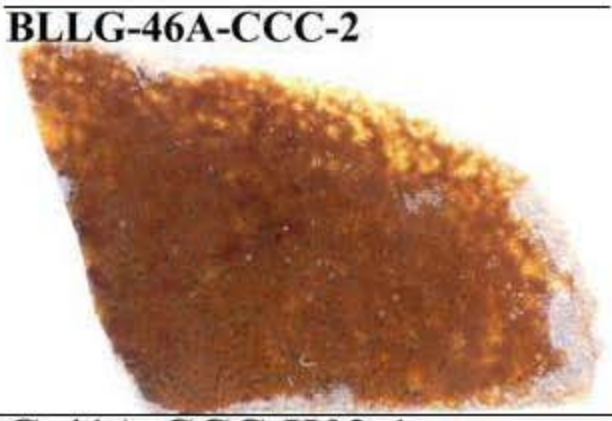

2)

3)

Figure 3.3d. 1) Scanned image of thin sections of BLL-G-41A after CCC; 2)-3) Scanned images of the thin sections of BLL-G-41A after 2 and 6 hours of truncated CCC.

1)

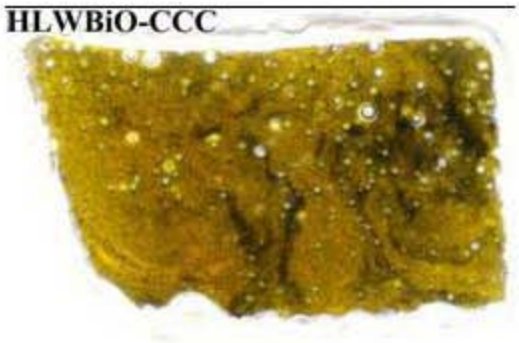

2)

3)

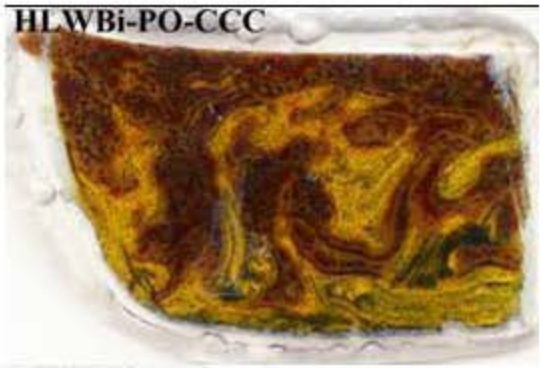

4)

Figure 3.3e. 1) Scanned image of thin section of HLW-Bi-Bi0 after CCC; 2) Scanned image of the thin section of HLW-Bi-F0 after CCC; 3) Scanned image of the thin section of HLW-Bi-P0 after CCC; 4) Scanned images of the thin section of HLW-Bi-BiP0 after CCC.

1)

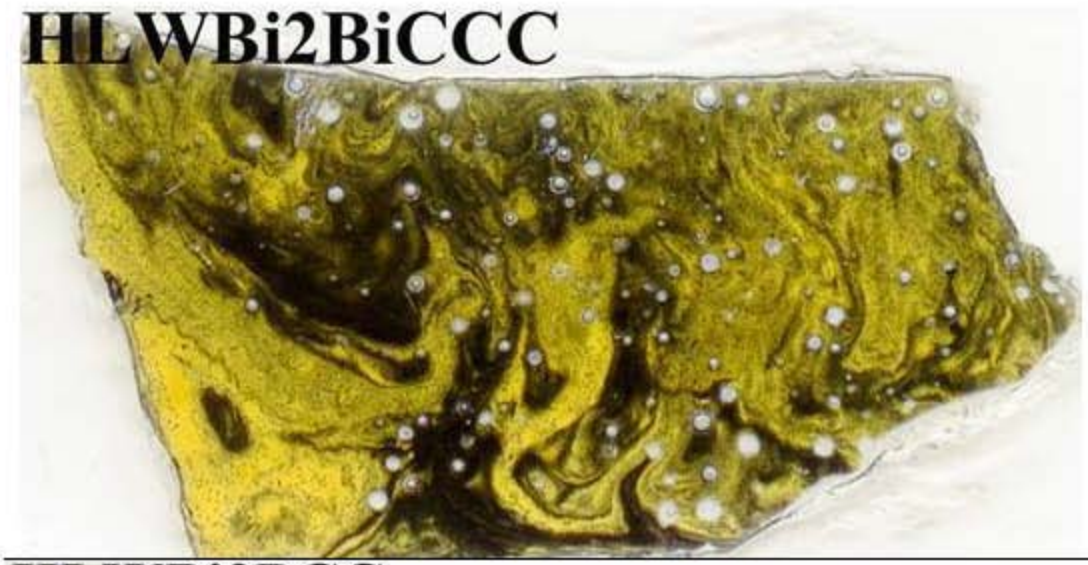

2)

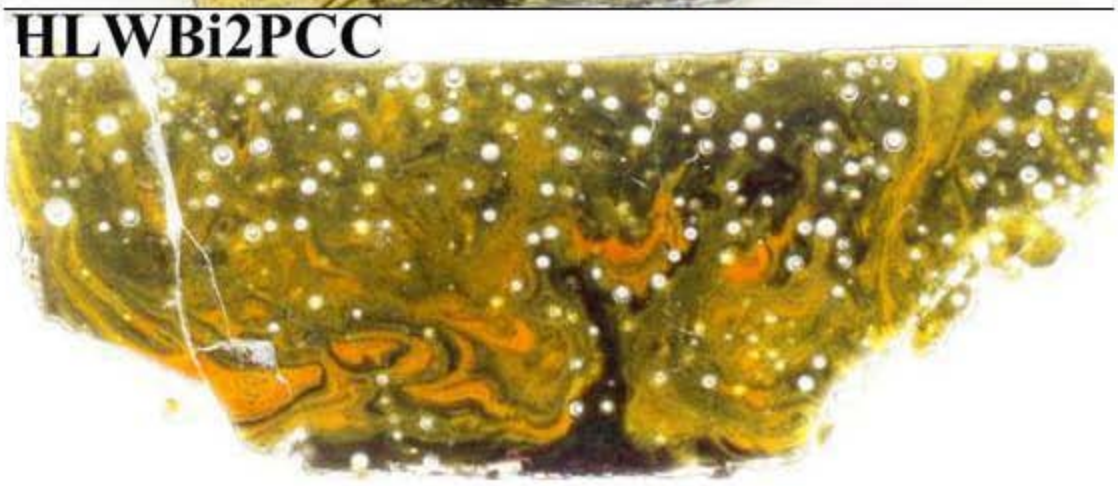

Figure 3.3f. 1) Scanned image of thin section of HLW-Bi-2Bi after CCC; 2) Scanned image of the thin section of HLW-Bi-2P after CCC.

Figure 3.3g. Scanned image of thin section of HLW-Bi-2P0Cr after CCC.

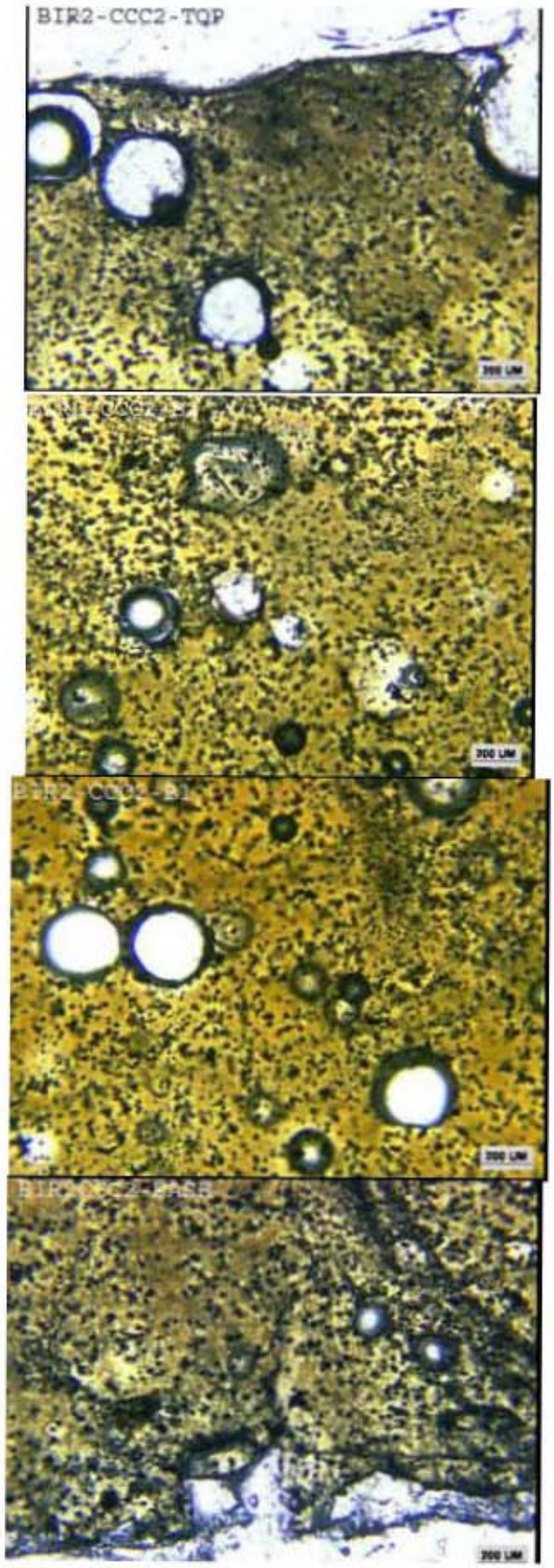

Figure 3.4a. Transmission optical microscopic images of HLW-E-Bi6r after CCC.

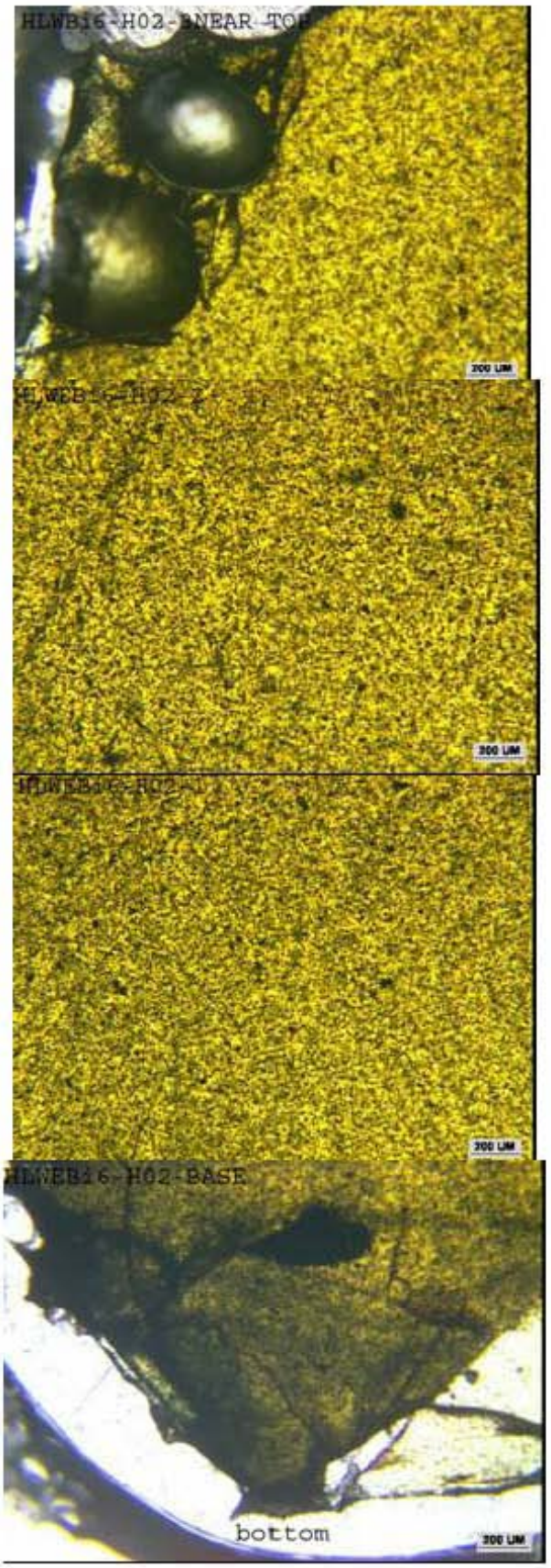

Figure 3.4b. Transmission optical microscopic images of HLW-E-Bi6 after truncated 2 hour CCC.

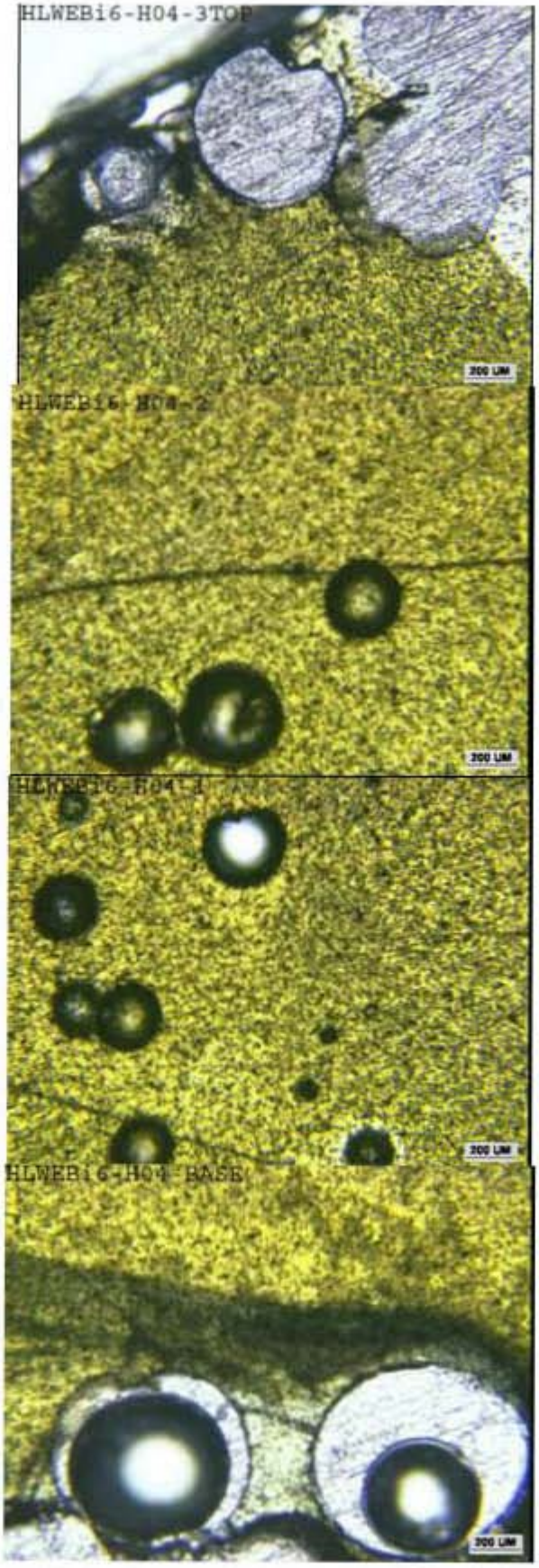

Figure 3.4c. Transmission optical microscopic images of HLW-E-Bi6 after truncated 4 hour CCC.

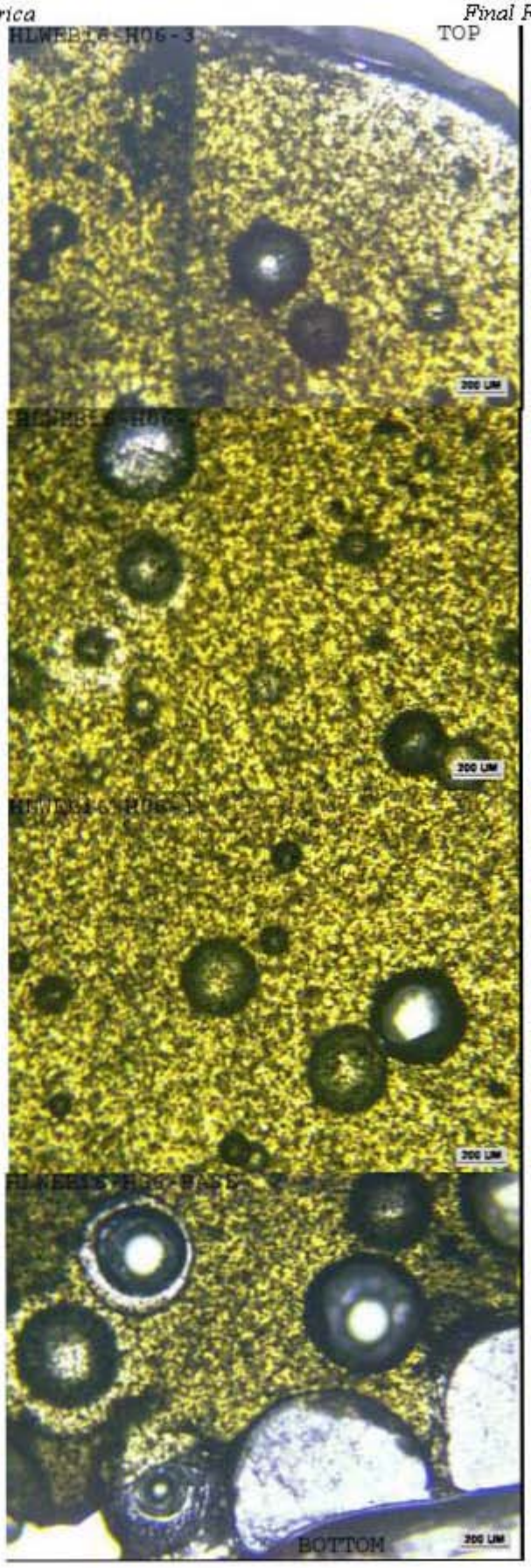

Figure 3.4d. Transmission optical microscopic images of HLW-E-Bi6 after truncated 6 hour CCC.

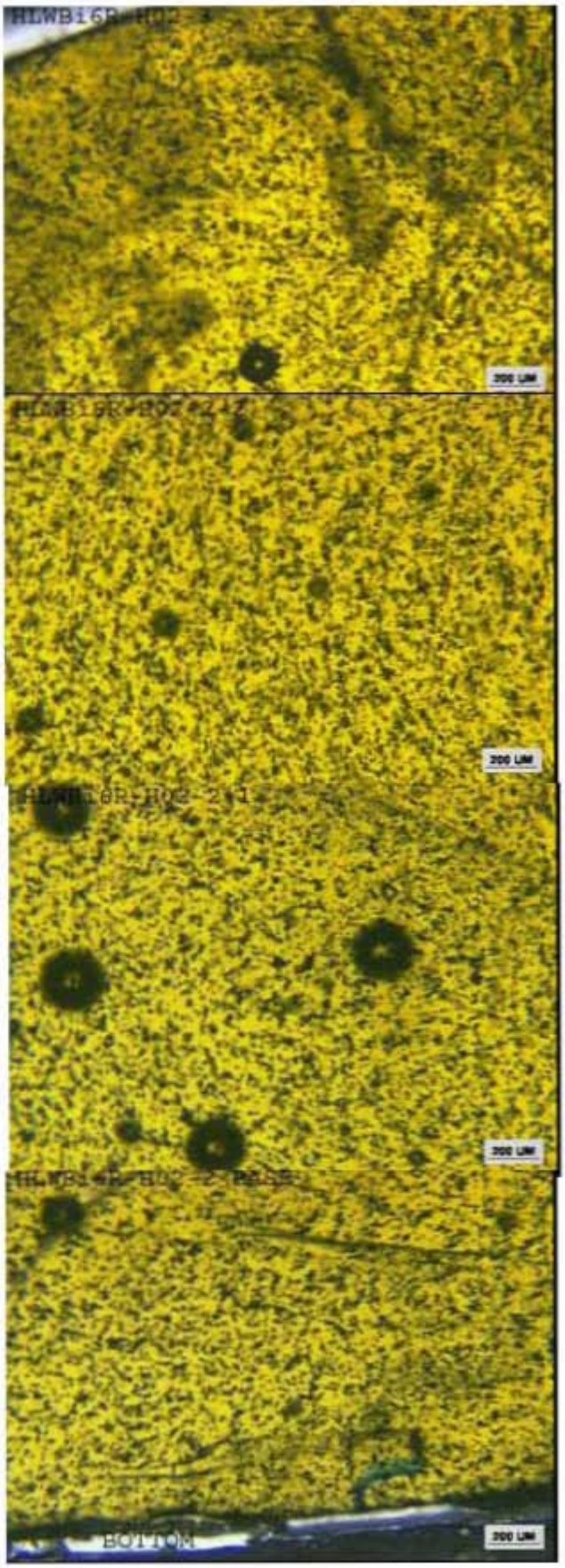

Figure 3.4e. Transmission optical microscopic images of HLW-E-Bi6r after truncated 2 hour CCC.

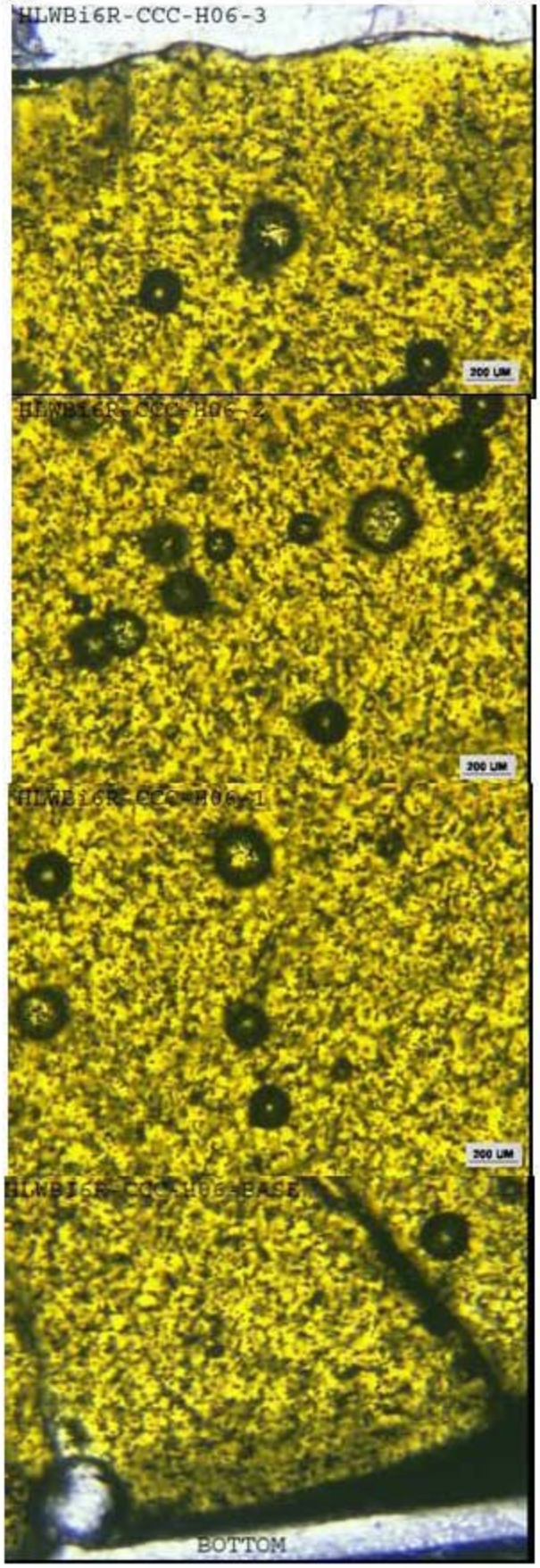

Figure 3.4f. Transmission optical microscopic images of HLW-E-Bi6r after truncated 6 hour CCC.

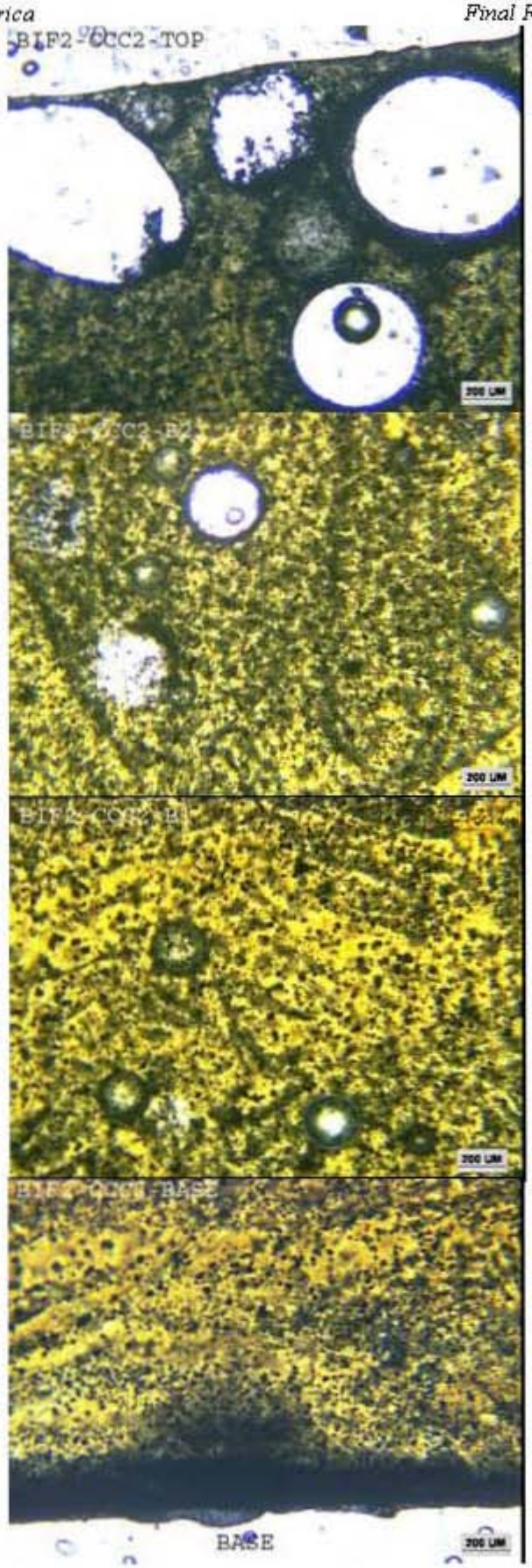

Figure 3.4g. Transmission optical microscopic images of HLW-Bi-F2 after CCC.

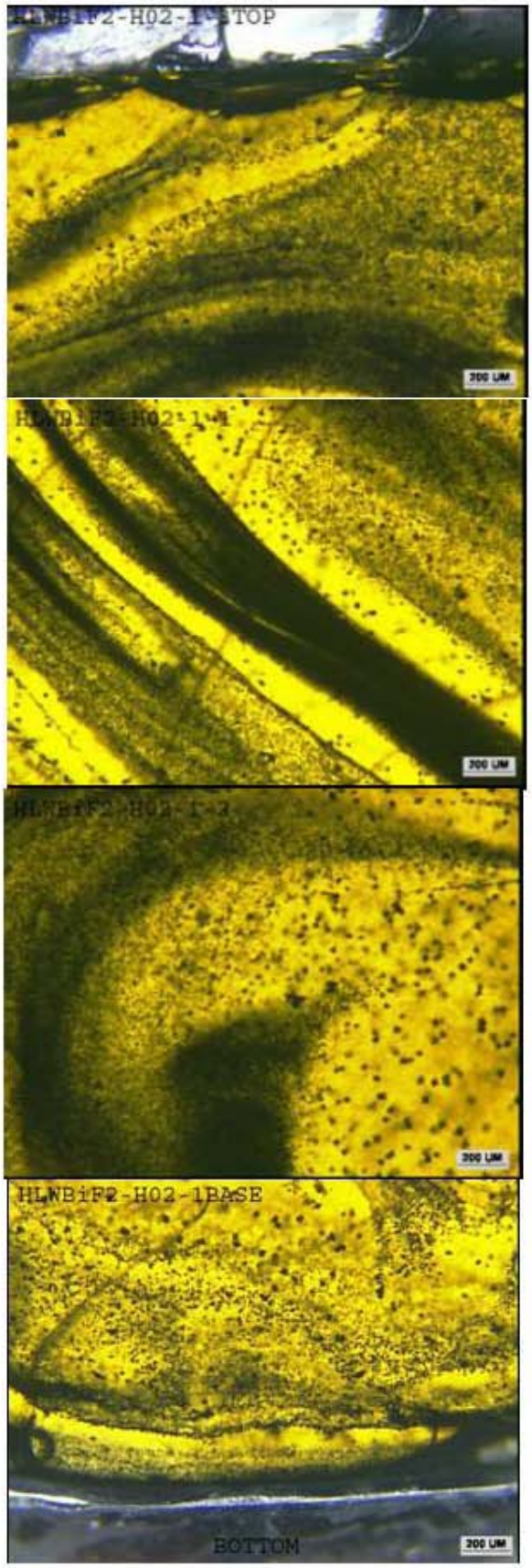

Figure 3.4h. Transmission optical microscopic images of HLW-Bi-F2 after truncated 2 hour CCC.

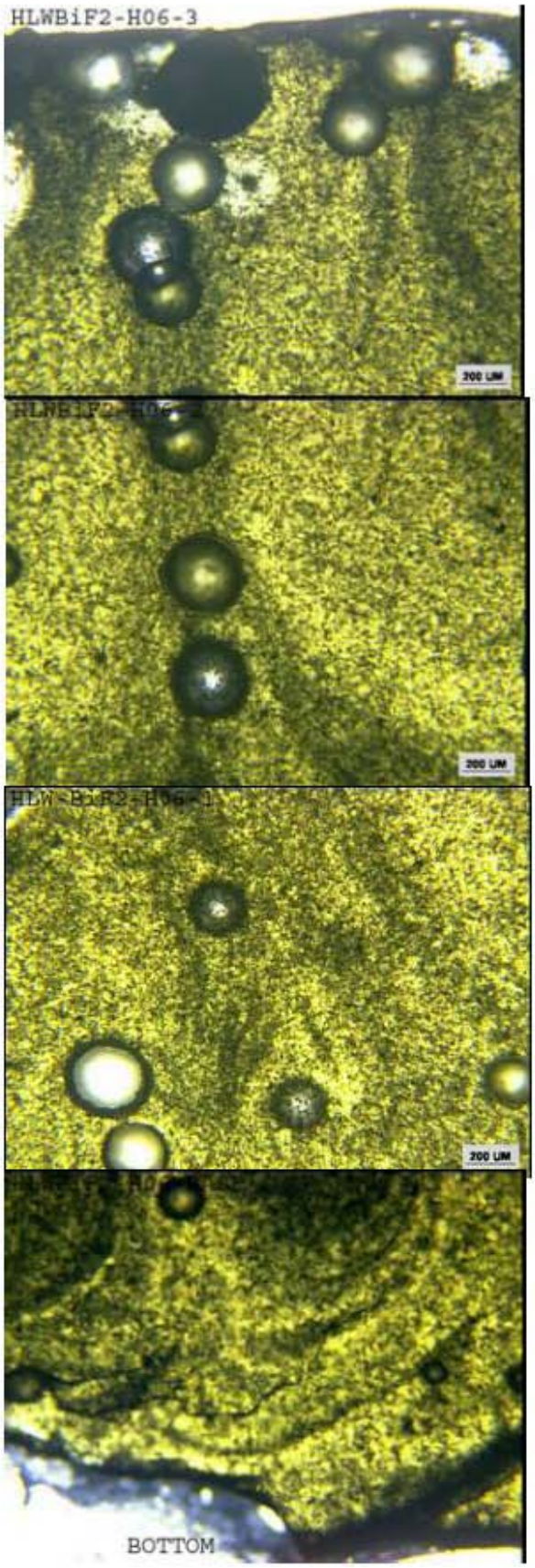

Figure 3.4i. Transmission optical microscopic images of HLW-Bi-F2 after truncated 6 hour CCC.

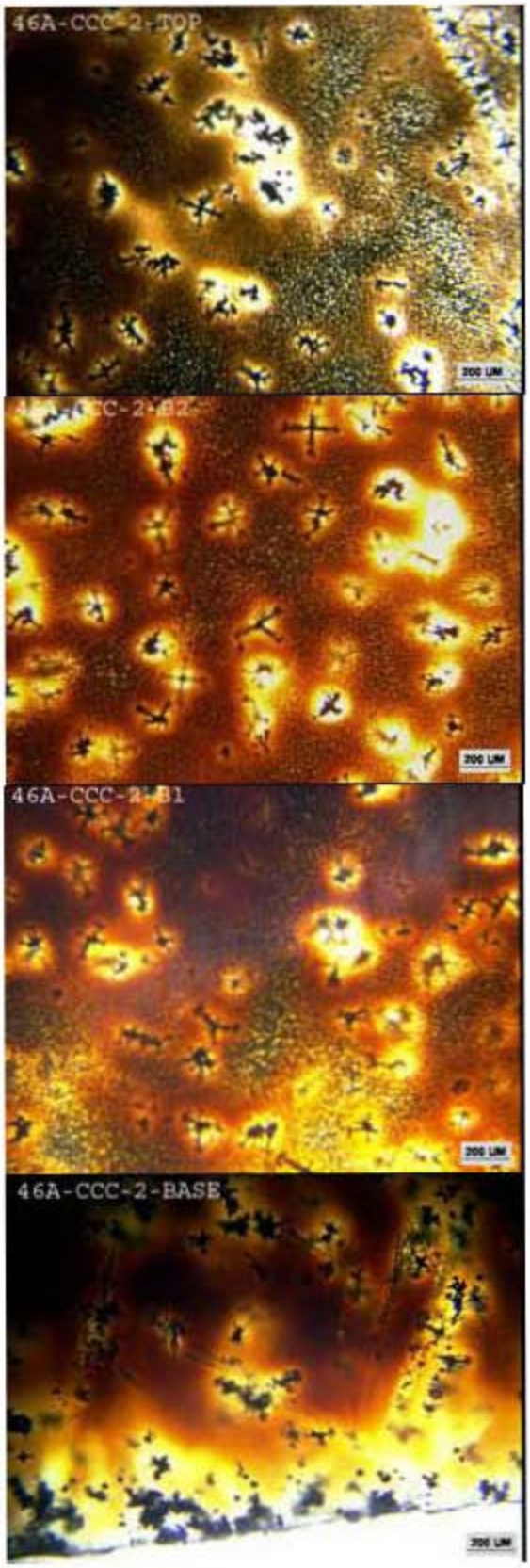

Figure 3.4j. Transmission optical microscopic images of BLL-G-46A after CCC.

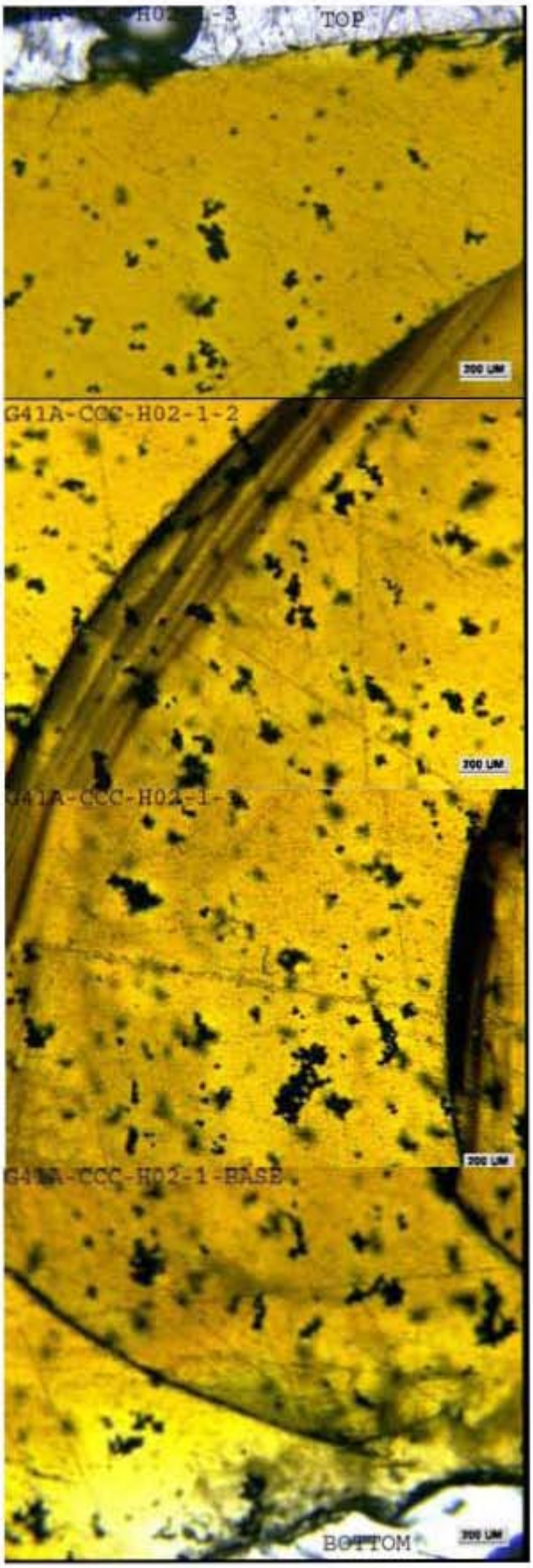

Figure 3.4k. Transmission optical microscopic images of BLL-G-46A after truncated 2 hour CCC.

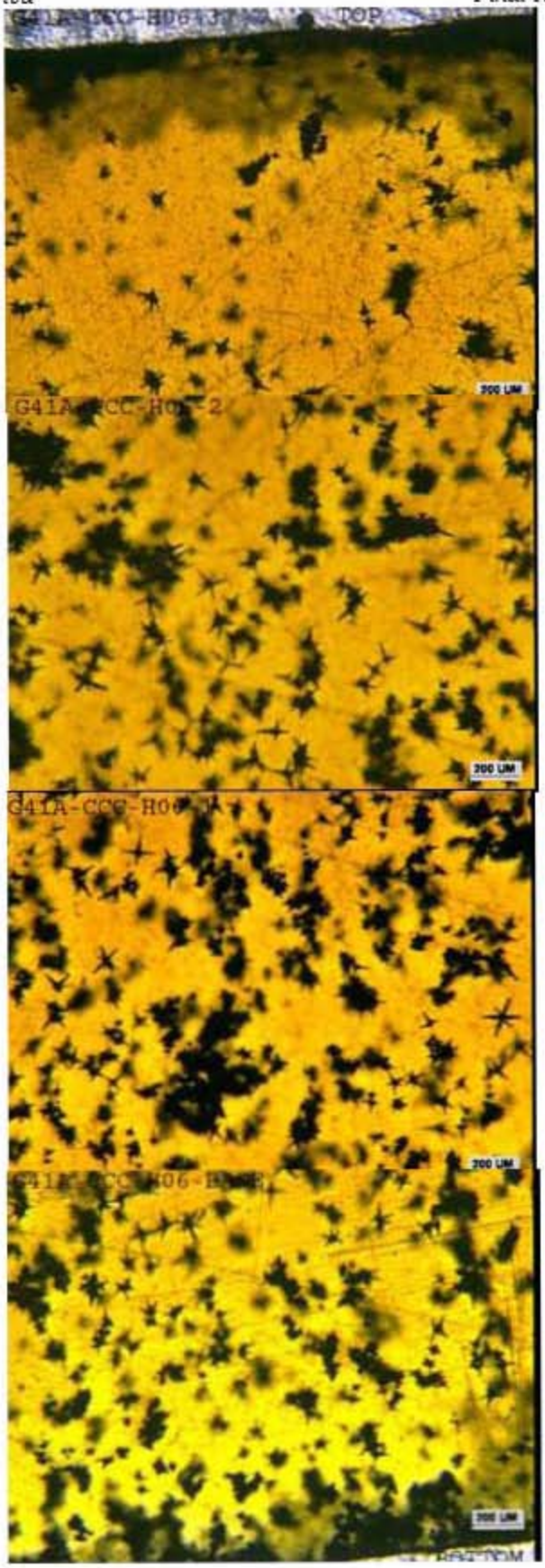

Figure 3.4l. Transmission optical microscopic images of BLL-G-46A after truncated 6 hour CCC.

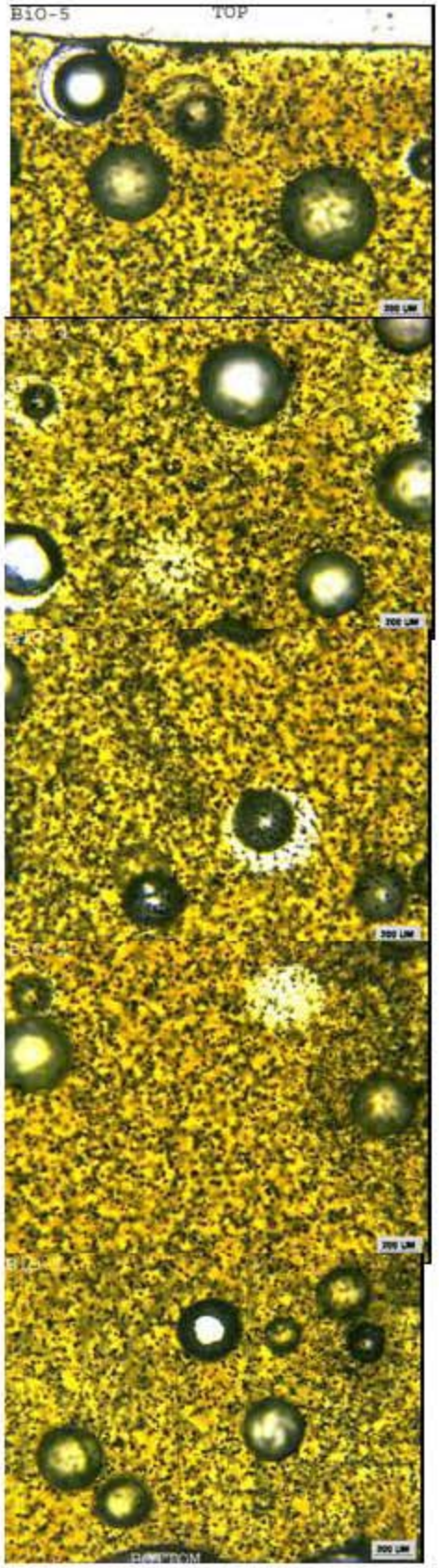

Figure 3.4m. Transmission optical microscopic images of HLW-Bi-Bi0 after CCC.

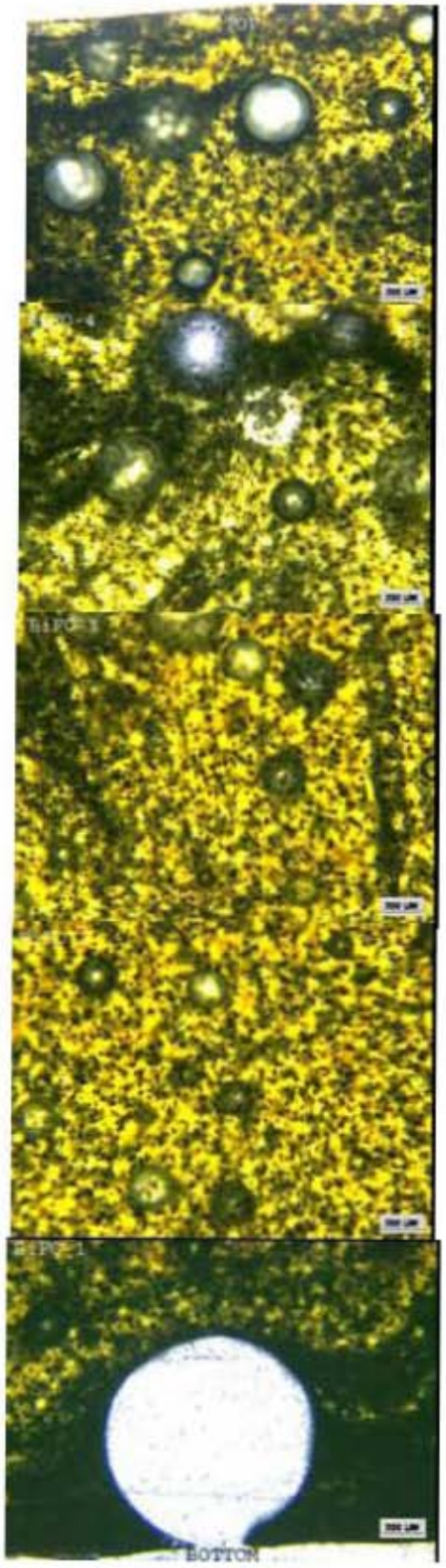

Figure 3.4n. Transmission optical microscopic images of HLW-Bi-F0 after CCC.

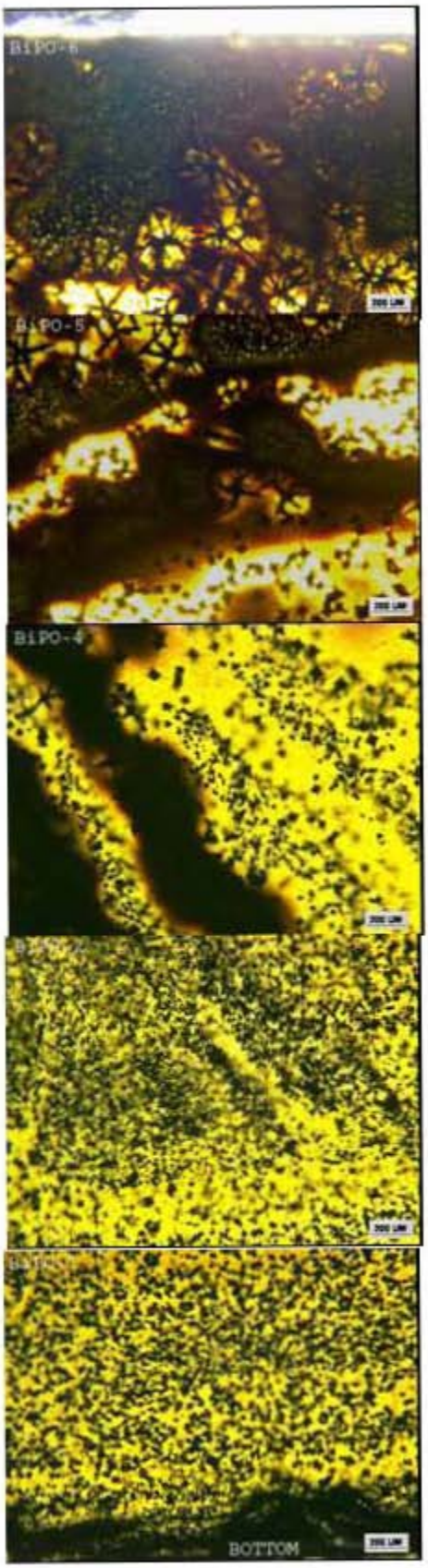

Figure 3.4o. Transmission optical microscopic images of HLW-Bi-P0 after CCC.

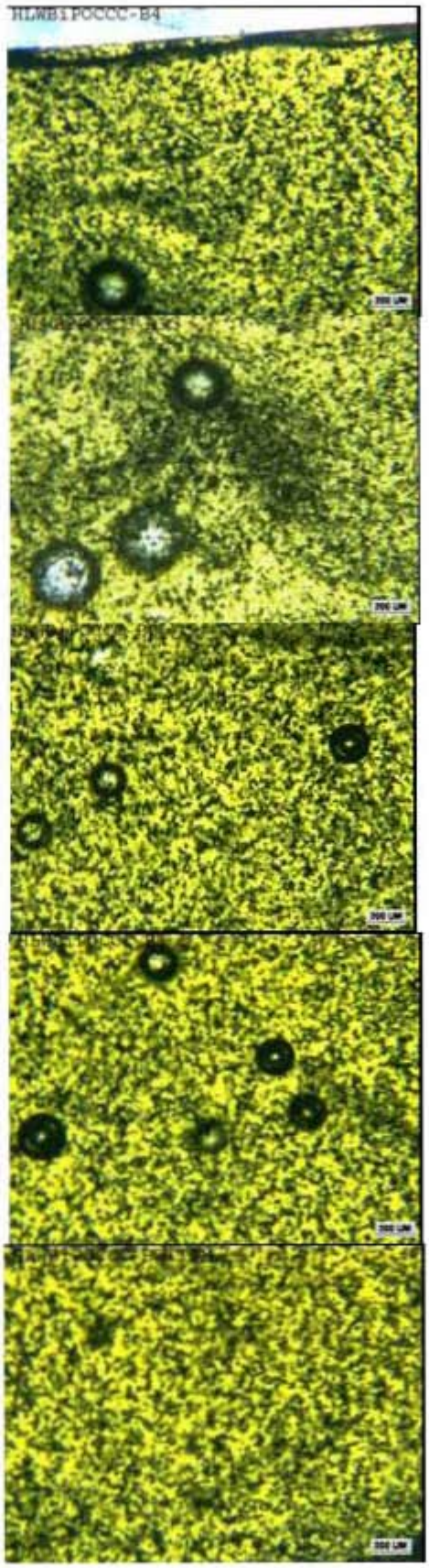

Figure 3.4p. Transmission optical microscopic images of HLW-Bi-BiP0 after CCC.

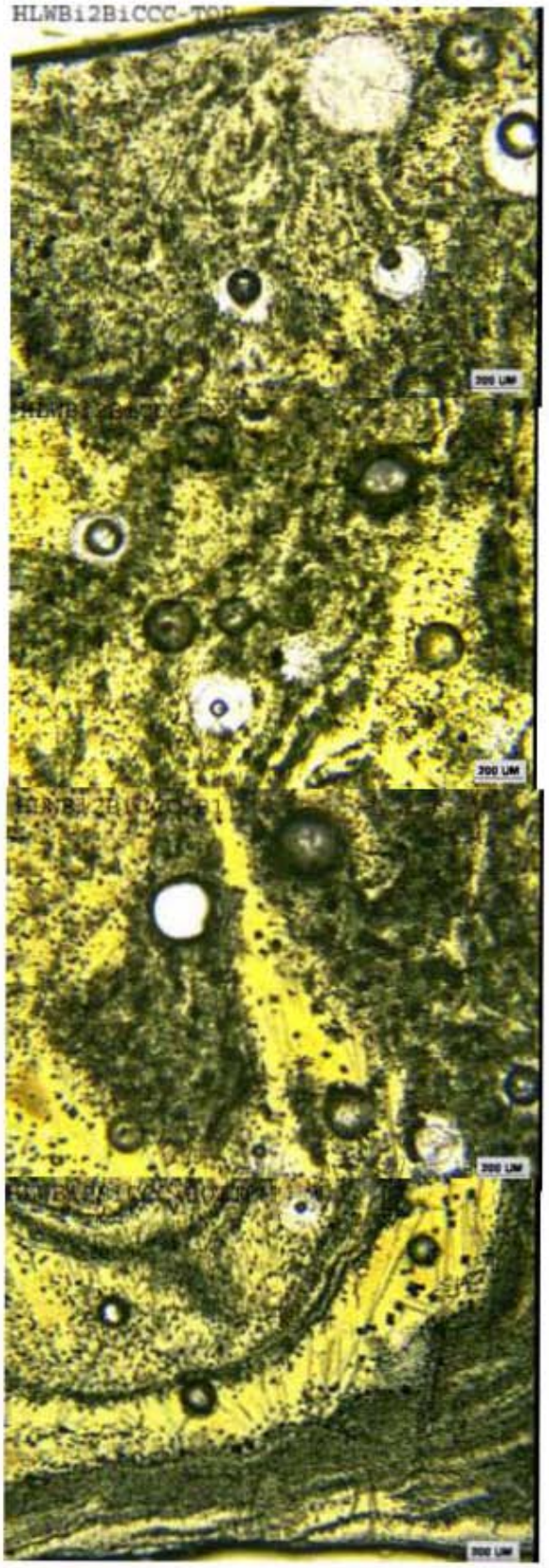

Figure 3.4q. Transmission optical microscopic images of HLW-Bi-2Bi after CCC.

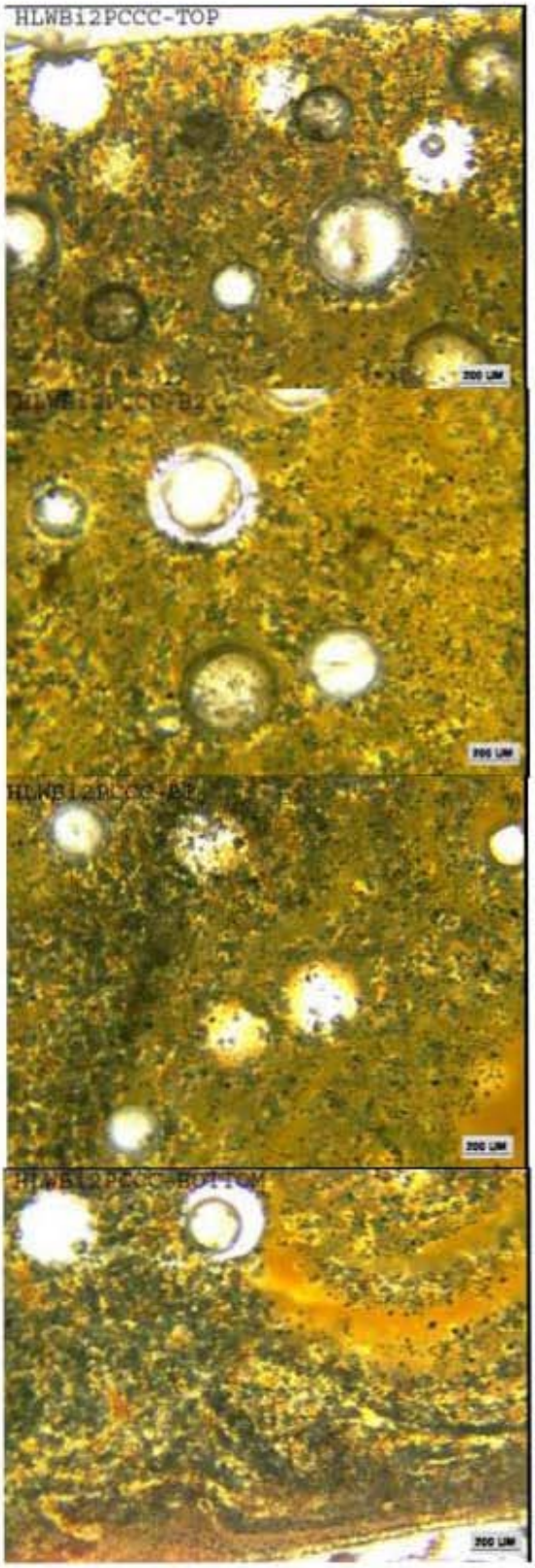

Figure 3.4r. Transmission optical microscopic images of HLW-Bi-2P after CCC.

Figure 3.4s. Transmission optical microscopic images of HLW-Bi-2P0Cr after CCC.

Figure 3.5a. Feed conversion after 30 minute VGF experiments: top view and cross section of HLW-E-Bi6.

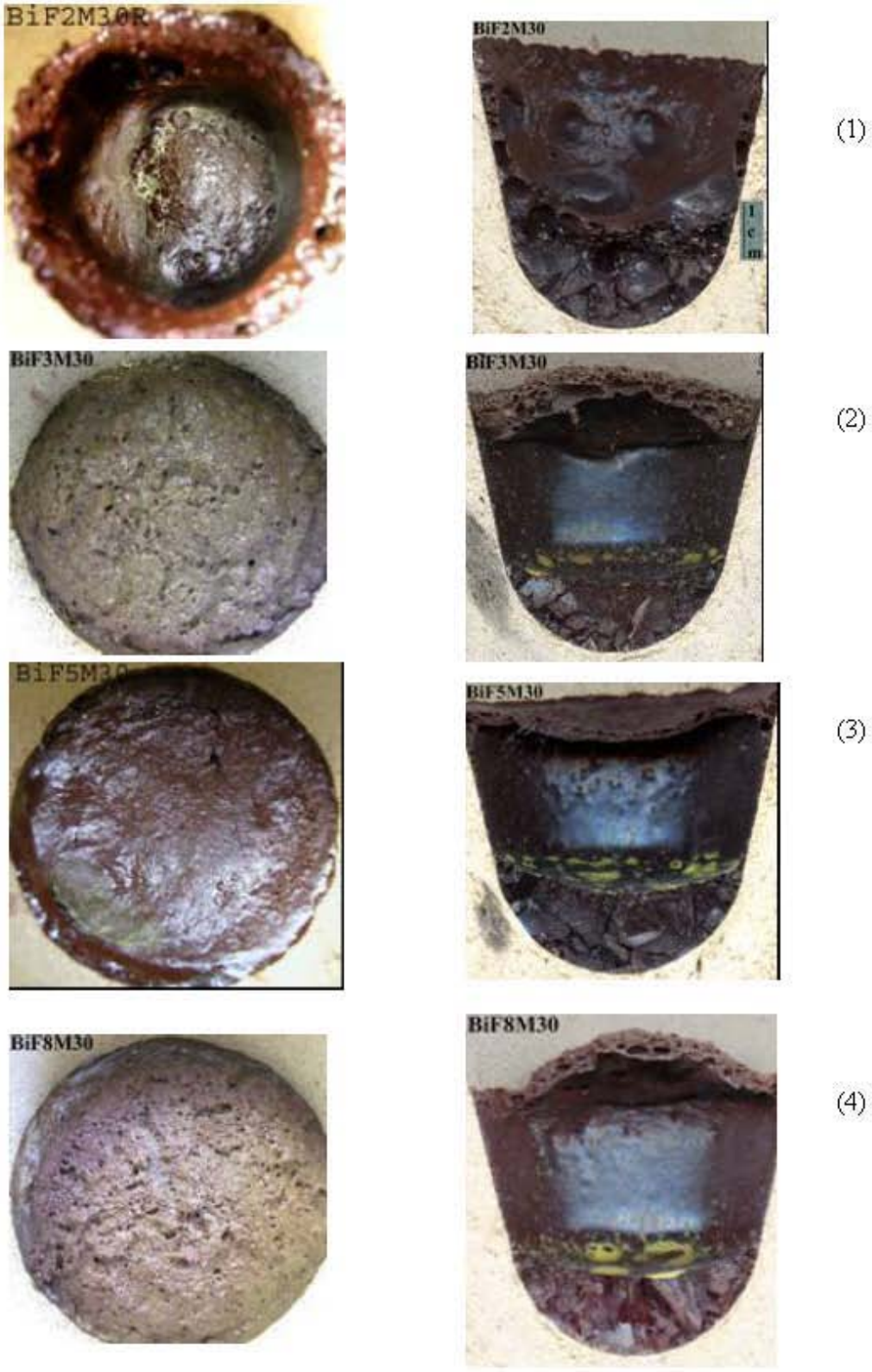

Figure 3.5b. Feed conversion after 30 minute VGF experiments: top view and cross section of 1) HLW-Bi-F2; 2) HLW-Bi-F3; 3) HLW-Bi-F5; and 4) HLW-Bi-F8.

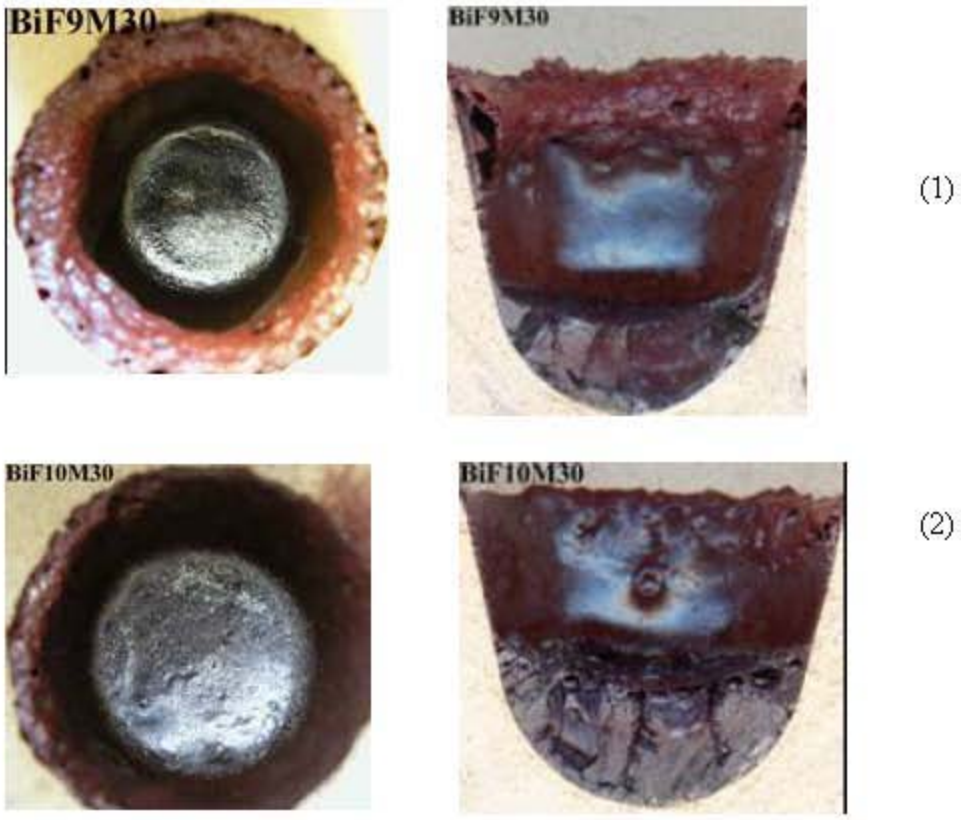

Figure 3.5c. Feed conversion after 30 minute VGF experiments: top view and cross section of 1) HLW-Bi-F9; 2) HLW-Bi-F10.

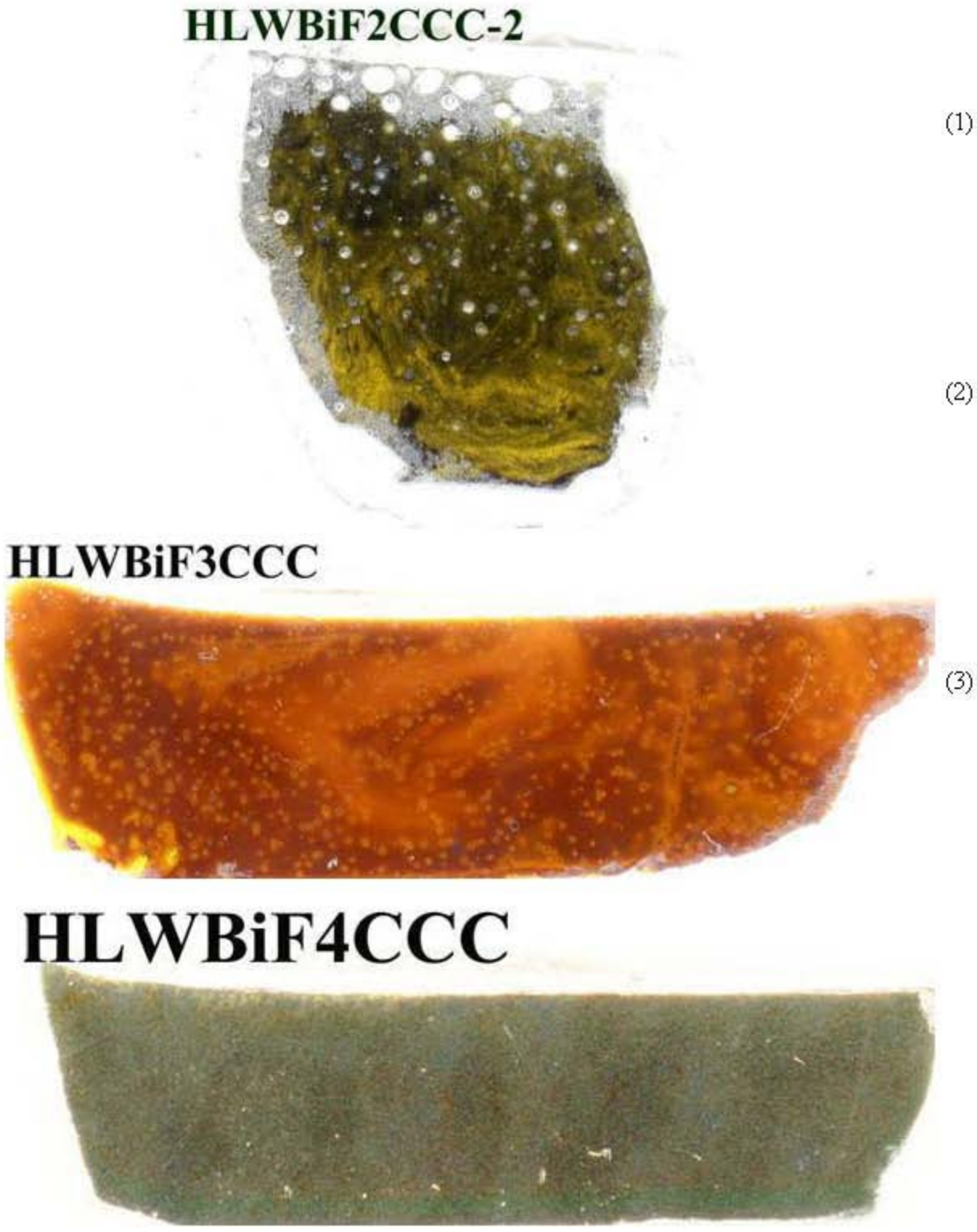

Figure 3.6a. Scanned images of thin sections of 1) HLW-Bi-F2 after CCC; 2) HLW-Bi-F3 after CCC; 3) HLW-Bi-F4 after CCC.

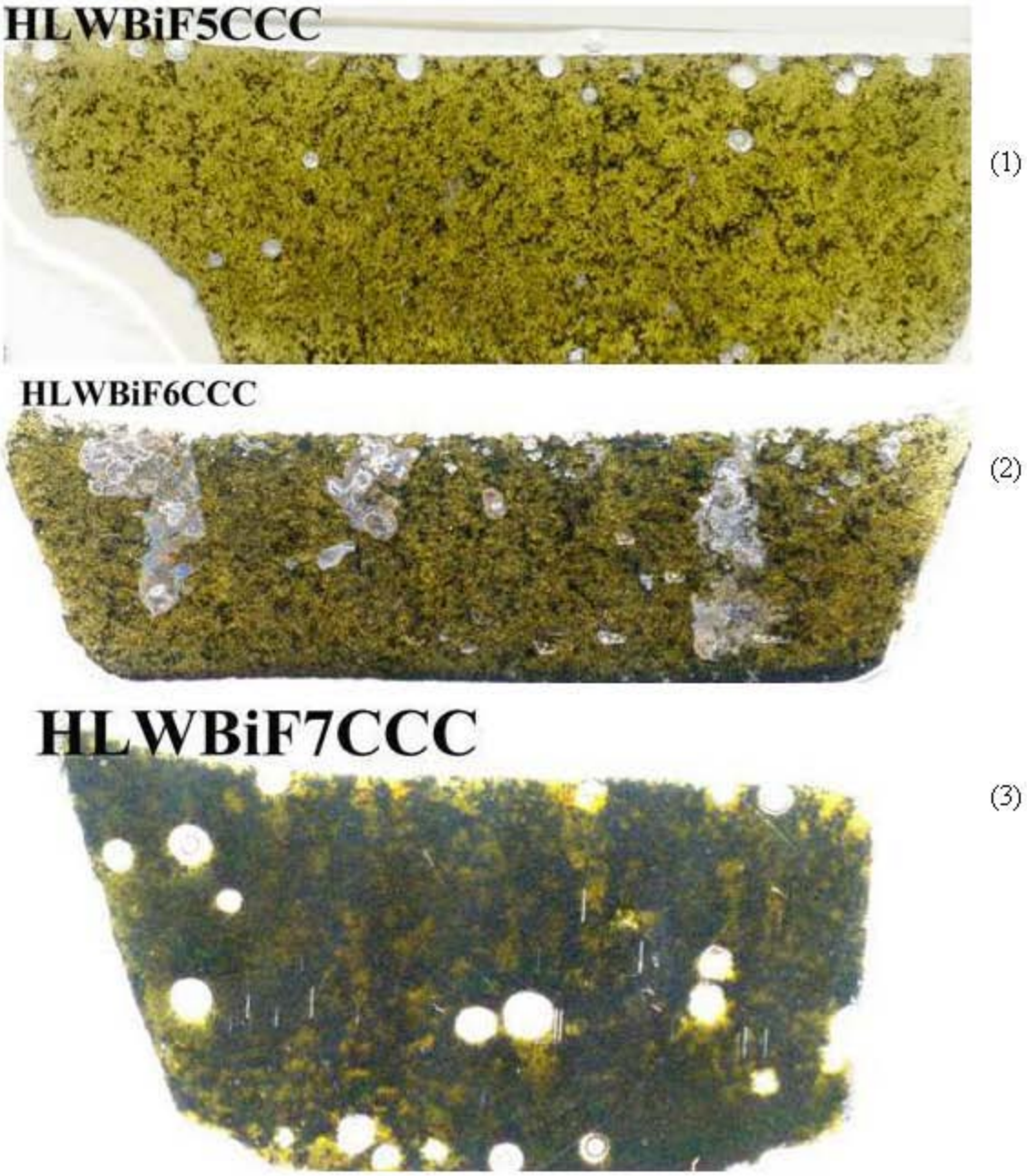

Figure 3.6b. Scanned images of thin sections of 1) HLW-Bi-F5 after CCC; 2) HLW-Bi-F6 after CCC; 3) HLW-Bi-F7 after CCC.

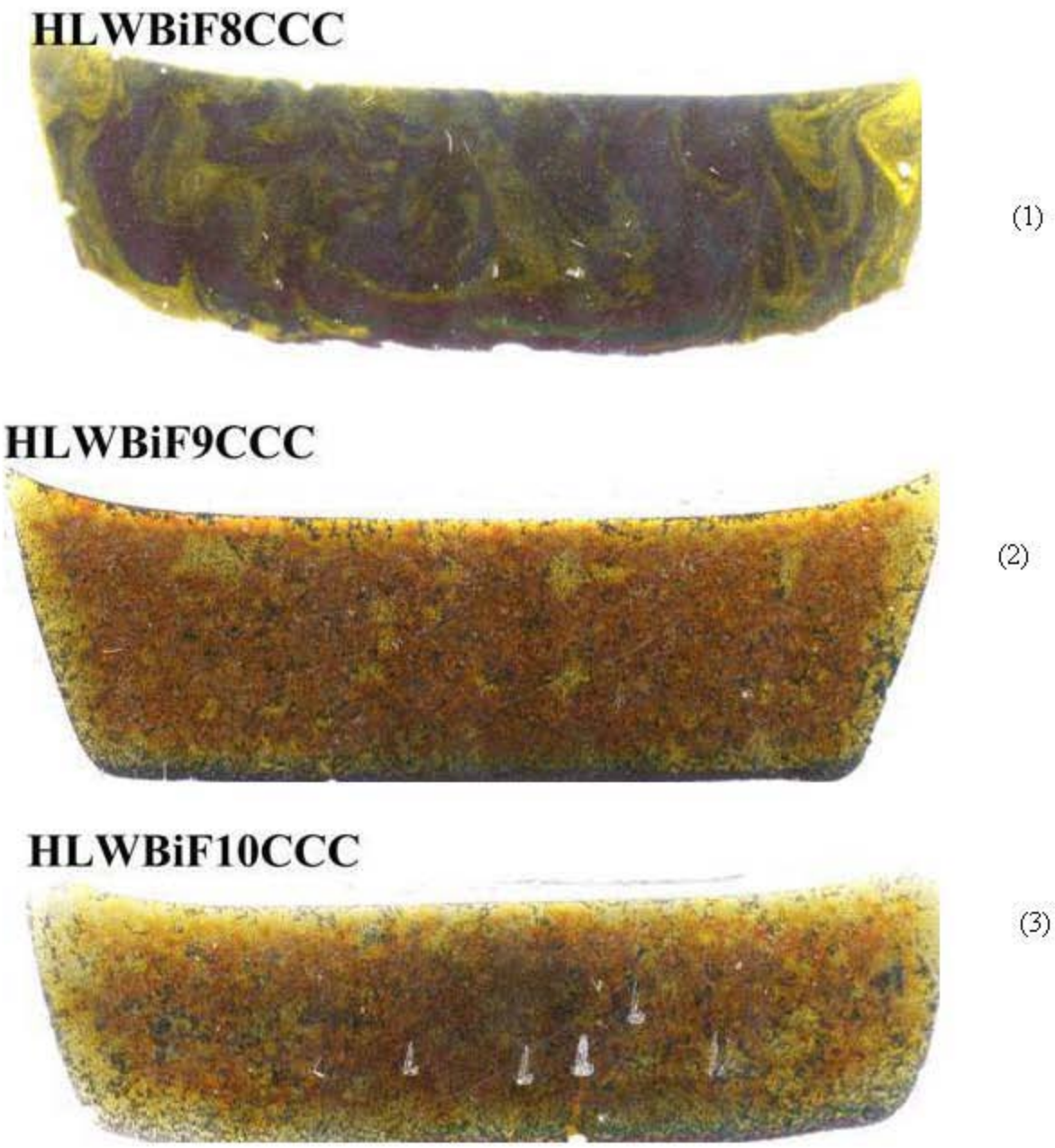

Figure 3.6c. Scanned images of thin sections of 1) HLW-Bi-F8 after CCC; 2) HLW-Bi-F9 after CCC; 3) HLW-Bi-F10 after CCC.

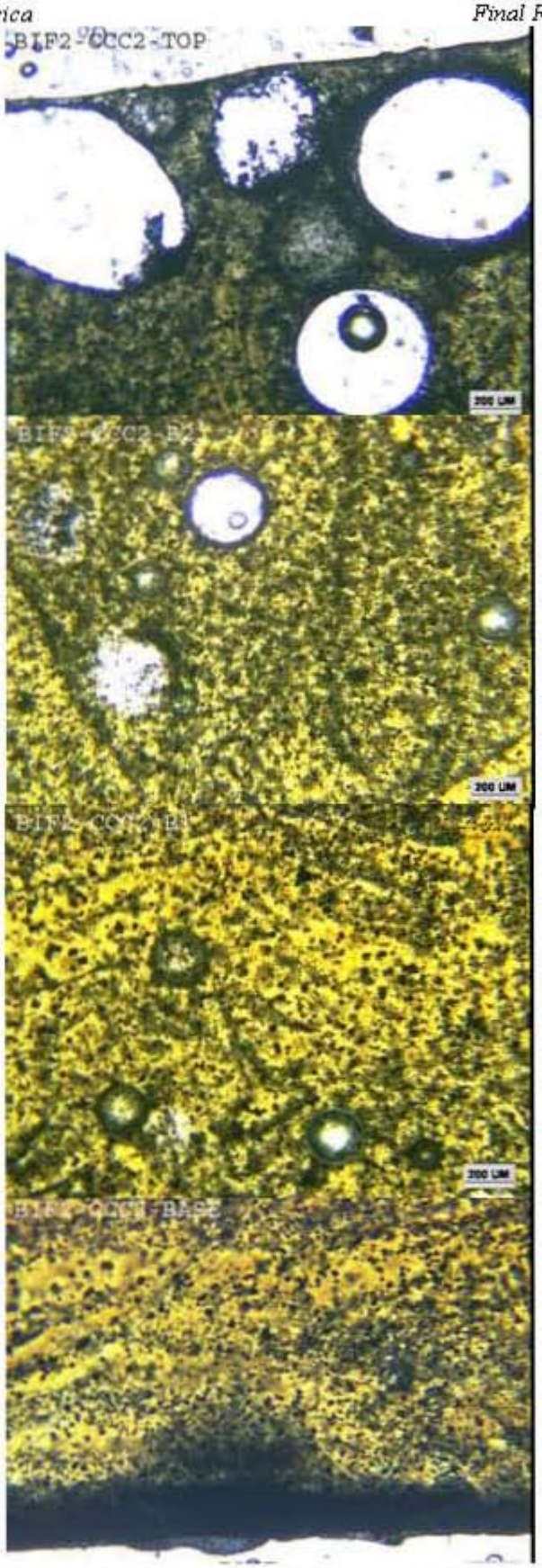

Figure 3.7a. Transmission optical microscopic images of thin section HLW-Bi-F2 after CCC.

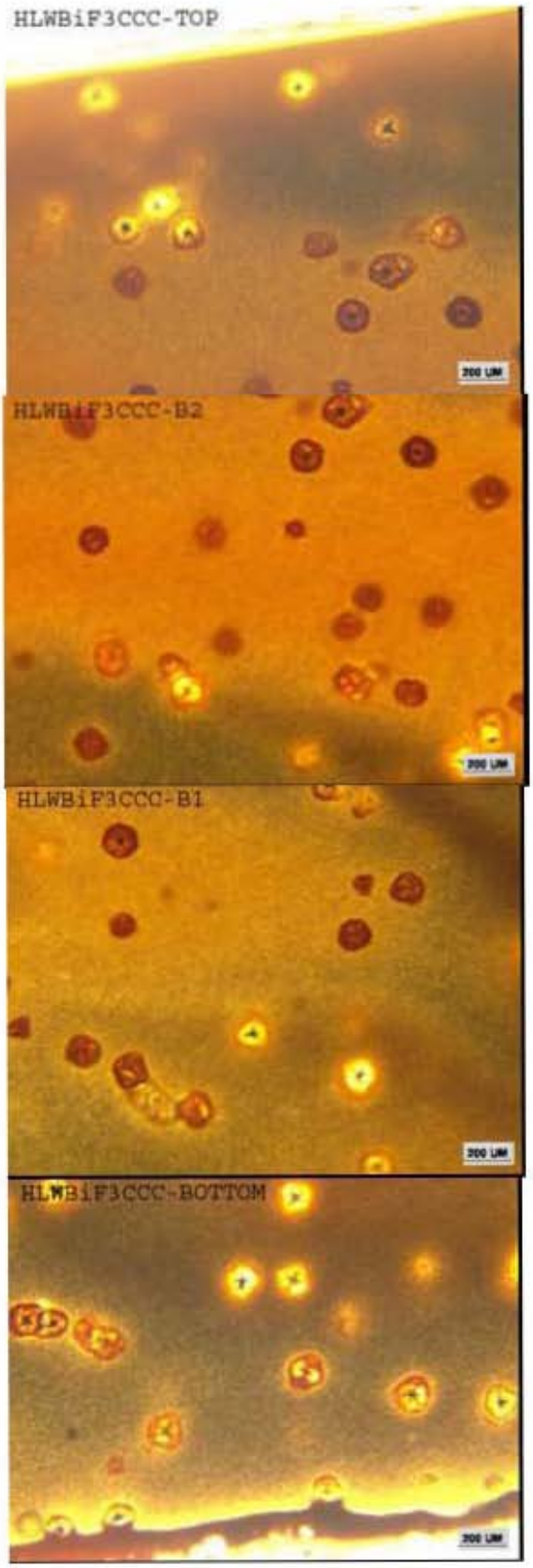

Figure 3.7b. Transmission optical microscopic images of thin section HLW-Bi-F3 after CCC.

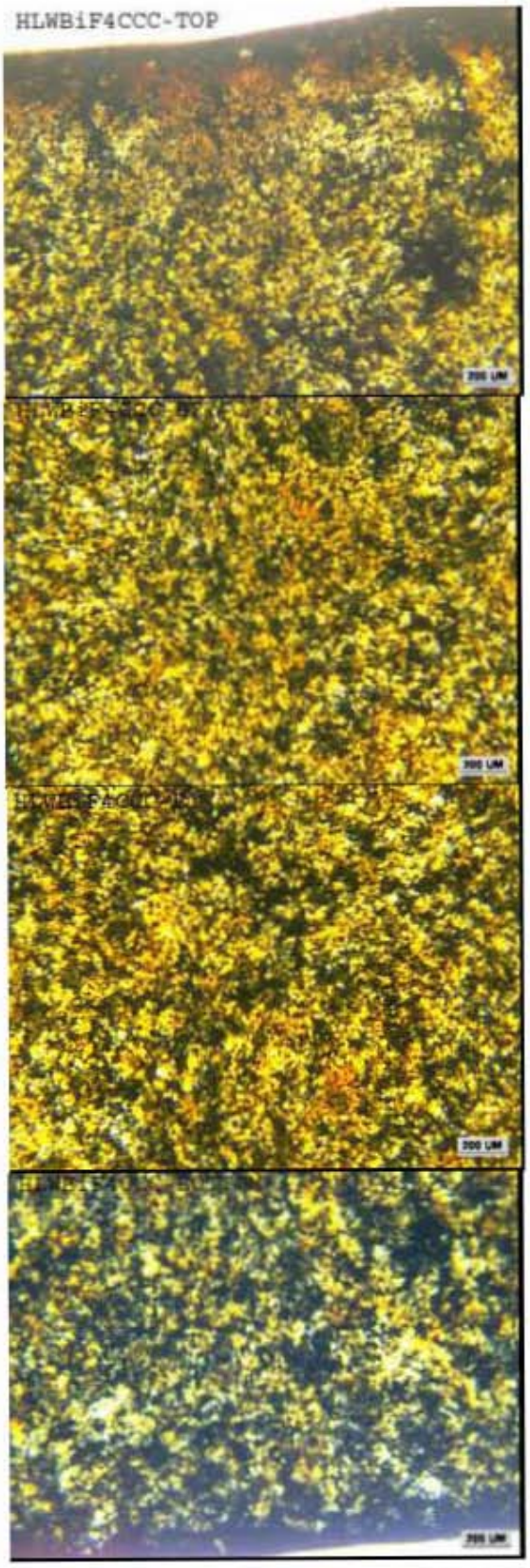

Figure 3.7c. Transmission optical microscopic images of thin section HLW-Bi-F4 after CCC.

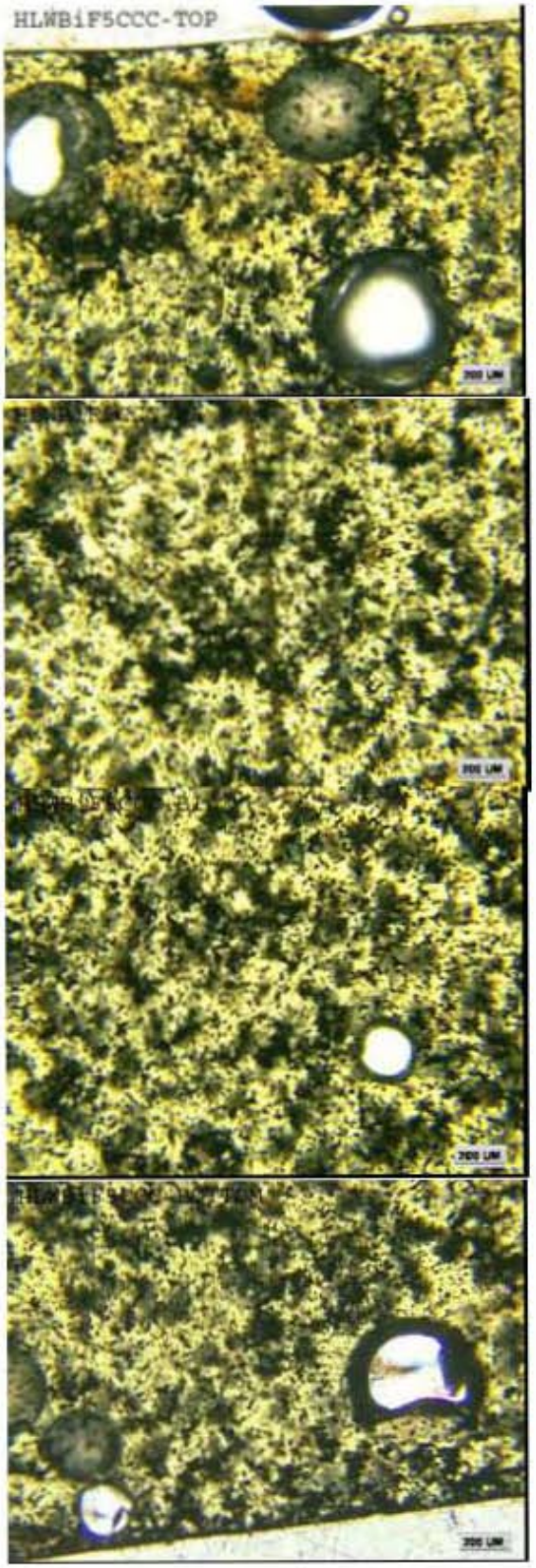

Figure 3.7d. Transmission optical microscopic images of thin section HLW-Bi-F5 after CCC.

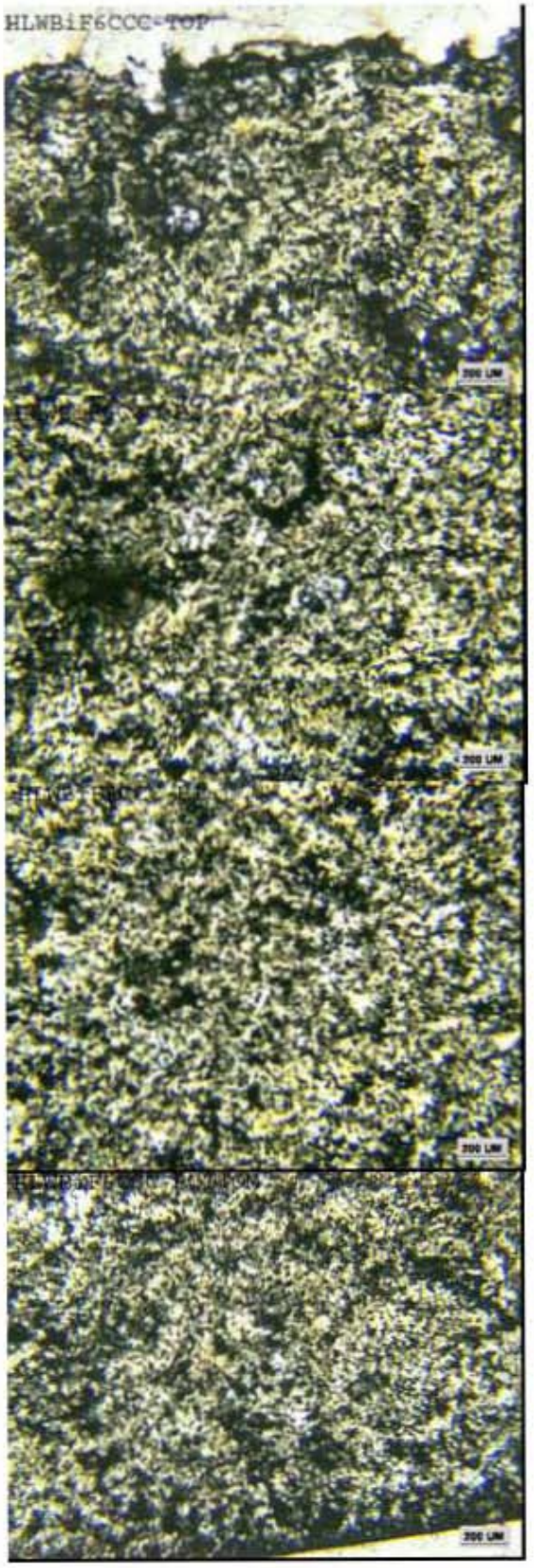

Figure 3.7e. Transmission optical microscopic images of thin section HLW-Bi-F6 after CCC.

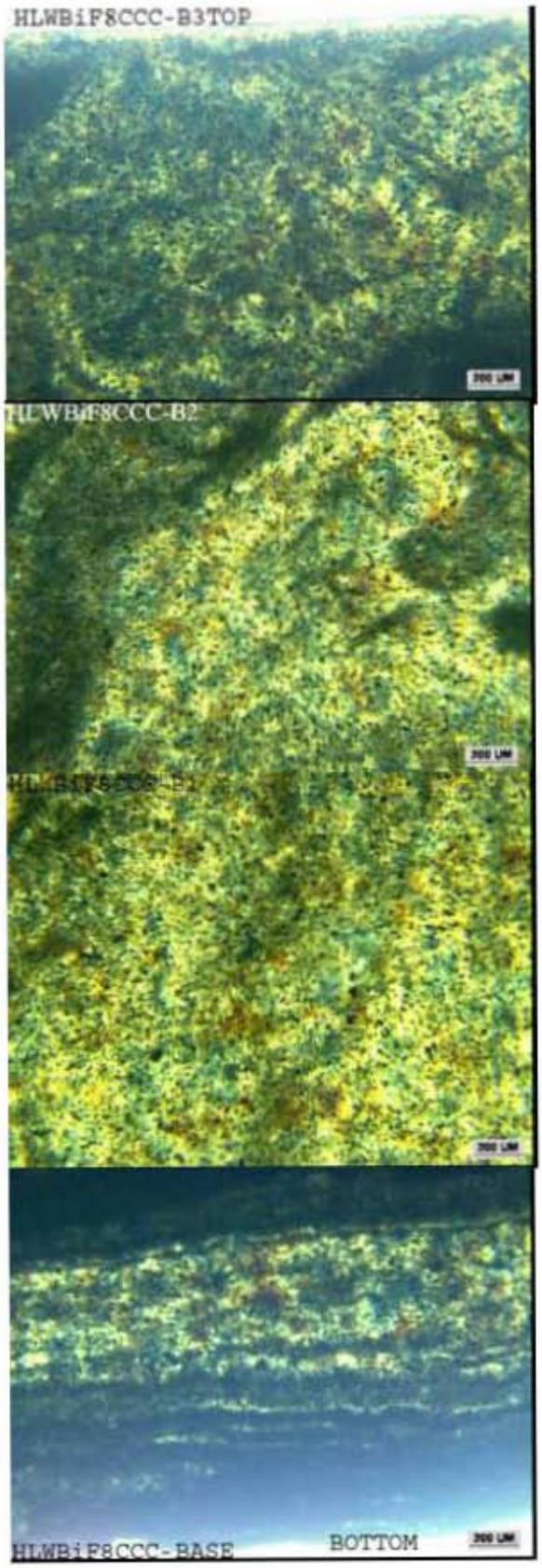

Figure 3.7f. Transmission optical microscopic images of thin section HLW-Bi-F8 after CCC.

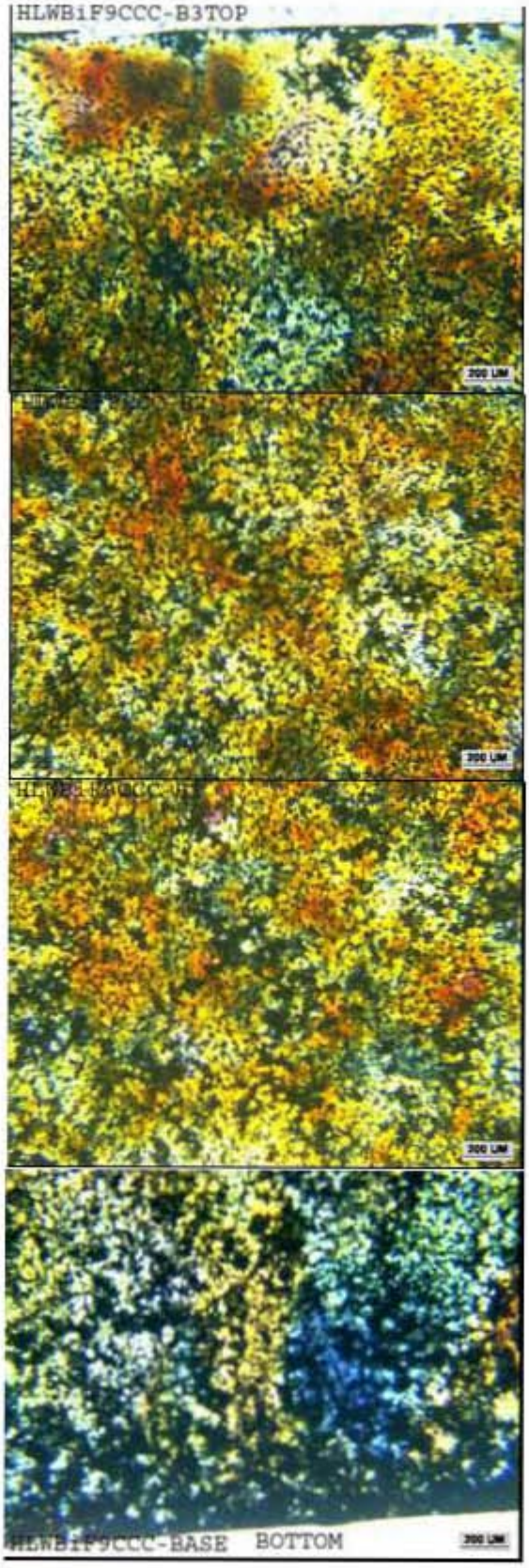

Figure 3.7g. Transmission optical microscopic images of thin section HLW-Bi-F9 after CCC.

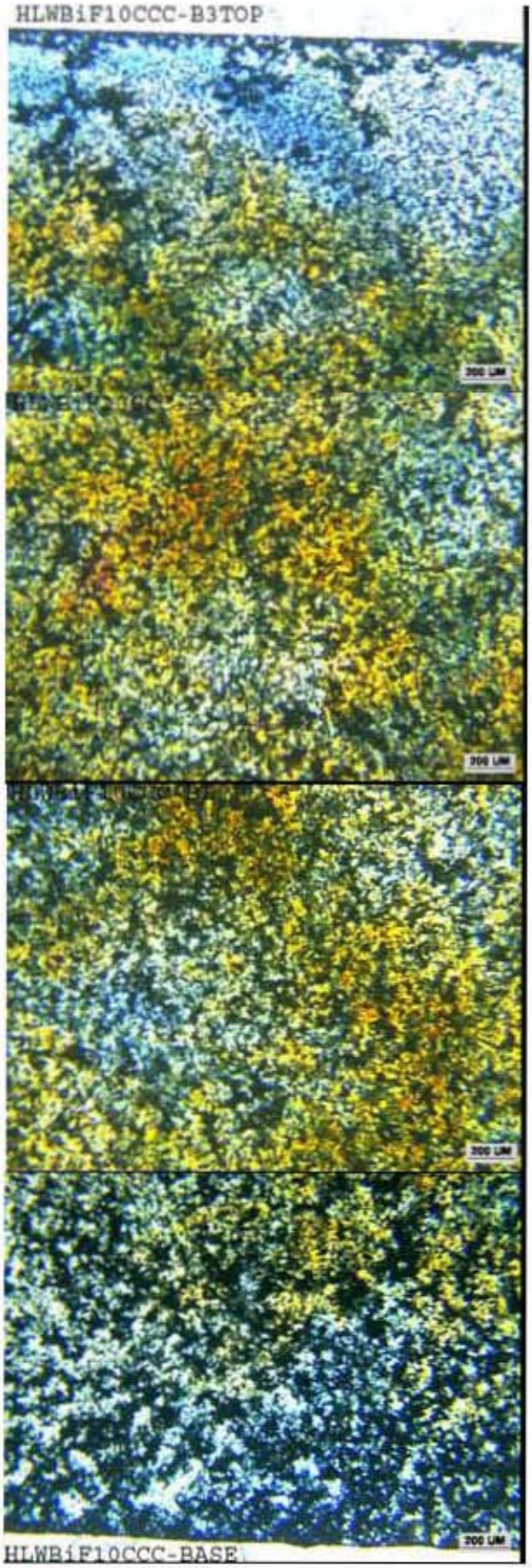

Figure 3.7h. Transmission optical microscopic images of thin section HLW-Bi-F10 after CCC.

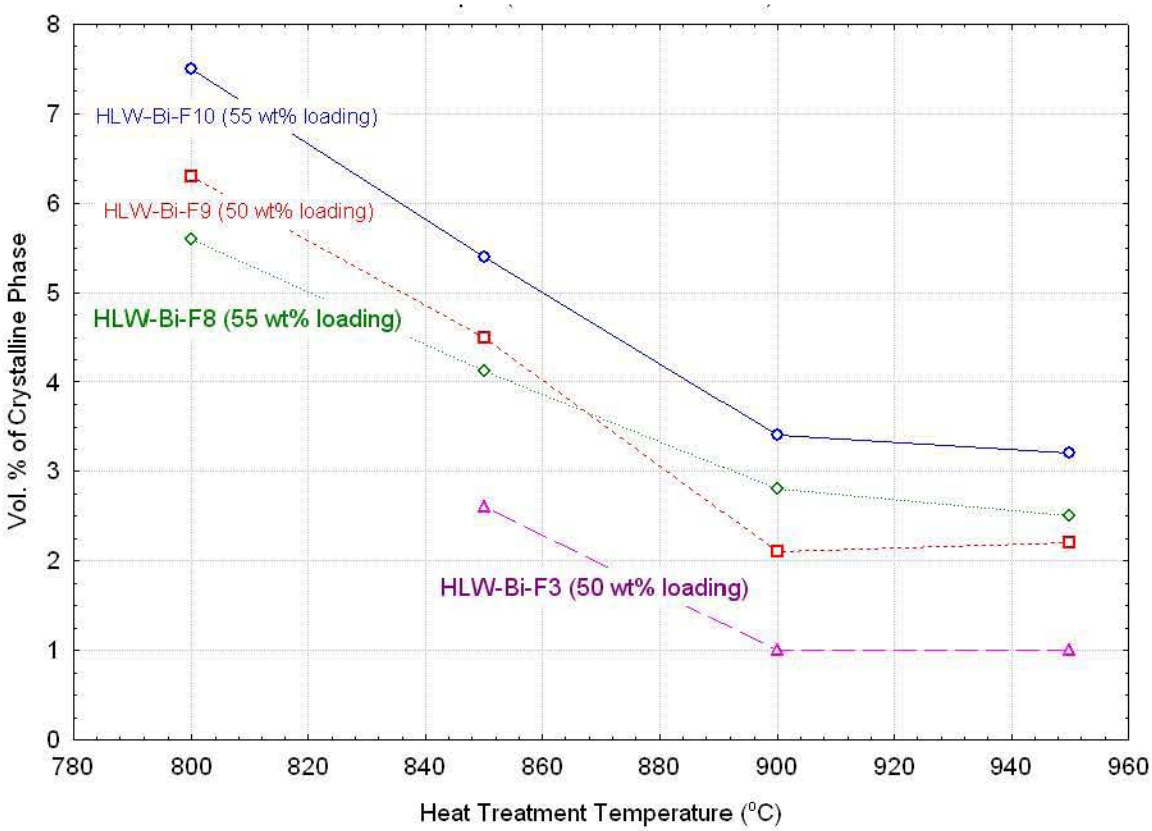

Figure 3.8. Crystallinity (vol%) after 70 hours isothermal heat treatments of four candidate HLW-Bi glasses.

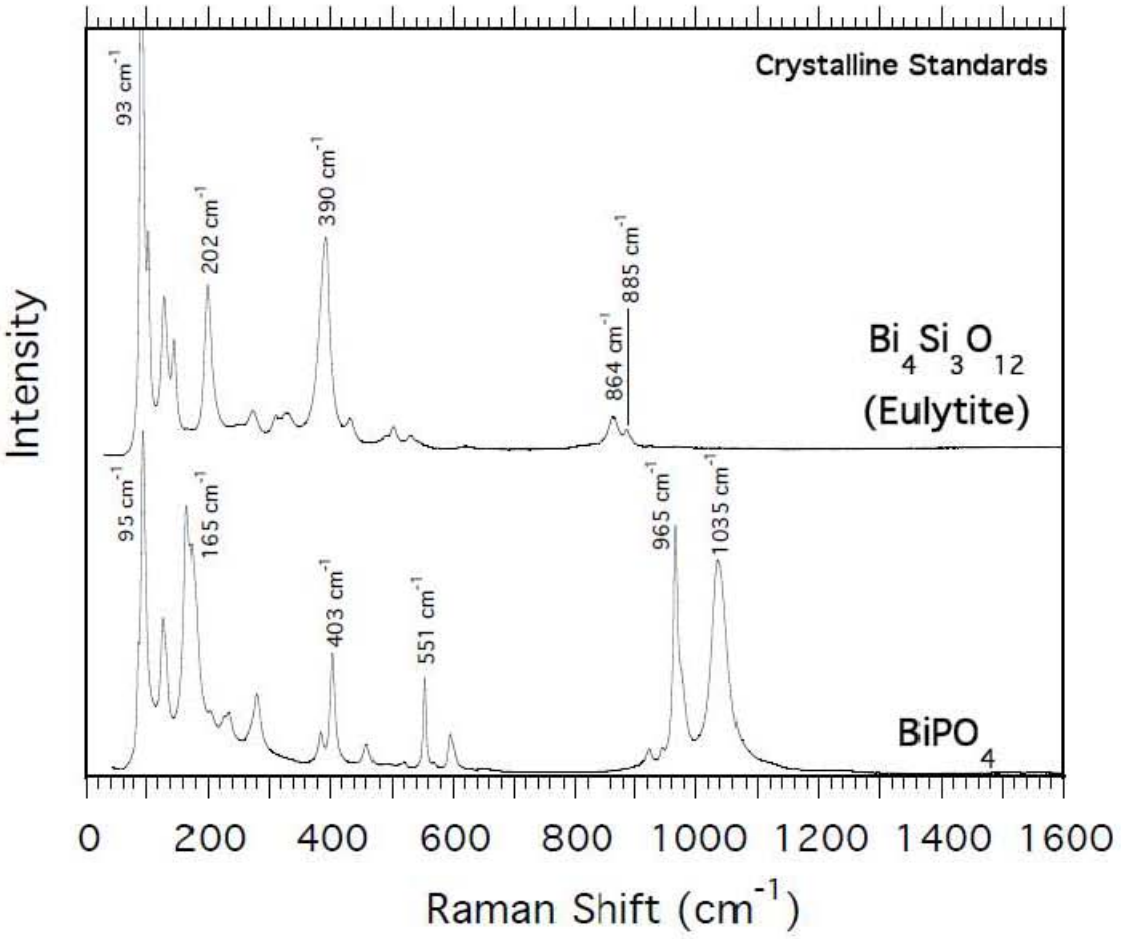

Figure 3.9. VV polarized Raman spectra of the two crystalline Bi-standards. Some prominent peak frequencies are listed.

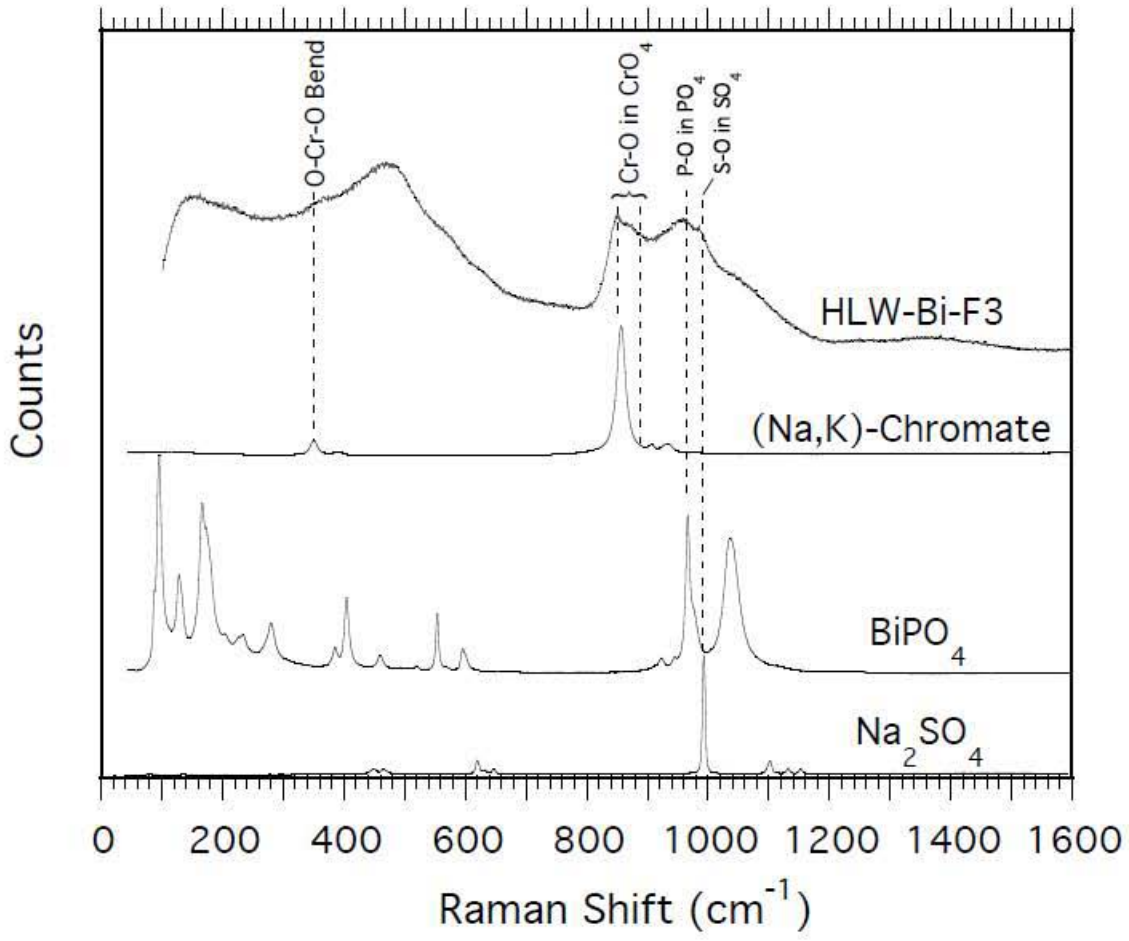

Figure 3.10. VV polarized Raman spectra of a representative waste glass HLW-Bi-F3 and three crystalline samples depicting Cr-O stretch and O-Cr-O bend in chromate, P-O stretch in phosphate, and S-O stretch in sulfate modes.

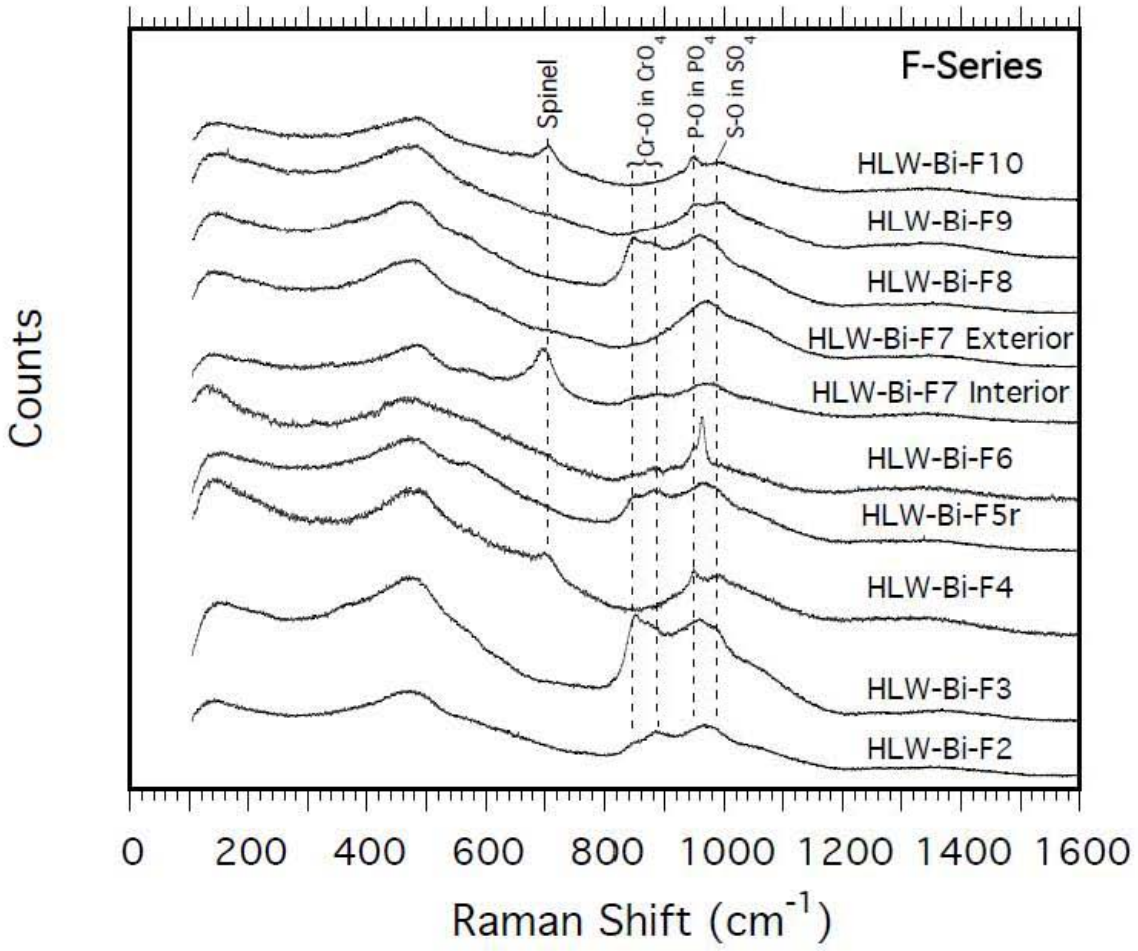

Figure 3.11. VV polarized spectra of the waste glasses (F-series) where Bi_2O_3 and P_2O_5 waste-loading was varied; these spectra were collected at points having the least amount of crystals. HLW-Bi-F7 Interior is a representative spectrum of an interior fracture surface of the sample; HLW-Bi-F7 Exterior is a representative spectrum of the outer sample surface. Several spectra are rescaled to highlight differences. Some vibrational assignments are indicated.

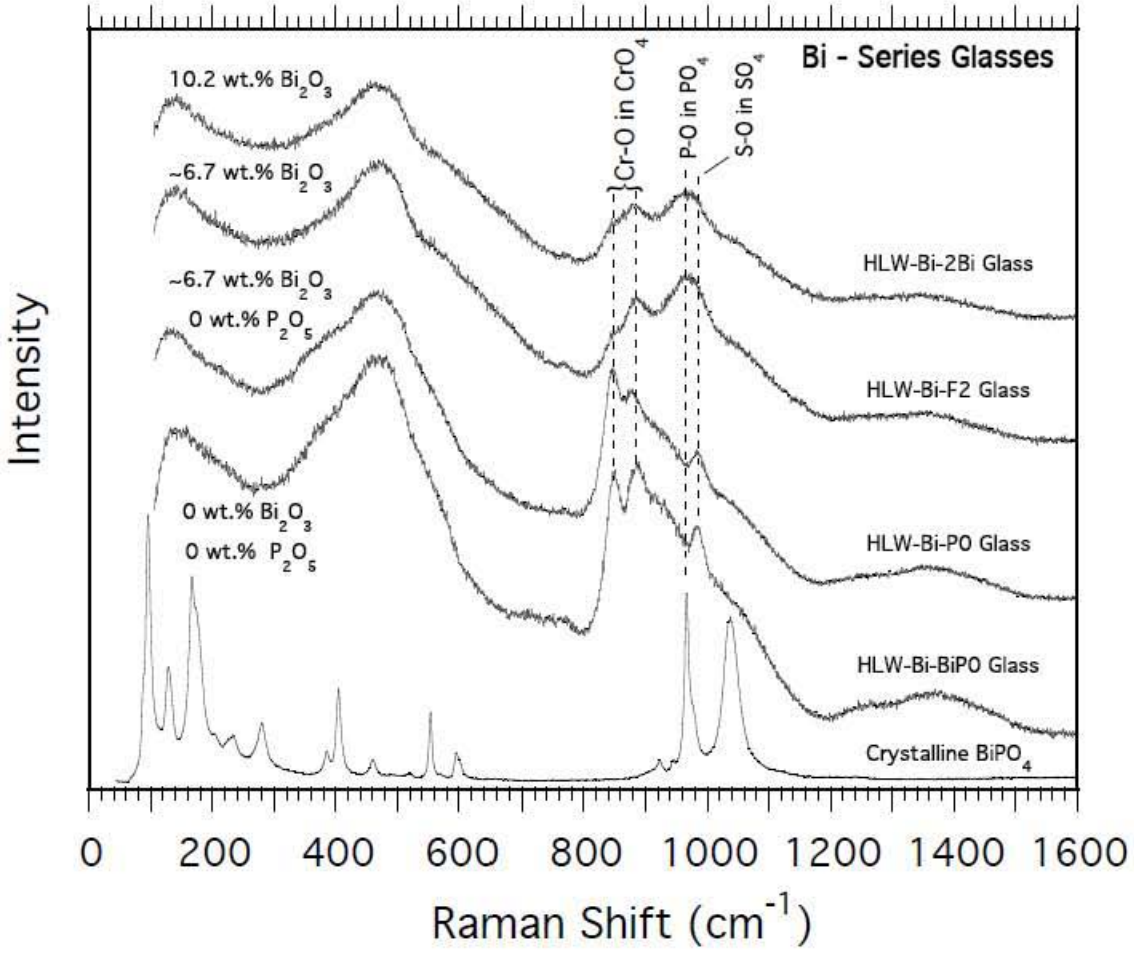

Figure 3.12. VV polarized spectra of the Bi-series glasses where Bi_2O_3 content was varied. Some of the higher frequency glass vibration assignments are indicated.

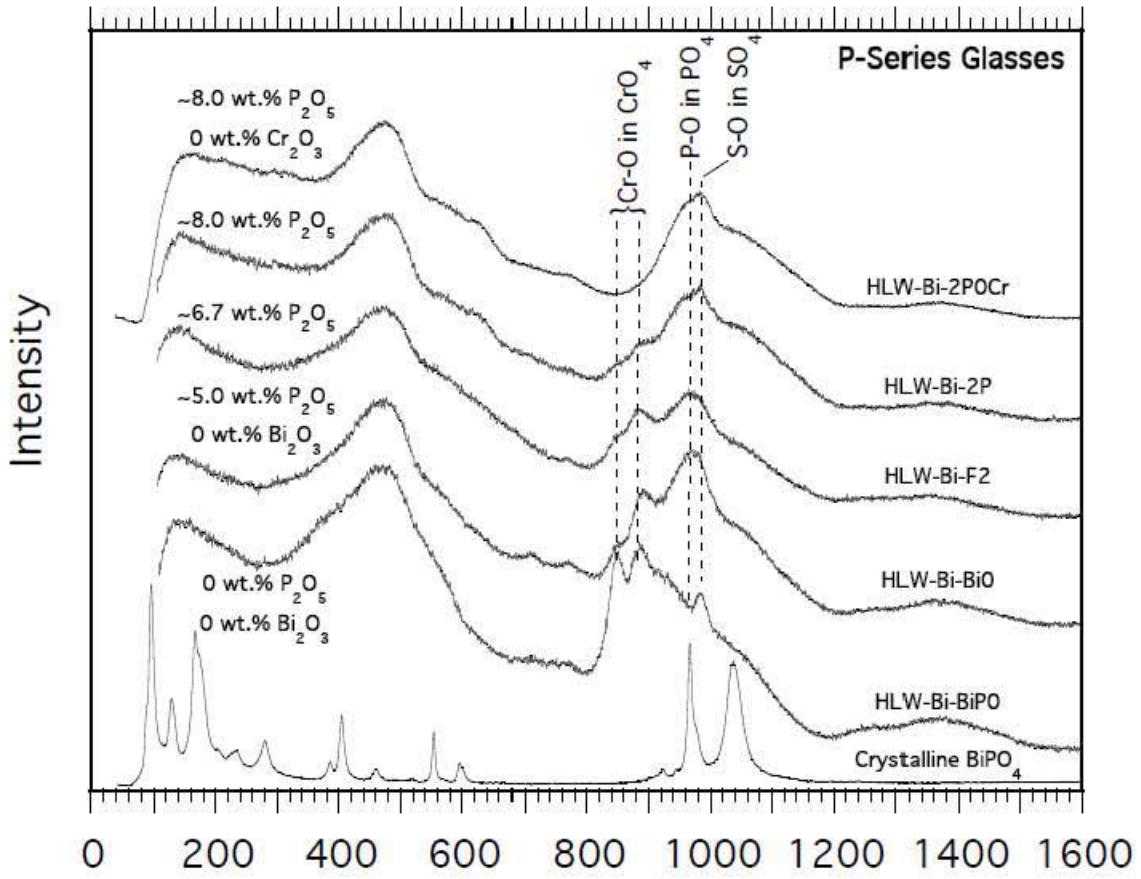

Figure 3.13. VV polarized spectra of the P-series glasses where P_2O_5 content was varied. Some of the higher frequency glass vibration assignments are indicated. HLW-Bi-2P0Cr (without Cr) is included to indicate the absence of chromate modes.

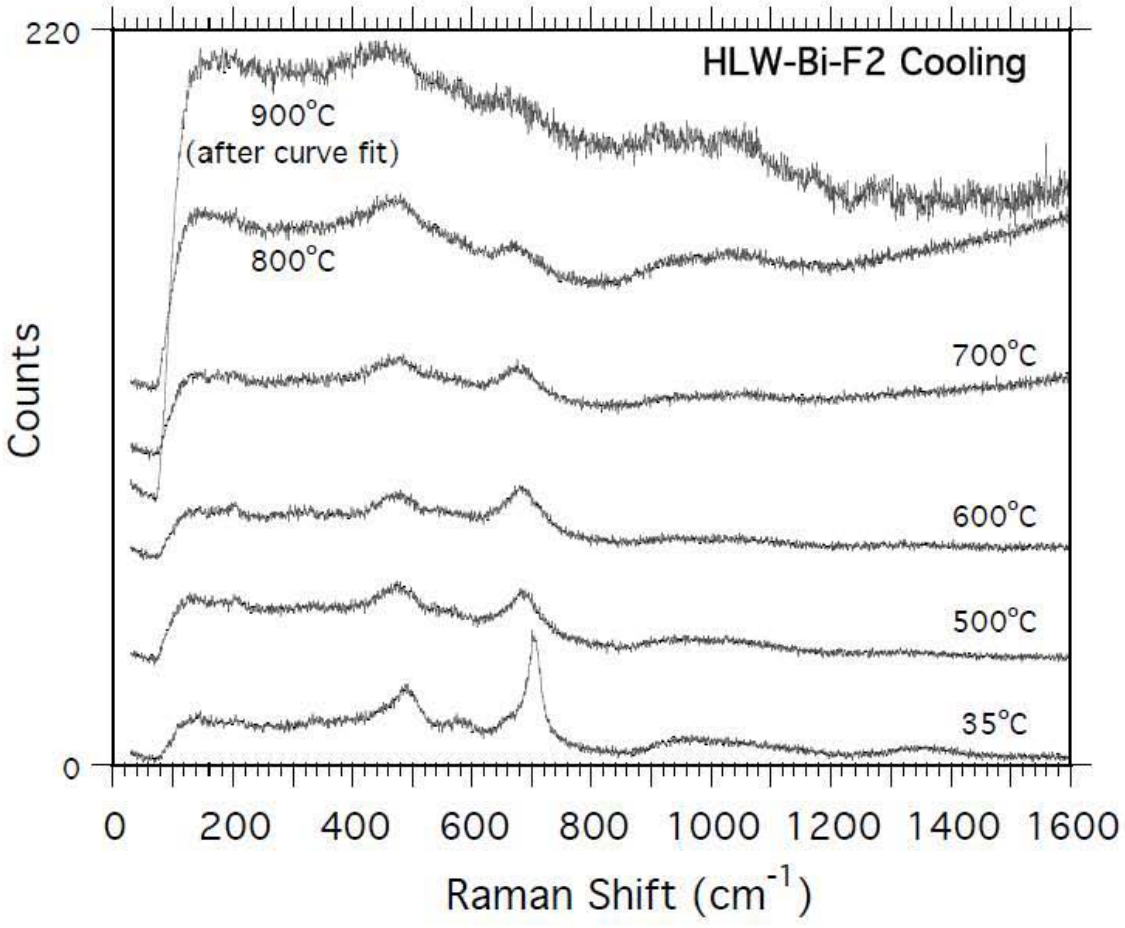

Figure 3.14. VV polarized spectra of the HLW-Bi-F2 glass during the cooling stage of a heating run. Note the spinel peak near 680 cm^{-1}. A curve-fit to the black body radiation contribution was subtracted from the 900°C spectrum (top plot).

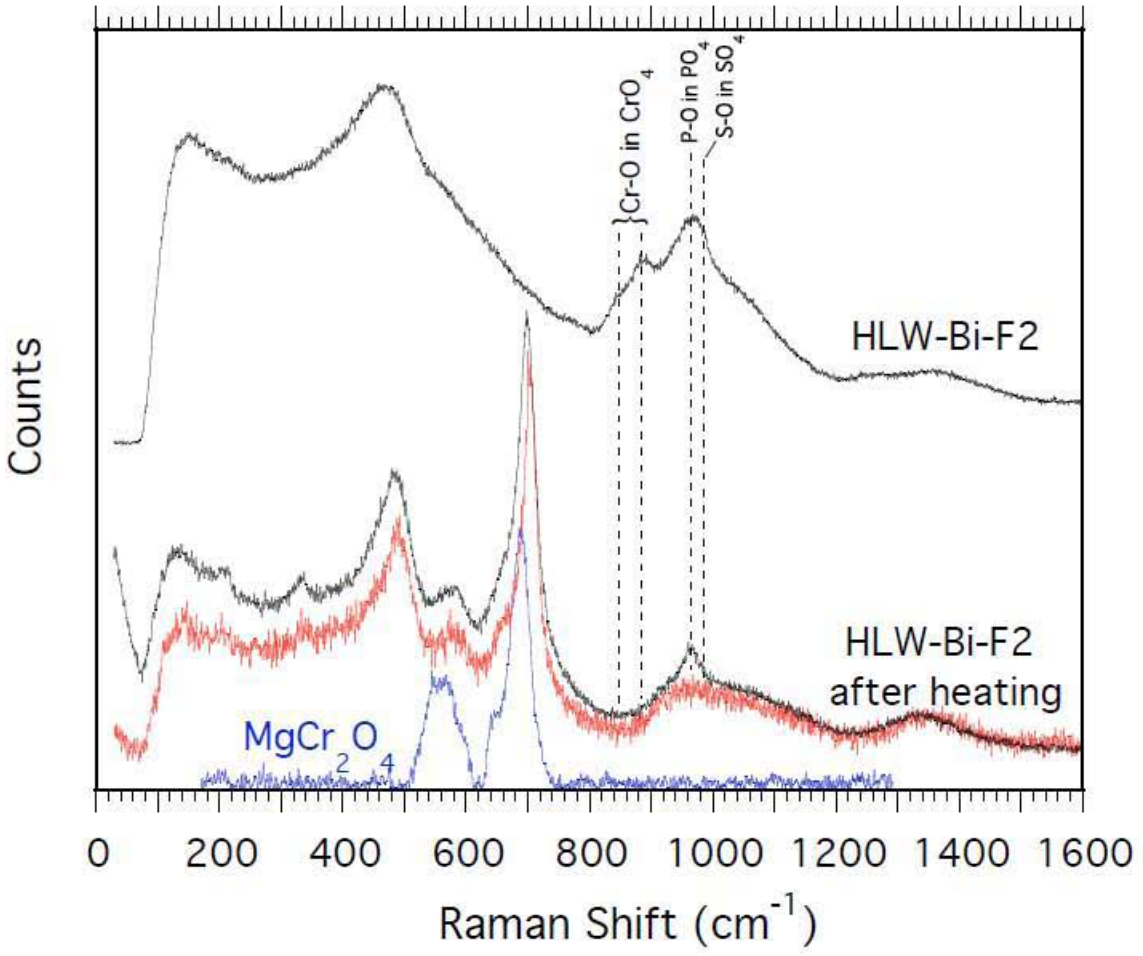

Figure 3.15. VV polarized spectra of the HLW-Bi-F2 glass before and after heating runs (black and red plots). The unpolarized spectrum of $MgCr_2O_4$ spinel [49] (blue plot) is included as a comparison with some relatively narrow peaks in the run product (after heating) spectra. Note the absence of chromate modes in both run product spectra.

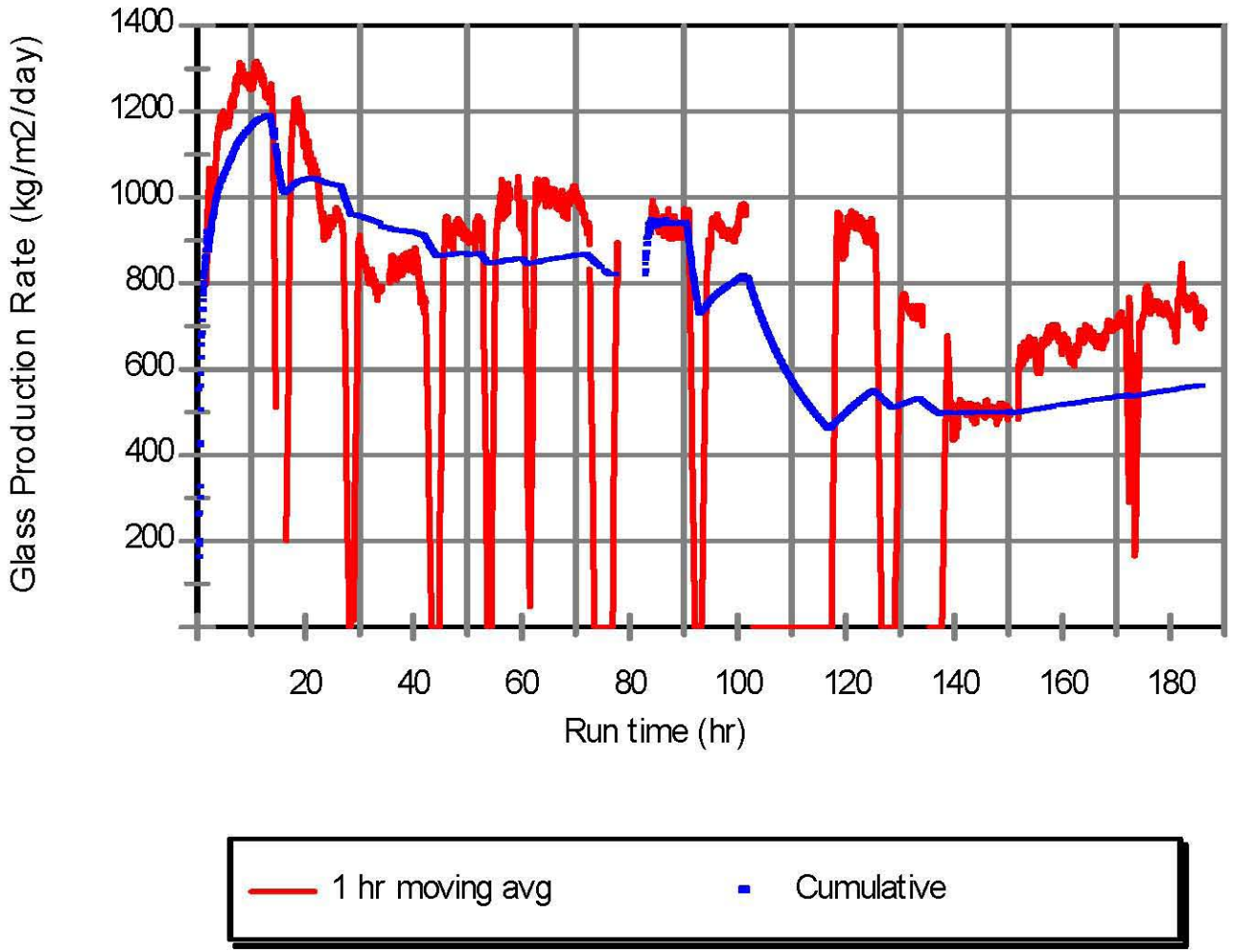

Figure 4.1. Production rates for DM1200 Tests.

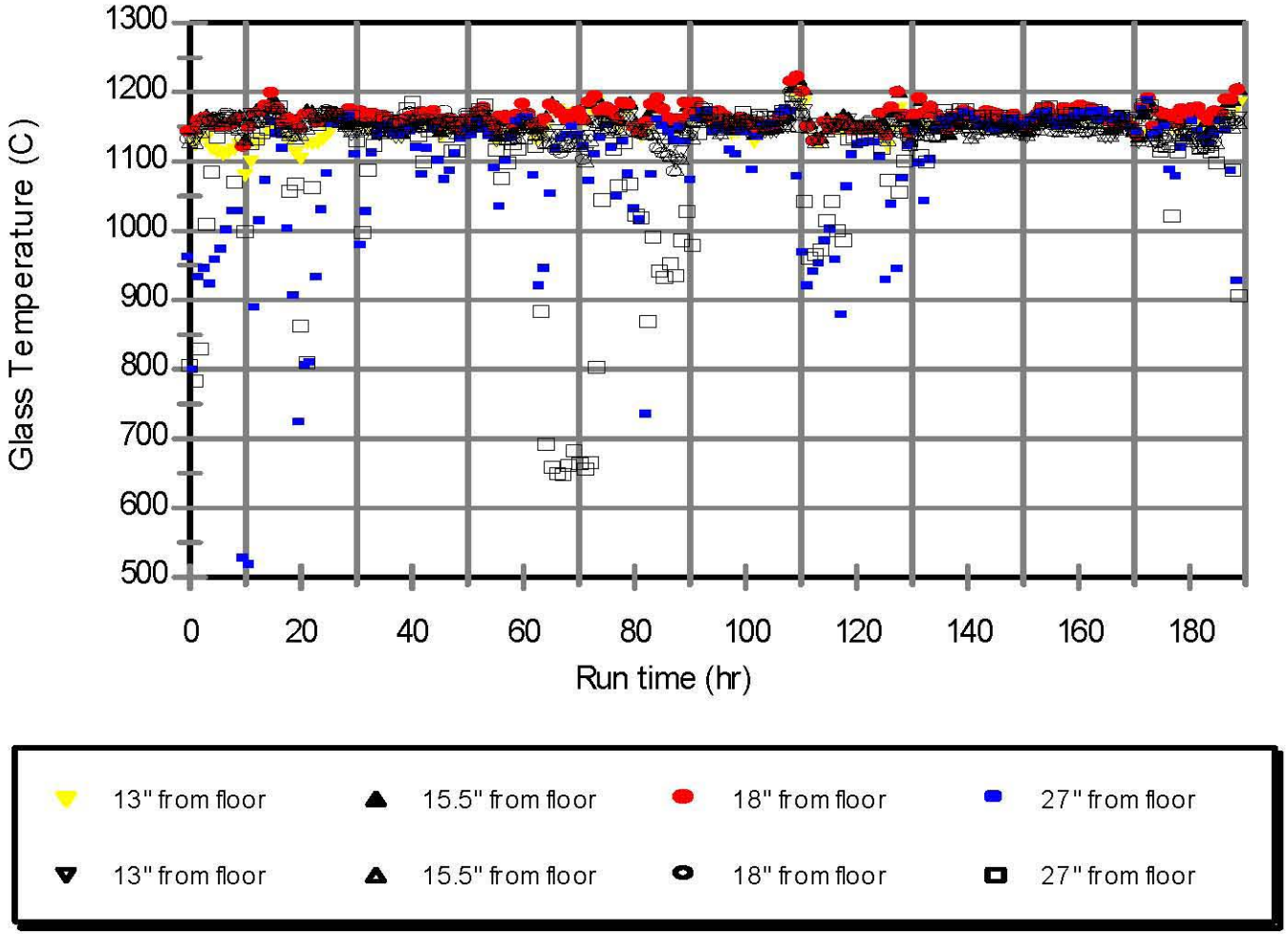

Figure 4.2. Glass temperatures (hourly averages) for DM1200 Tests.

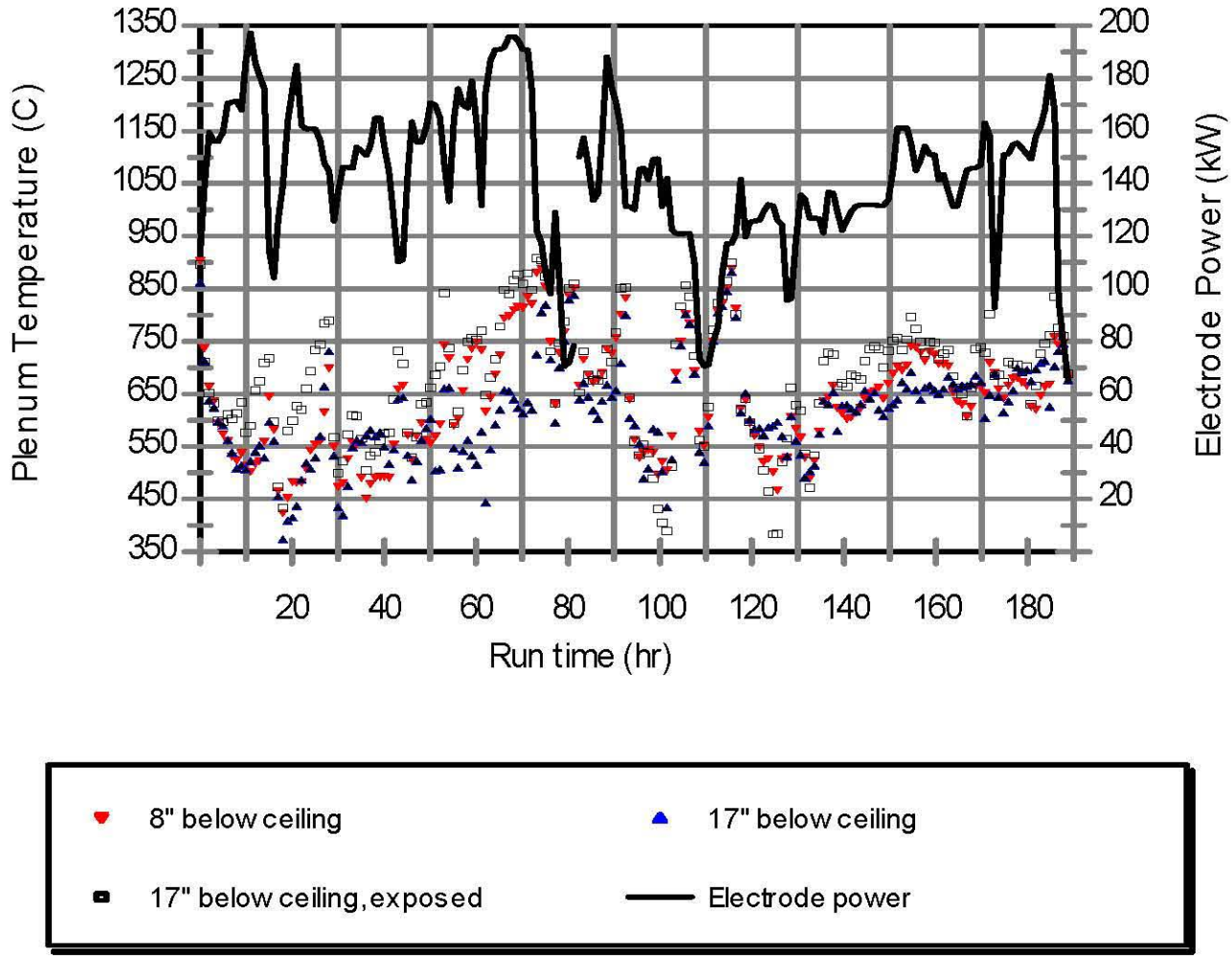

Figure 4.3. Plenum temperatures and electrode power (hourly averages) for DM1200 Tests.

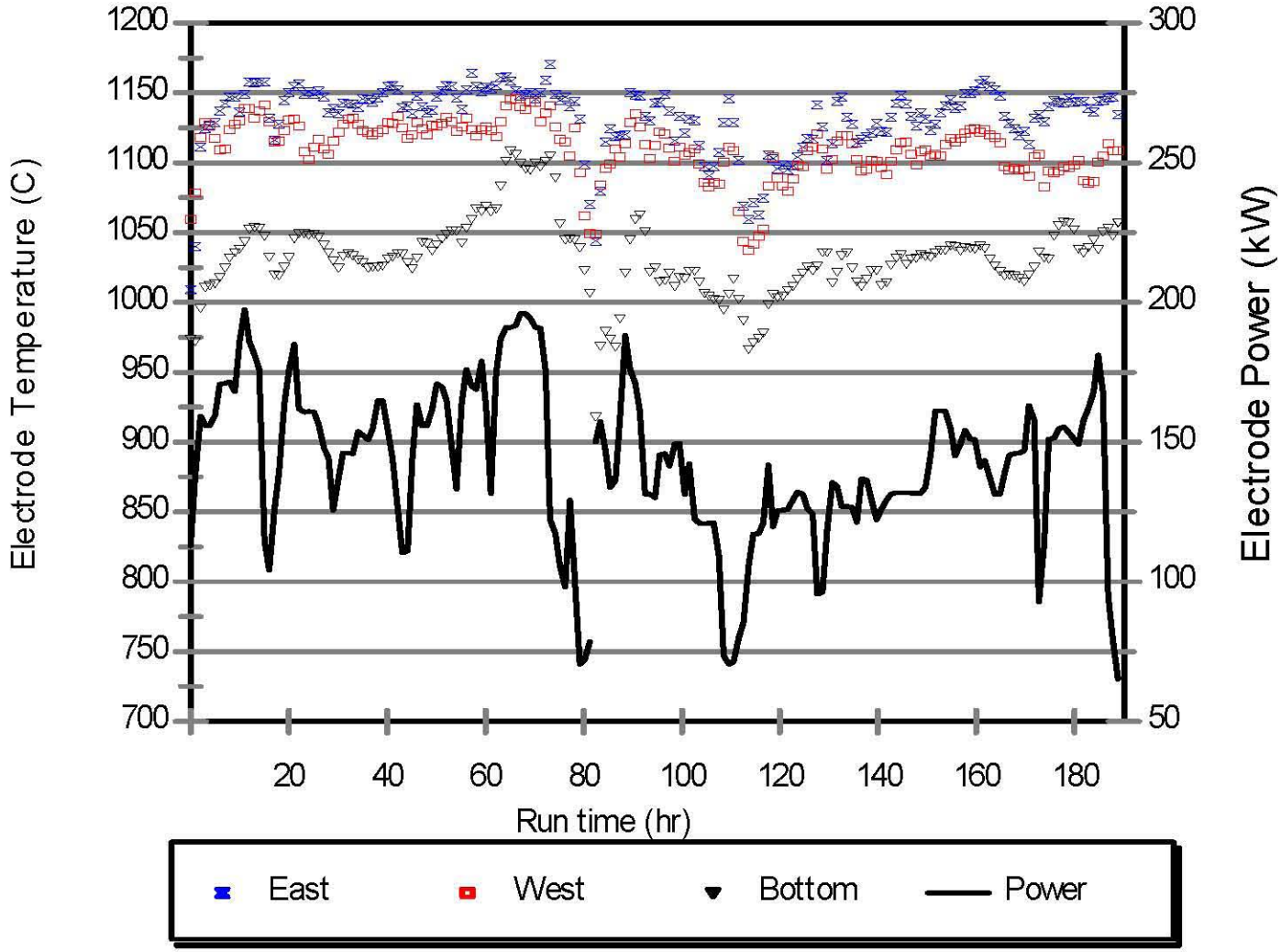

Figure 4.4. Electrode temperatures and power (hourly averages) for DM1200 Tests.

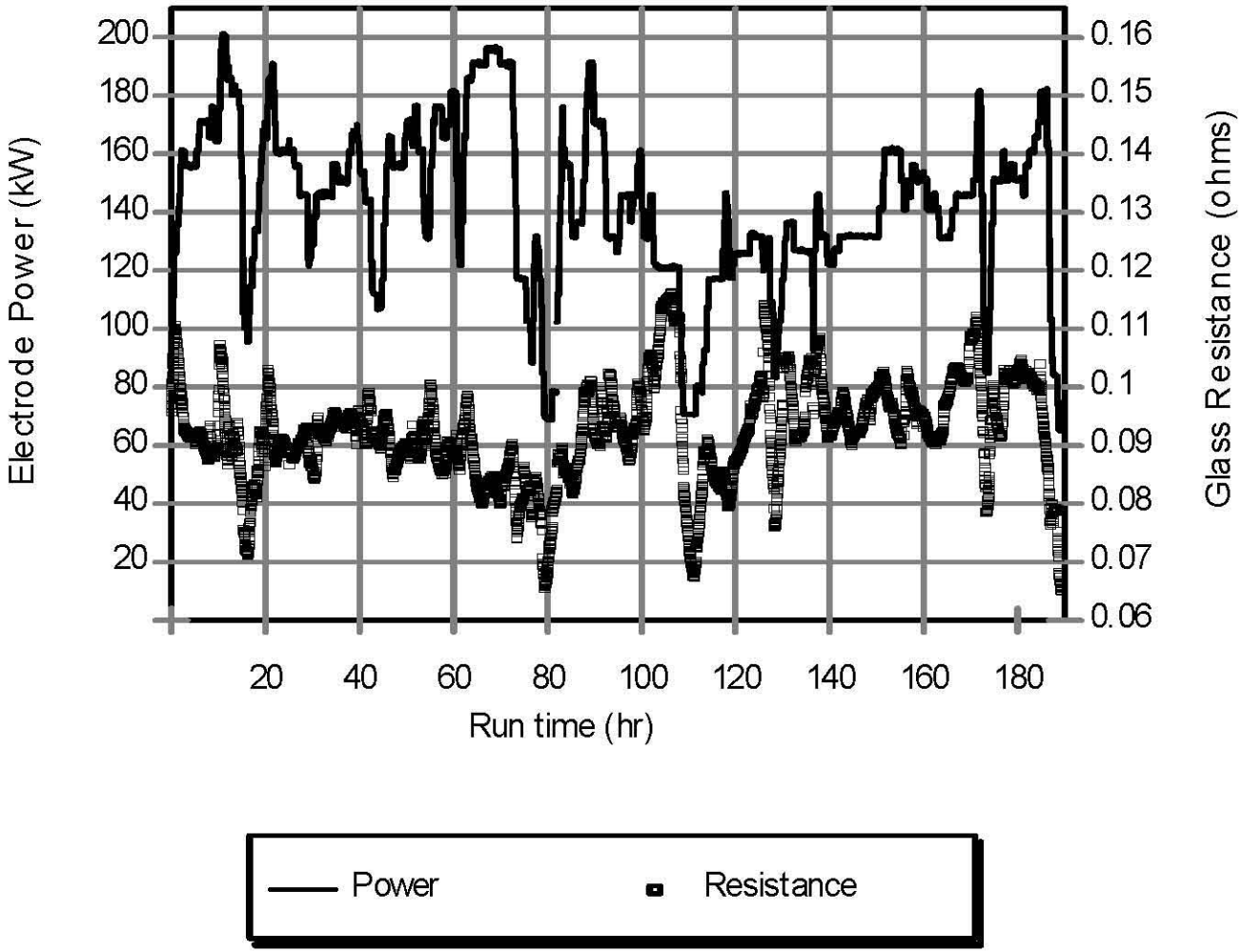

Figure 4.5. Electrode power and glass resistance for DM1200 Tests.

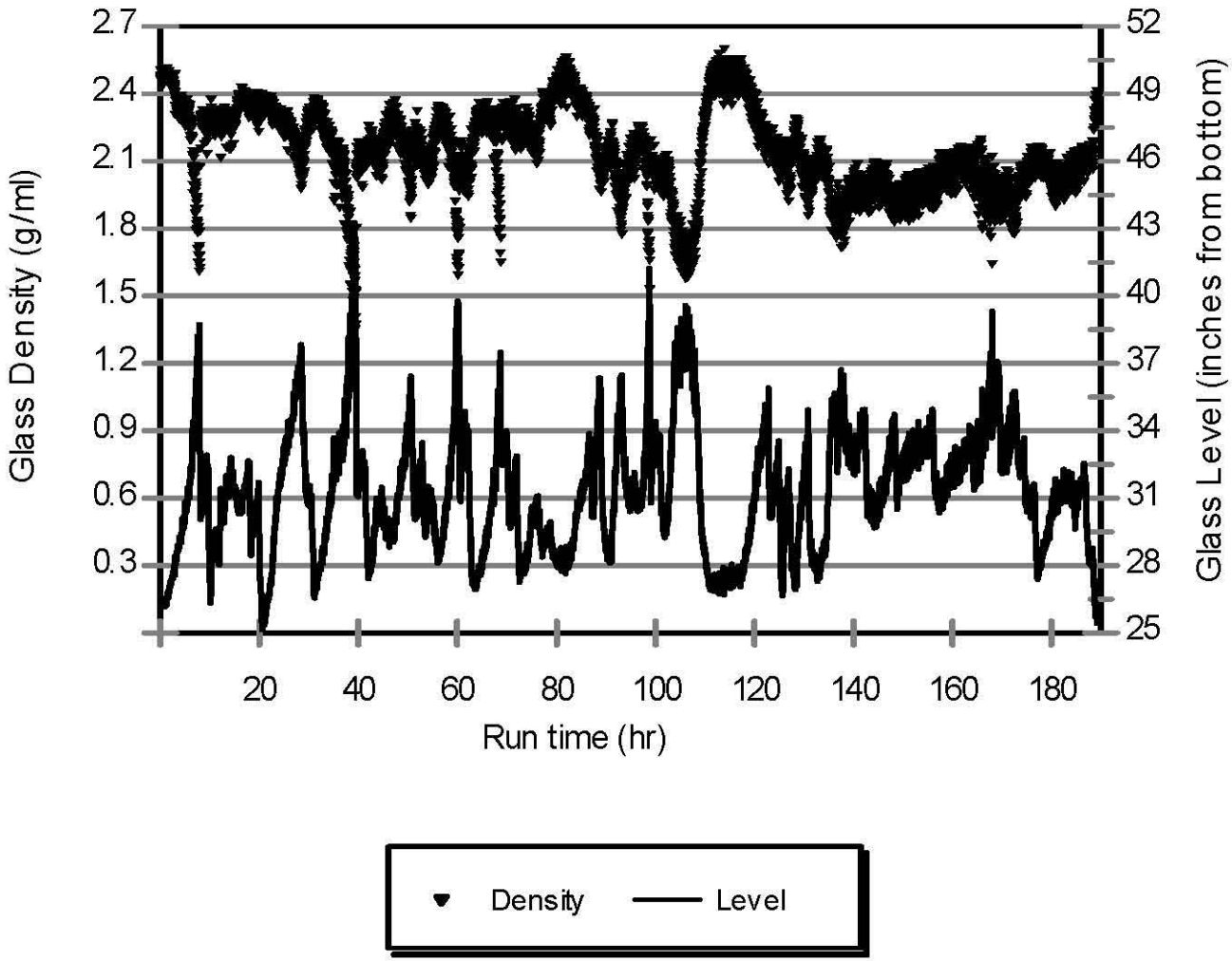

Figure 4.6. Glass density and level for DM1200 Tests.

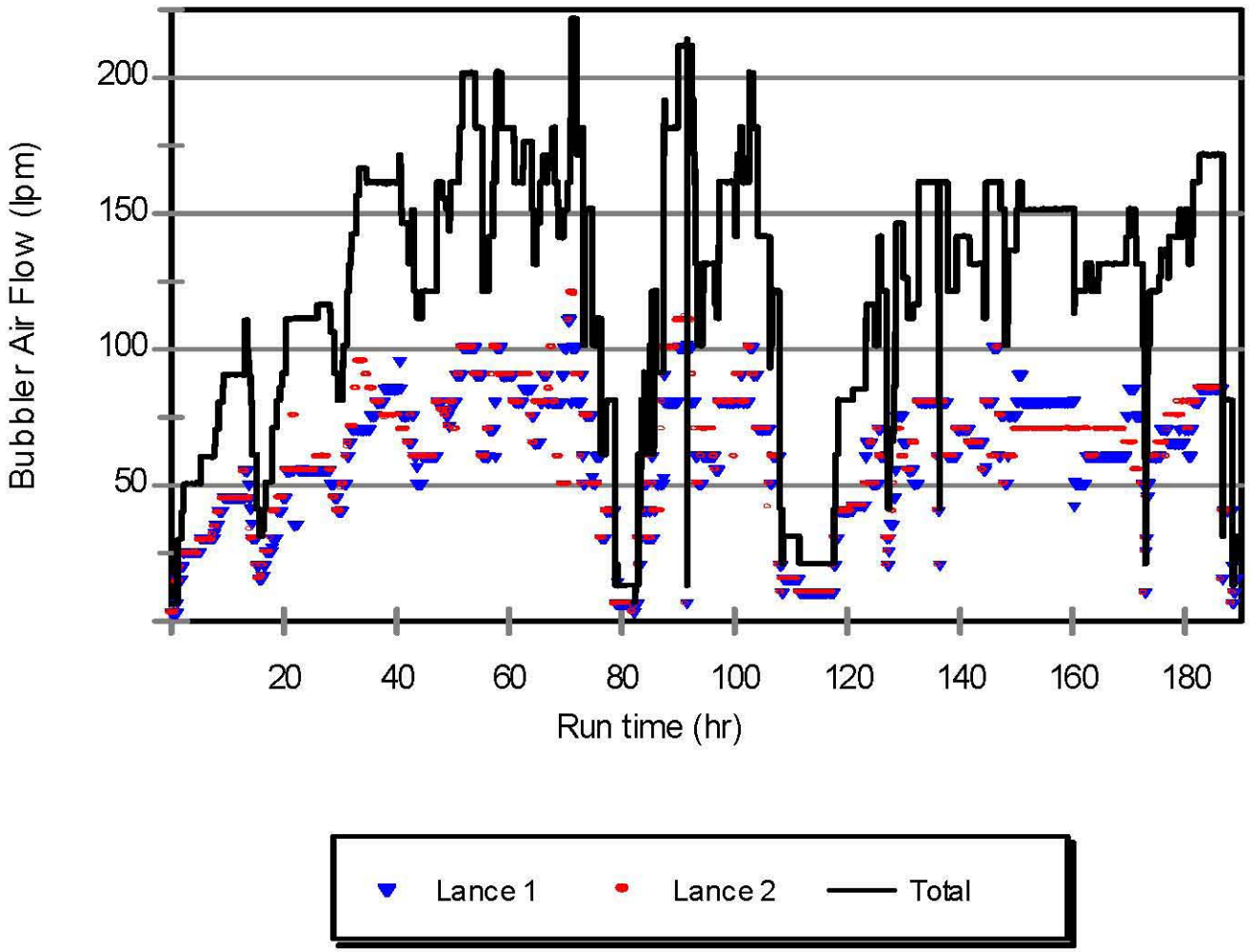

Figure 4.7. Glass pool bubbling for DM1200 Tests.

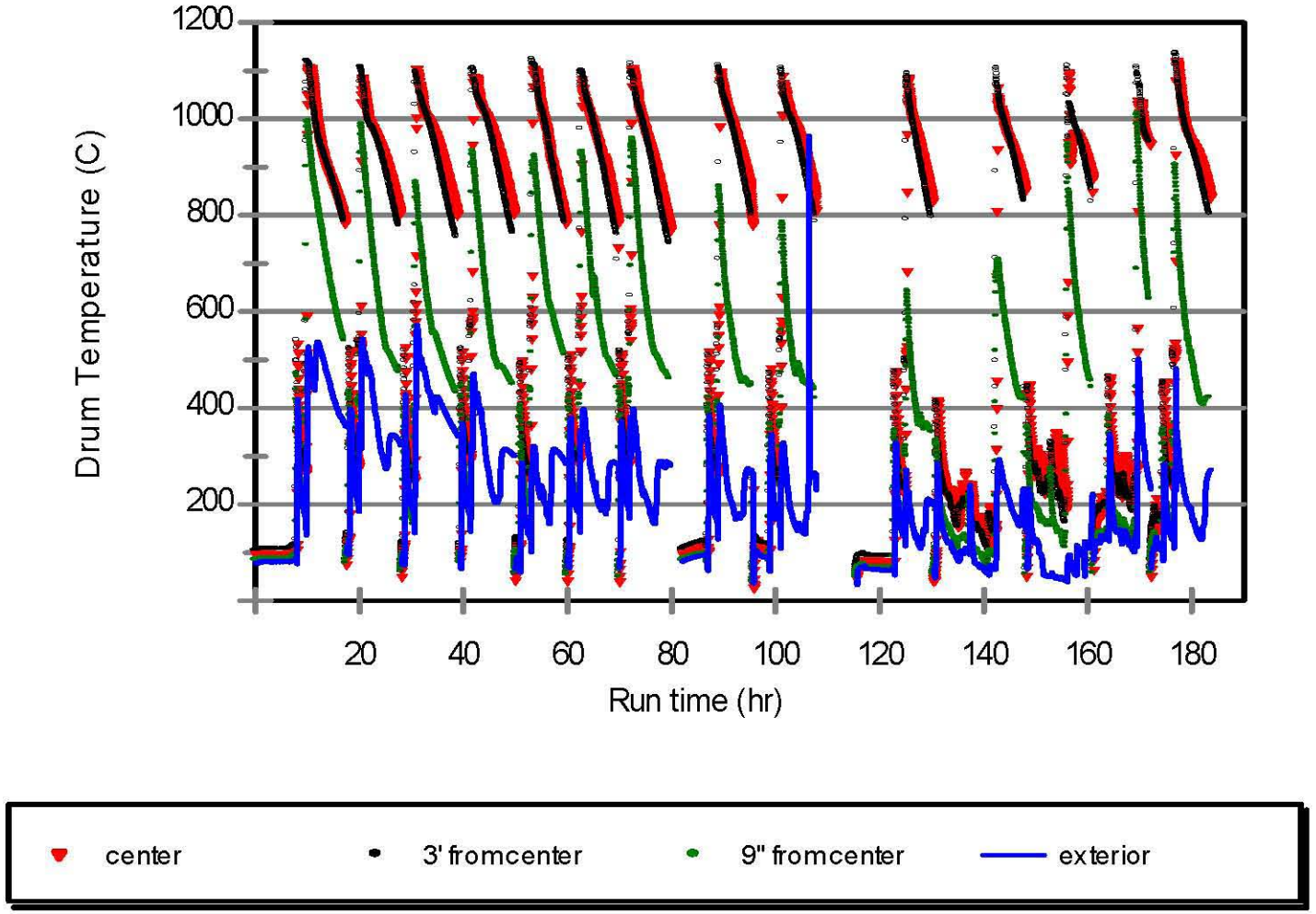

Figure 4.8. Measured temperatures from canister cooling experiments.

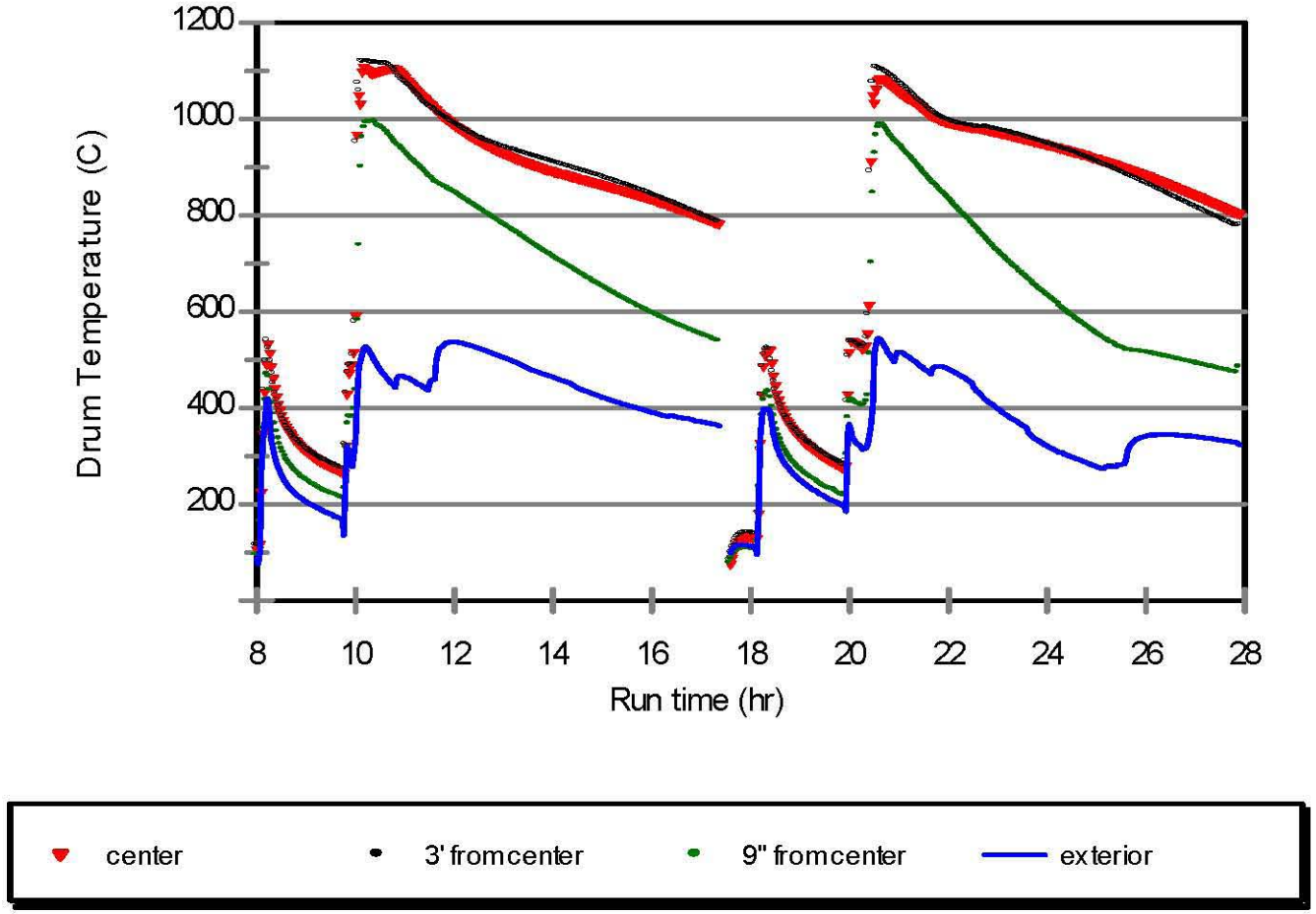

Figure 4.9. Measured temperatures from first two canister cooling experiments.

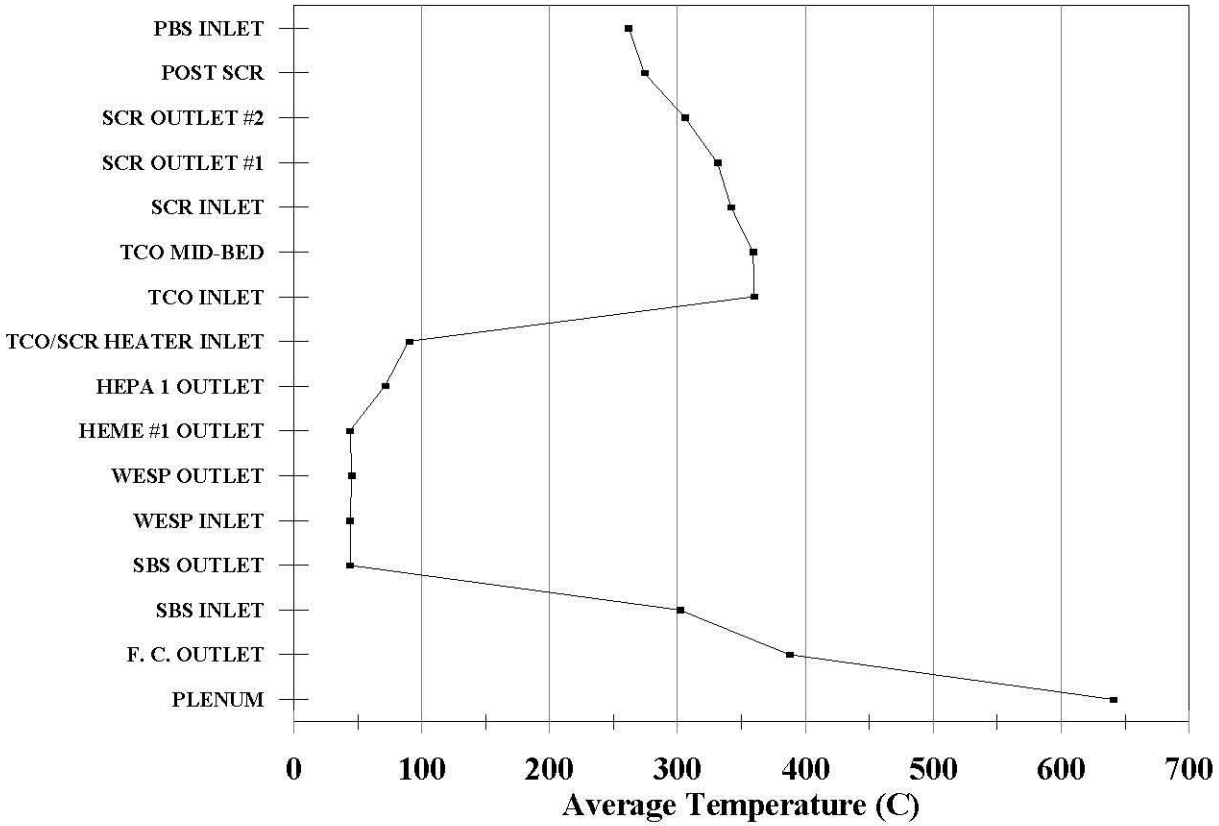

Figure 4.10.a. Average gas temperatures along the DM1200 off-gas train during the first portion of testing.

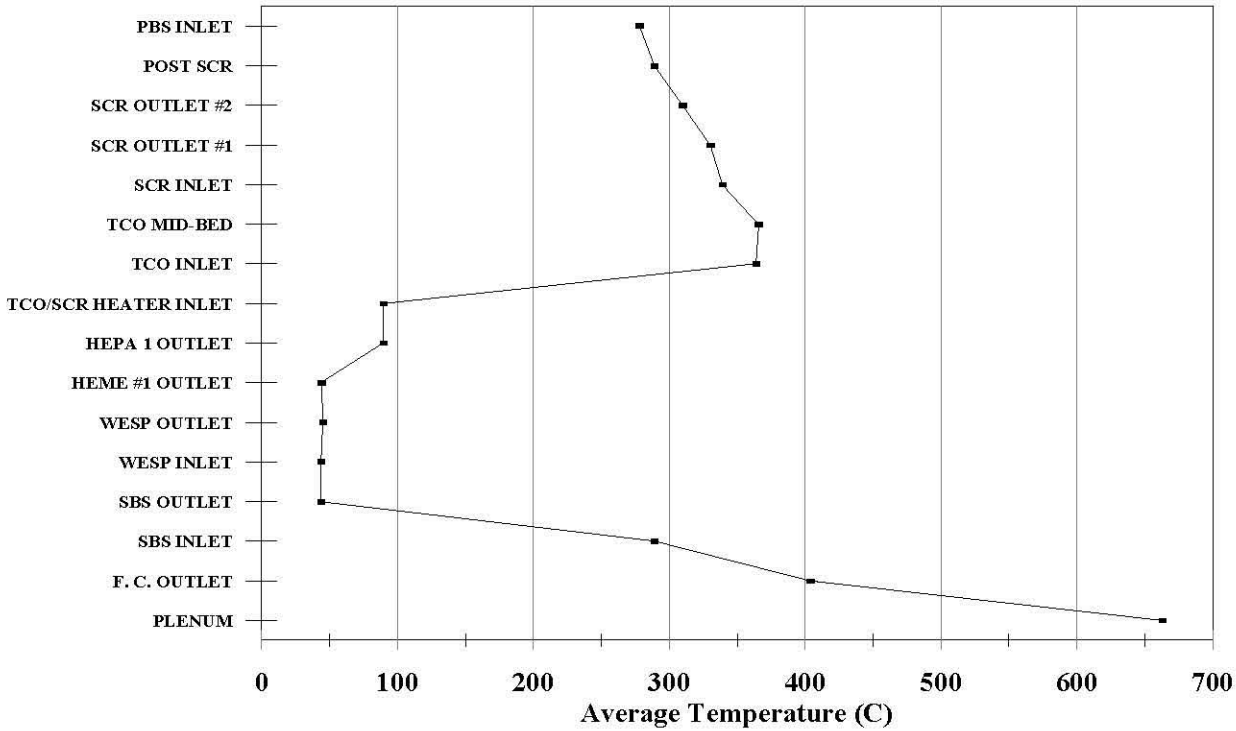

Figure 4.10b. Average gas temperatures along theDM1200 off-gas train during the second portion of testing.

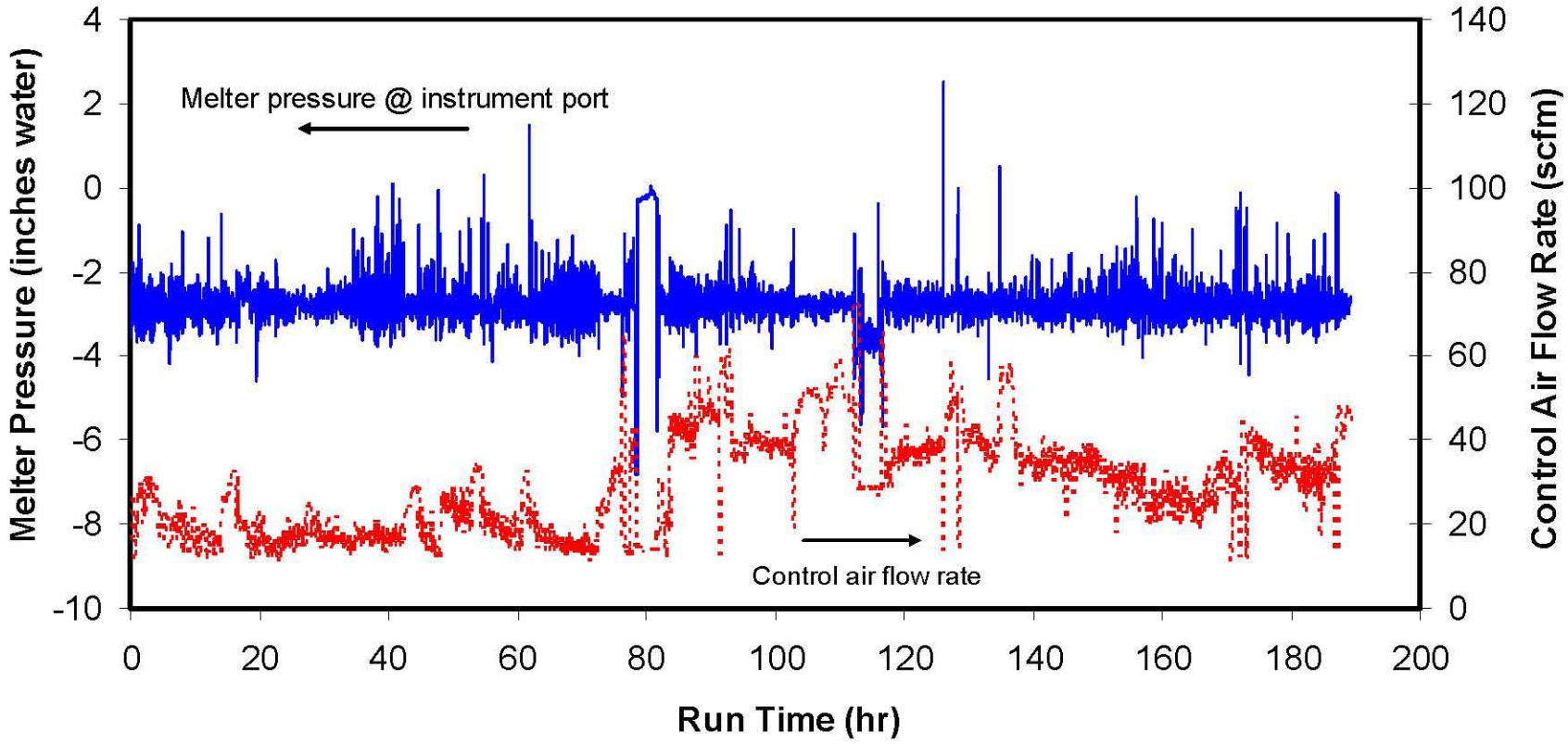

Figure 4.11. Melter pressure at instrument port and control air flow rate during testing.

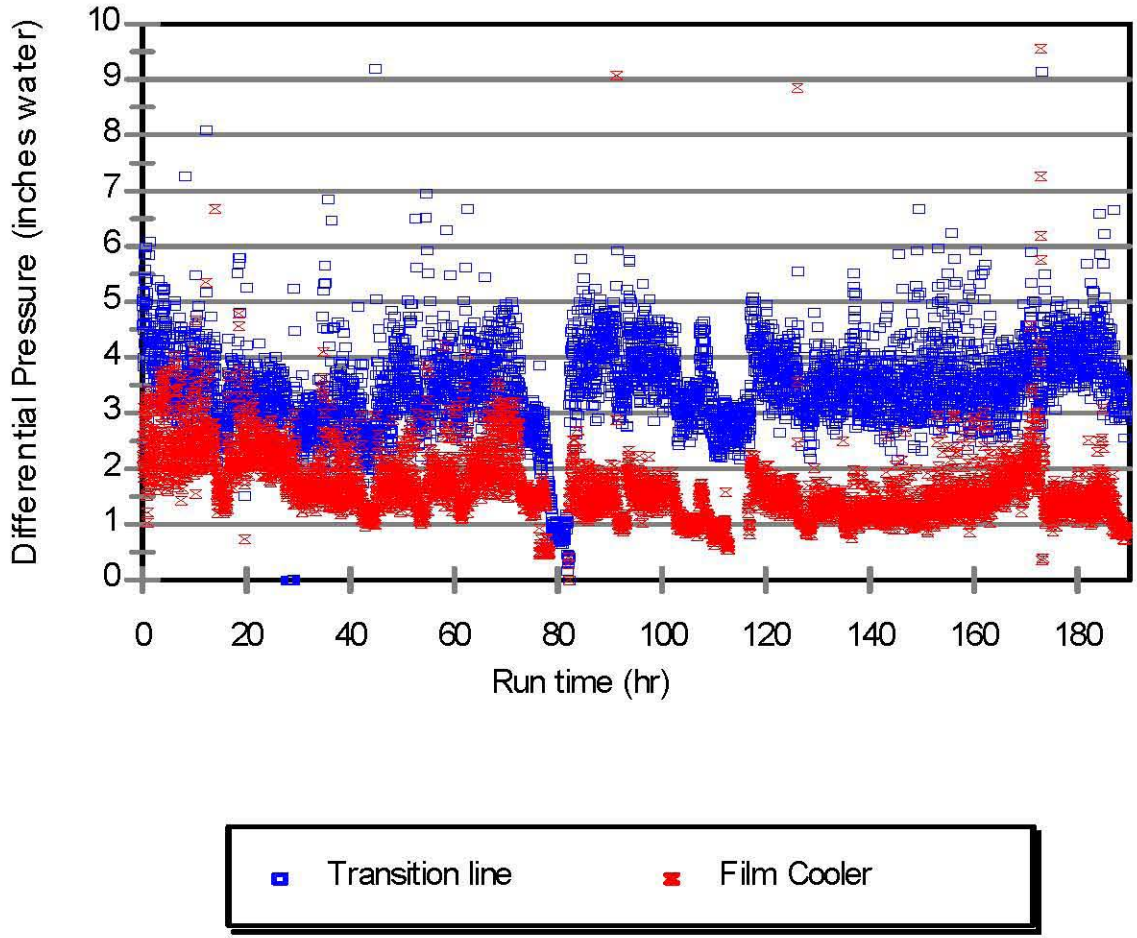

Figure 4.12. Differential pressure across the transition line and film cooler during testing.

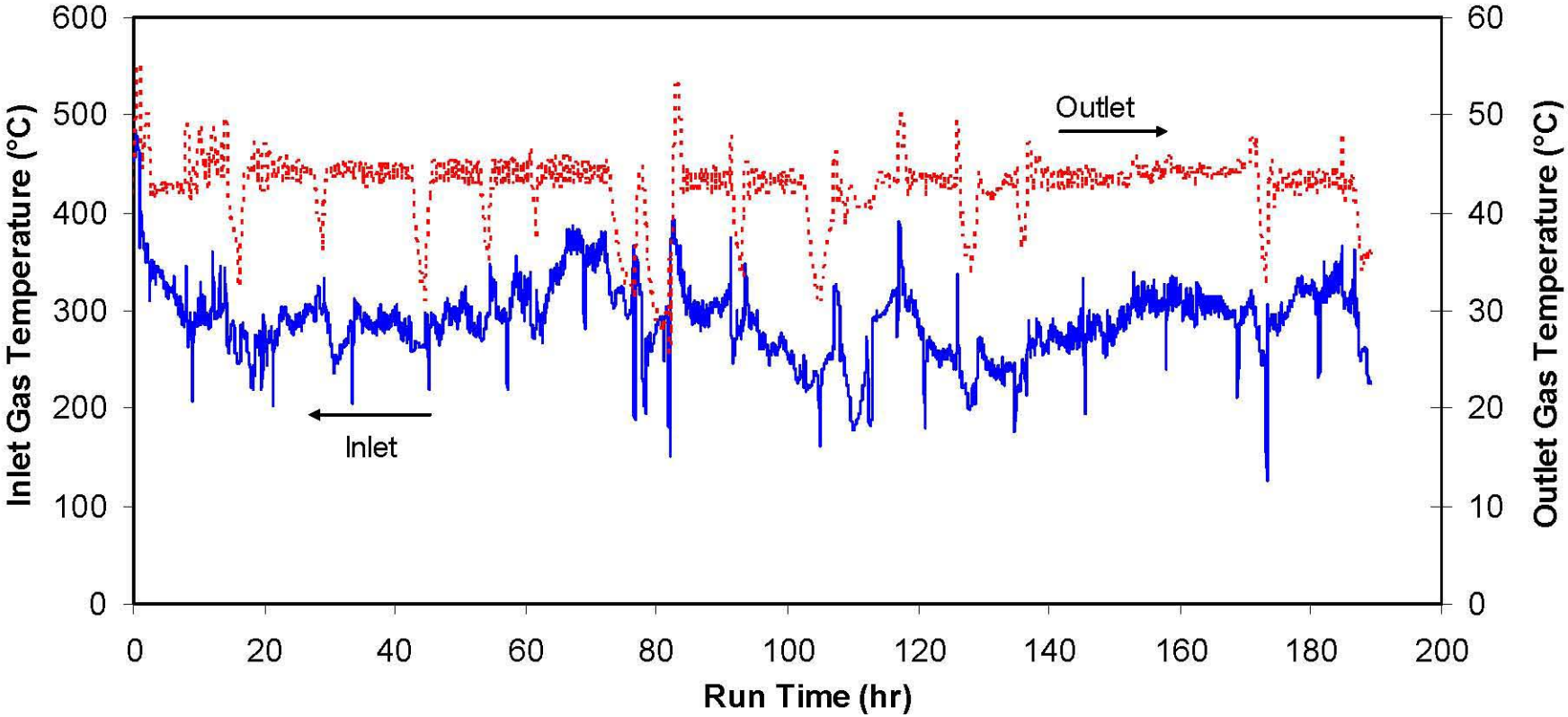

Figure 4.13. SBS inlet and outlet gas temperatures during testing.

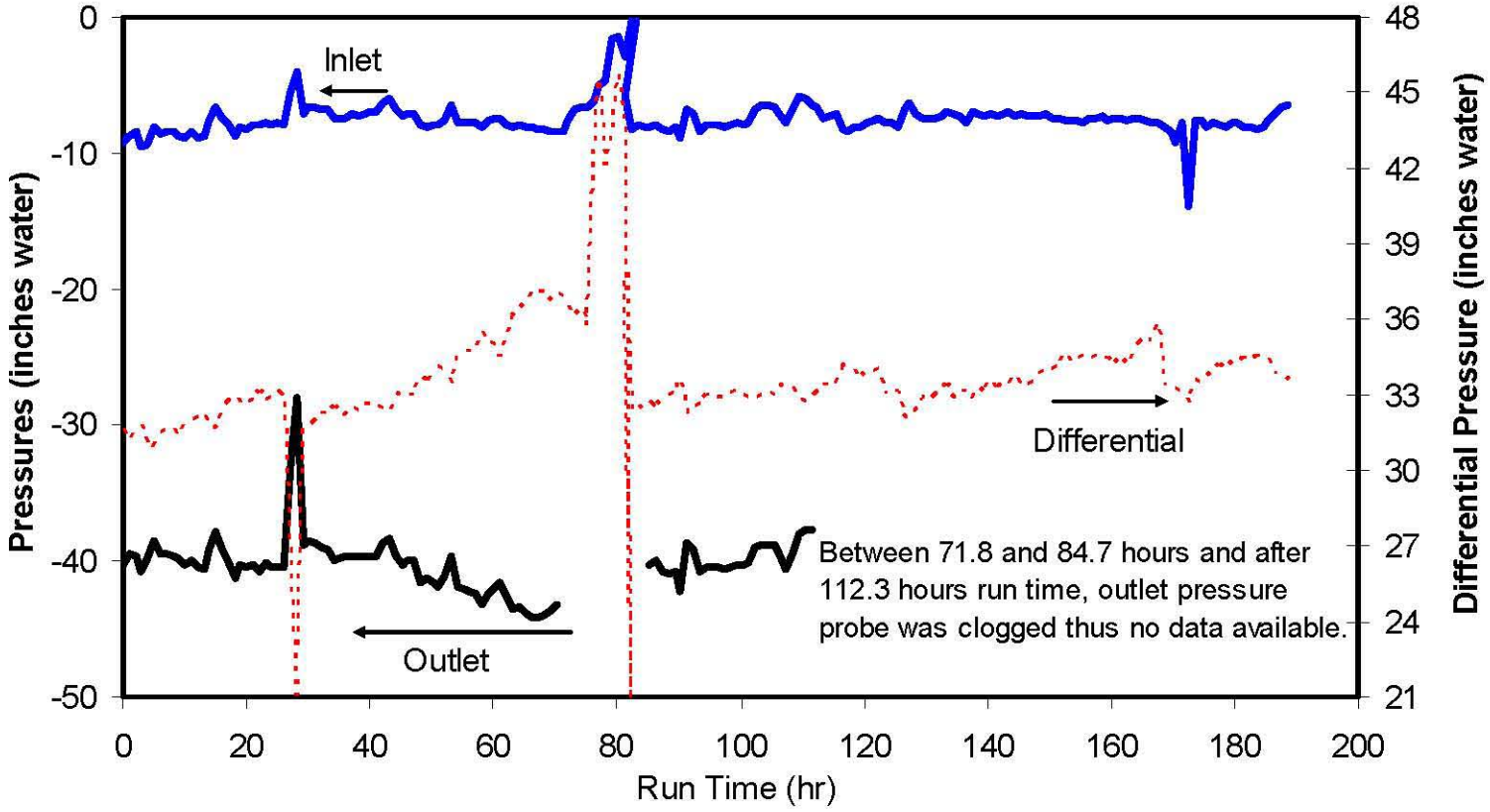

Figure 4.14. SBS inlet, outlet, and differential pressures (hourly average values) during testing.

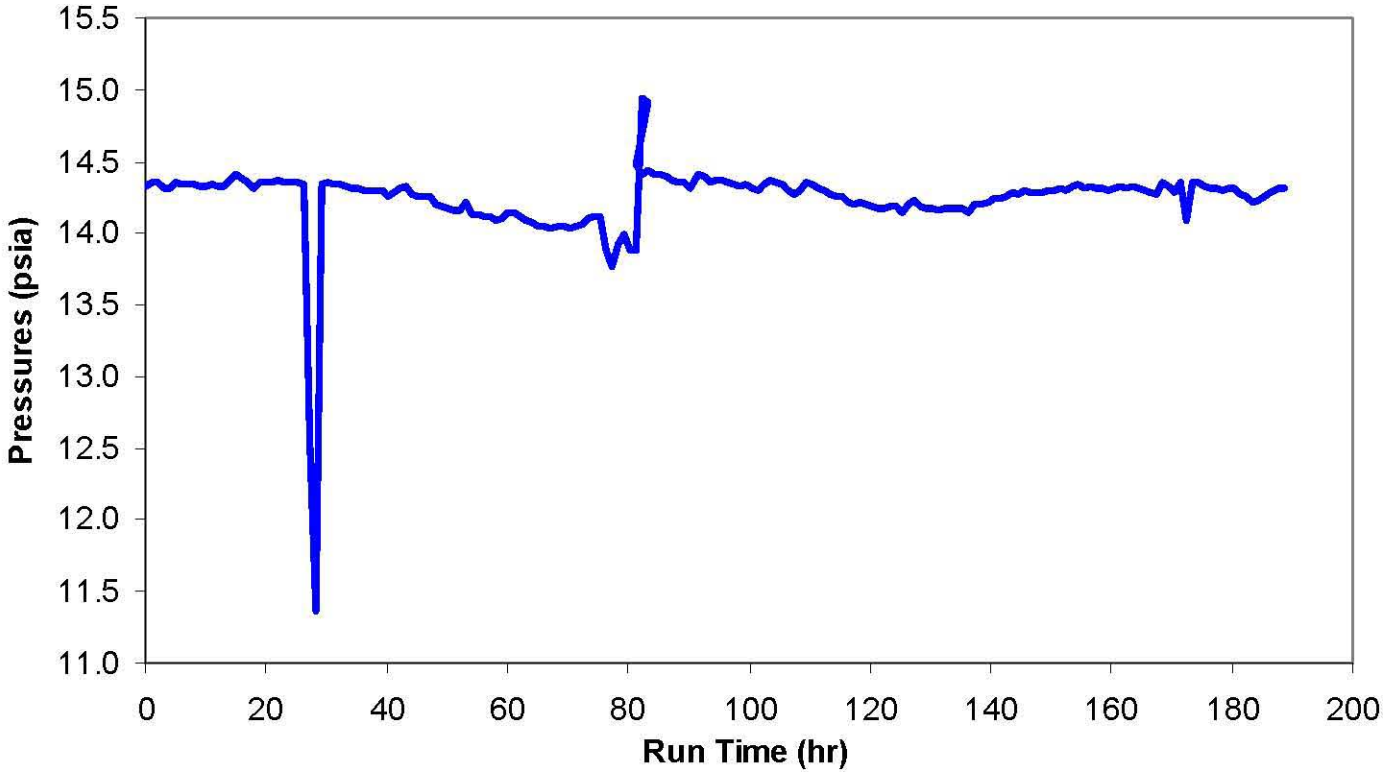

Figure 4.15. SBS downcomer annulus pressure (hourly average values) during testing.

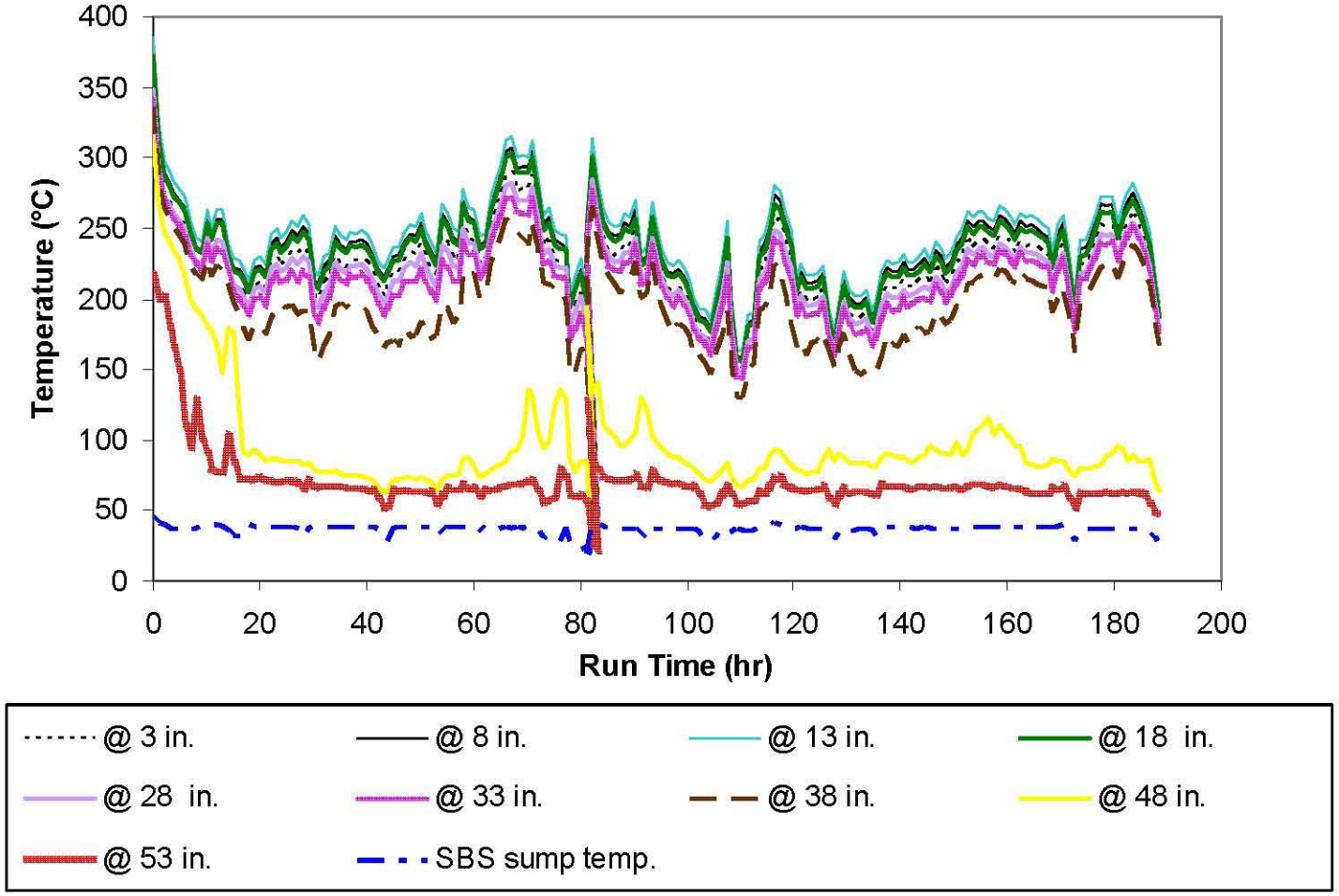

Figure 4.16. Off-gas temperatures in the SBS downcomer and sump water temperatures (hourly average values) during testing.

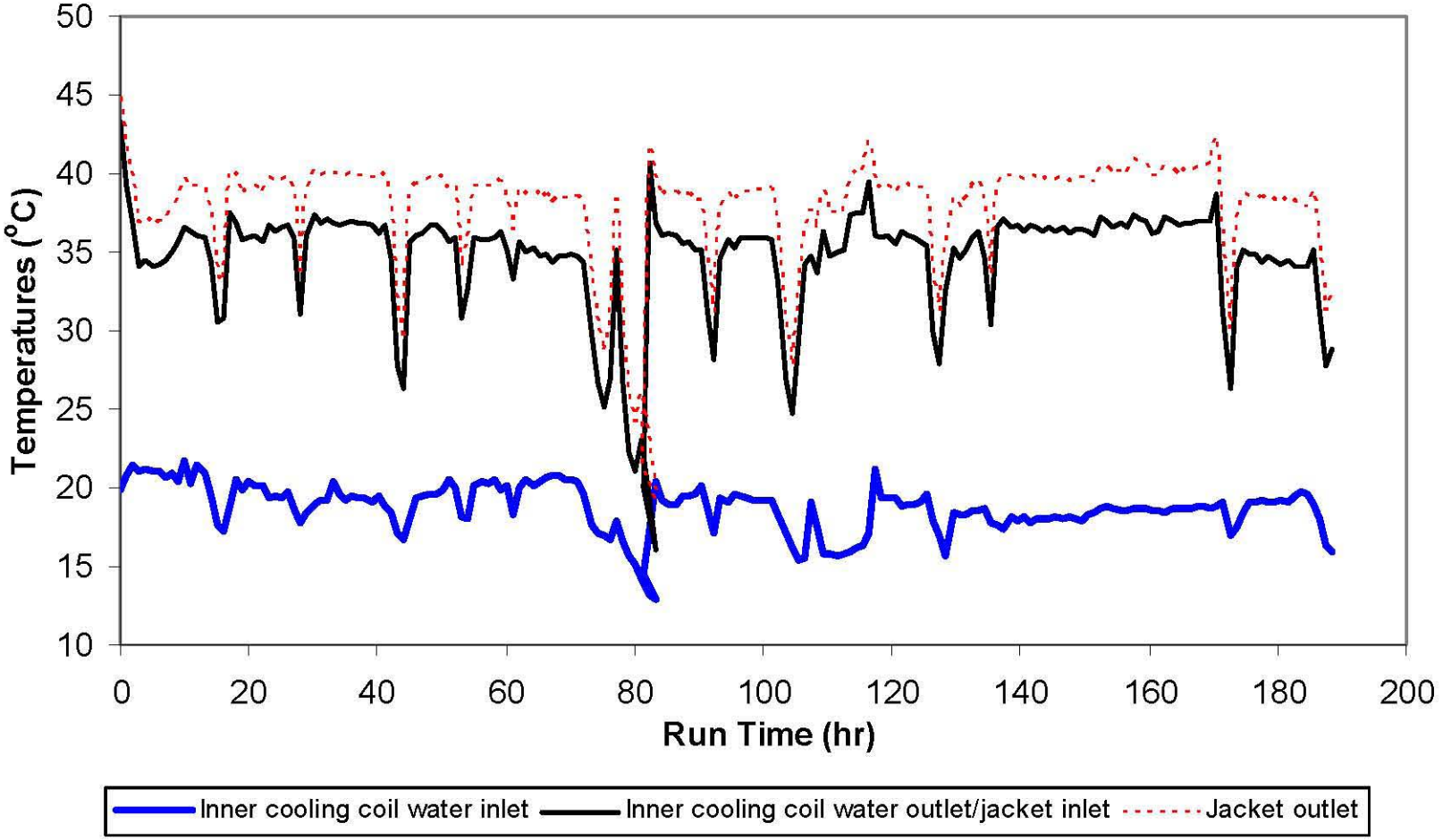

Figure 4.17. SBS cooling coil inlet, cooling coil outlet/jacket inlet and jacket outlet water temperatures (hourly average values) during testing.

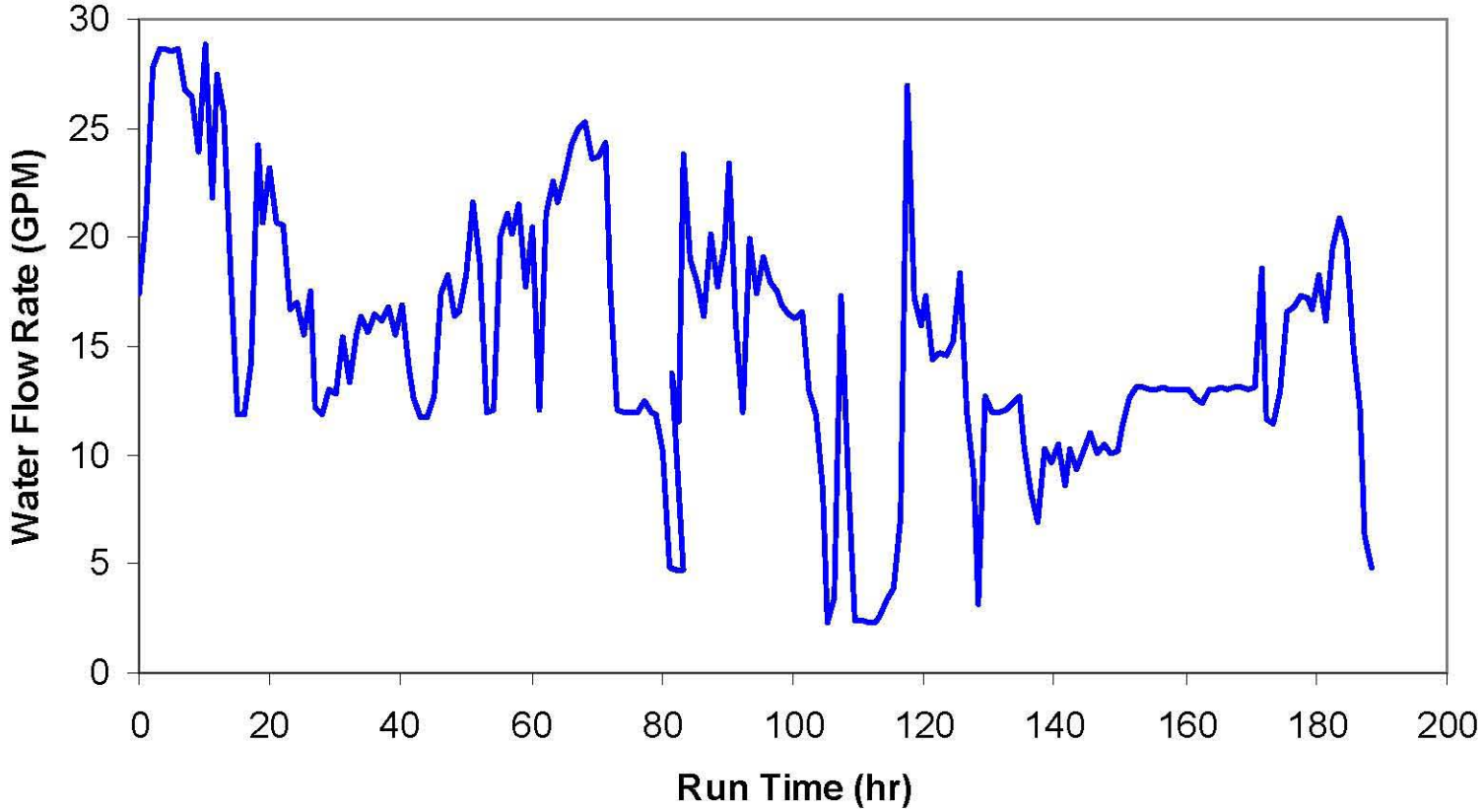

Figure 4.18. SBS cooling coil/jacket water flow rate (hourly average values) during testing.

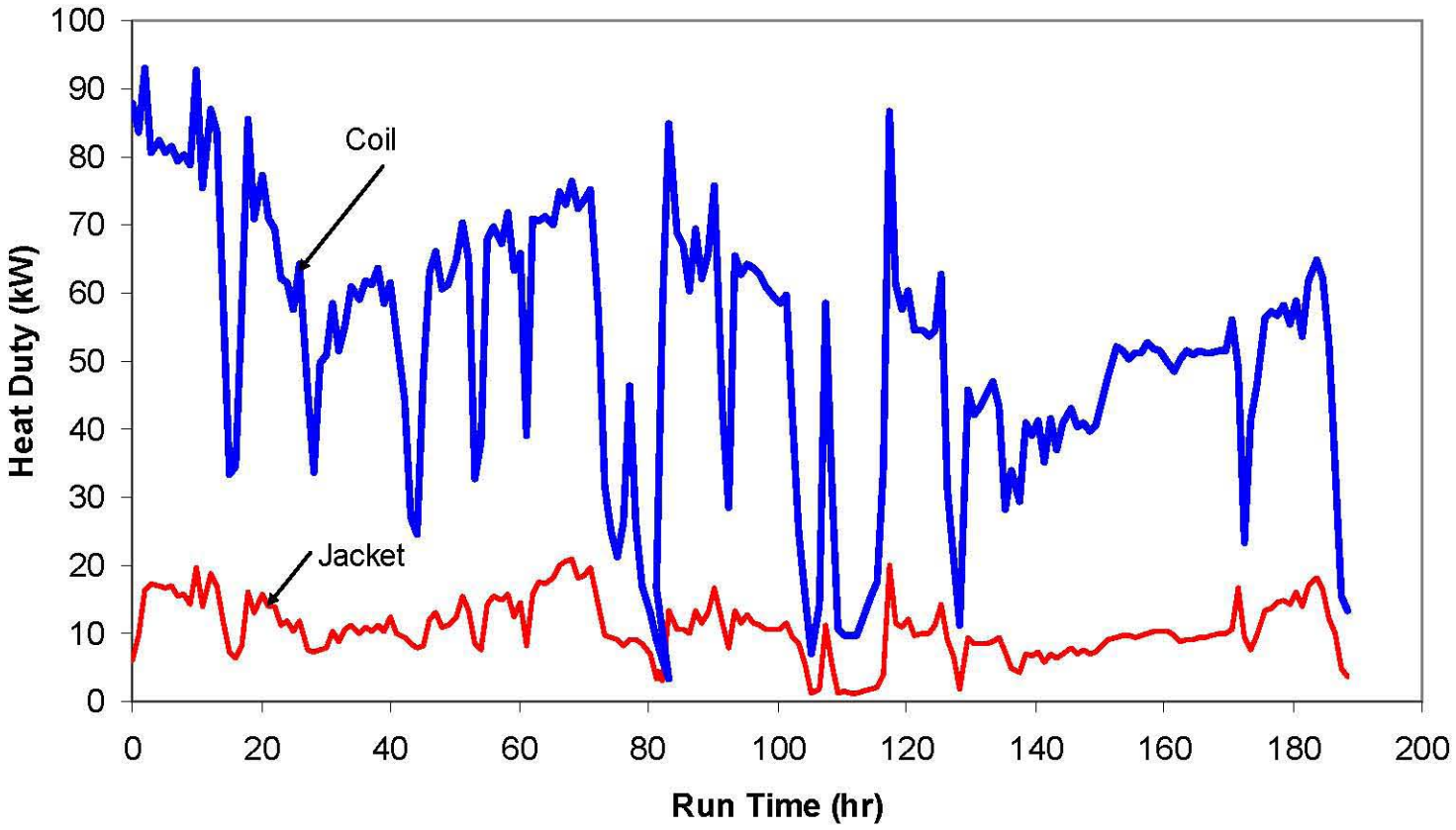

Figure 4.19. Calculated heat loads on the inner coil and jacket (hourly average values) during testing.

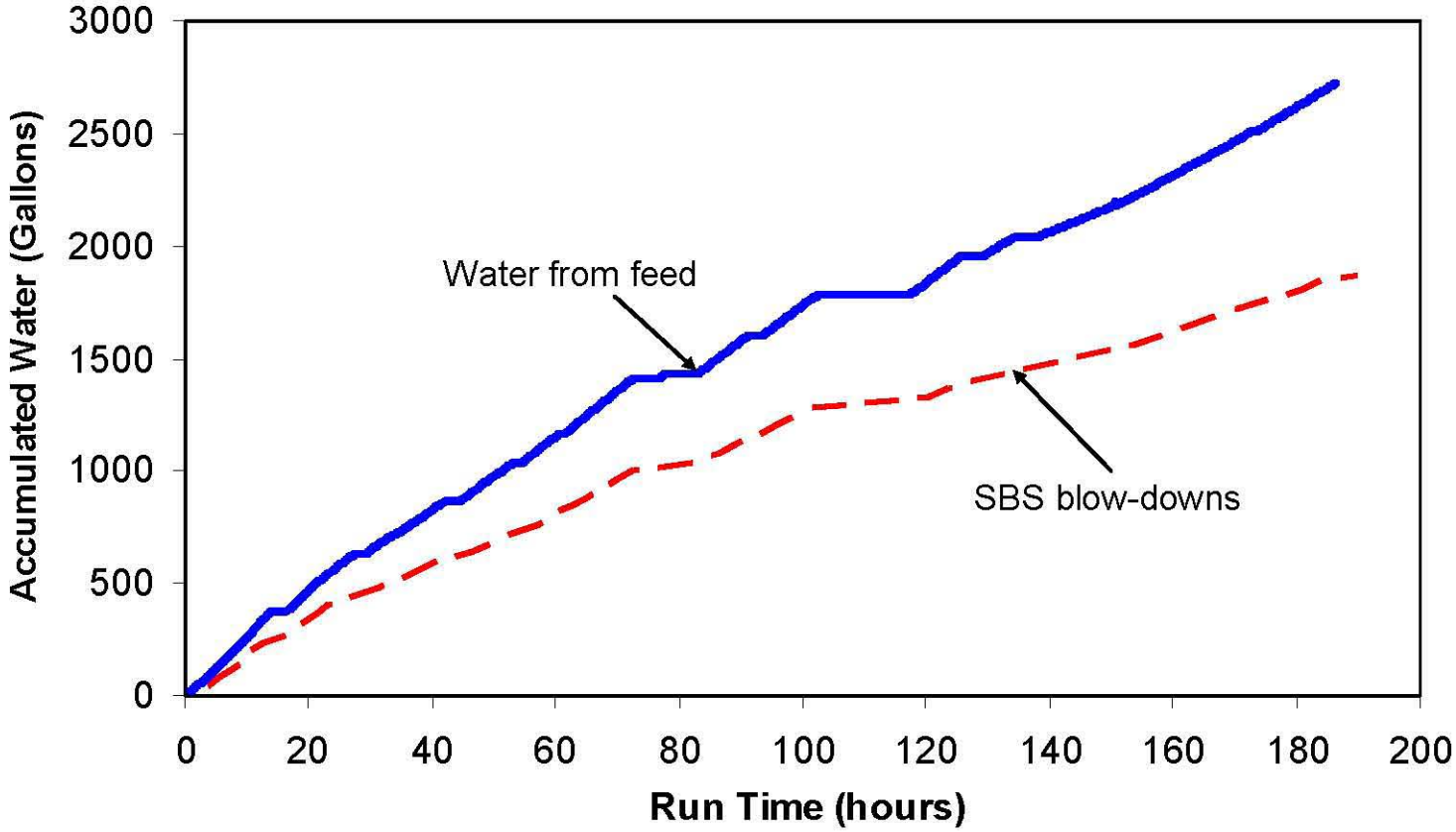

Figure 4.20. Accumulated SBS blowdown volume and accumulated feed water during testing.

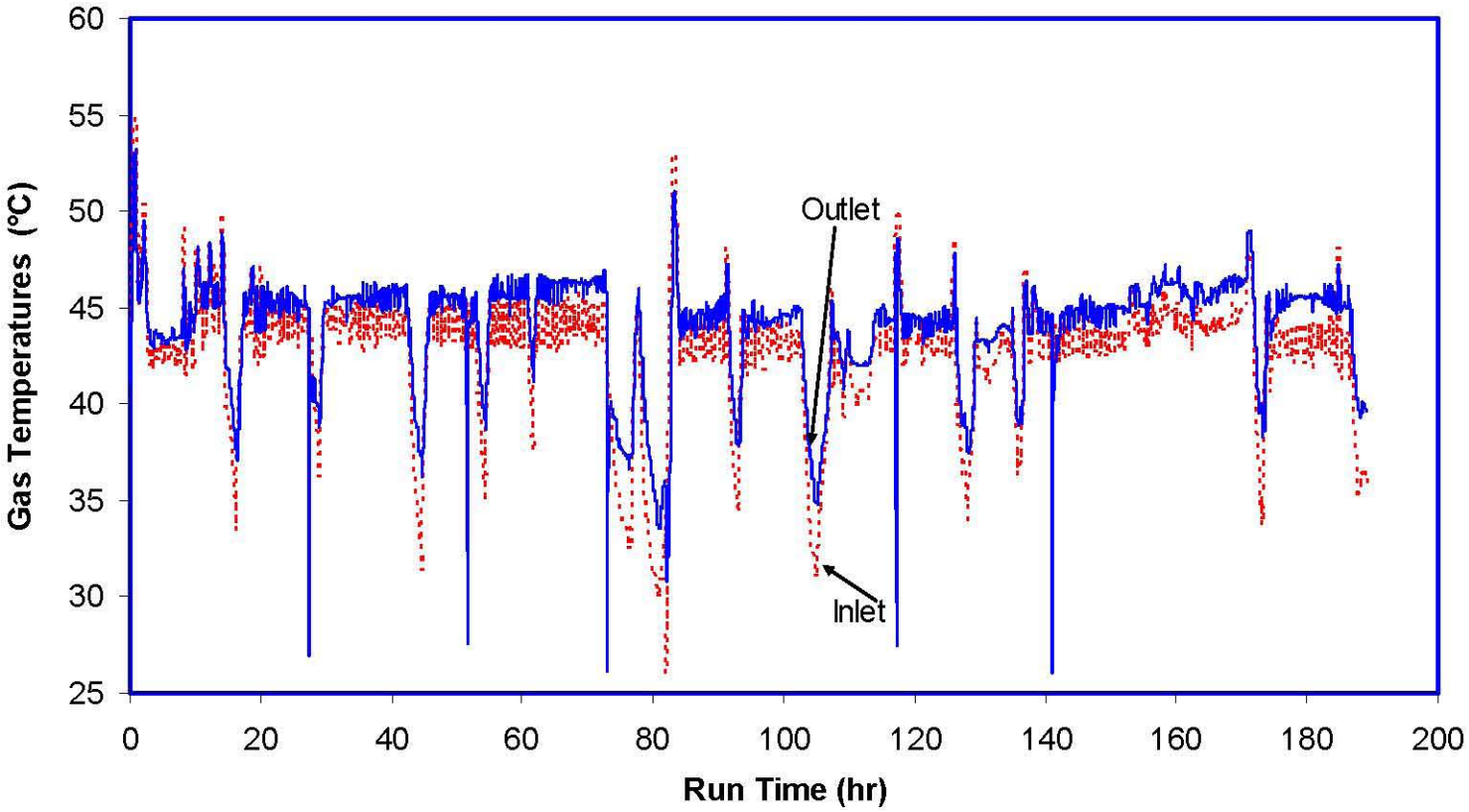

Figure 4.21. WESP inlet and outlet gas temperatures during testing.
(Note: downward outlet temperature spikes are the result of WESP deluges.)

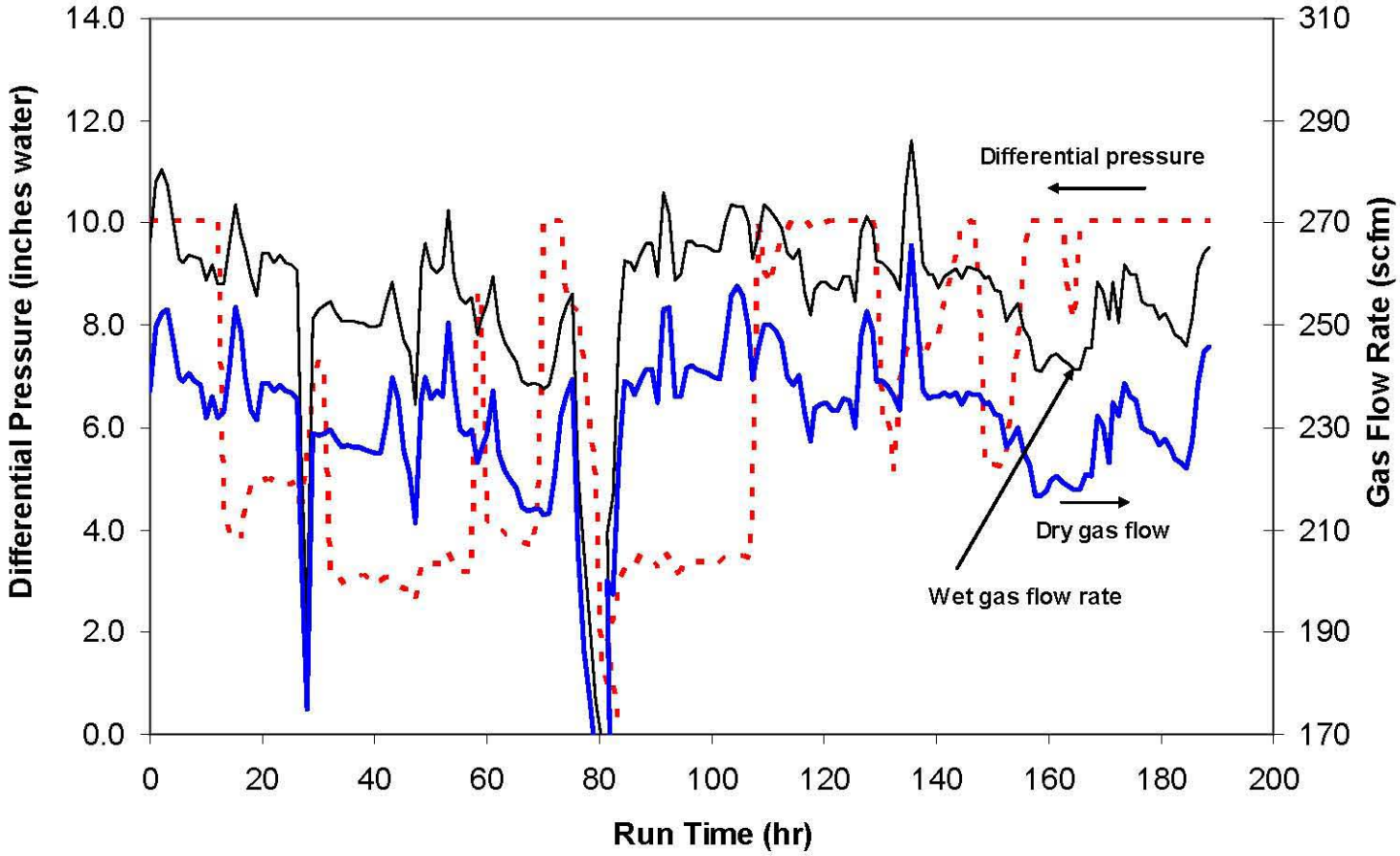

Figure 4.22. WESP differential pressure and outlet gas flow rate (hourly average values) during testing.

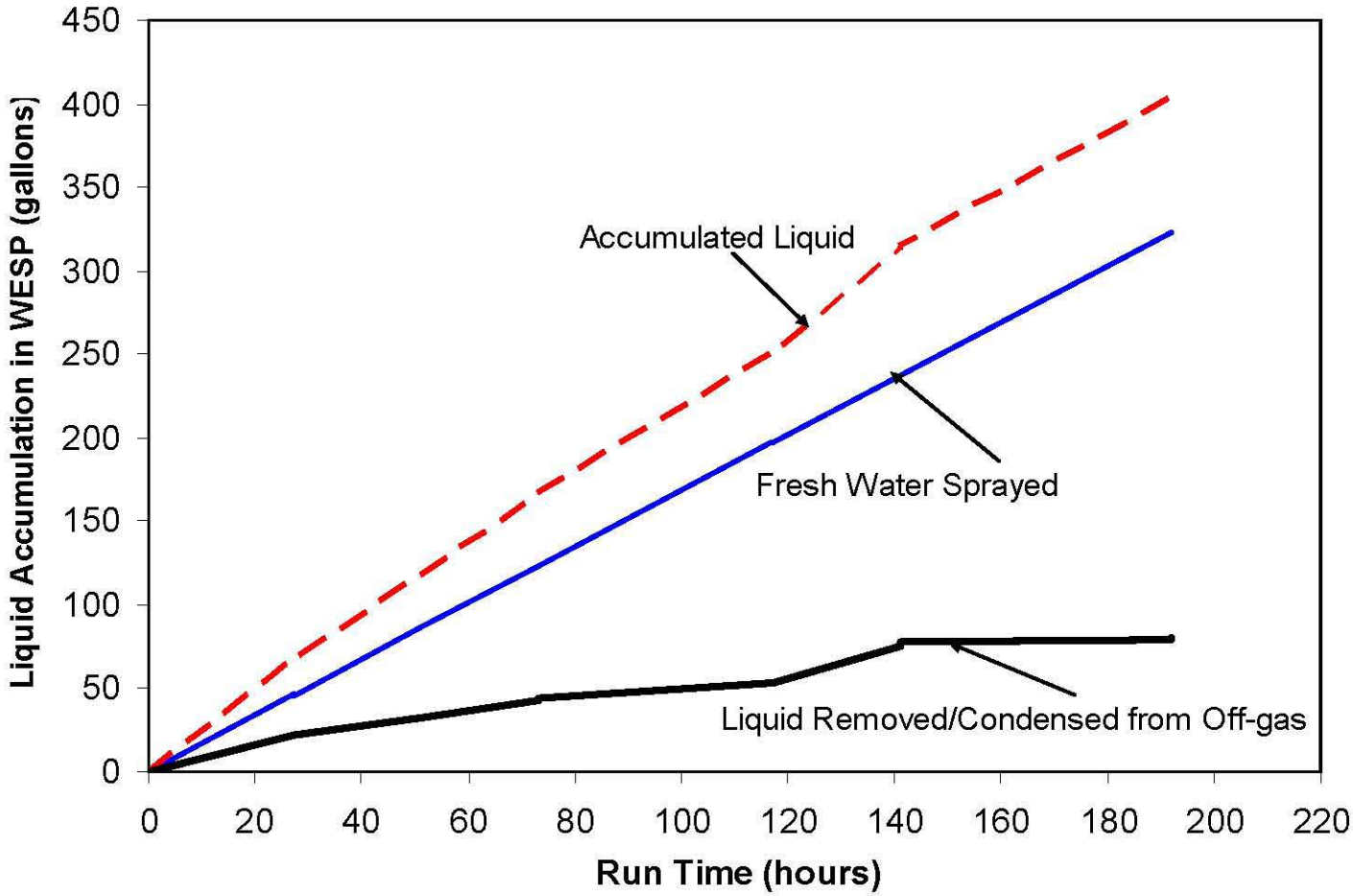

Figure 4.23. Accumulated WESP blowdown volume, accumulated fresh spray water, and water removed from off-gas during testing.

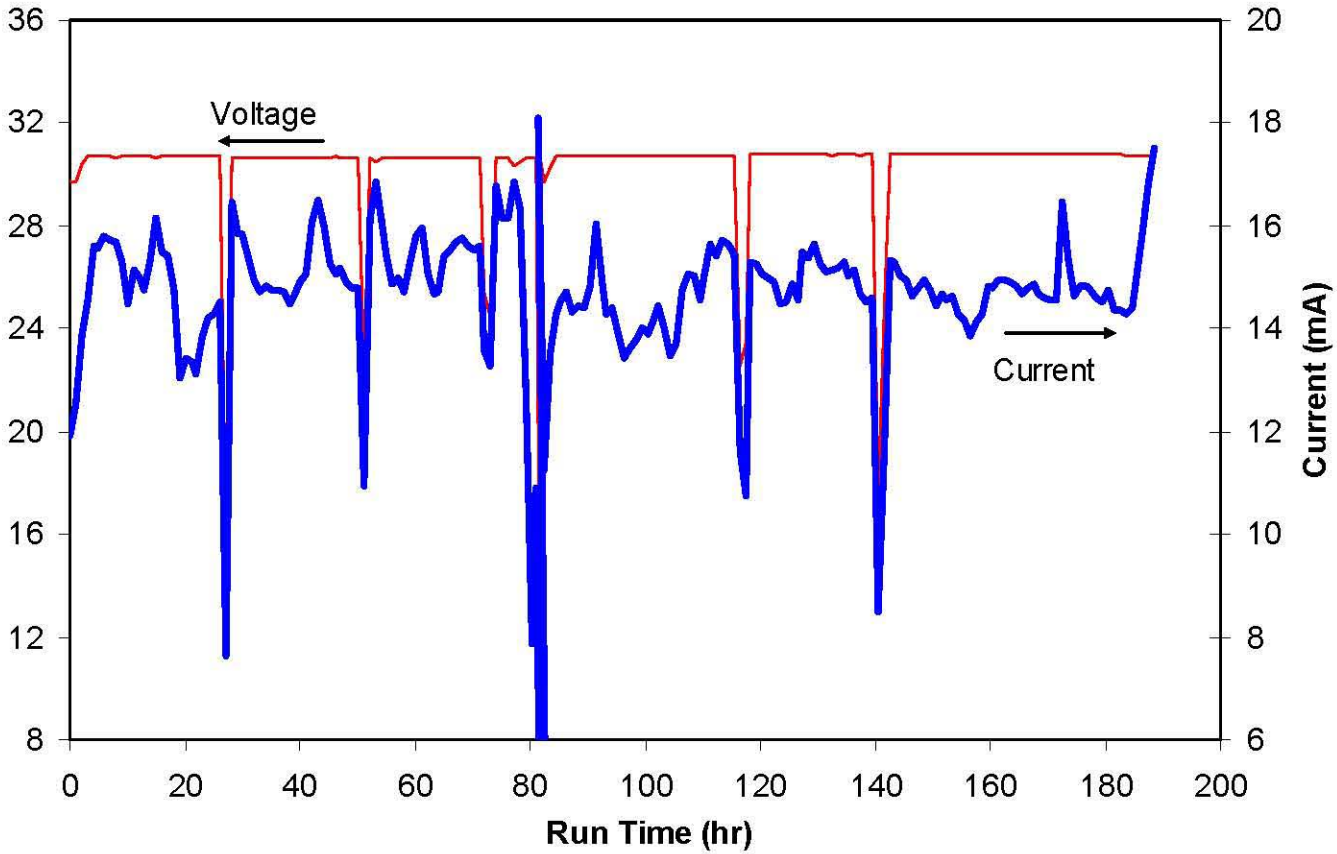

Figure 4.24. Voltage and current across the WESP during testing.

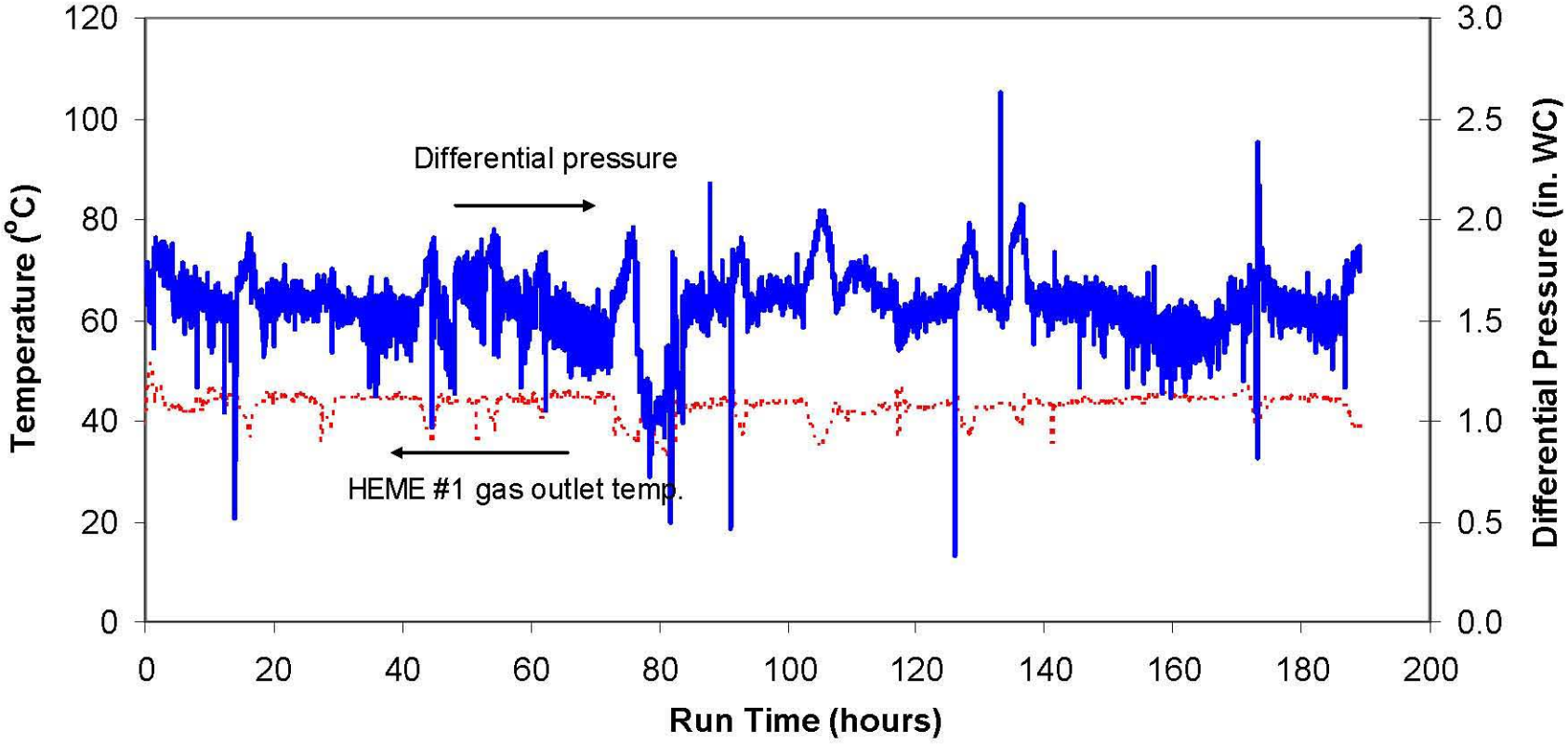

Figure 4.25. Outlet gas temperature and differential pressure for HEME #1 during testing.

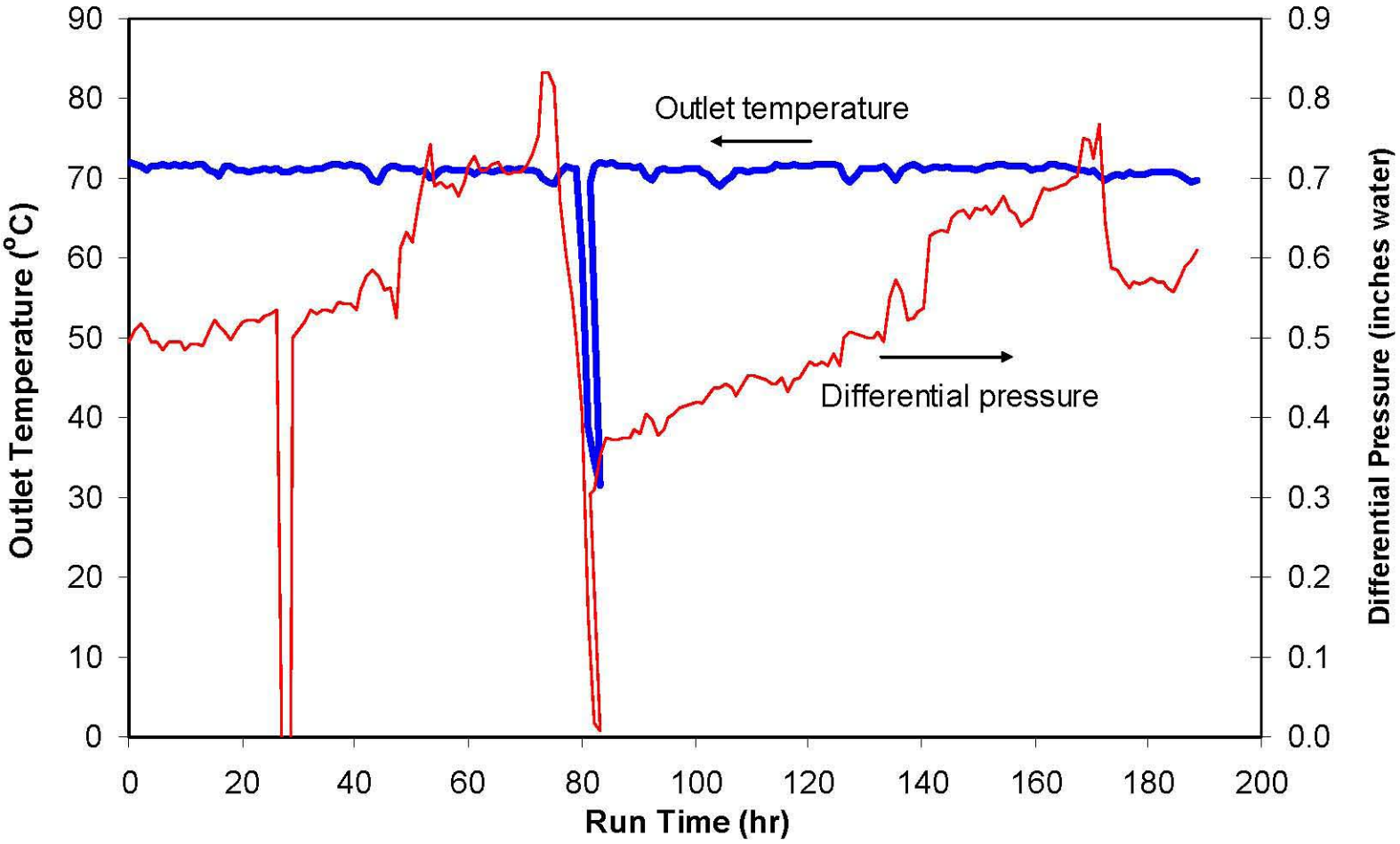

Figure 4.26. Outlet temperature and differential pressure for HEPA #1 (hourly average values) during testing.

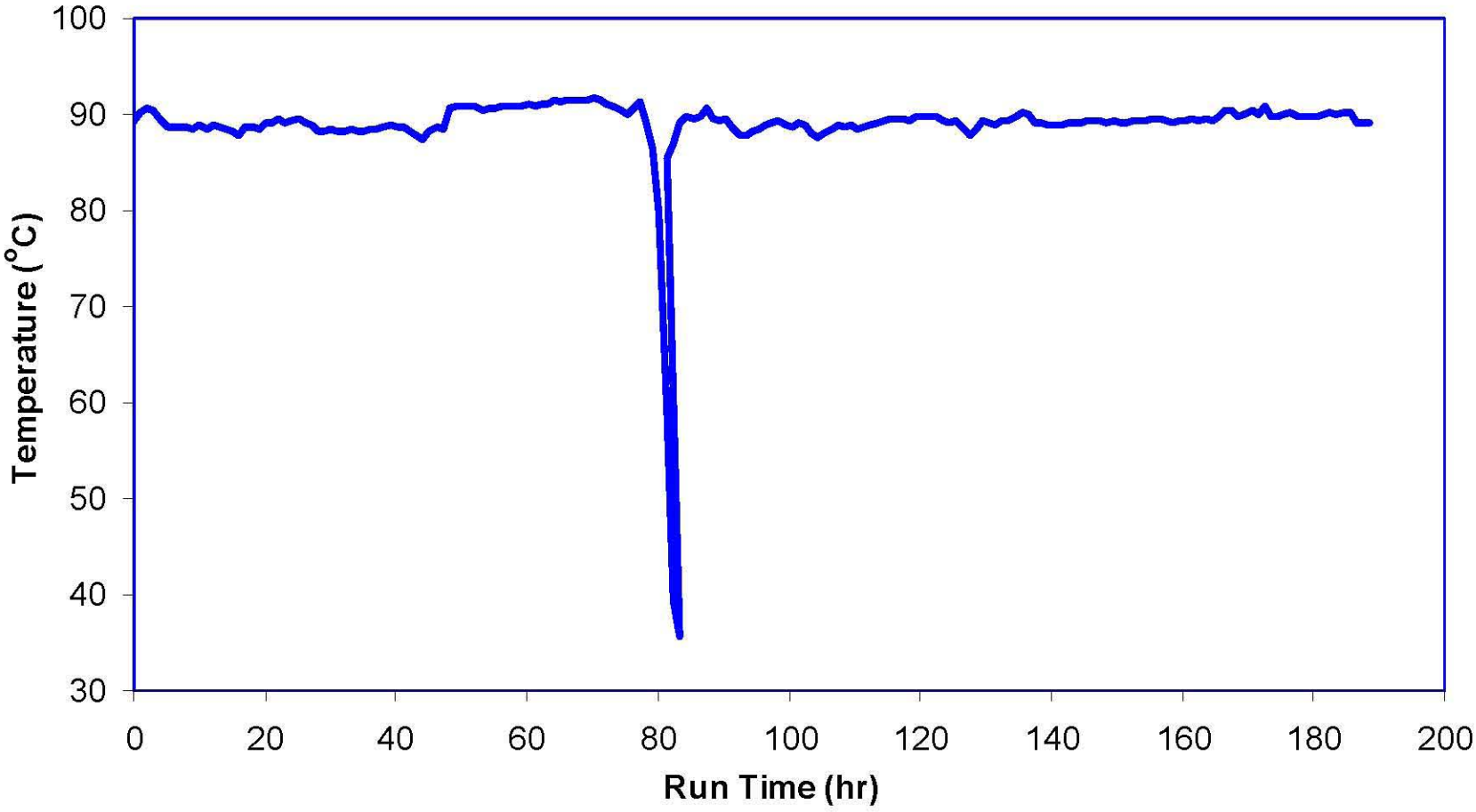

Figure 4.27. TCO/SCR heater gas inlet temperatures during testing.

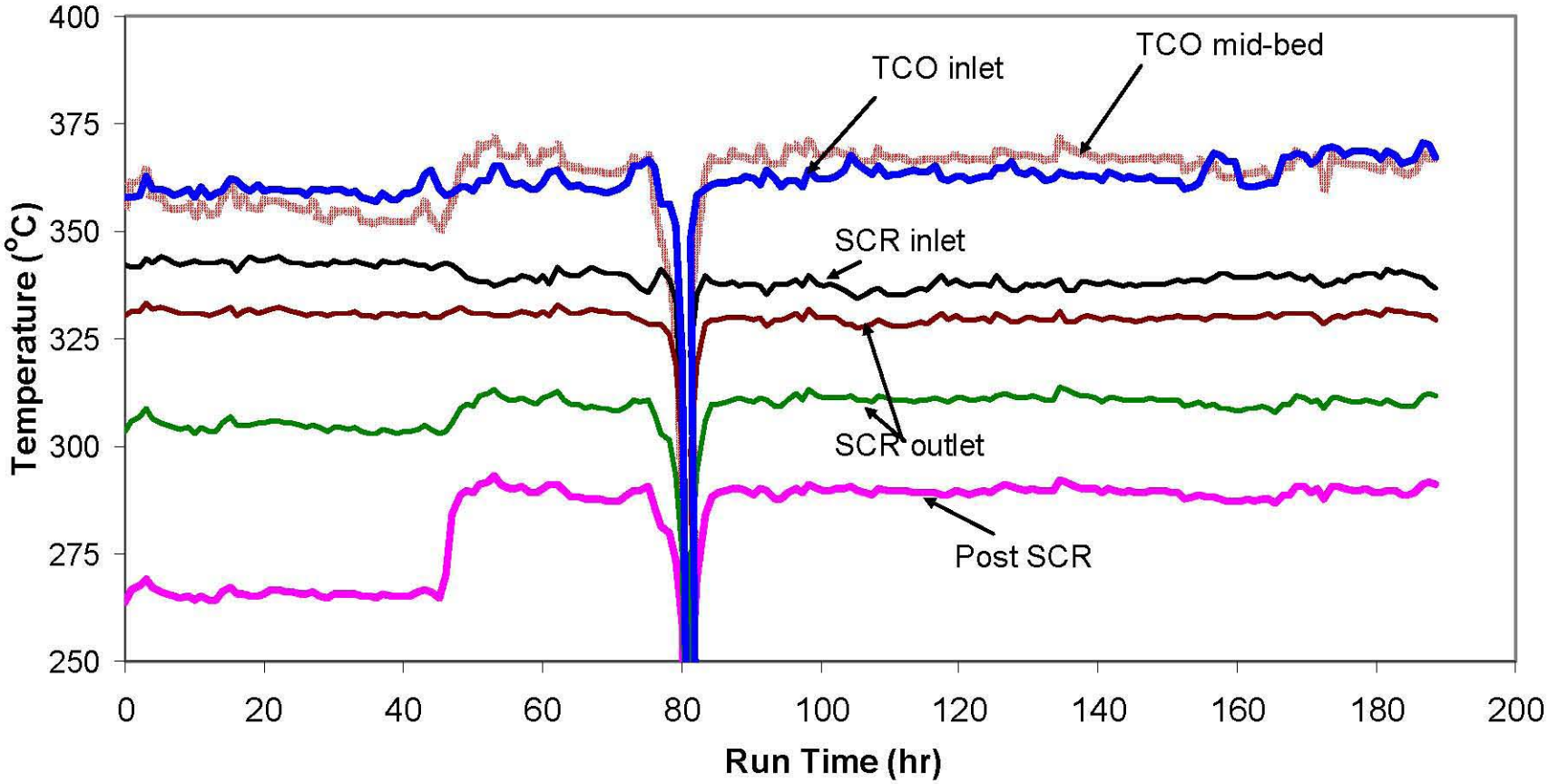

Figure 4.28. TCO/SCR temperatures (average hourly values) during testing.

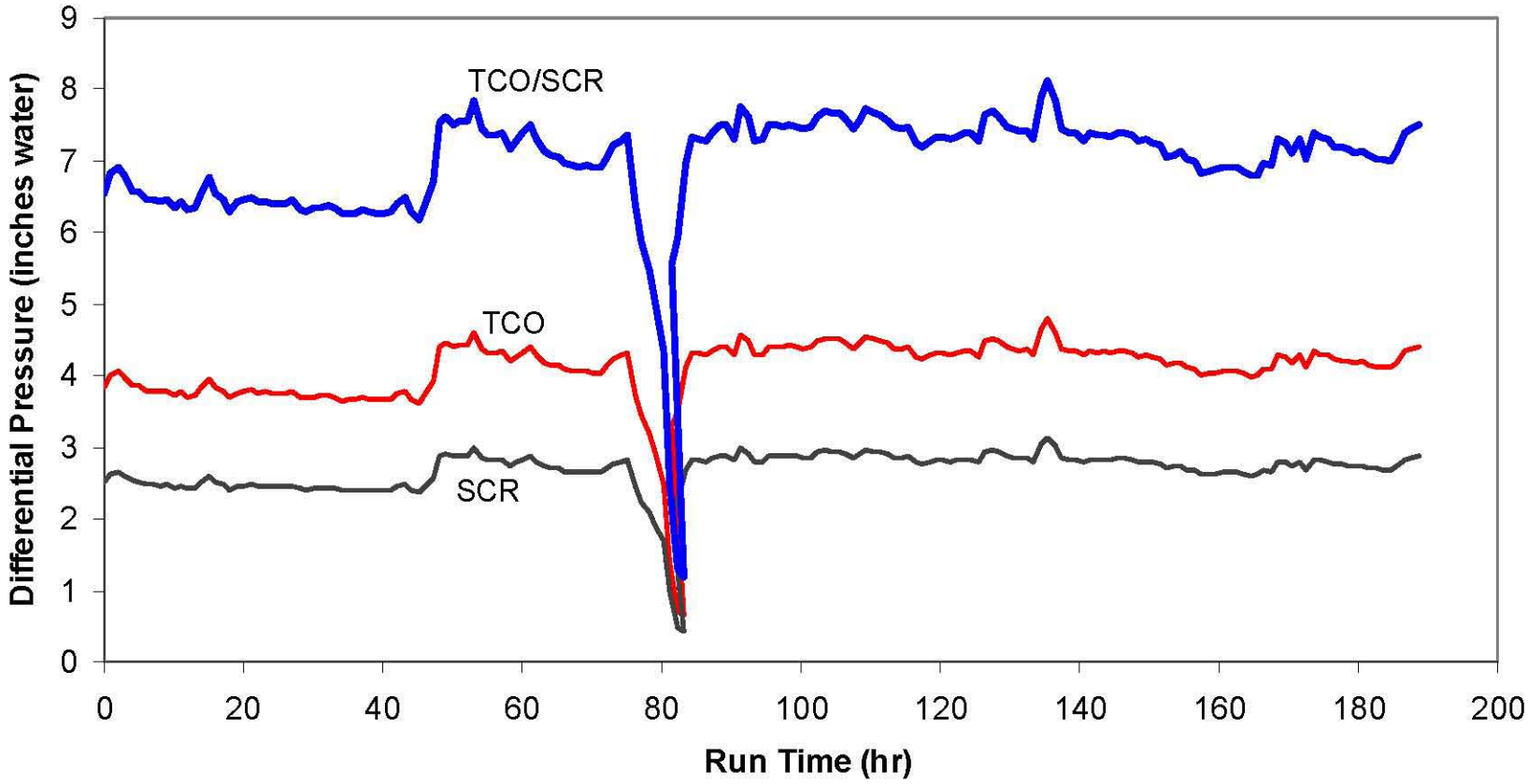

Figure 4.29. TCO/SCR differential pressures (average hourly values) during testing.

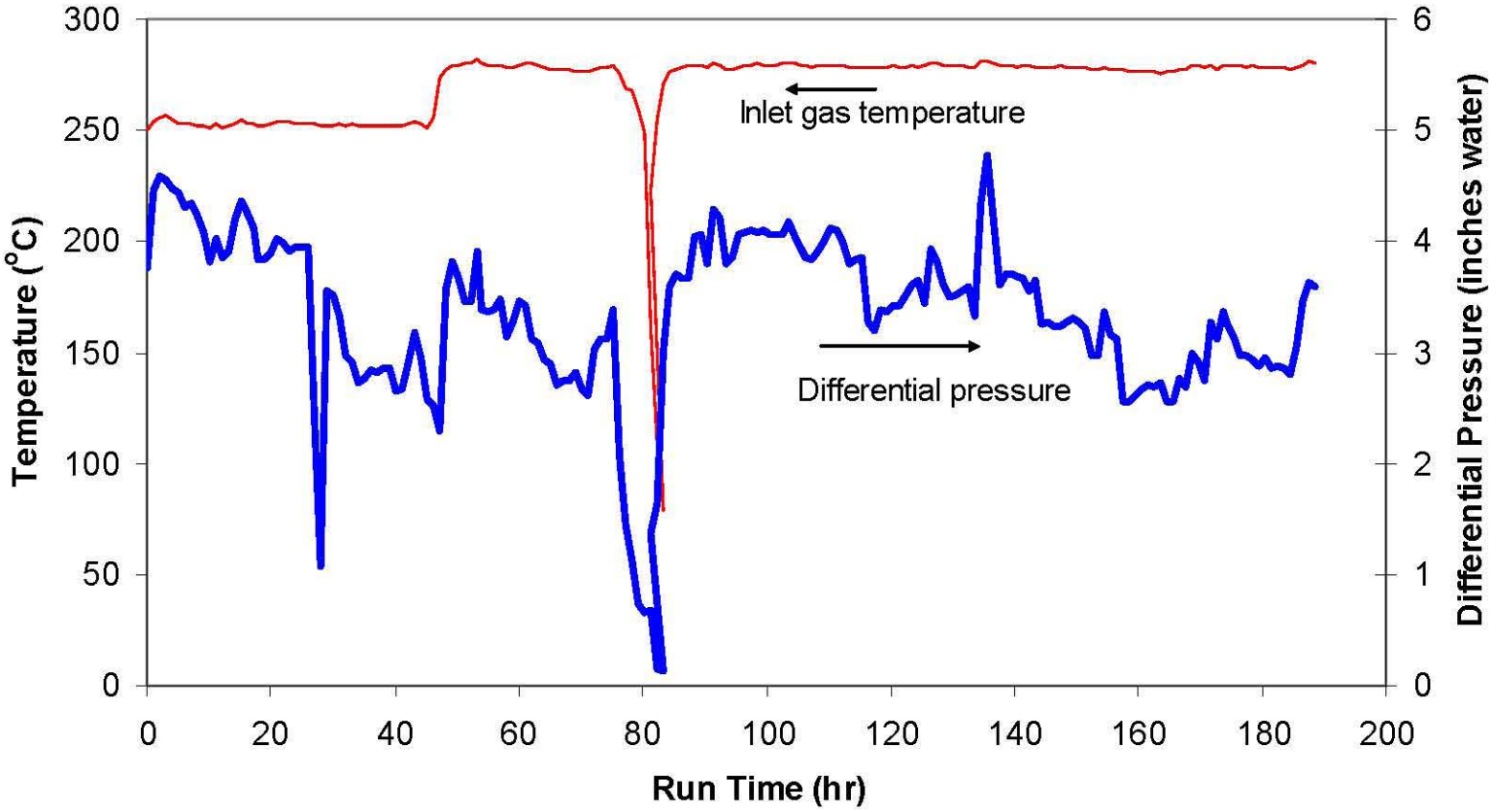

Figure 4.30. Inlet gas temperature and differential pressure for PBS (hourly average values) during testing.

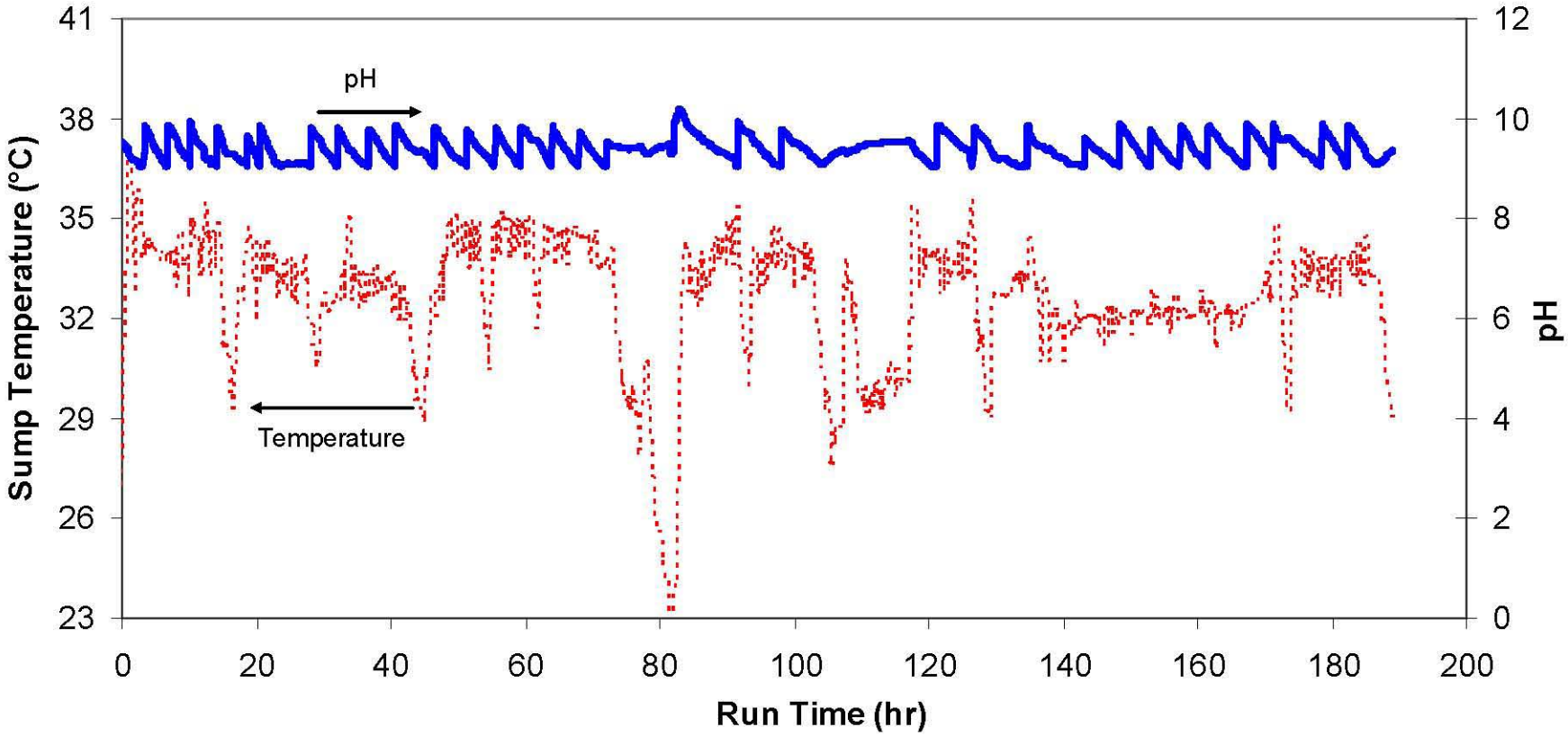

Figure 4.31. Sump temperature and pH for PBS (hourly average values) during testing.

Figure 5.1. Discharge glass G-12N-151A. No foamy glass observed.

Figure 5.2. Discharge glass G-12O-20A. No foamy glass observed.

Figure 5.3. Discharge glass G-12O-37A. No foamy glass observed.

Figure 5.4.a. Discharge glass G-12O-53A. Foam observed.

Figure 5.4.b. Foam in discharge glass G-12O-53A.

Figure 5.5. Discharge glass G-12O-69A. Foam observed.

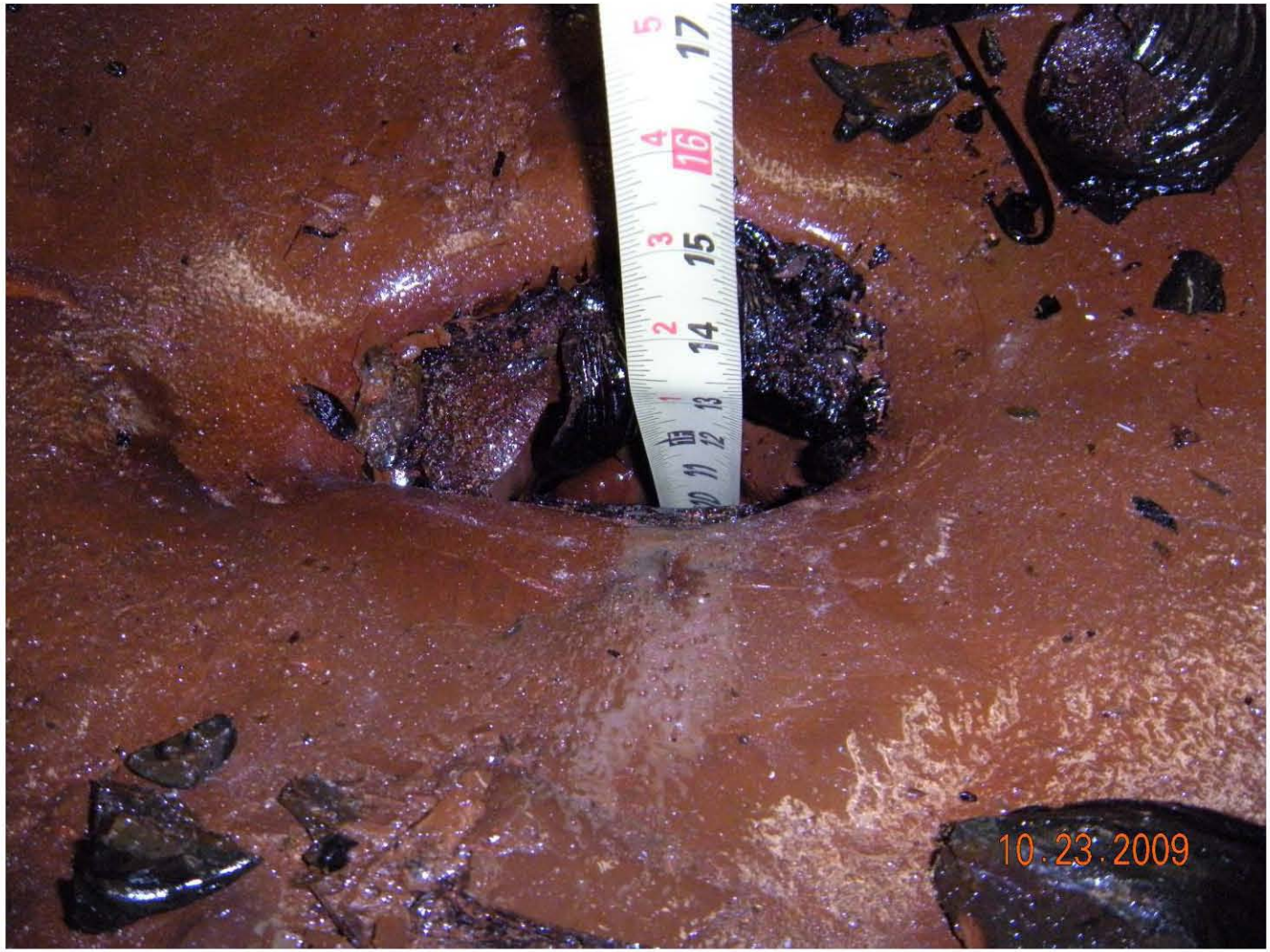

Figure 5.6. Discharge glass G12O-85A. Foam and large cavity observed.

Figure 5.7. Discharge glass G12O-101A. Foam observed.

Figure 5.8. Discharge glass G12O-133A. Foam observed.

Figure 5.9. Discharge glass G12O-150A. Foam observed.

Figure 5.10. Discharge glass G-12P-32A. Foam observed.

Figure 5.11a. Discharge G-12P-53A. Foam observed.

Figure 5.11.b. Foam in discharge glass G-12P-53A.

Figure 5.12. Discharge glass G-12P-72A. Foam observed.

Figure 5.13. Discharge glass G-12P-88A. Foam observed.

Figure 5.14. Discharge glass G-12P-101A. Foam observed.

Figure 5.15. Discharge glass G-12P-116A. Foam observed.

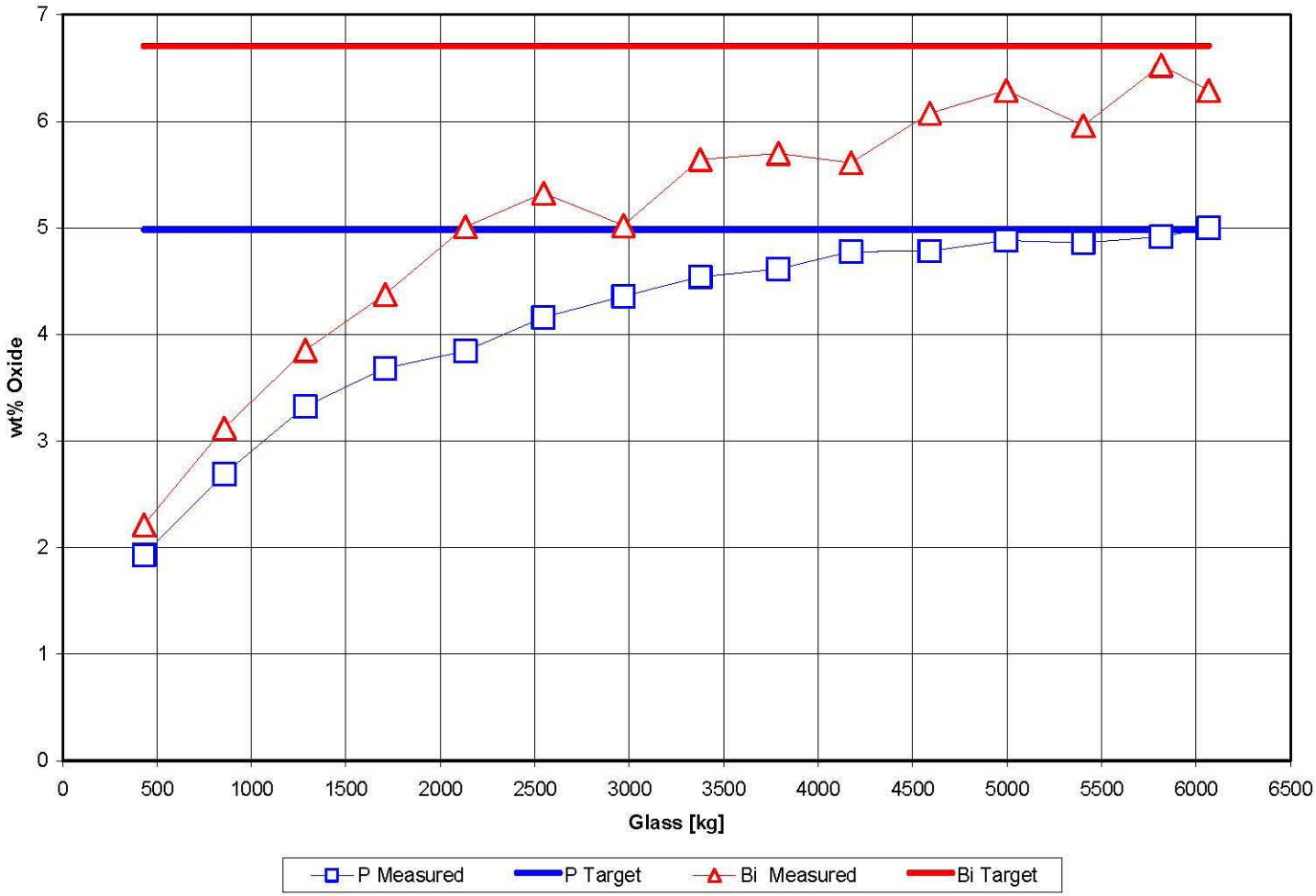

Figure 5.16.a. DM1200 product and target glass compositions determined by XRF.

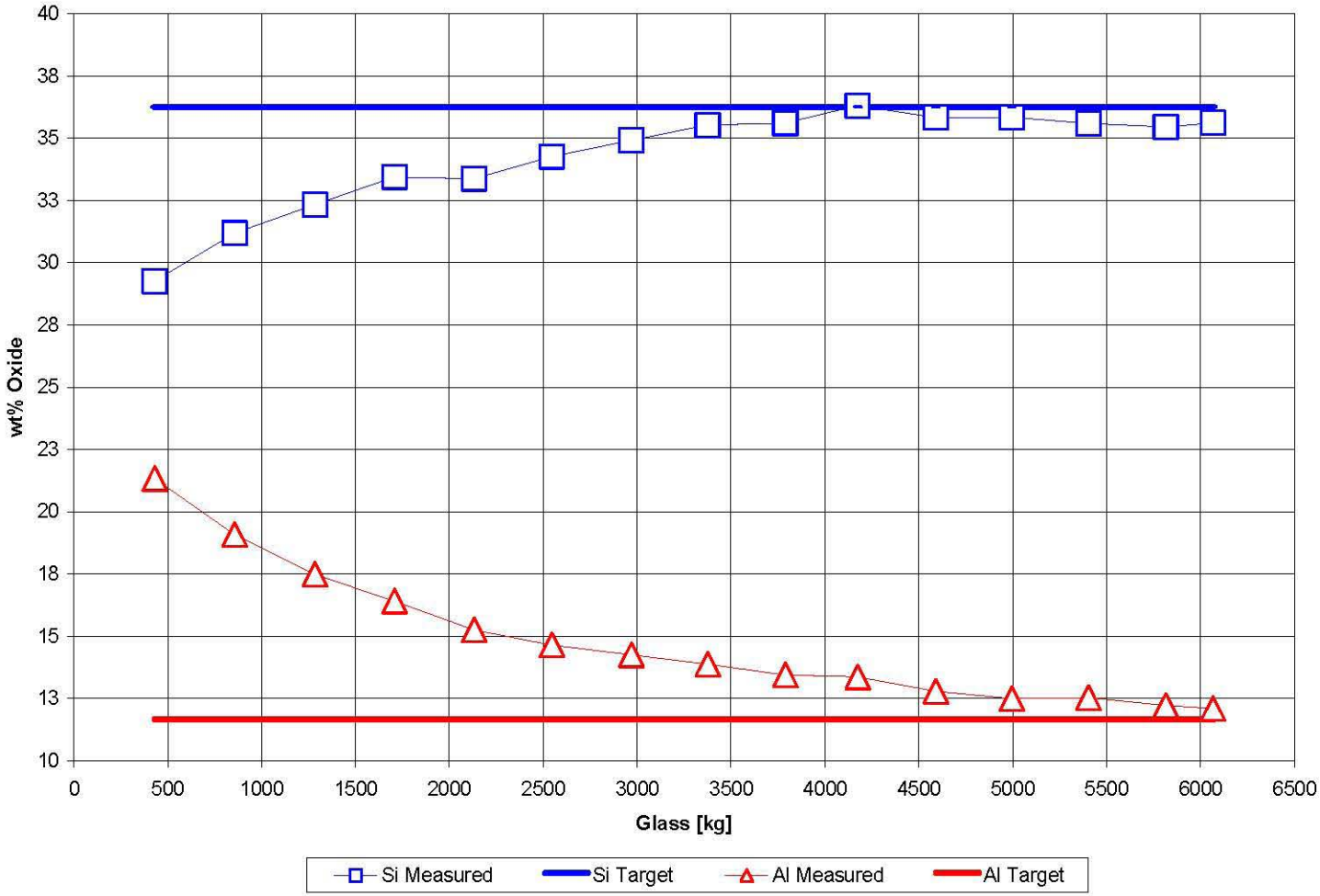

Figure 5.16.b. DM1200 product and target glass compositions determined by XRF.

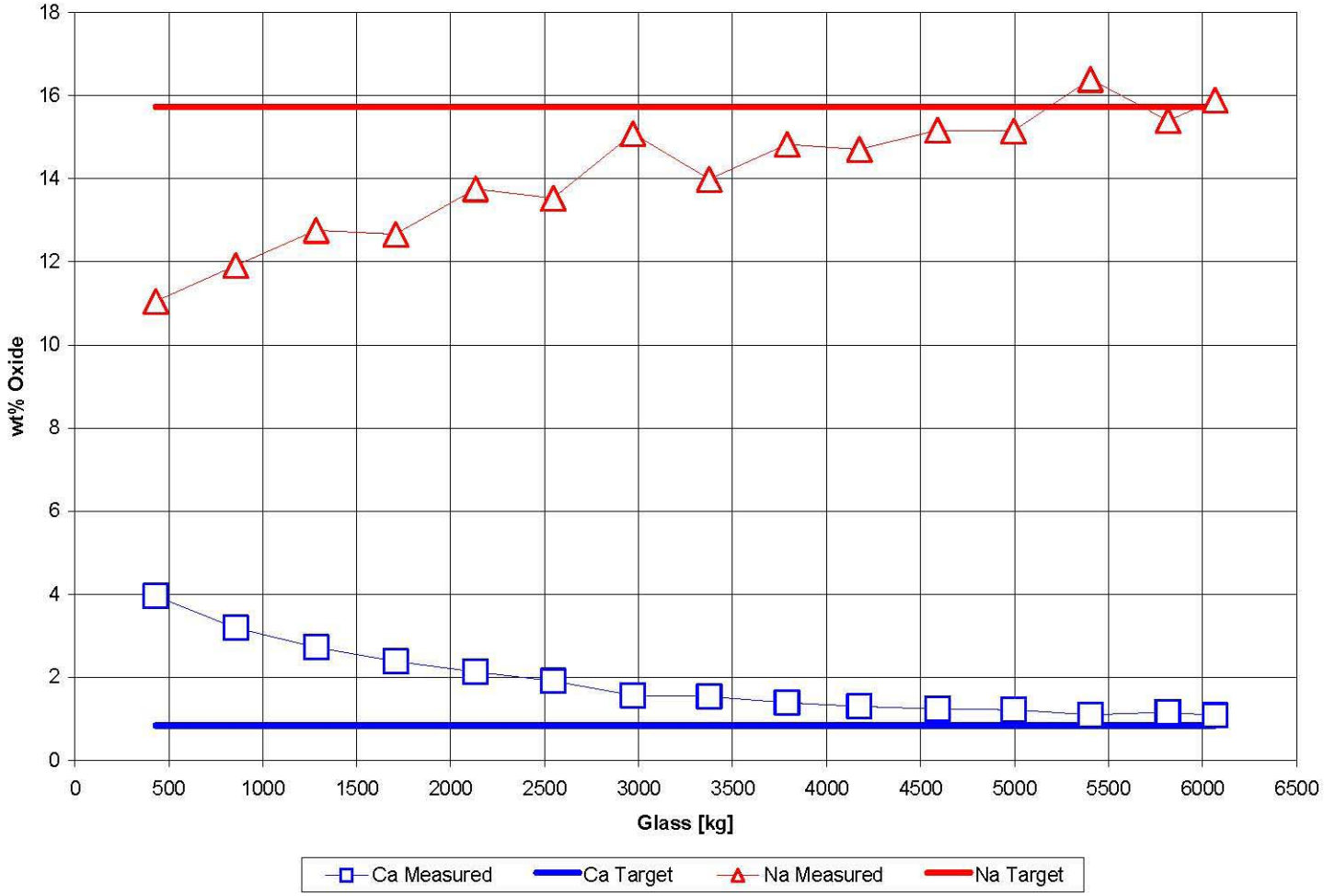

Figure 5.16.c. DM1200 product and target glass compositions determined by XRF.

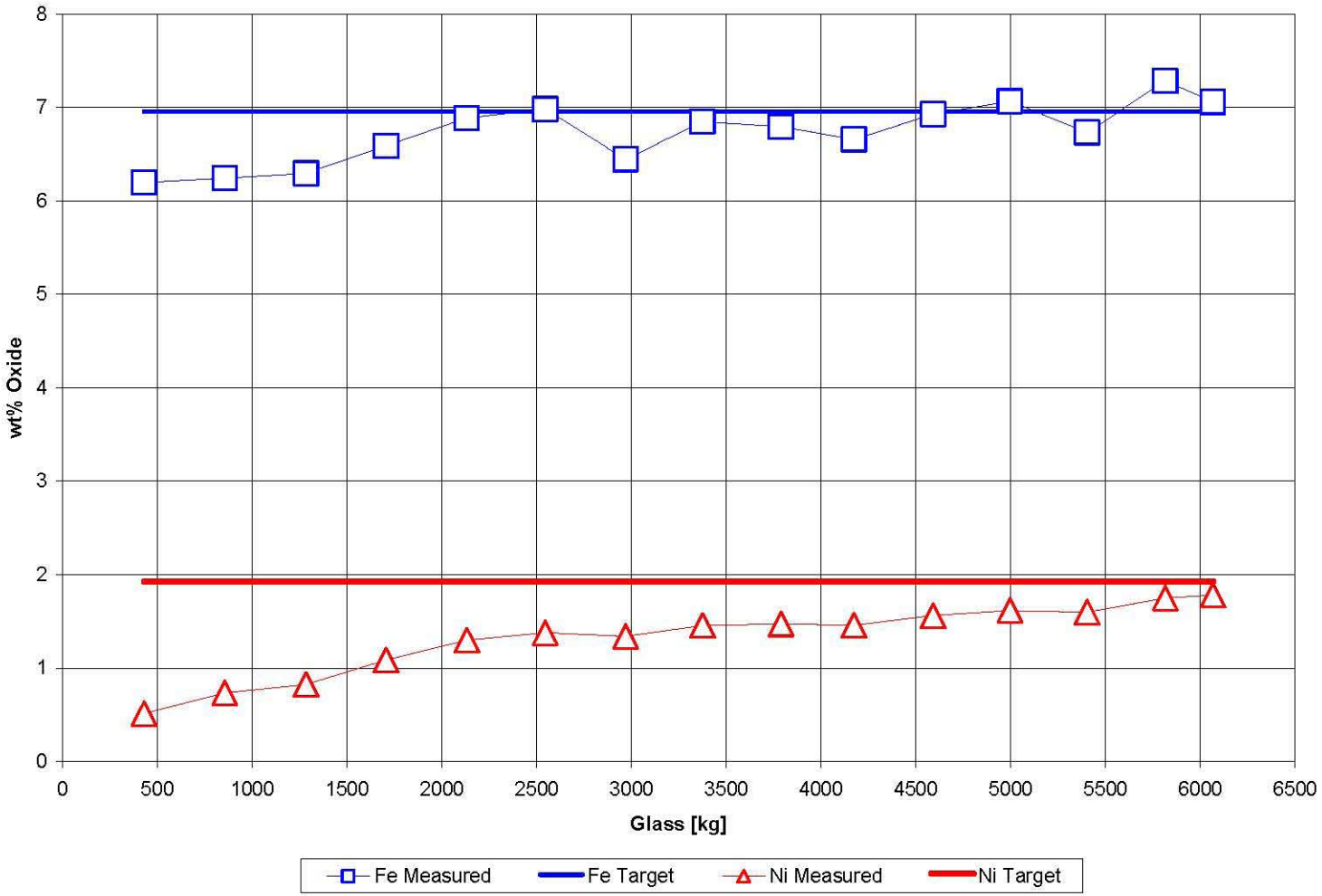

Figure 5.16.d. DM1200 product and target glass compositions determined by XRF.

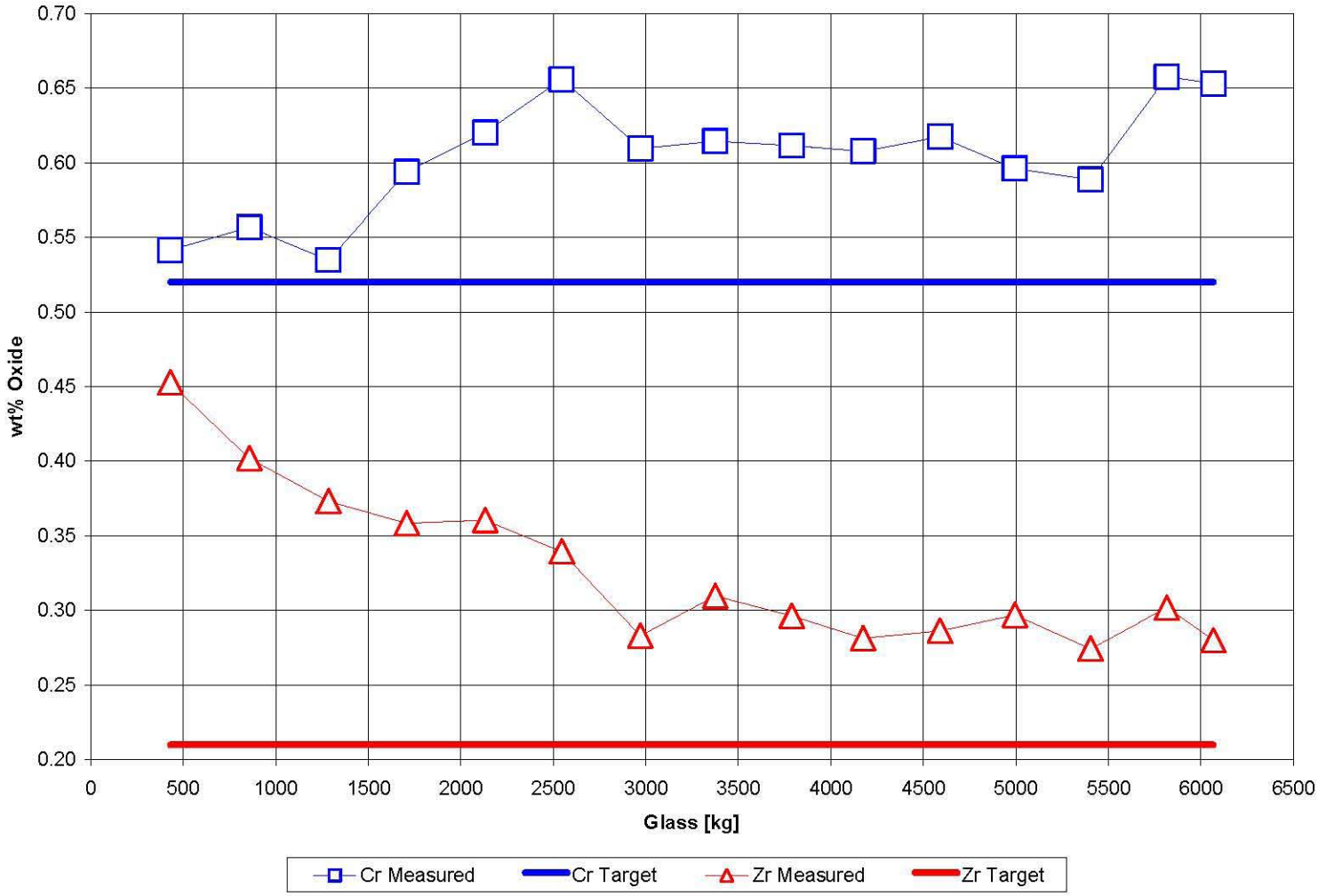

Figure 5.16.e. DM1200 product and target glass compositions determined by XRF.

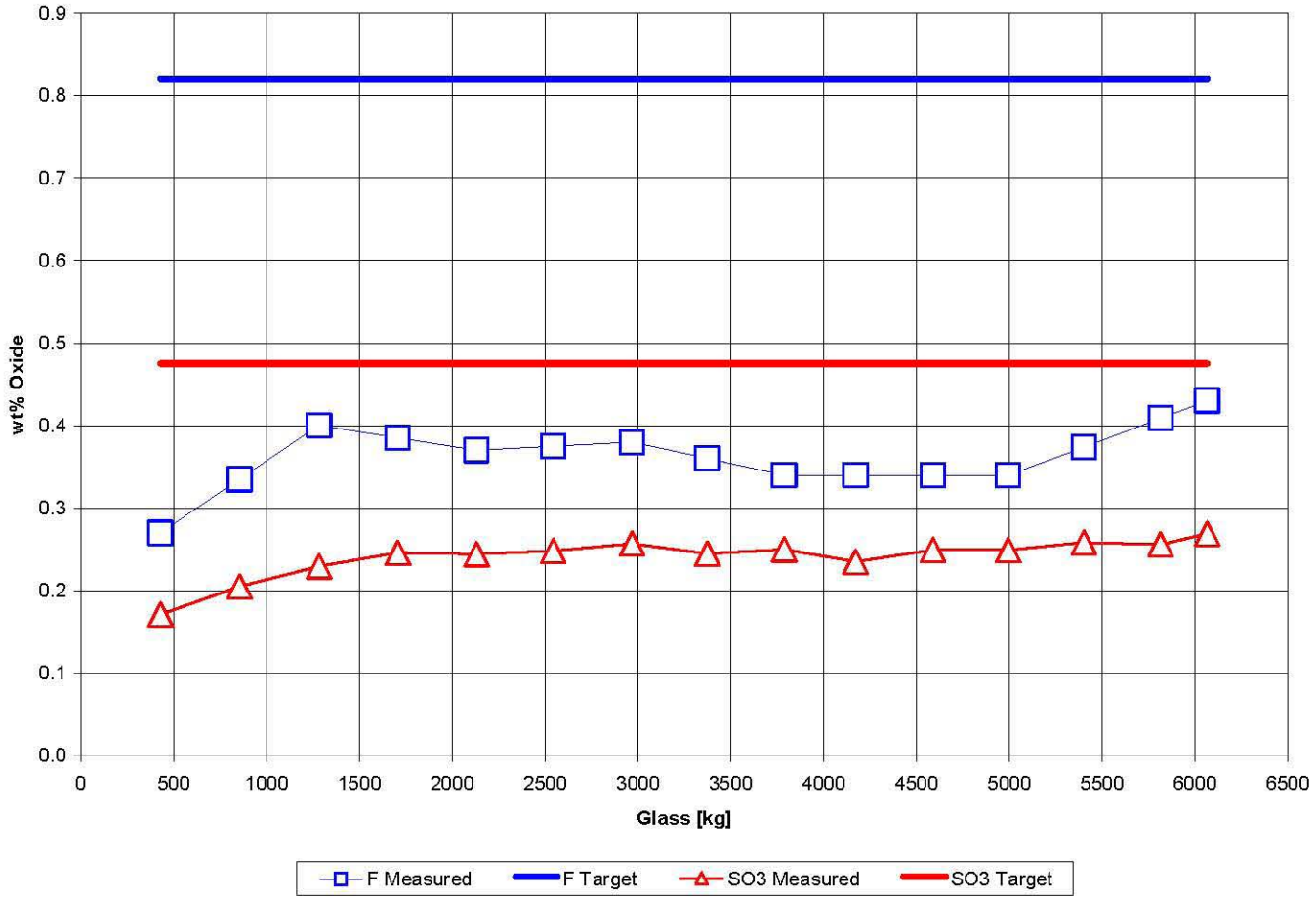

Figure 5.16.f. DM1200 product and target glass compositions determined by XRF.

Figure 5.17.a View of drum cutting rig and setup.

Figure 5.17.b View of drum cutting rig and setup.

Figure 5.17.c View of drum cutting rig and setup.

Figure 5.17.d. View of drum cutting rig and setup.

Figure 5.17.e View of drum cutting rig and setup.

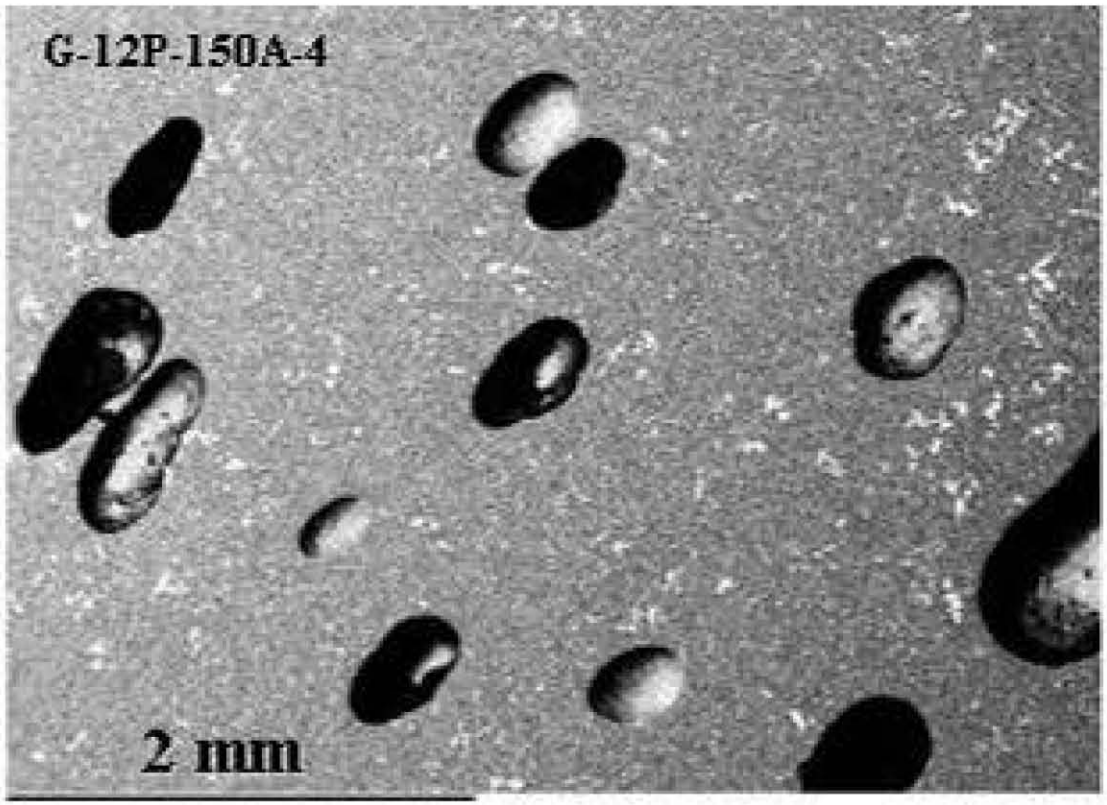

Figure 5.18. SEM image of porosity in glass (G-12P-150A) discharged and cooled at prototypic rates, 3789 kg total production at time of discharge.

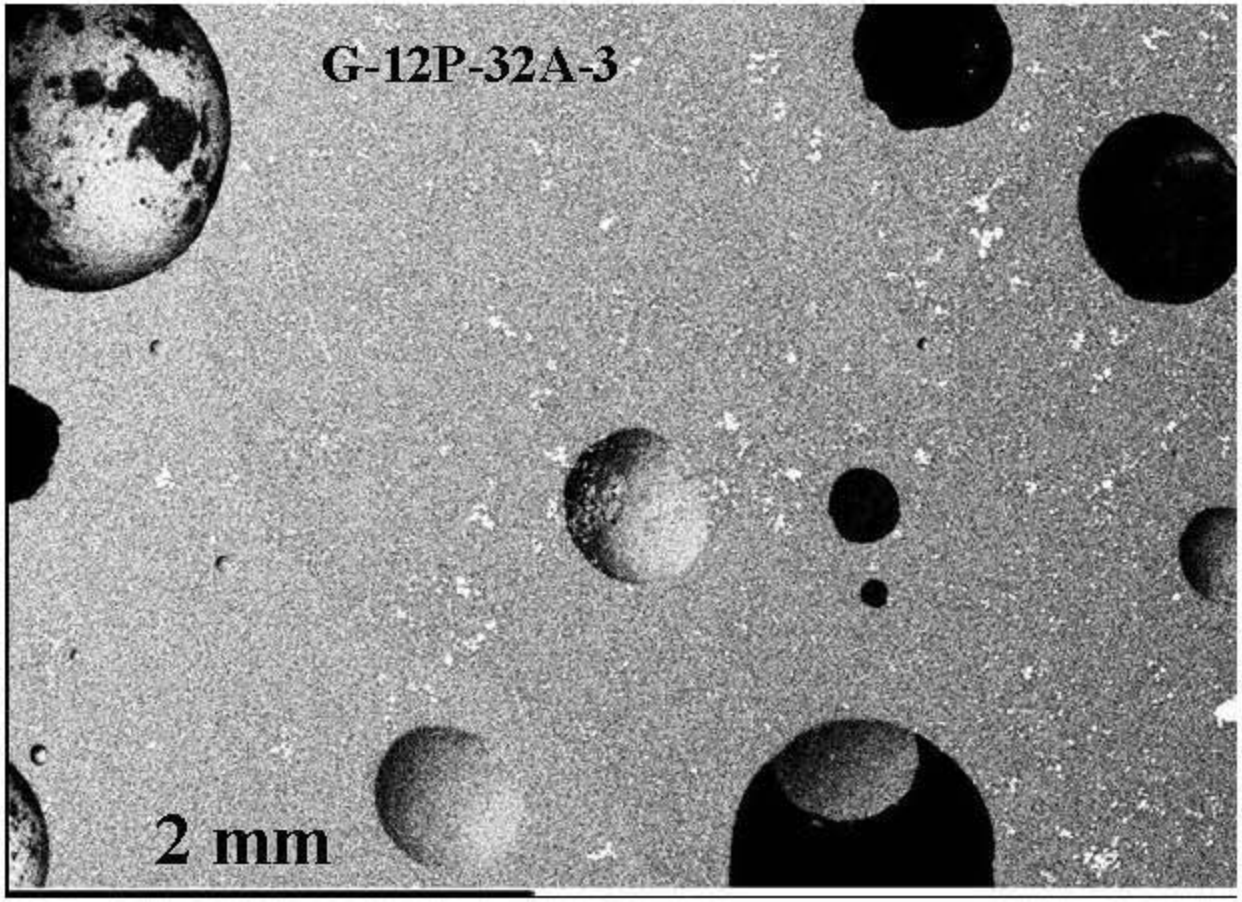

Figure 5.19. SEM image of porosity in glass (G-12P-32A) discharged and cooled at prototypic rates, 4174 kg total production at time of discharge.

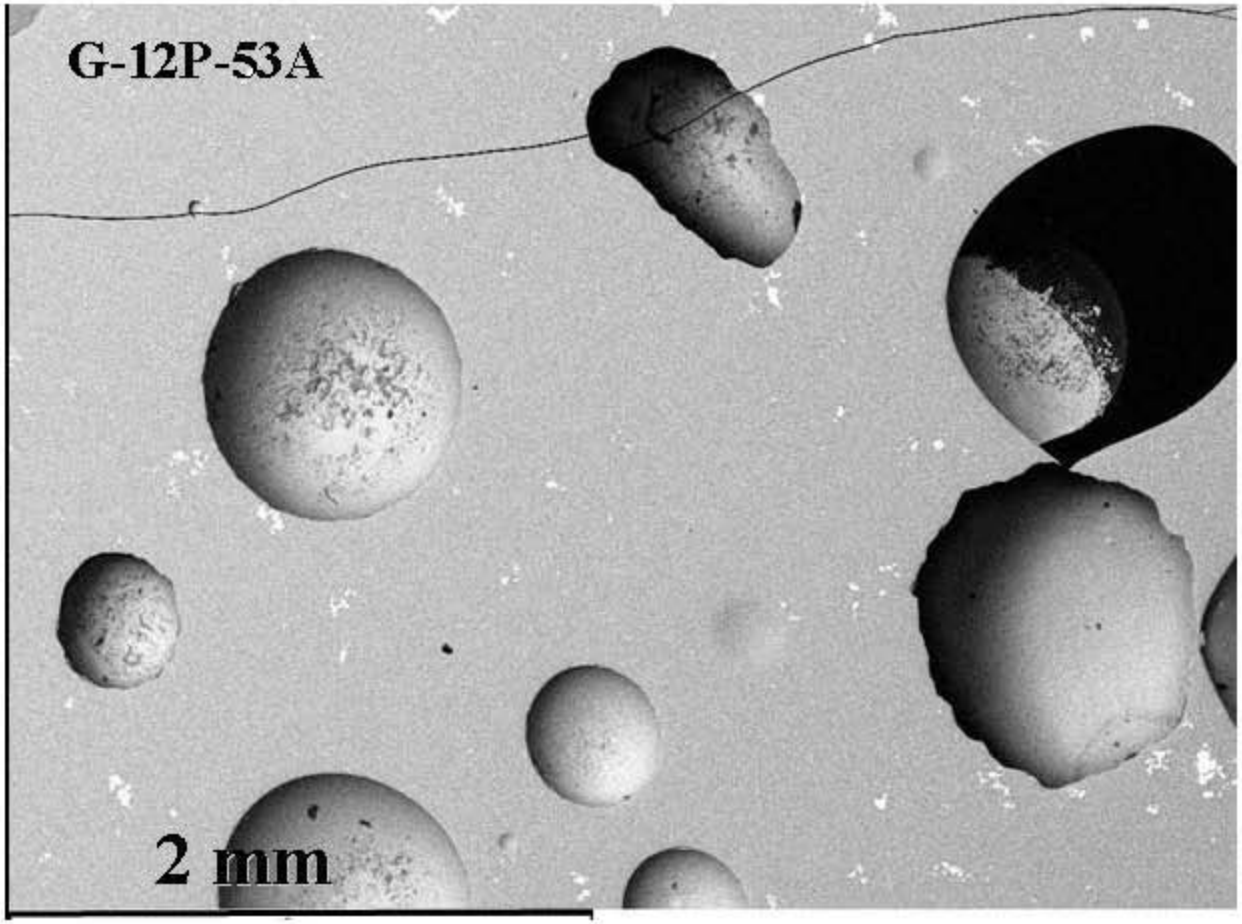

Figure 5.20. SEM image of porosity in glass (G-12P-53A) discharged and cooled at prototypic rates, 4591 kg total production at time of discharge.

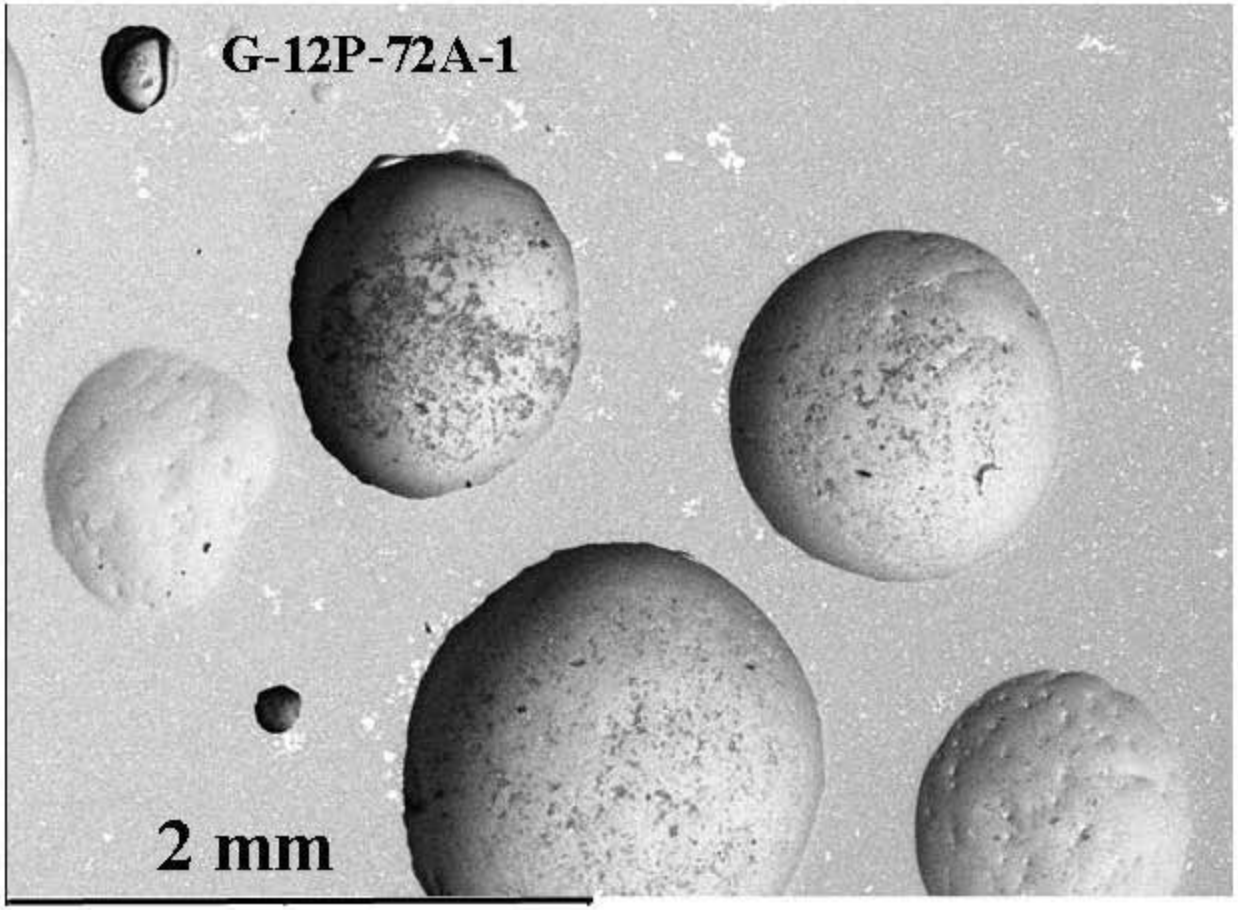

Figure 5.21. SEM image of porosity in glass (G-12P-150A) discharged and cooled at prototypic rates, 4995 kg total production at time of discharge.

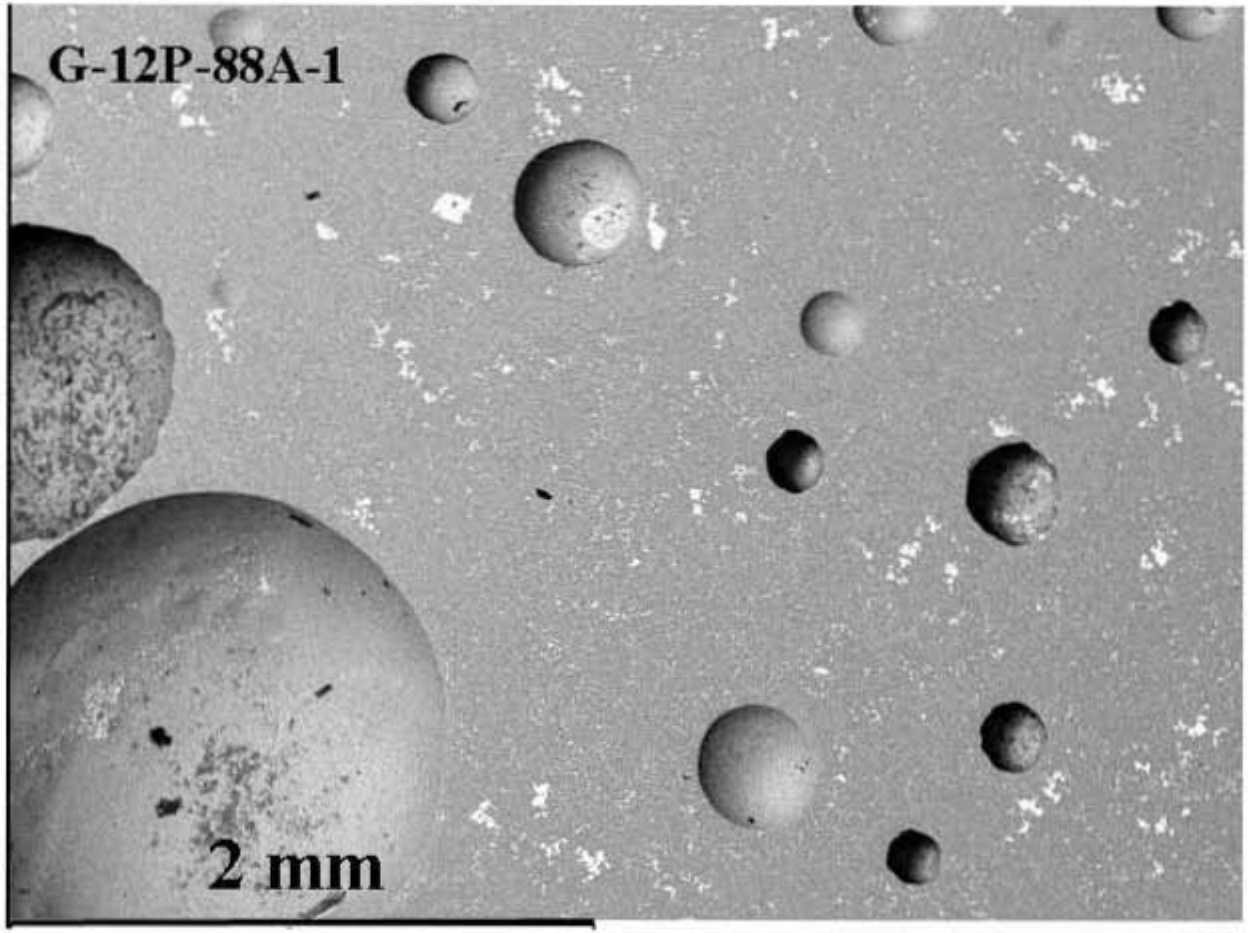

Figure 5.22. SEM image of porosity in glass (G-12P-88A) discharged and cooled at prototypic rates, 5403 kg total production at time of discharge.

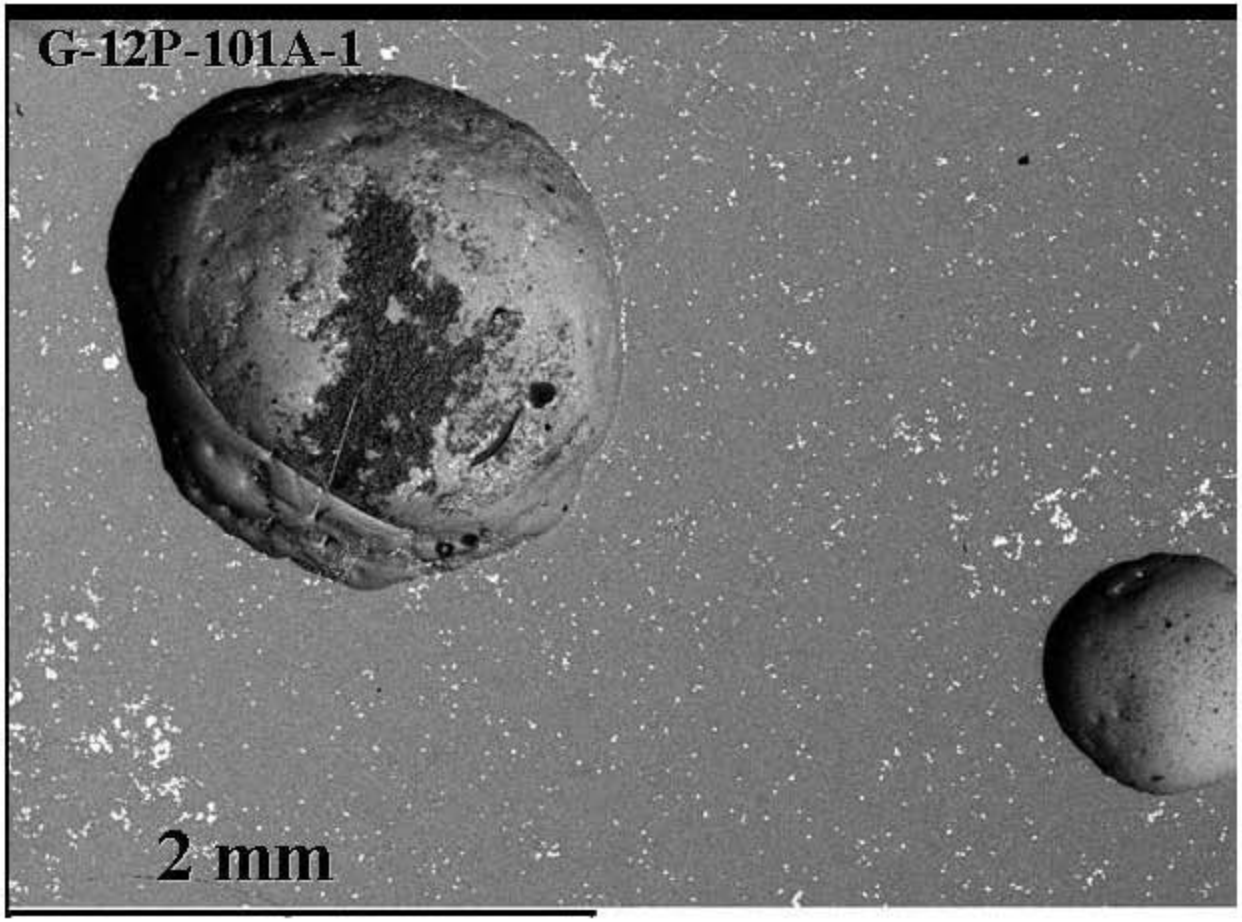

Figure 5.23. SEM image of porosity in glass (G-12P-101A) discharged and cooled at prototypic rates, 5816 kg total production at time of discharge.

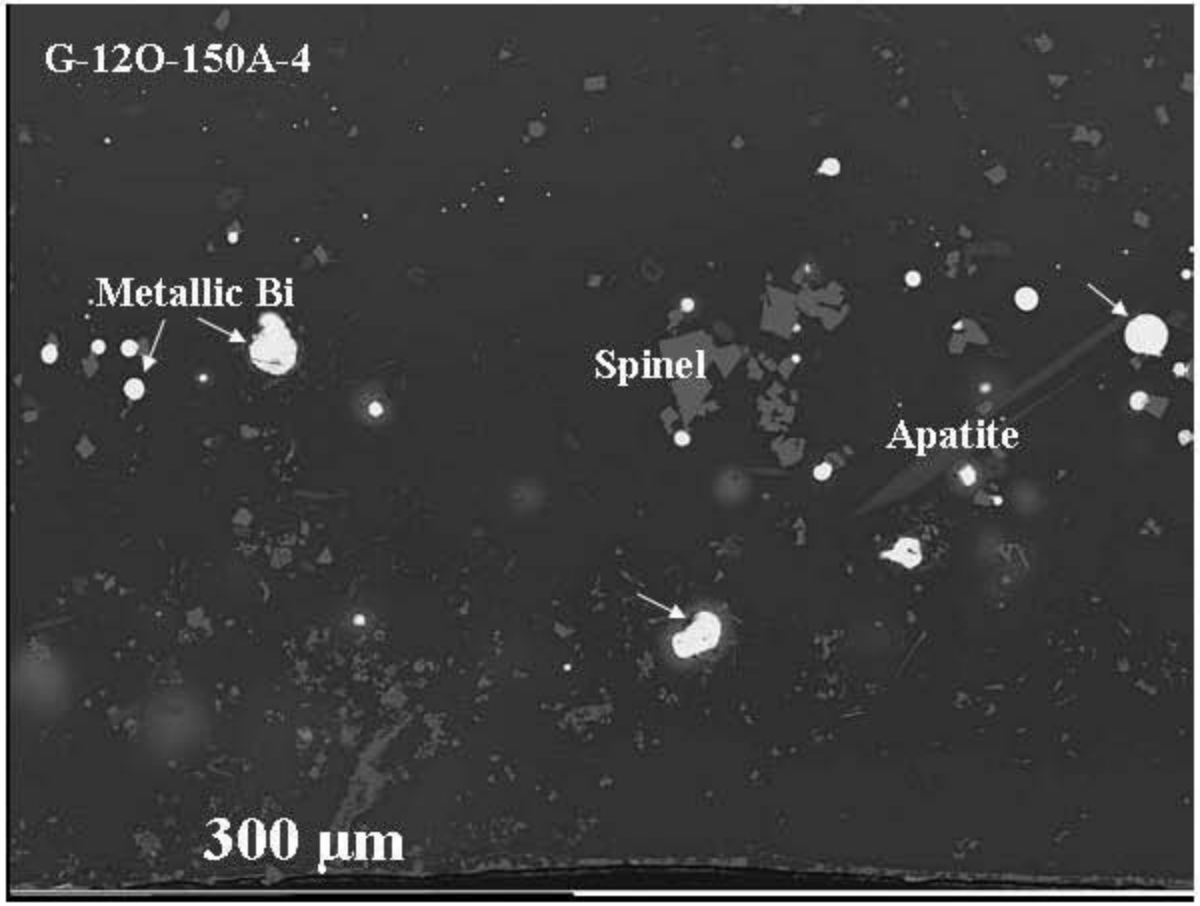

Figure 5.24. SEM image of crystalline phase in glass (G-12P-150A) discharged and cooled at prototypic rates, 3789 kg total production at time of discharge.
Note: Round bright areas are metallic bismuth

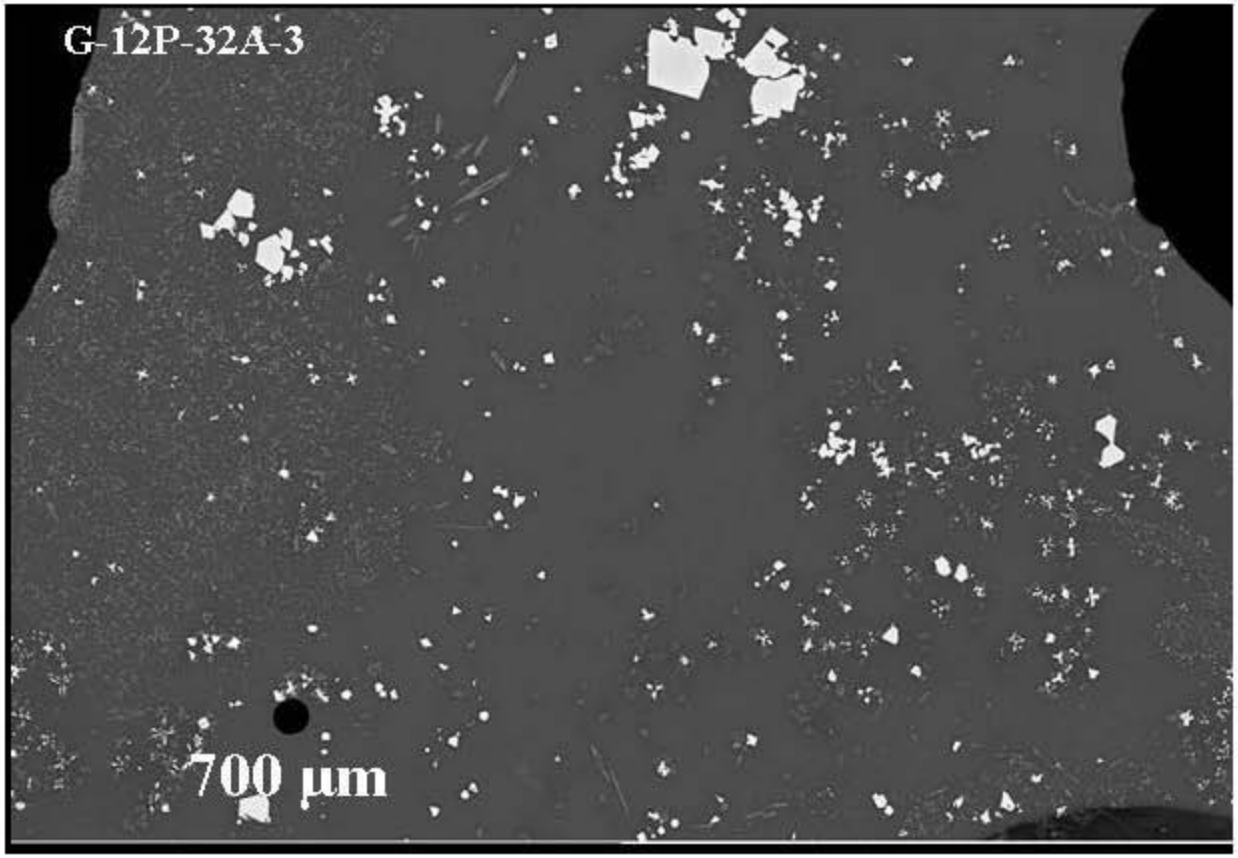

Figure 5.25. SEM image of crystalline phases in glass (G-12P-32A) discharged and cooled at prototypic rates, 4174 kg total production at time of discharge.
Note: Bright crystals spinel, dark needles apatite.

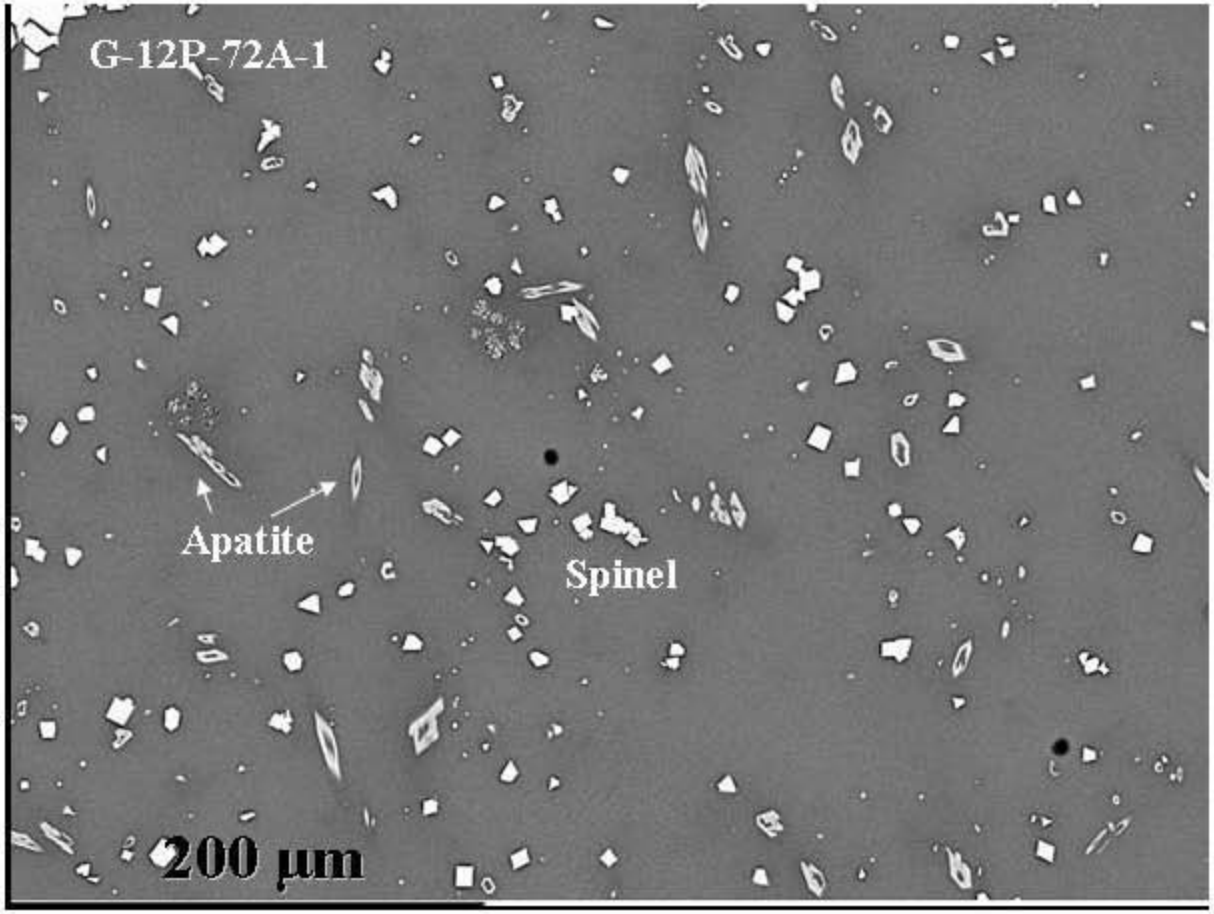

Figure 5.26. SEM image of crystalline phases in glass (G-12P-150A) discharged and cooled at prototypic rates, 4995 kg total production at time of discharge.

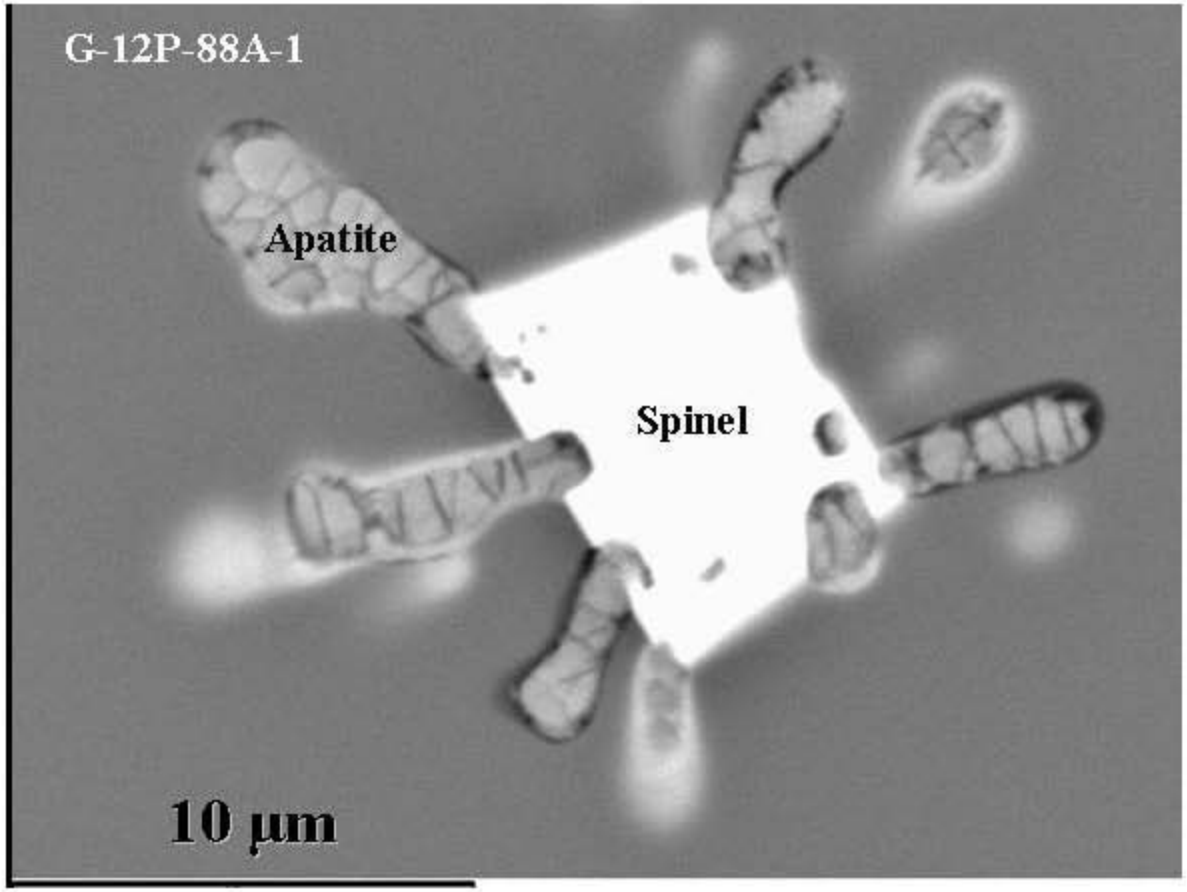

Figure 5.27. SEM image of secondary phases in glass (G-12P-88A) discharged and cooled at prototypic rates, 5403 kg total production at time of discharge.

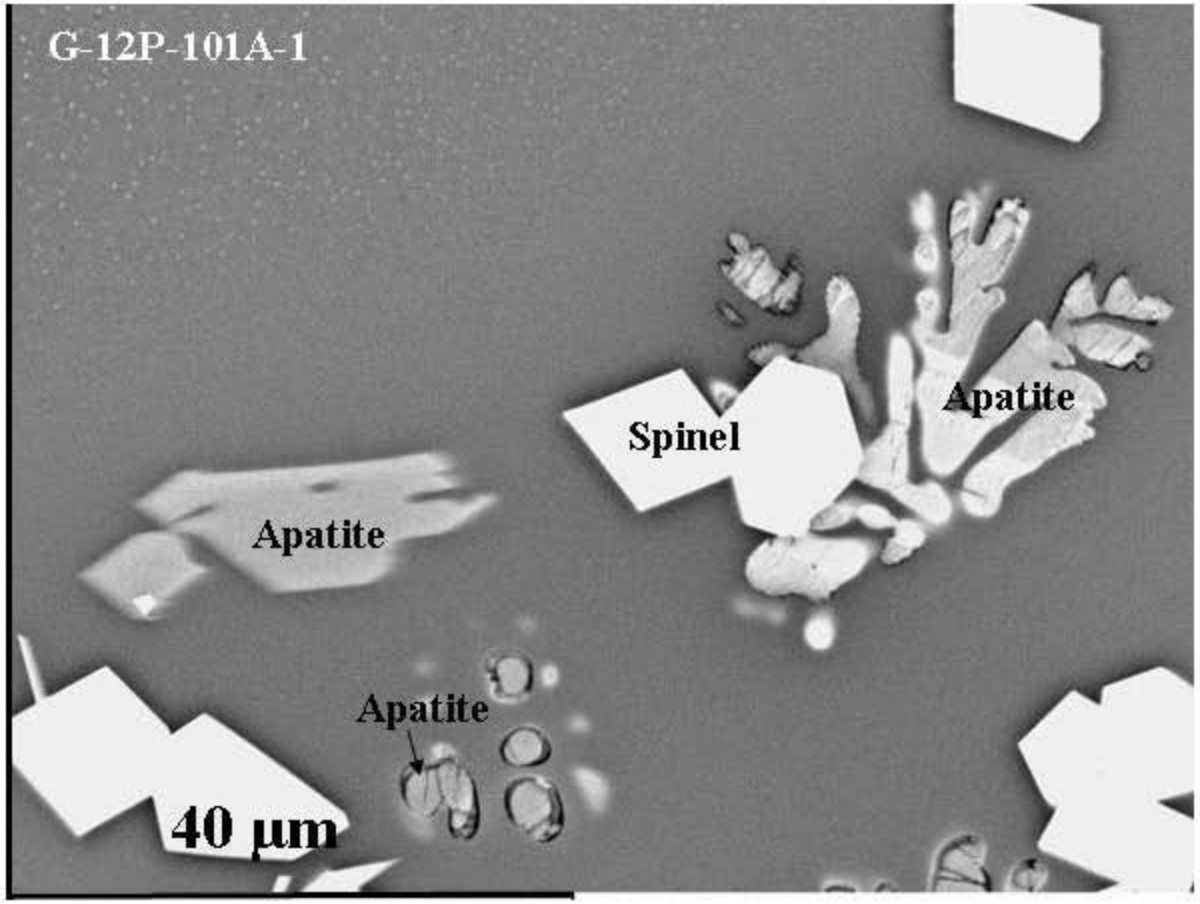

Figure 5.28. SEM image of crystalline phases in glass (G-12P-101A) discharged and cooled at prototypic rates, 5816 kg total production at time of discharge.

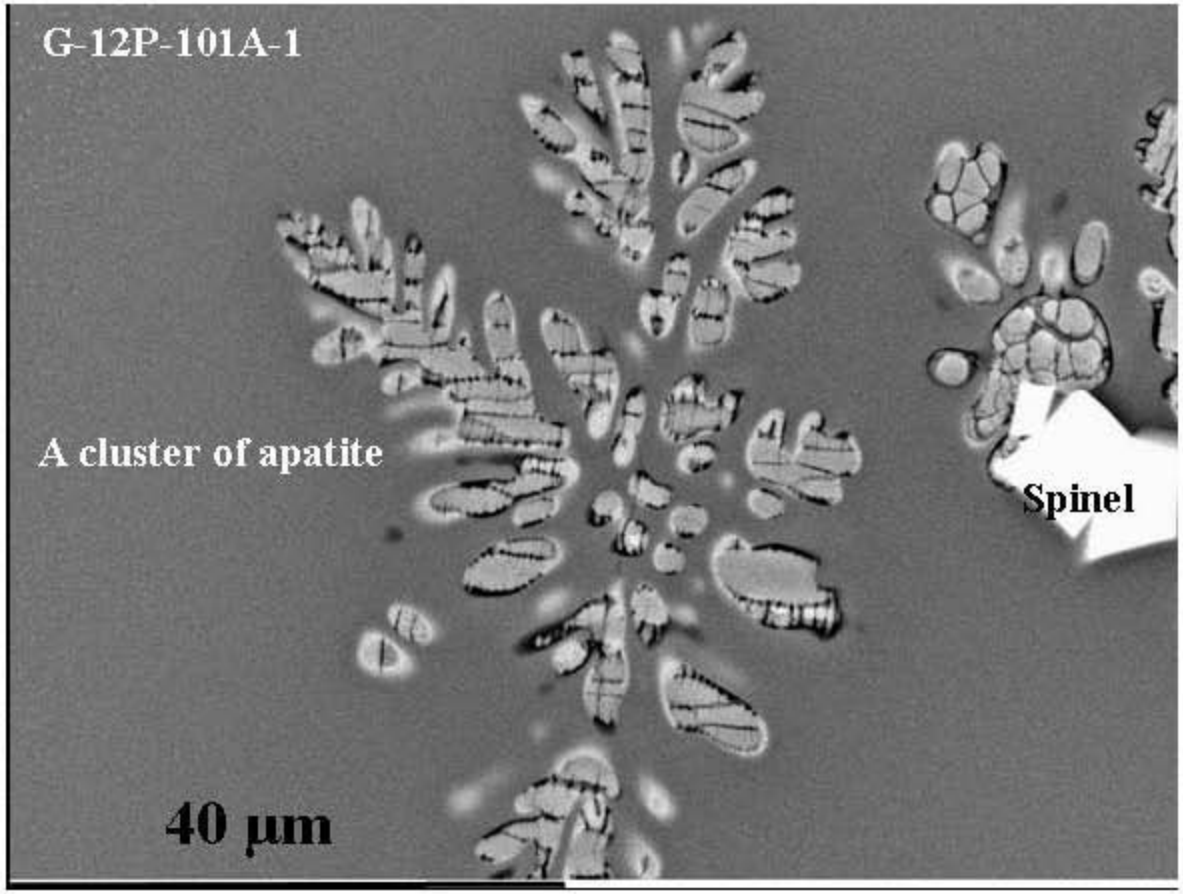

Figure 5.29. SEM image of secondary phases in glass (G-12P-101A) discharged and cooled at prototypic rates, 5816 kg total production at time of discharge.

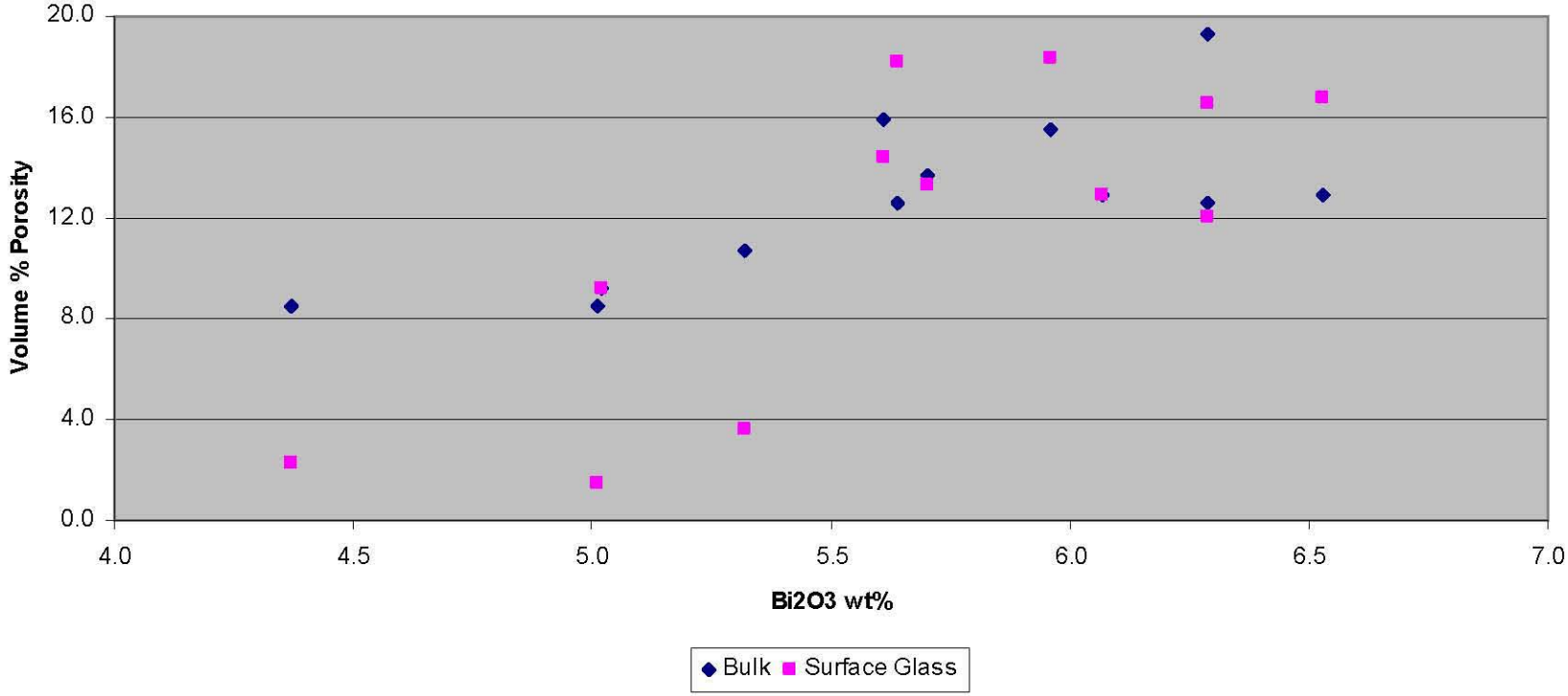

Figure 5.30. Relationship between bismuth concentration and void space in glass discharged from the DM1200.

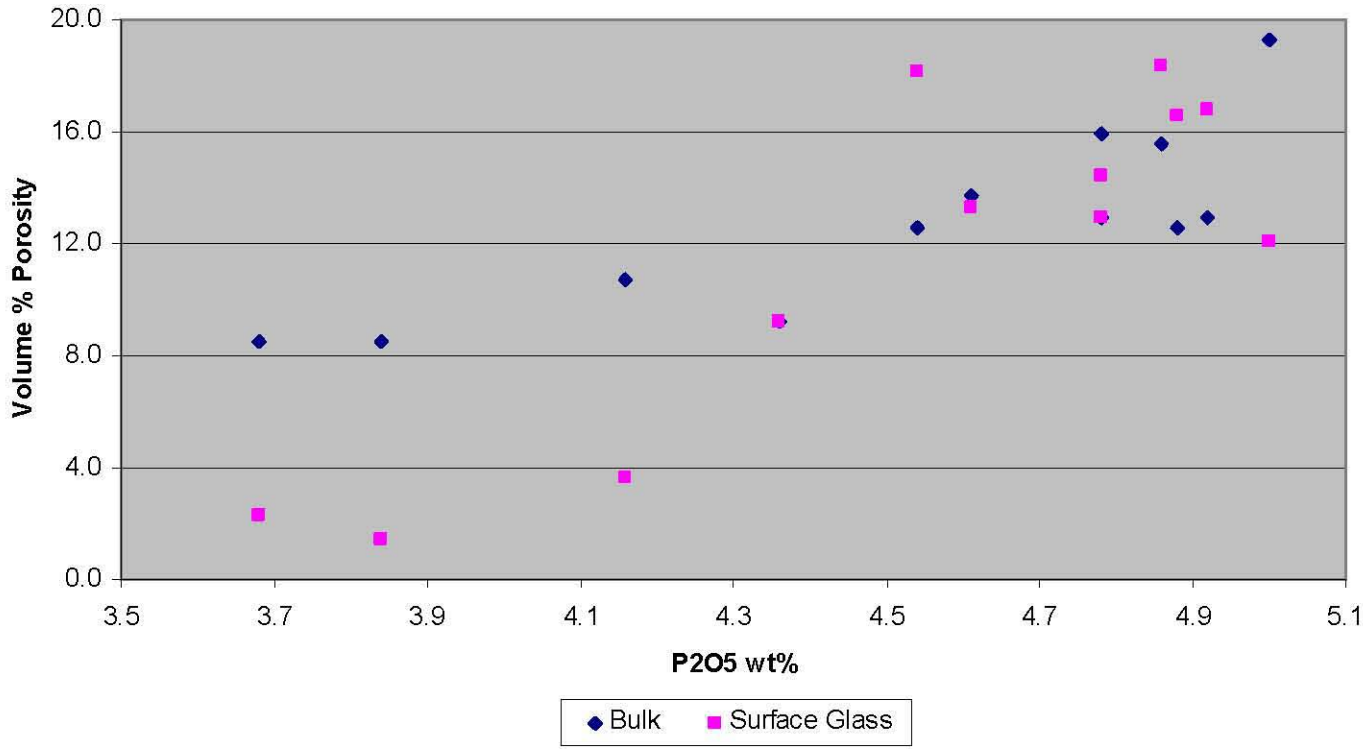

Figure 5.31. Relationship between phosphorus concentration and void space in glass discharged from the DM1200.

Figure 5.32. Bubbler (DB-3) tip prior to installation in the high bismuth tests.

Figure 5.33. Bubbler (DB-4) tip prior to installation in the high bismuth tests.

Figure 5.34. Bubbler (DB-3) tip after exposure to the high bismuth glass.

Figure 5.35. Bubbler (DB-4) tip after exposure to the high bismuth glass.

Figure 5.36. Bubbler (DB-4) after exposure to the high bismuth glass.

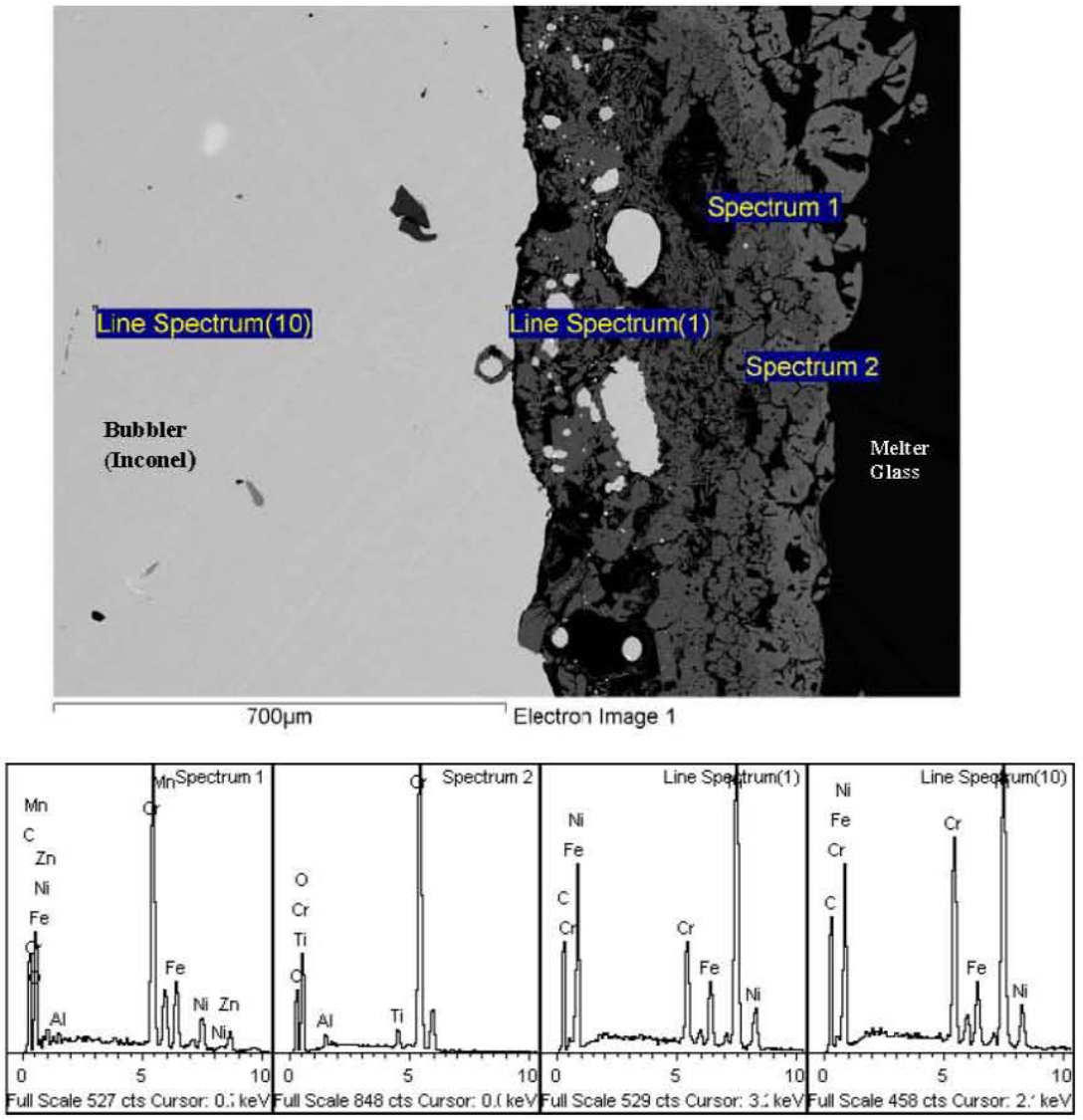

Figure 5.37. Glass-Inconel reaction interface and EDS spectra at selected points.

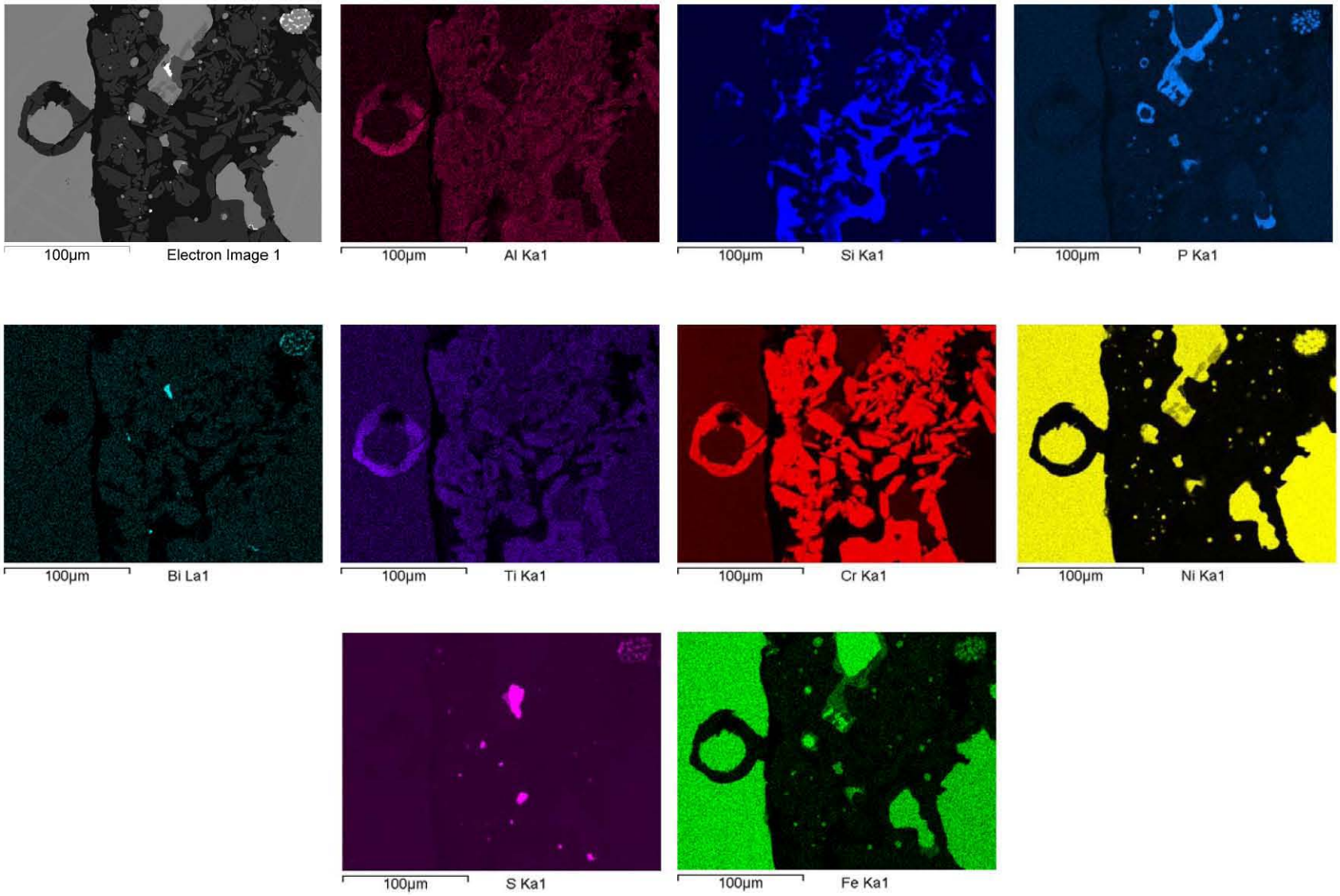

Figure 5.38. X-ray maps of reaction interface on O-12Q-31B.

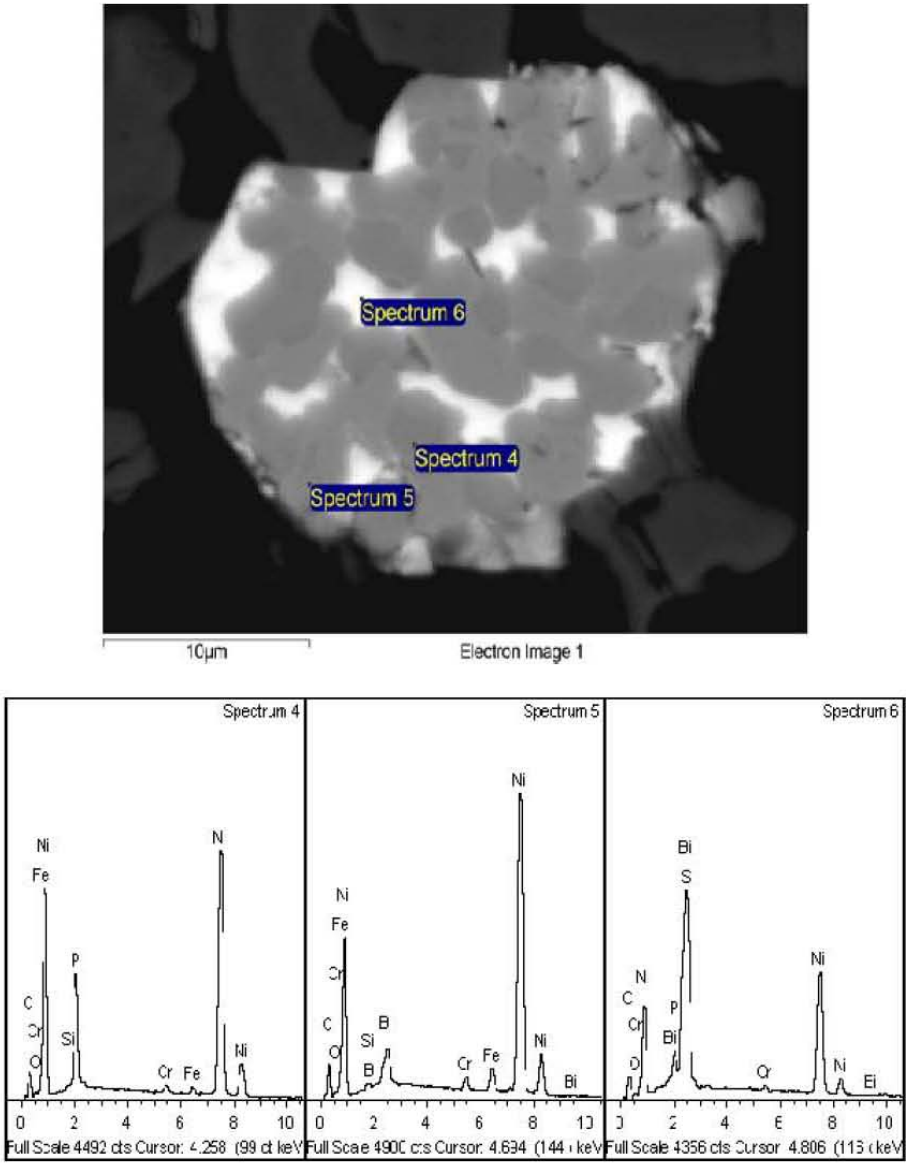

Figure 5.39. Detail of nodule in Figure 5.38 with spectra of typical areas. Spectra probably do not represent exclusive sampling.

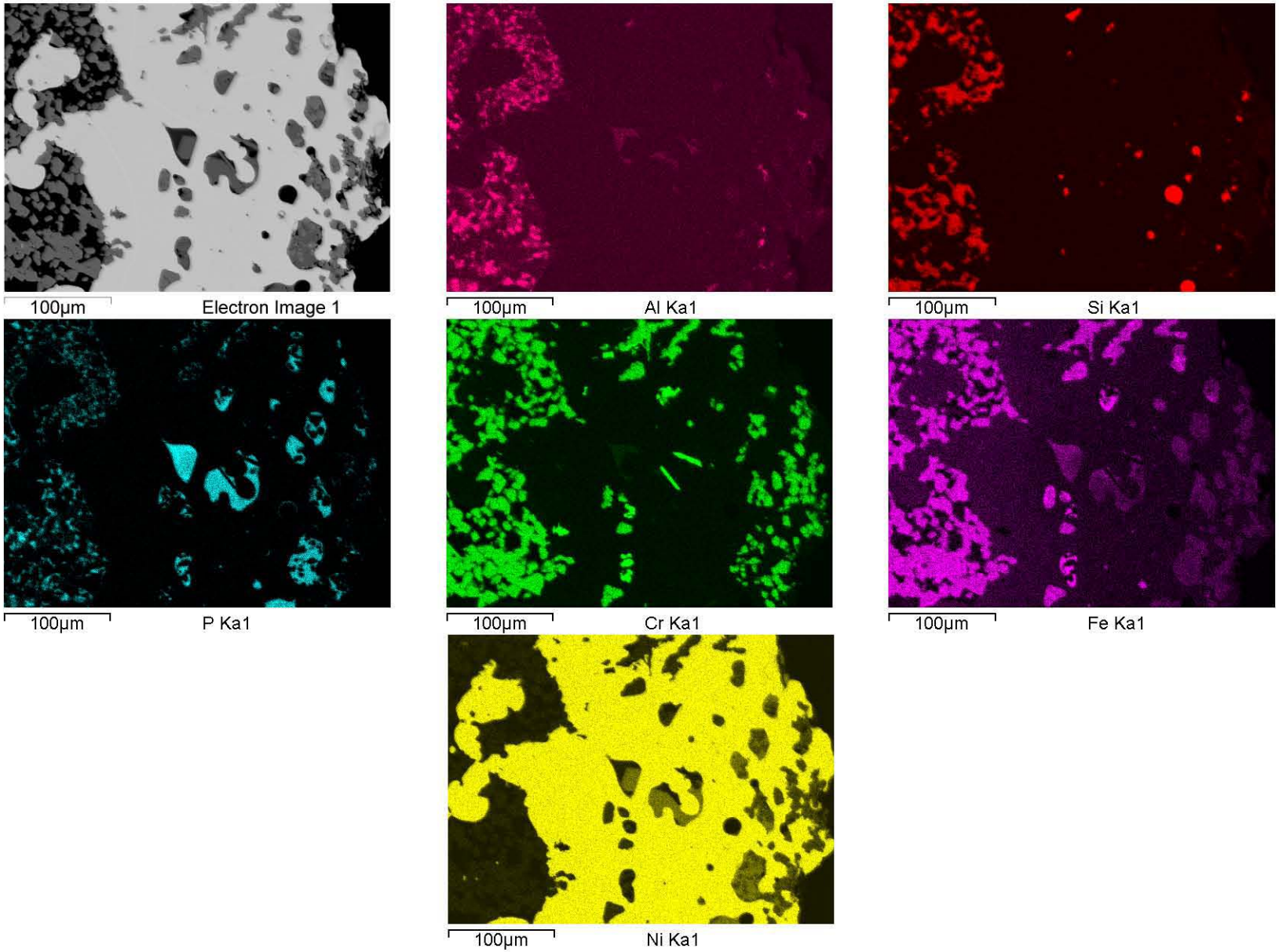

Figure 5.40. Detached nodule in corroded area of O-12Q-31C. Mixed phosphates, no bismuth, no sulfur, silicon rich areas seem to be pure silica.

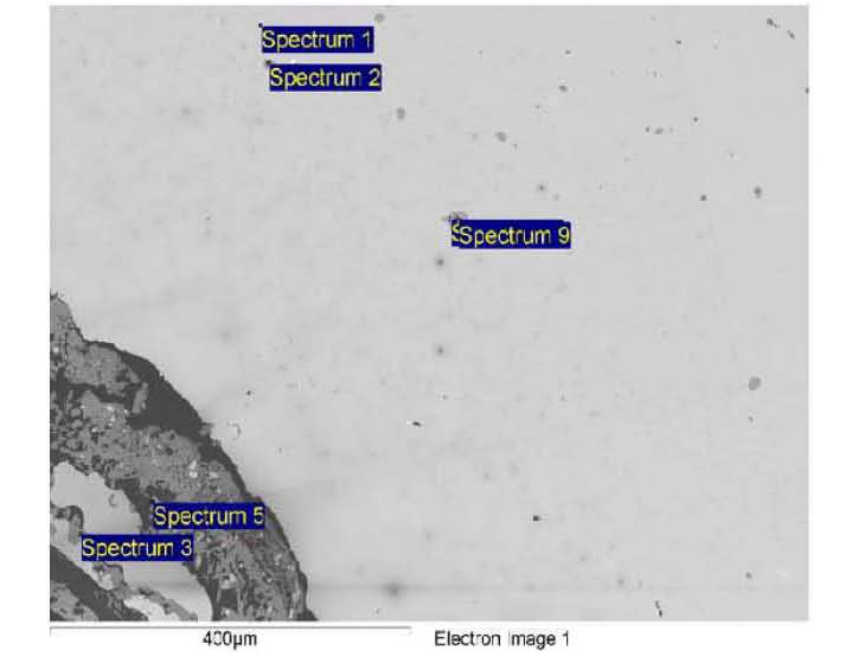

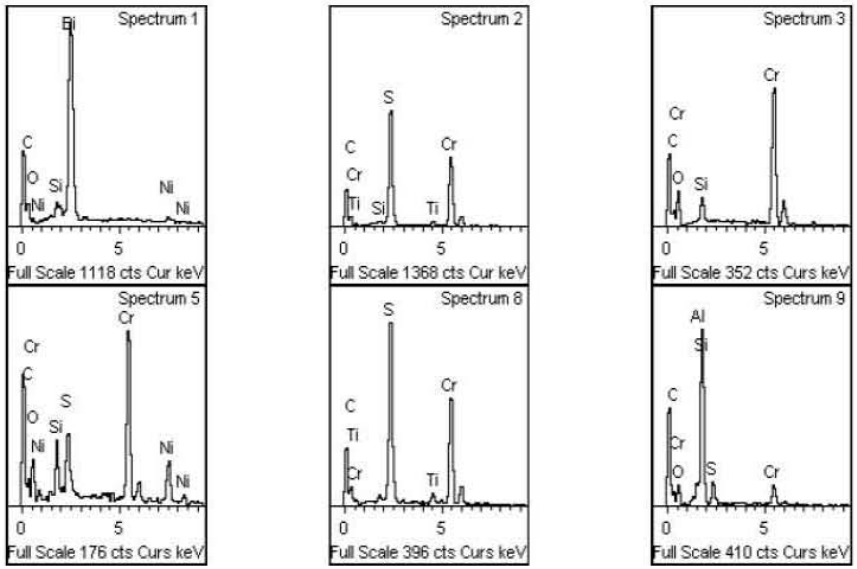

Figure 5.41. SEM image in O-12Q-31C and EDS analyses at points of interest.

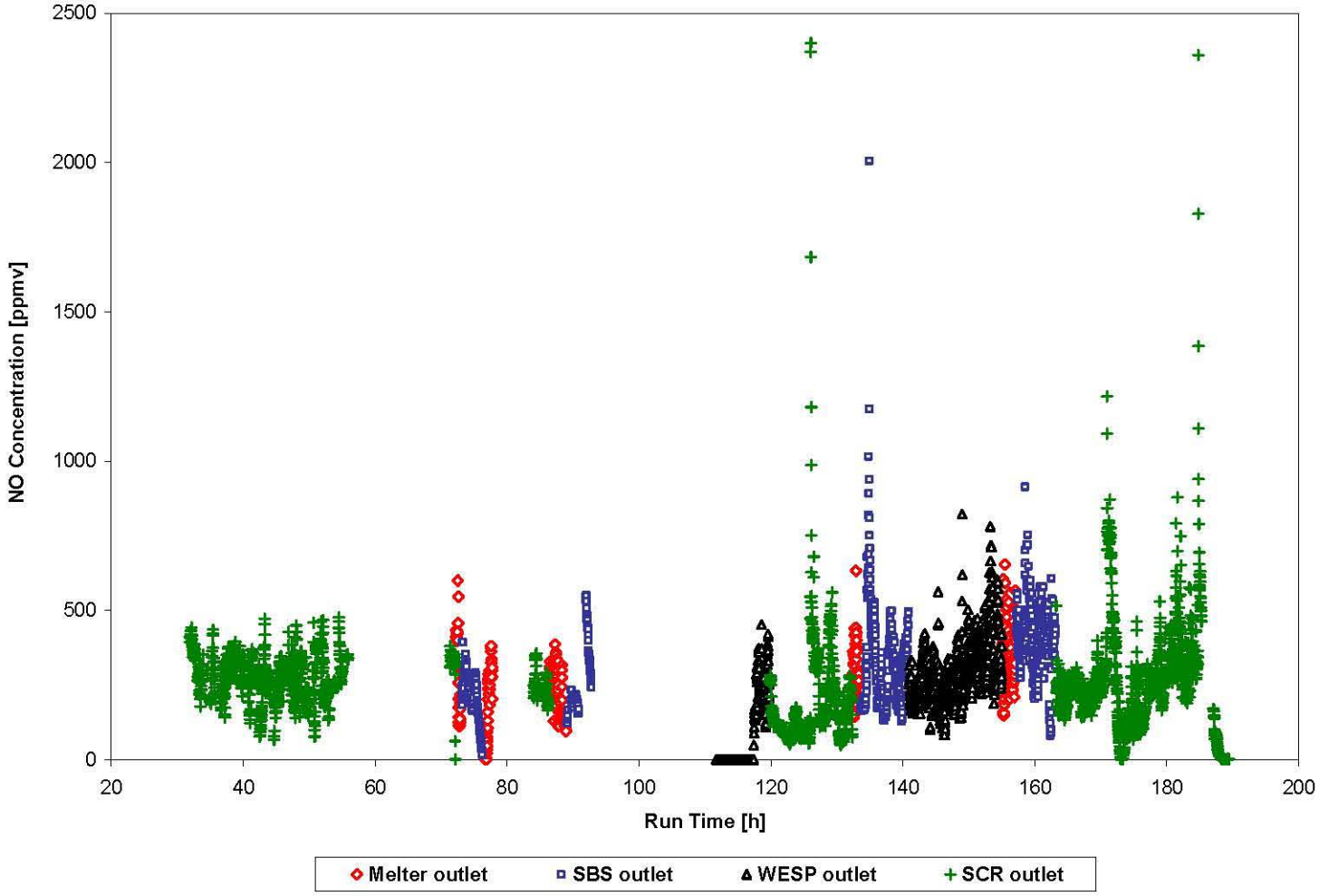

Figure 6.1. FTIR monitored NO emissions during DM1200 tests.

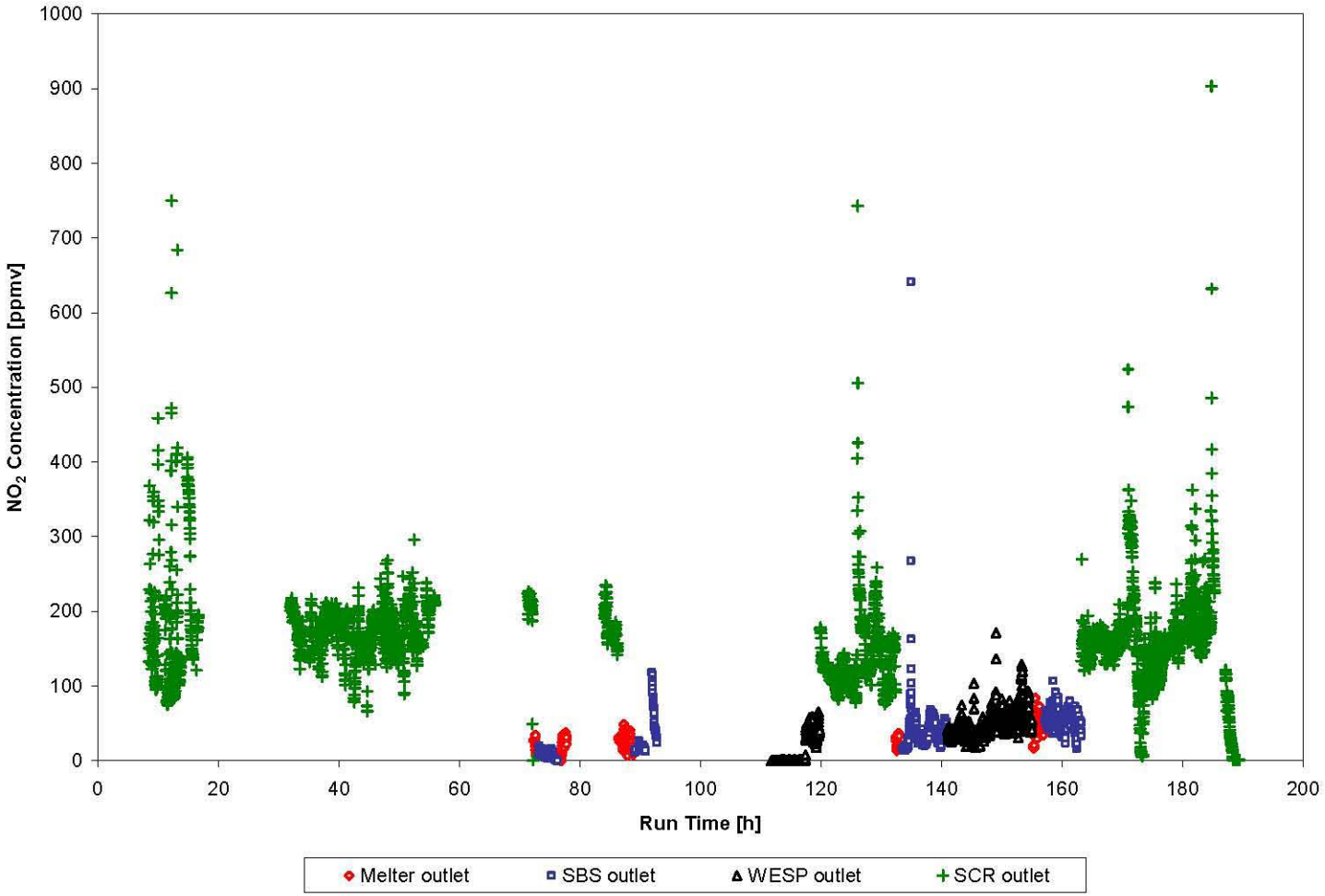

Figure 6.2. FTIR monitored NO_2 emissions during DM1200 tests.

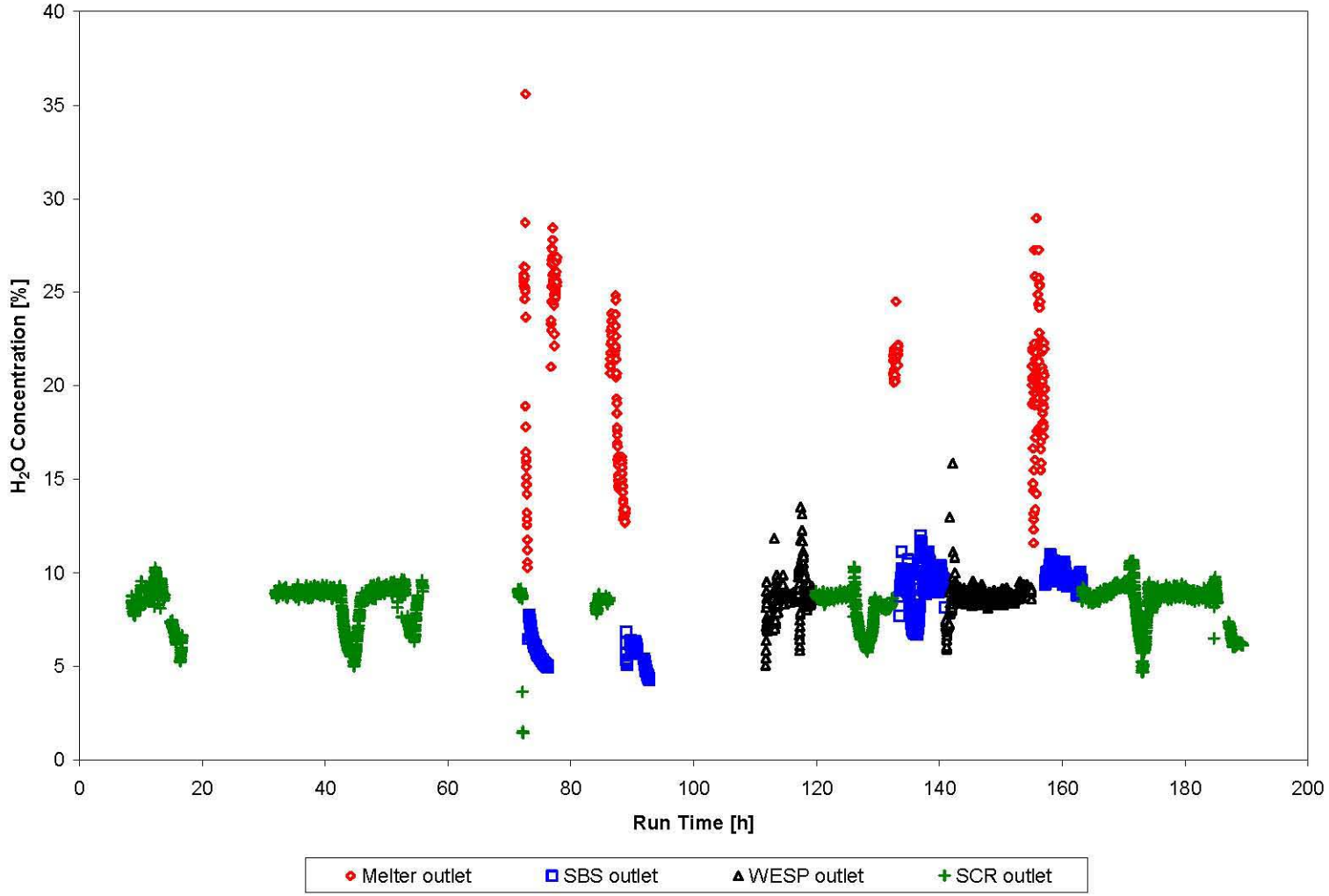

Figure 6.3. FTIR monitored H_2O emissions during DM1200 tests.

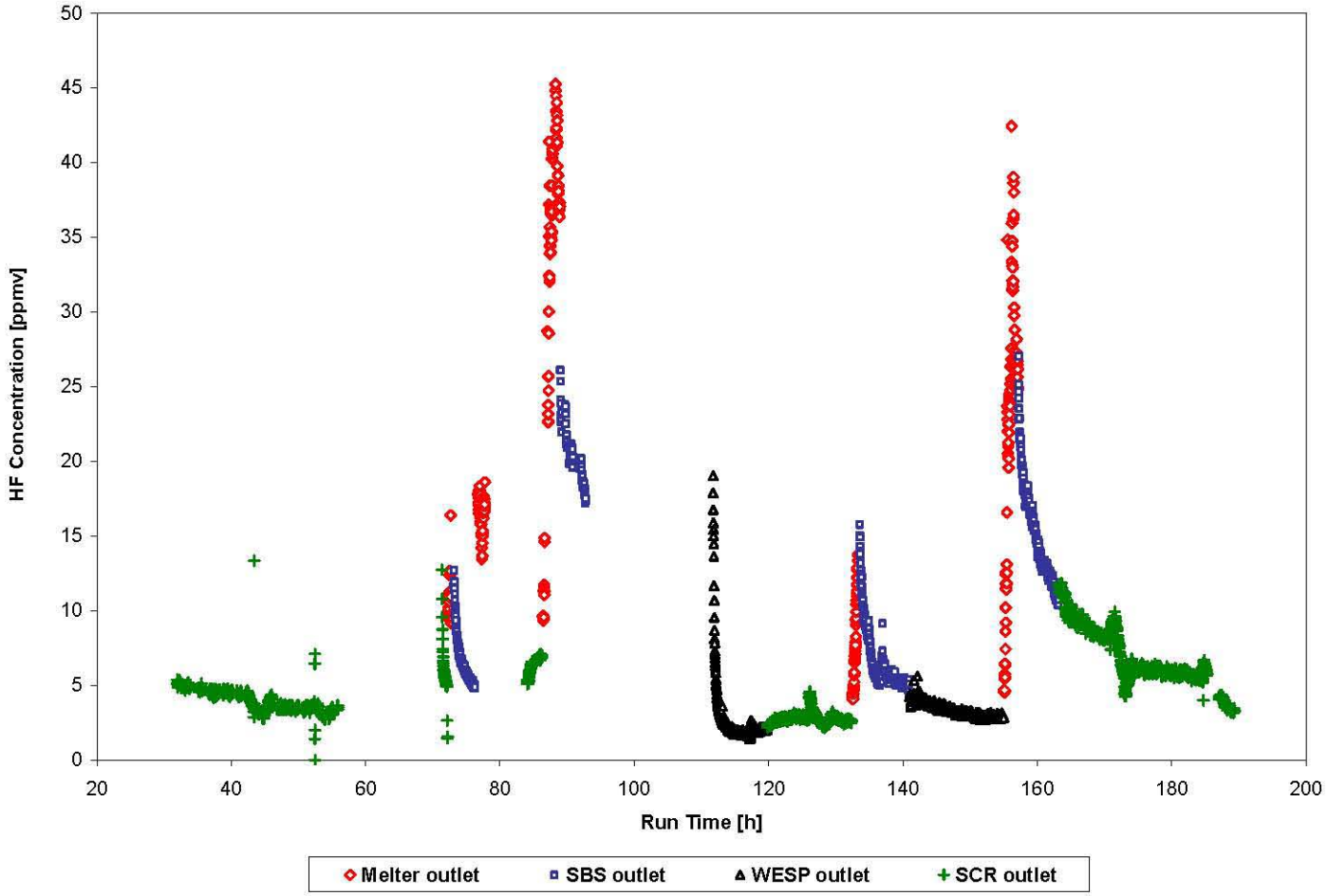

Figure 6.4. FTIR monitored HF emissions during DM1200 tests.

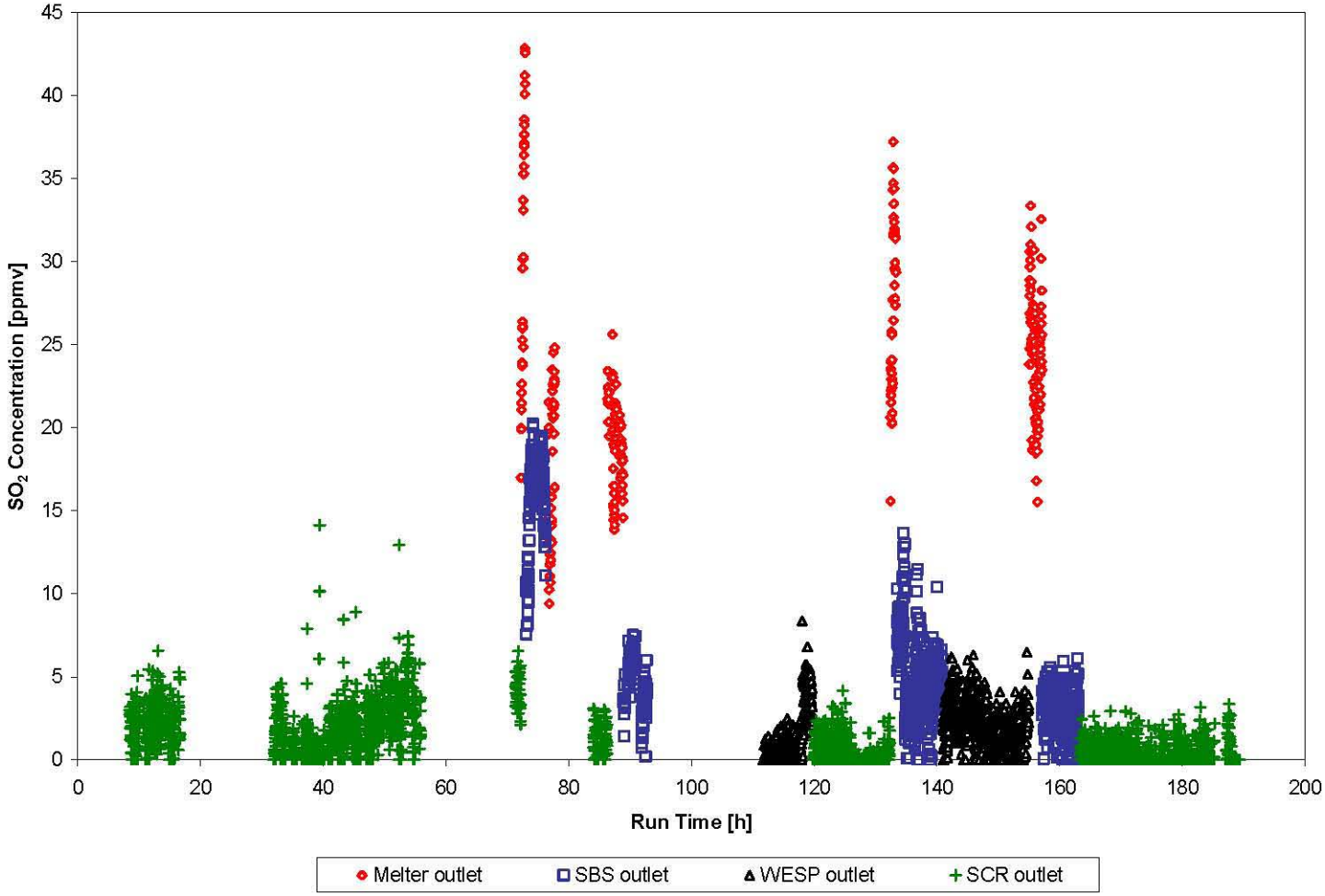

Figure 6.5. FTIR monitored SO_2 emissions during DM1200 tests.

Appendix A
Internal Drum Inspection Log

Sample: G-120-133A

1/15/2010

LEFT HALF

Picture Ref. #2 & 3
overall view of left
half of drum

Note 1: On both halves, there is a "foamy" layer of glass ~2-3" thick on top

NOTE 2: NO METALLIC PHASES OBSERVED THROUGHOUT THE GLASS

NOTE 3: NO SECONDARY PHASES OBSERVED THROUGHOUT THE GLASS

RIGHT HALF

Picture Ref. #4
overall view of right
half of drum

Picture Ref. #1 of void area around t/w on right half of drum

Note 4: void around t/w is ~ 6"x 6" x 6"

Measurements of glass from the bottom of the glass to the top of glass in inches.

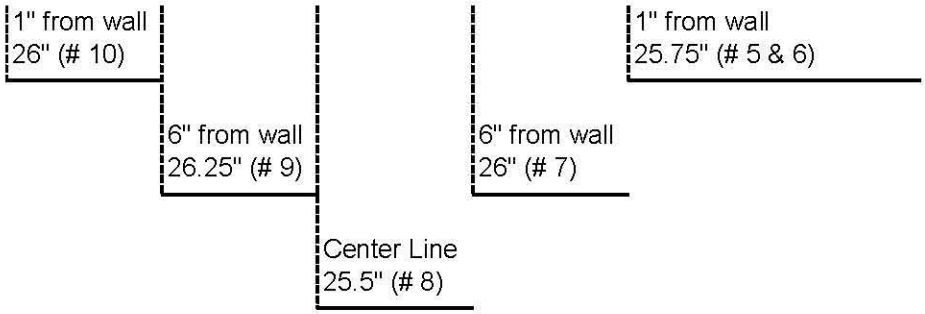

View into right half of drum showing void area, partial split.

View into left half of drum, partial split.

View of left half of drum, full split open.

View of right half of drum, full split open, shows void around t/w.

View of measure @ 1" from right side of right half of drum.

View of measure @ 1" from right side of right half of drum.

View of measure @ 6" from right side of right half of drum.

View of measure @ center line of right half of drum.

View of measure @ 6" from left side of right half of drum.

View of measure @ 1" from left side of right half of drum.

G-12P-116A
1/19/10

LEFT HALF

Picture Ref. # 1
overall view of left
half of drum

Note 1: Foamy glass layer ~1-2" on top of glass and ~2-3" at bottom of drum

NOTE 2: NO METALLIC PHASES OBSERVED THROUGHOUT THE GLASS

NOTE 3: NO SECONDARY PHASES OBSERVED THROUGHOUT THE GLASS

NOTE 4: TAN/BROWN STIATIONS OBSERVED THROUGHOUT THE GLASS, PRIMARILY AT OUTER 2-3"

RIGHT HALF

Picture Ref. # 2
overall view of right
half of drum

Picture Ref. # n/a

Note 4: void's in glass ~3-8" below surface w/ largest being egg shaped 3" x 4" x 4", several more voids ~2-3" diameter

Measurements of glass from the bottom of the glass to the top of glass in inches.

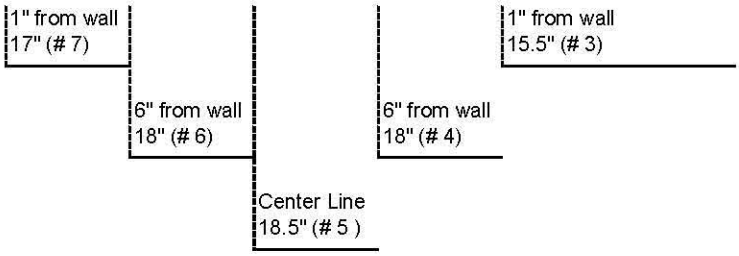

Overall view, left half of drum after cut.

Overall view, right half of drum after cut.

Glass measured @ 1" from right wall of right half of drum.

Glass measured @ 6" from right wall of right half of drum.

Glass measured @ 6" from left wall of right half of drum.

Glass measured @ 1" from left wall of right half of drum.

G-12P-101A
1/19/10

LEFT HALF

Picture Ref. #1
overall view of left
half of drum

Note 1: Glass mostly foamy throughout, but progressively more at towards the surface

NOTE 2: NO METALLIC PHASES OBSERVED THROUGHOUT THE GLASS

NOTE 3: NO SECONDARY PHASES OBSERVED THROUGHOUT THE GLASS

NOTE 4: TAN/BROWN STIATIONS OBSERVED THROUGHOUT THE GLASS, PRIMARILY AT OUTER 2-3"

RIGHT HALF

Picture Ref. # 2
overall view of right
half of drum

Picture Ref. # N/A

Note 5: void around t/w is ~ 6.5" x 7.5" x 8"

Measurements of glass from the bottom of the glass to the top of glass in inches.

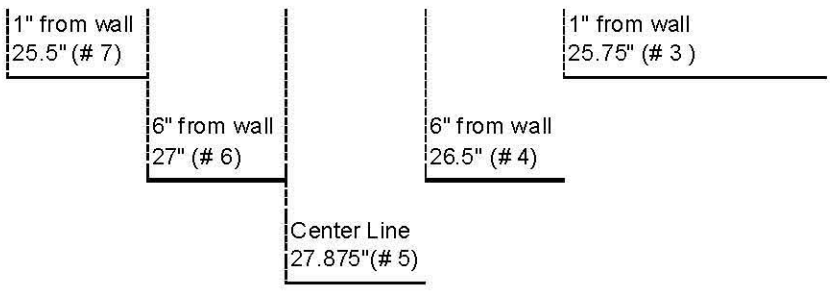

Overall view, left half of drum after cut.

Overall view, right half of drum after cut.

Glass measured @ 1" from right wall of right half of drum.

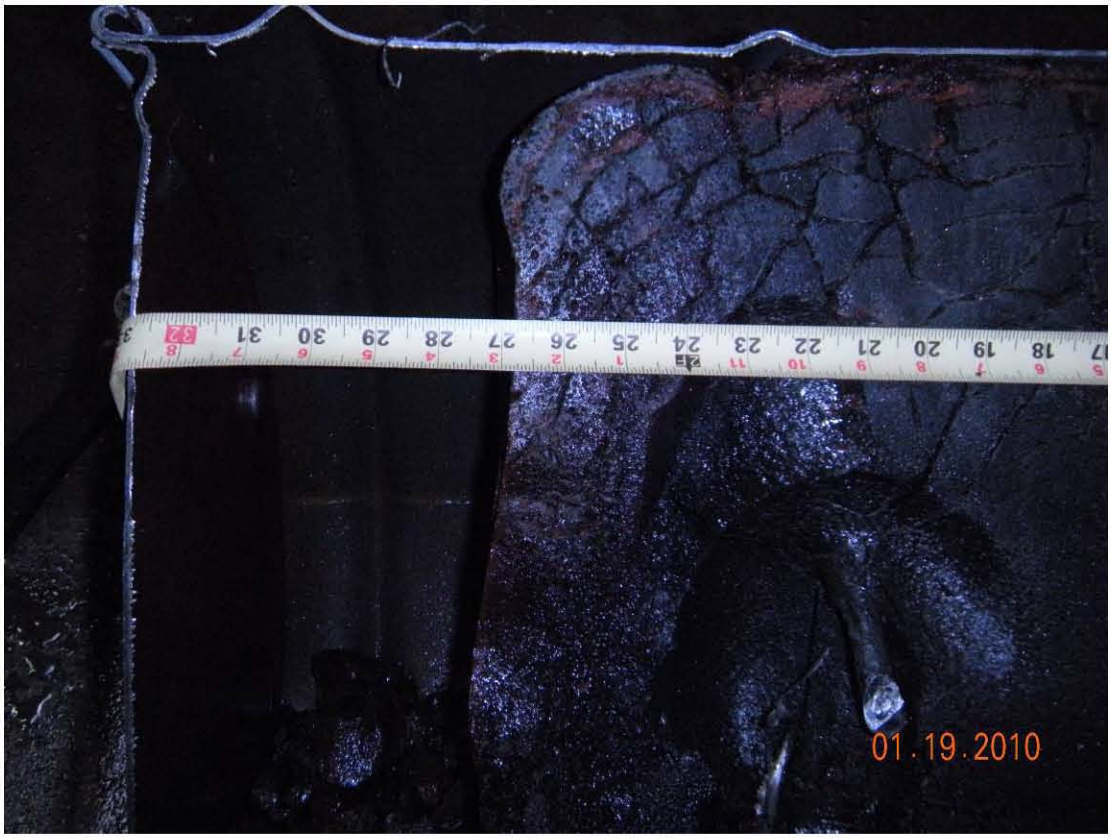

Glass measured @ 6" from right wall of right half of drum.

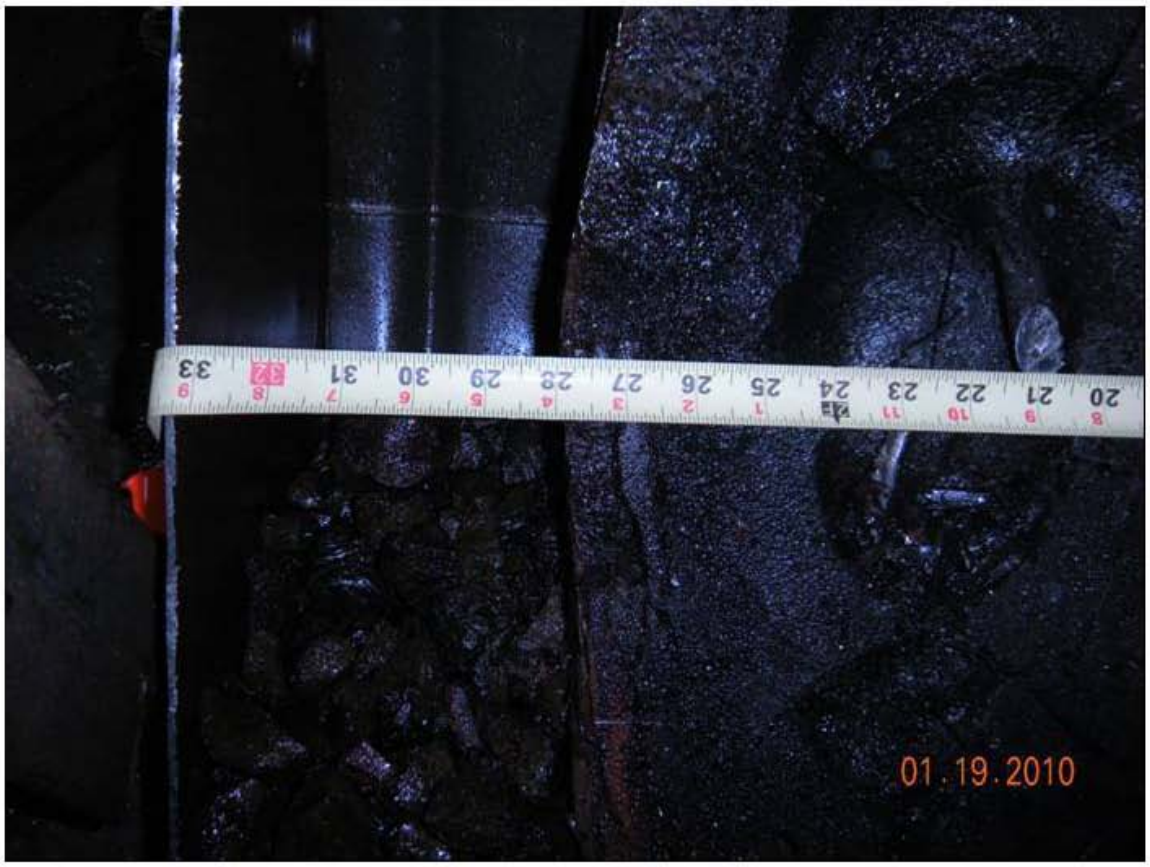

Glass measured @ center line of right half of drum.

Glass measured @ 6" from left wall of right half of drum.

Glass measured @ 1" from left wall of right half of drum.

G-12P-88A
1/20/2010

LEFT HALF

Picture Ref. # 1 overall view of left half of drum.
Picture #8 taken of glass on surface, left half.

Note 1: Mostly foamy at the top 1-2", slight foamy layer at bottom of dru.

NOTE 2: NO METALLIC PHASES OBSERVED THROUGHOUT THE GLASS

NOTE 3: NO SECONDARY PHASES OBSERVED THROUGHOUT THE GLASS

NOTE 4: TAN/BROWN STIATIONS OBSERVED THROUGHOUT THE GLASS.

RIGHT HALF

Picture Ref. # 2
overall view of right half of drum

Picture Ref. # N/A

Note 5: N/A

Measurements of glass from the bottom of the glass to the top of glass in inches.

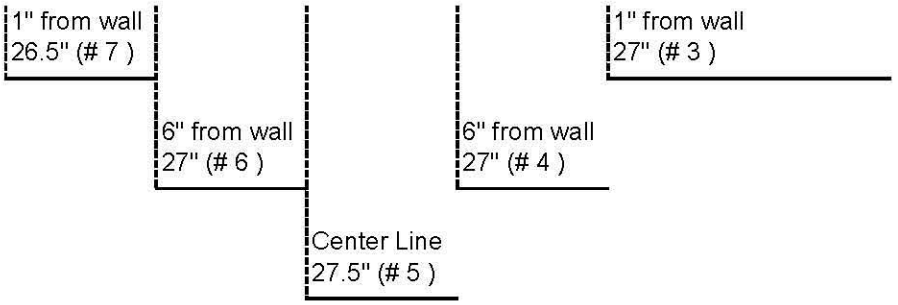

Overall view, left half of drum after cut.

Overall view, right half of drum after cut.

Glass measured @ 1" from right wall of right half of drum.

Glass measured @ 6" from right wall of right half of drum.

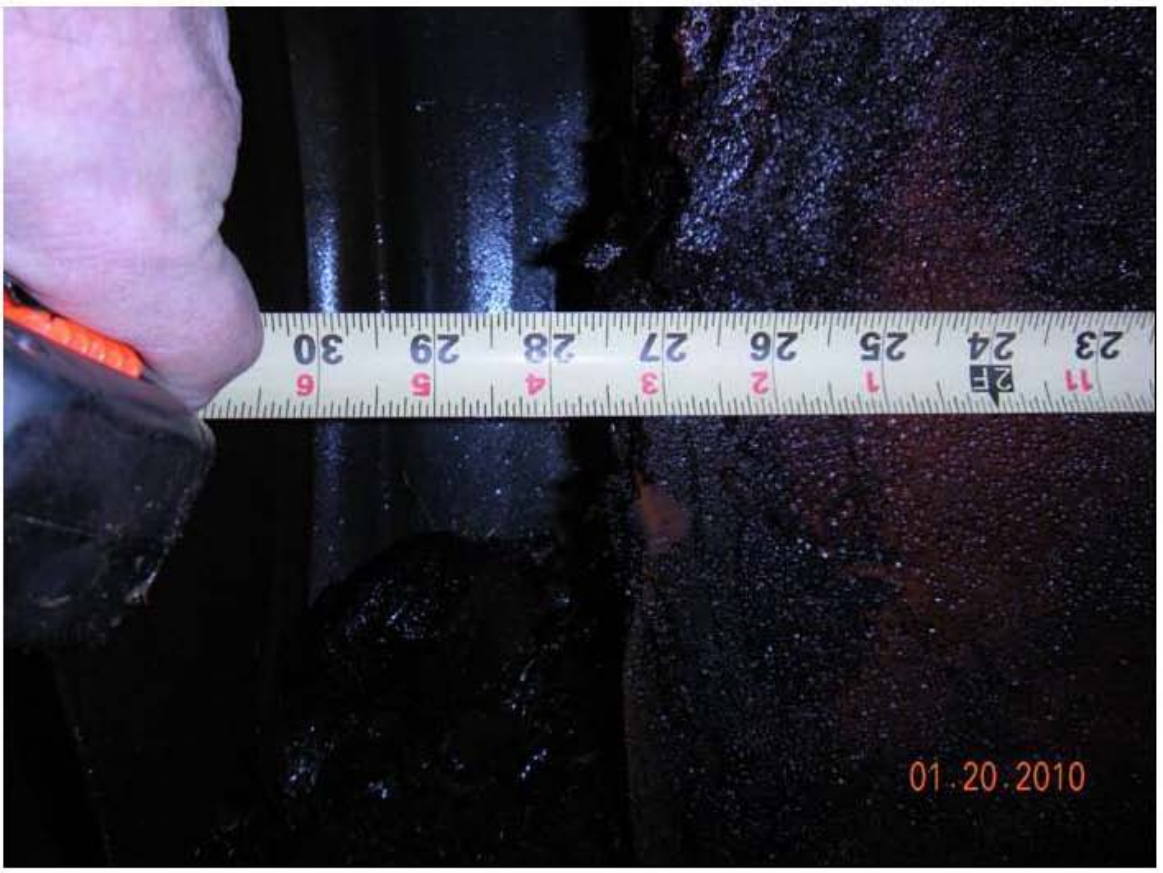

Glass measured @ center line of right half of drum.

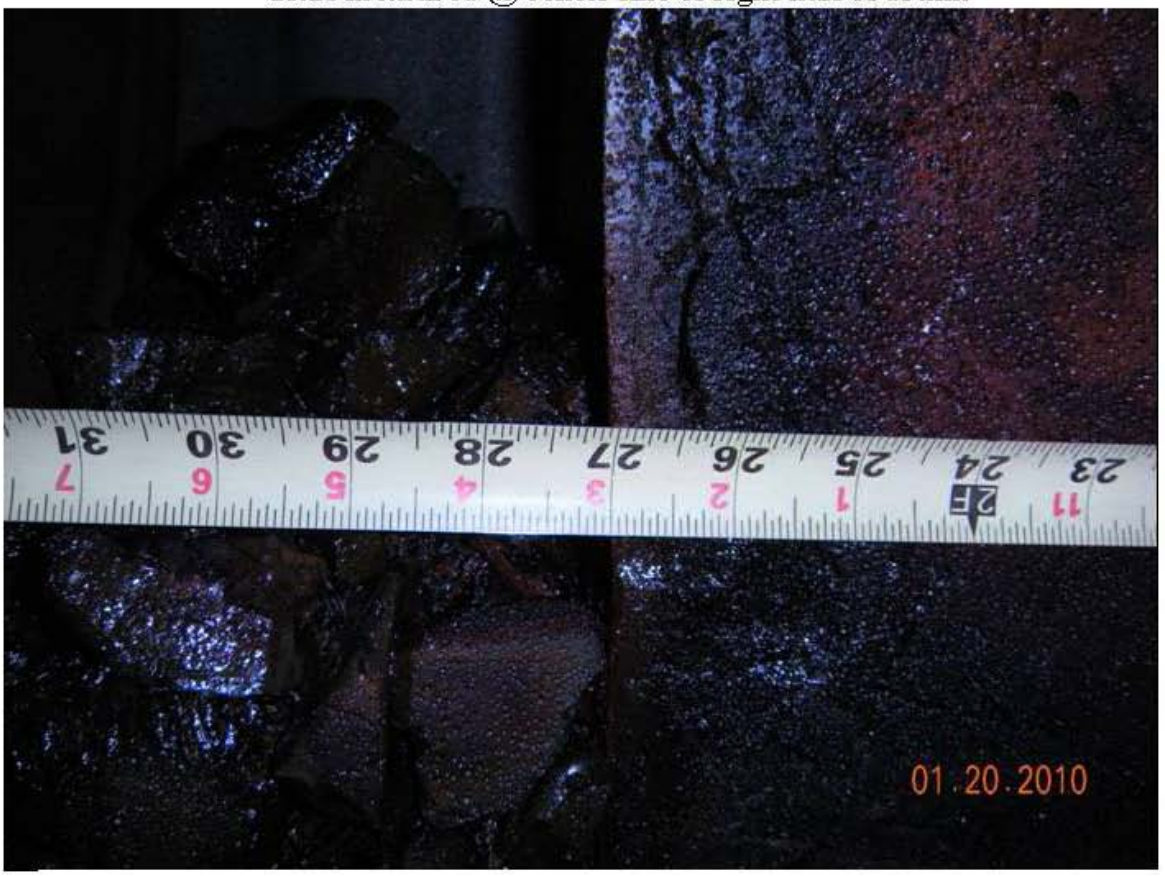

Glass measured @ 6" from left wall of right half of drum.

Glass measured @ 1" from left wall of right half of drum.

Glass surface on left half of drum.

G-12P-72A
1/20/10

LEFT HALF

Picture Ref. # 1
overall view of left
half of drum

Note 1: Pre pour glass shows very little foam & less brown striations.

NOTE 2: NO METALLIC PHASES OBSERVED THROUGHOUT THE GLASS

NOTE 3: NO SECONDARY PHASES OBSERVED THROUGHOUT THE GLASS

NOTE 4: TAN/BROWN STIATIONS OBSERVED THROUGHOUT THE GLASS.

RIGHT HALF

Picture Ref. # 2
overall view of right
half of drum

Picture Ref. # N/A

Note 5: N/A

Measurements of glass from the bottom of the glass to the top of glass in inches.

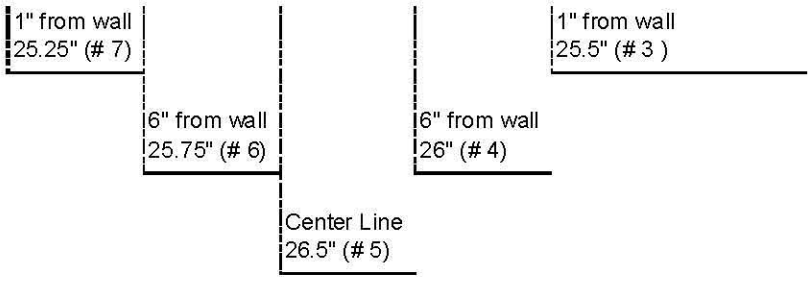

Overall view. left half of drum after cut.

Overall view, right half of drum after cut.

Glass measured @ 1" from right wall of right half of drum.

Glass measured @ 6" from right wall of right half of drum.

Glass measured @ center line of right half of drum.

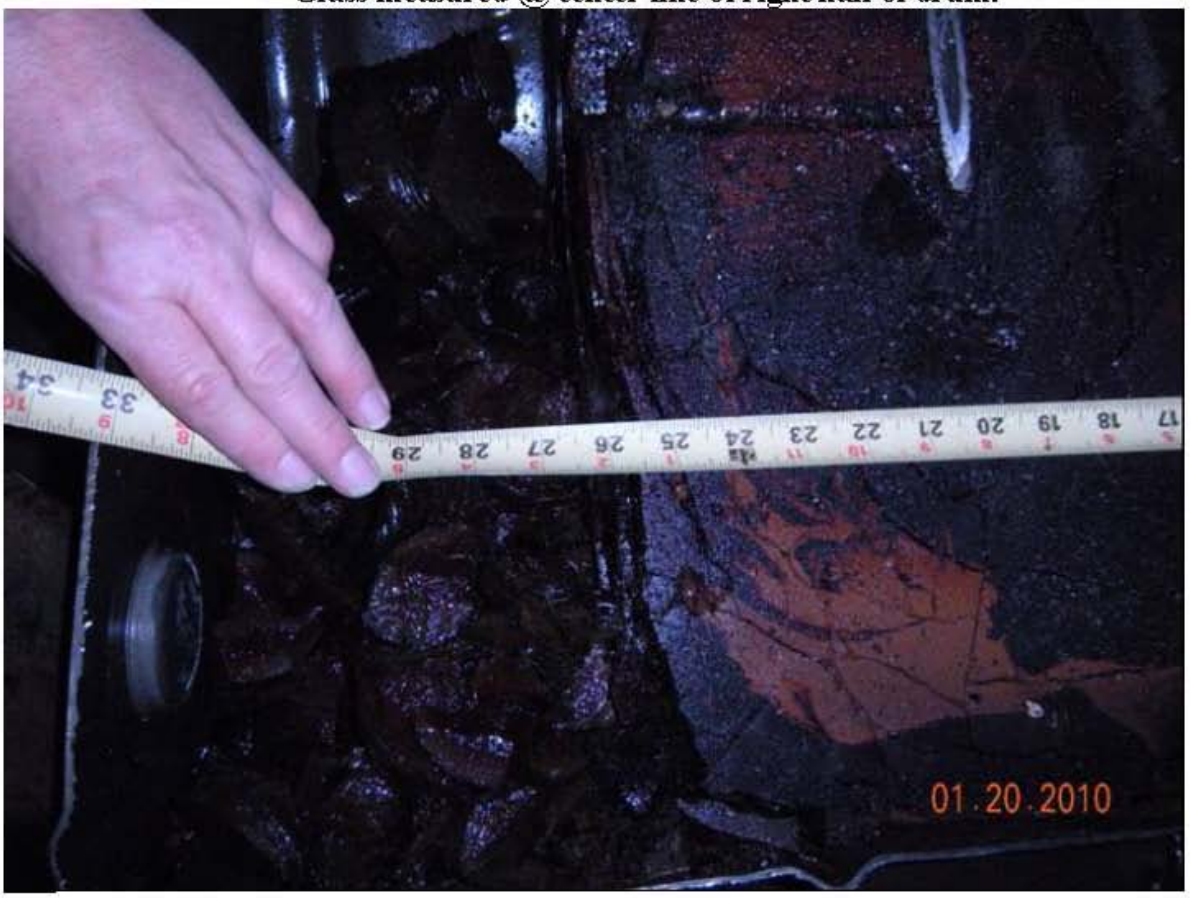

Glass measured @ 6" from left wall of right half of drum.

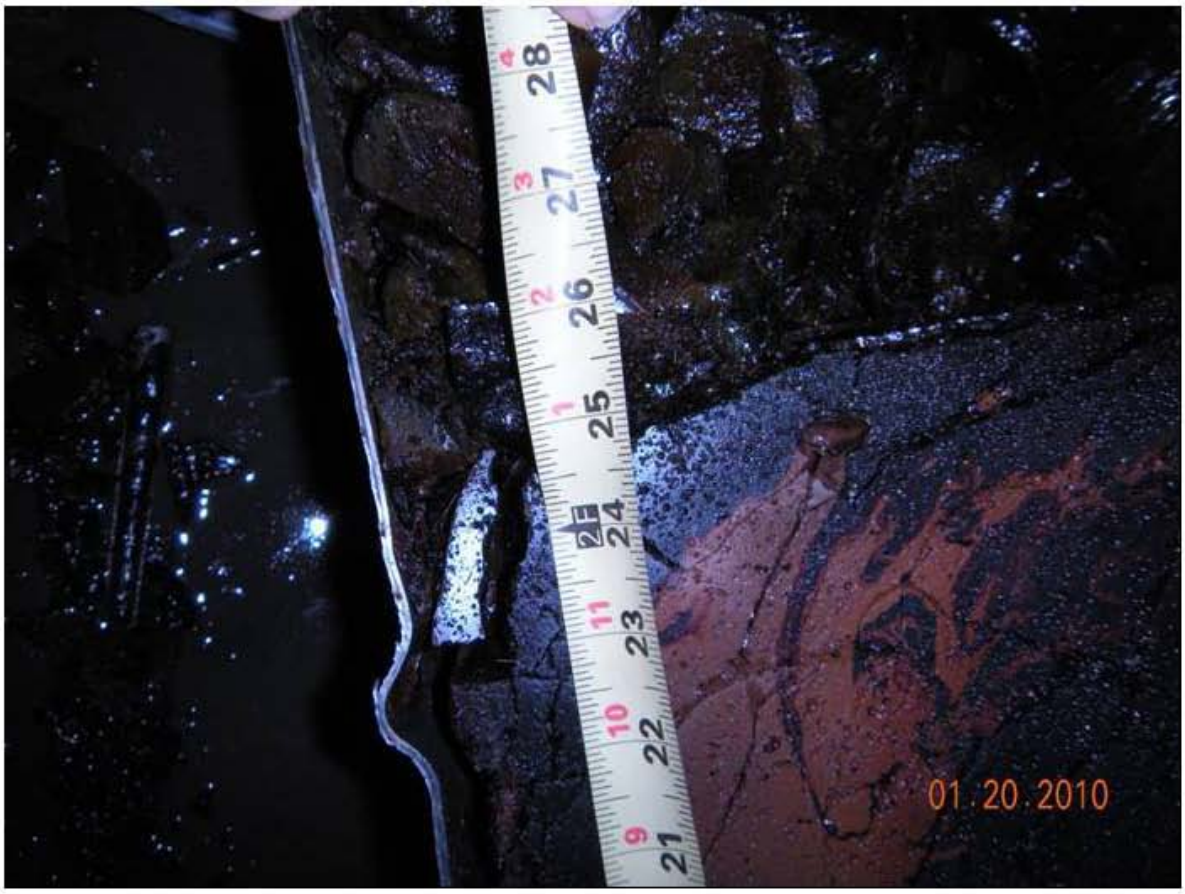

Glass measured @ 1" from left wall of right half of drum.

G-12P-53A
1/20/10

LEFT HALF

Picture Ref. # 1: overall view of left half of drum.
Ref. #9 & 10: Top of Left half of drum

Note 1: Surface glass is very "crumbly" for 2-3". Less foam and brown striations in pre-pour glass.

NOTE 2: NO METALLIC PHASES OBSERVED THROUGHOUT THE GLASS

NOTE 3: NO SECONDARY PHASES OBSERVED THROUGHOUT THE GLASS

NOTE 4: TAN/BROWN STIATIONS OBSERVED THROUGHOUT THE GLASS

RIGHT HALF

Picture Ref. # 2: overall view of right half of drum.
Ref. # 8: Top of right half of drum

Picture Ref. # N/A

Note 5: N/A

Measurements of glass from the bottom of the glass to the top of glass in inches.

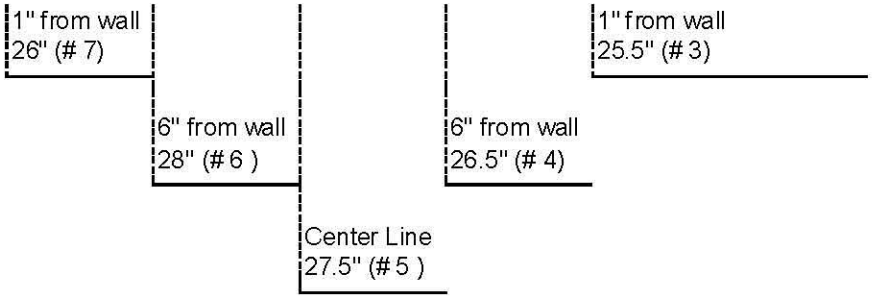

Overall view, left half of drum after cut.

Overall view, right half of drum after cut.

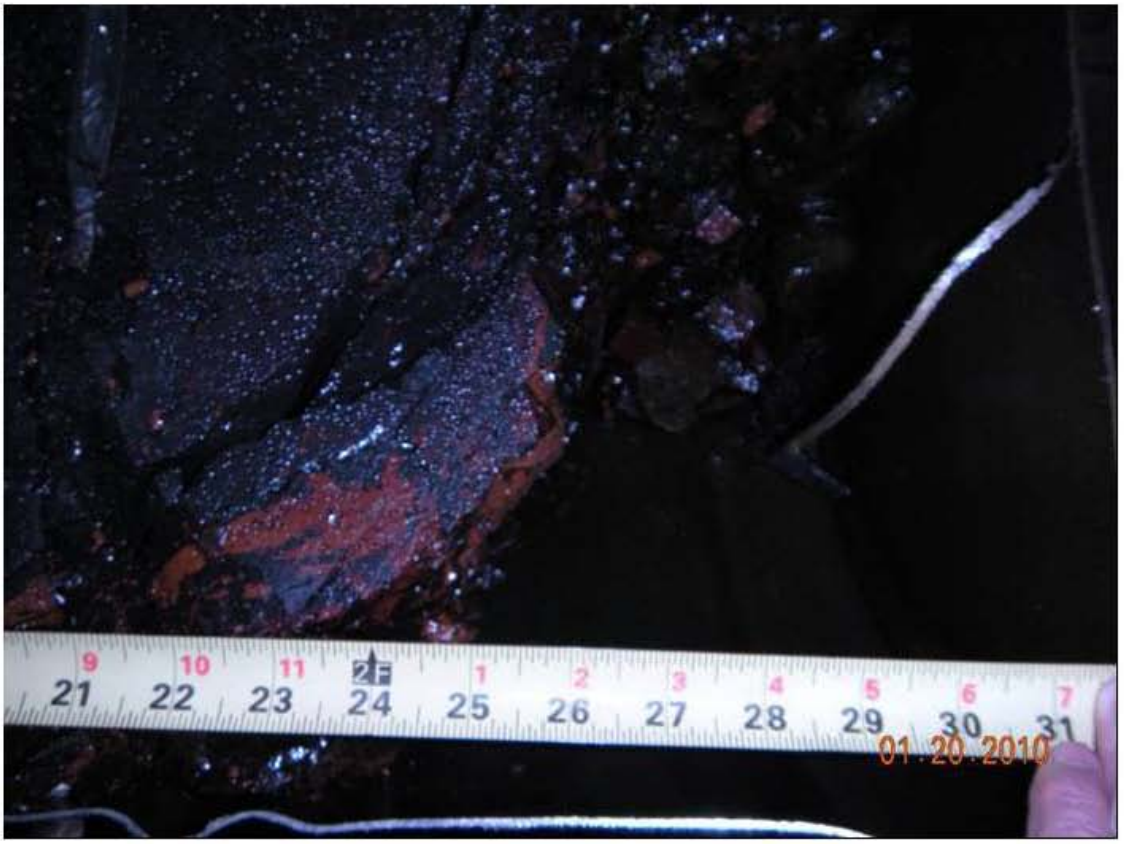

Glass measured @ 1" from right wall of right half of drum.

Glass measured @ 6" from right wall of right half of drum.

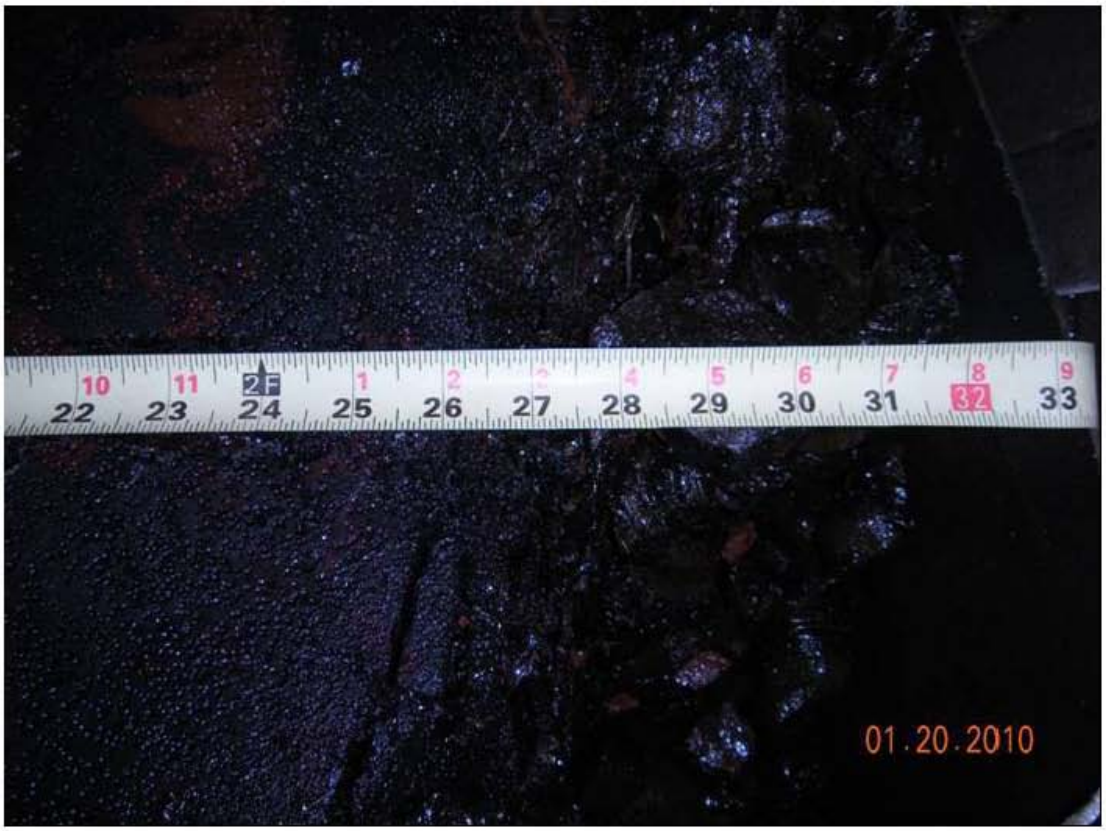

Glass measured @ center line of right half of drum.

Glass measured @ 6" from left wall of right half of drum.

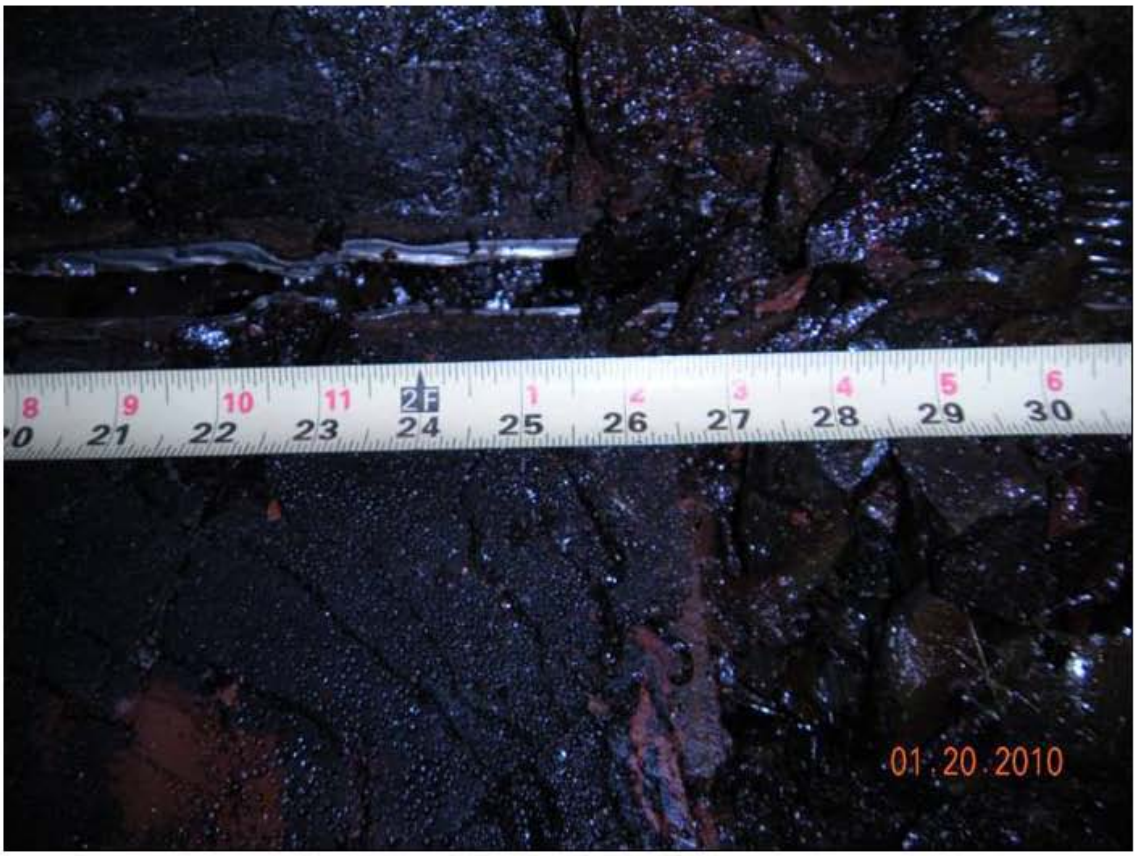

Glass measured @ 1" from left wall of right half of drum.

Glass surface right half of drum.

Glass surface left half of drum.

Glass surface left half of drum.

G-12P-32A
1/20/10

LEFT HALF

Picture Ref. # 1
overall view of left
half of drum

Note 1: Surface glass is very "crumbly" for 2-3". Less foam and brown striations in pre-pour glass.

NOTE 2: NO METALLIC PHASES OBSERVED THROUGHOUT THE GLASS

NOTE 3: SUSPECT SECONDARY PHASES OBSERVED THROUGHOUT THE GLASS

NOTE 4: RED/BROWN STIATIONS OBSERVED THROUGHOUT THE GLASS THAN ON LATER DISCHARGES

RIGHT HALF

Picture Ref. # 2
overall view of right
half of drum

Picture Ref. #

Note 5: Possible sliver of metal left in glass from cutting process,
see sample: G-12P-32A-1 (PIC# 8)

PIC# 9 TAKEN OF CAVITY BELOW SURFACE LEVEL OF GLASS, LOOKING FROM SURFACE VIEWPOINT

PIC# 10 TAKEN OF SUSPECT SECONDARY MATERIAL

Measurements of glass from the bottom of the glass to the top of glass in inches.

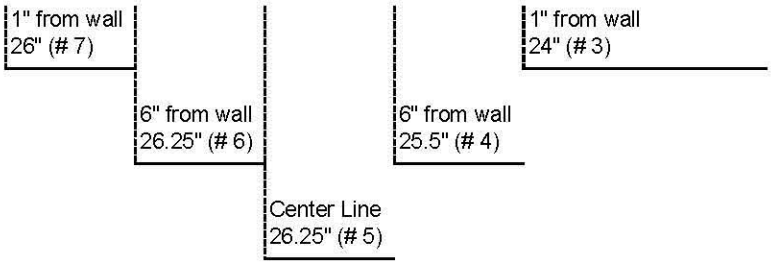

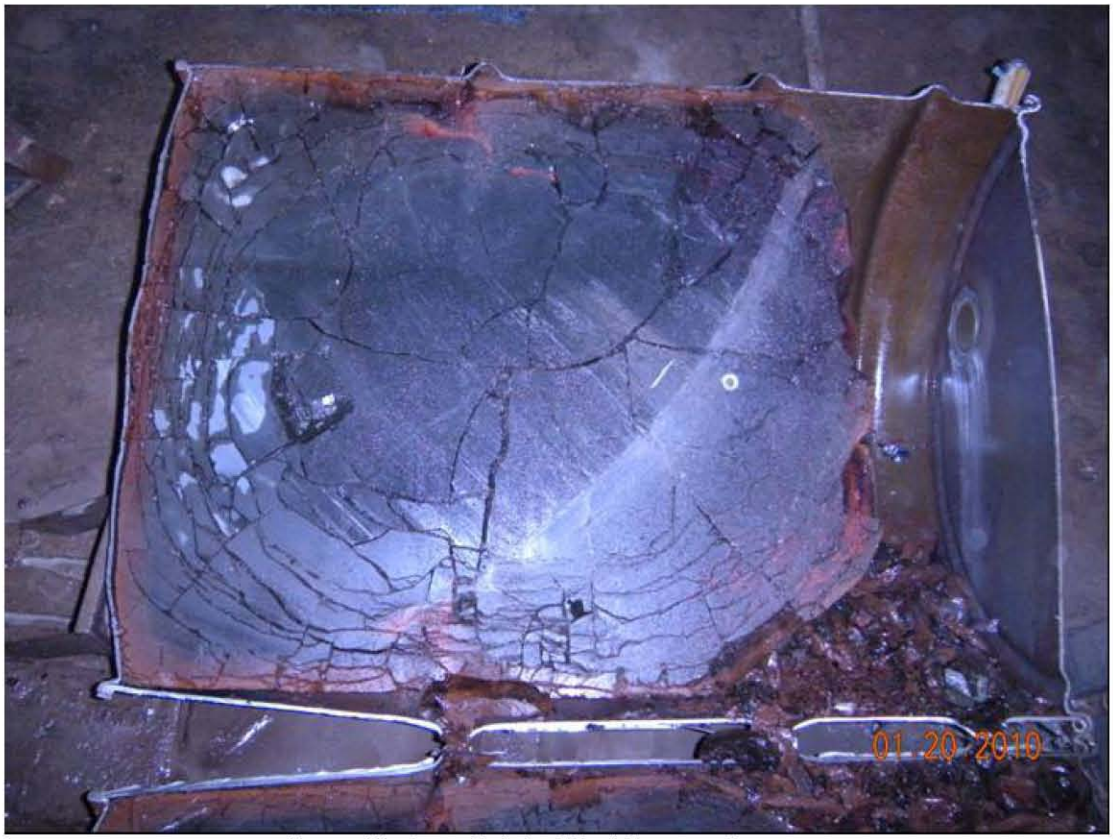

Overall view, left half of drum after cut.

Overall view, right half of drum after cut.

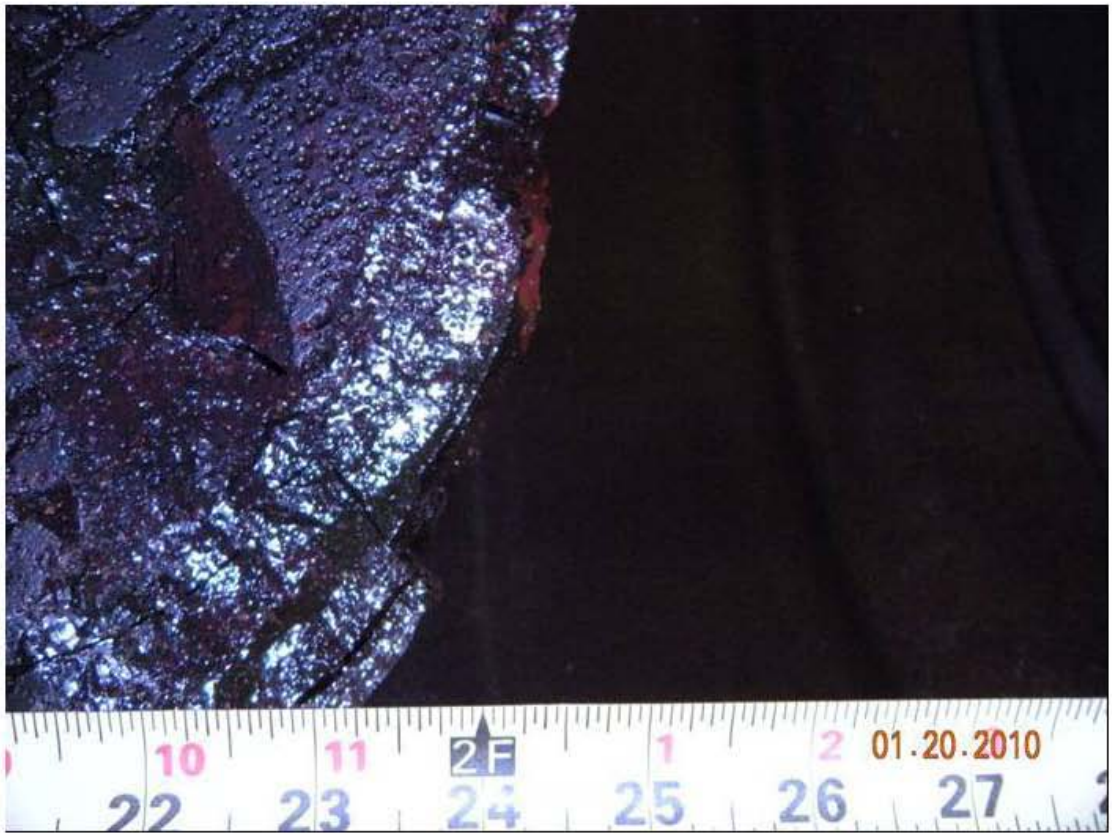

Glass measured @ 1" from right wall of right half of drum.

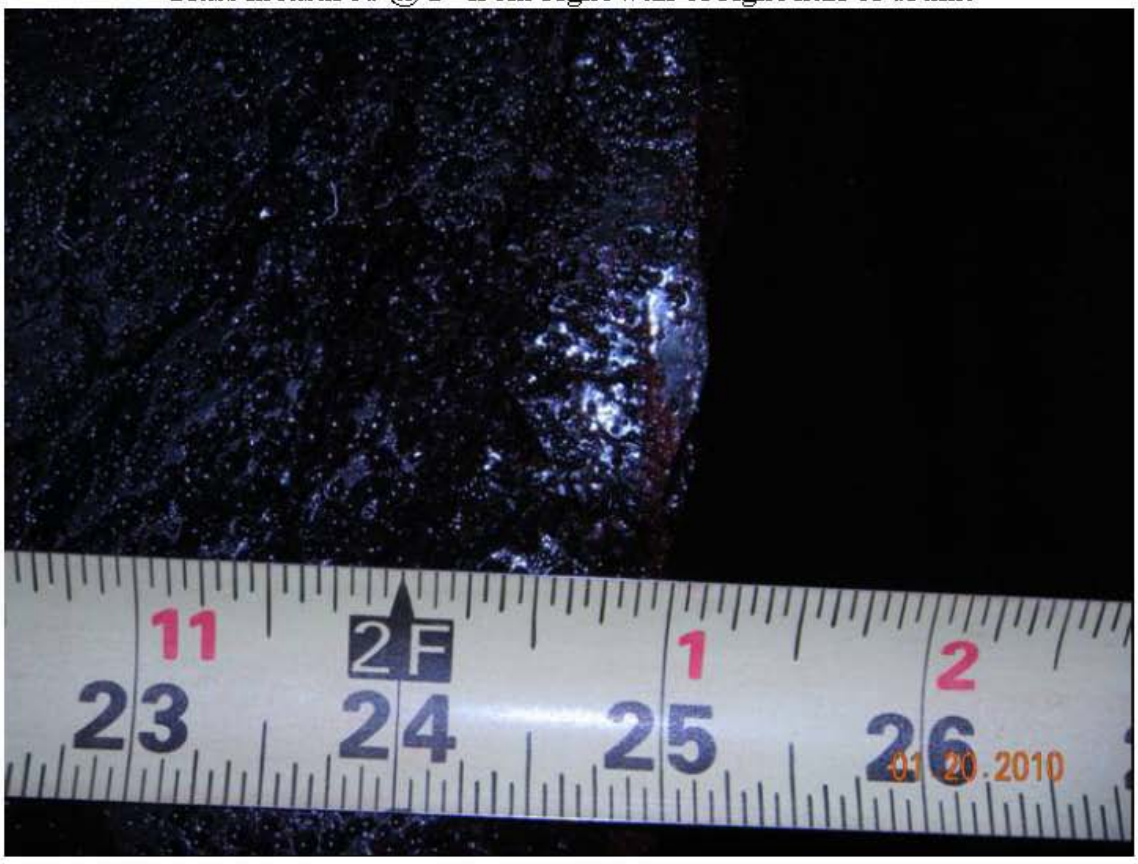

Glass measured @ 6" from right wall of right half of drum.

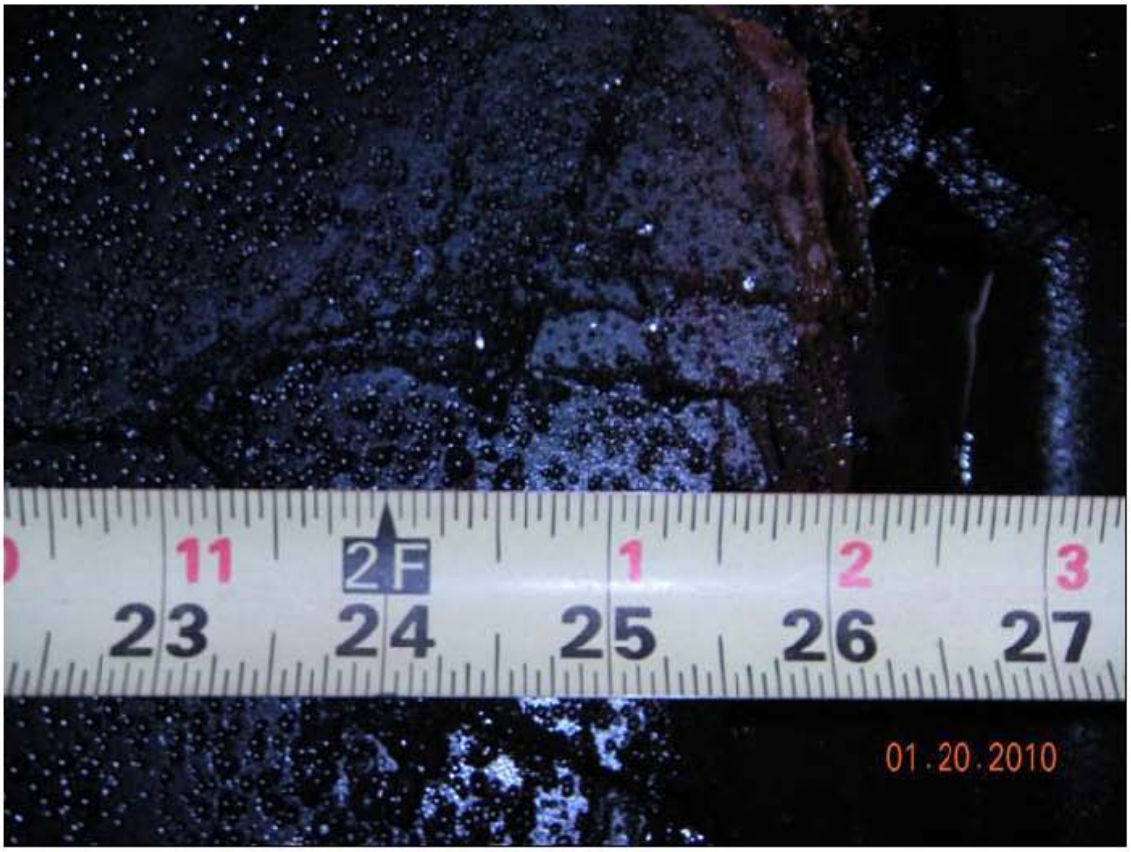

Glass measured @ center line of right half of drum.

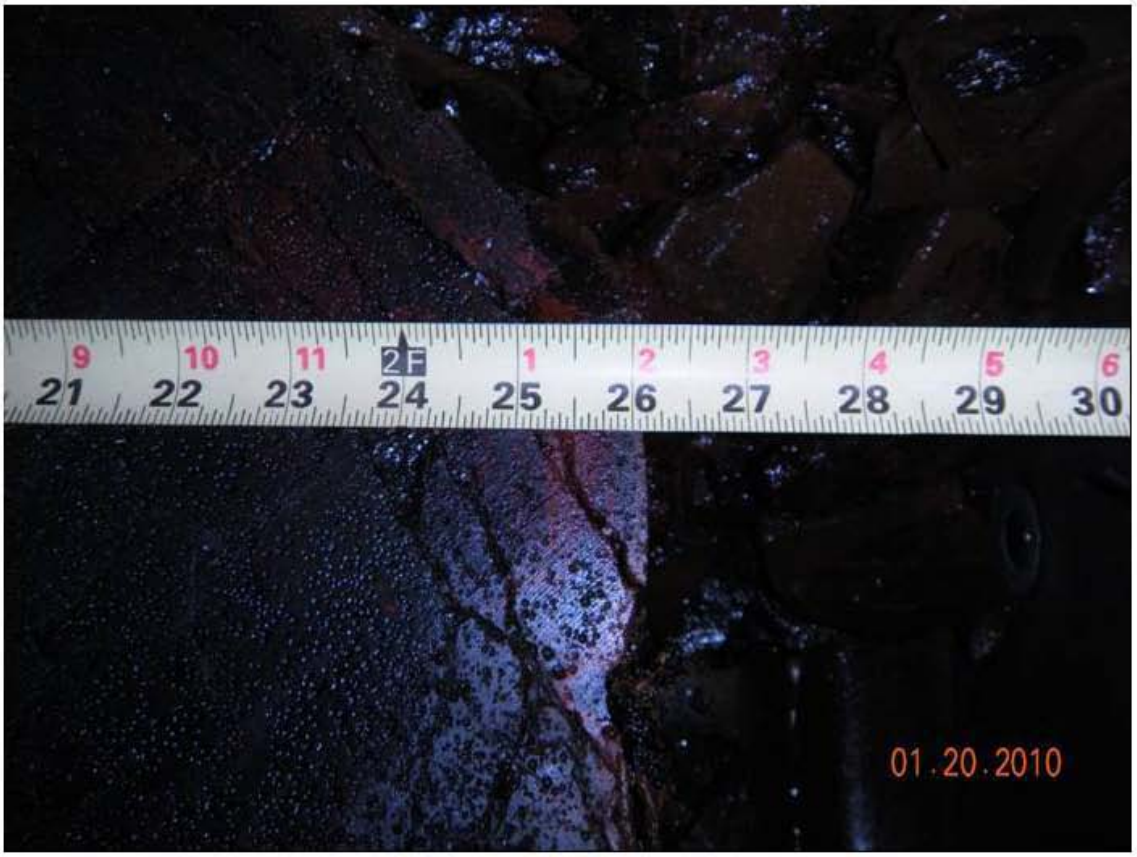

Glass measured @ 6" from left wall of right half of drum.

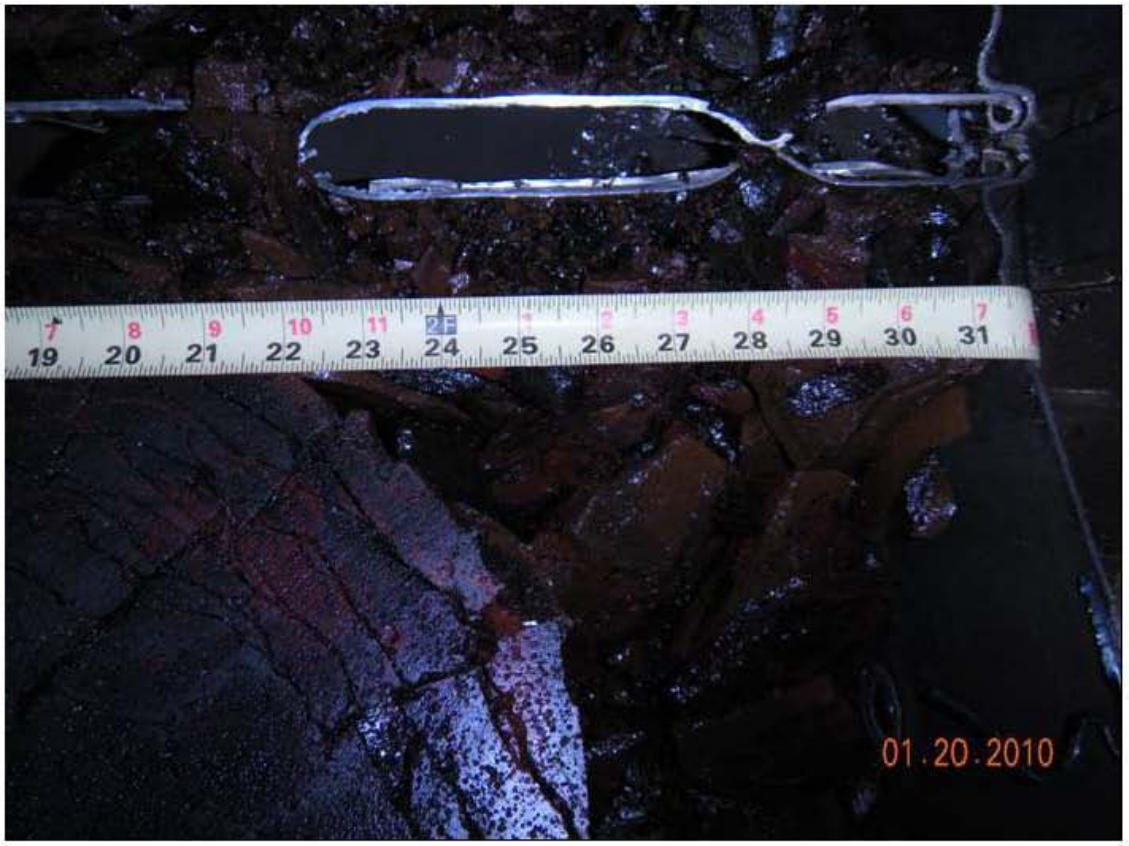

Glass measured @ 1" from left wall of right half of drum.

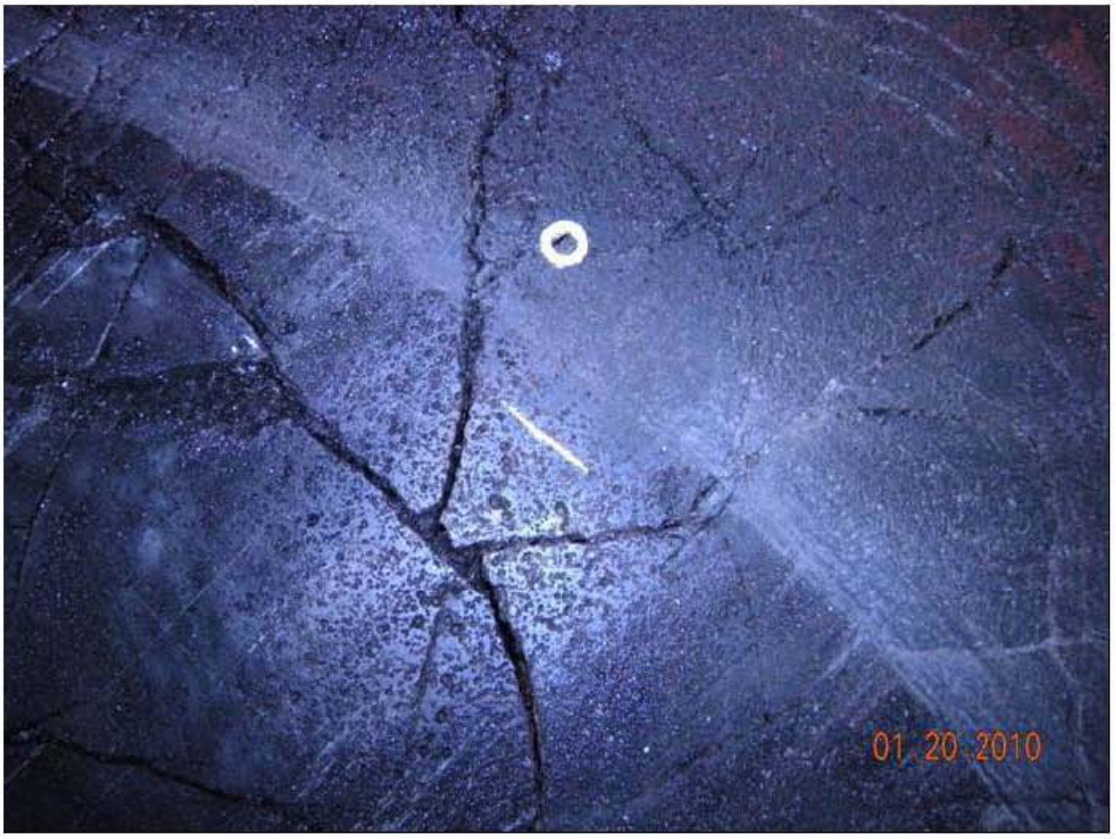

Glass area where sample: G-12P-32A-1 was collected.

Shows cavity below surface on right half of drum, looking downward.

Suspect secondary phase where sample G-12P-32A-3 was collected.

G-120-150A
1/20/10

LEFT HALF

Picture Ref. # 1
overall view of left
half of drum

Note 1: Mostly foamy at the top 1-2", slight foamy layer at bottom of drum.

NOTE 2: SUSPECT METALLIC PHASES OBSERVED IN THE GLASS

NOTE 3: SUSPECT SECONDARY PHASES OBSERVED THROUGHOUT THE GLASS

NOTE 4: RED/BROWN STIATIONS OBSERVED THROUGHOUT THE GLASS THAN ON LATER DISCHARGES

RIGHT HALF

Picture Ref. # 2
overall view of right
half of drum

Picture Ref. # 8 & 9: Void area around t/w.
Ref. # 10: glazed glass area near center.

Note 5: 2 voids
1st @ t/w is ~ 4" x 4" x 6",
2nd just above t/w ~ 3" x 2" x 2"

Picture Ref. # 11: Suspect secondary phase.

Measurements of glass from the bottom of the glass to the top of glass in inches.

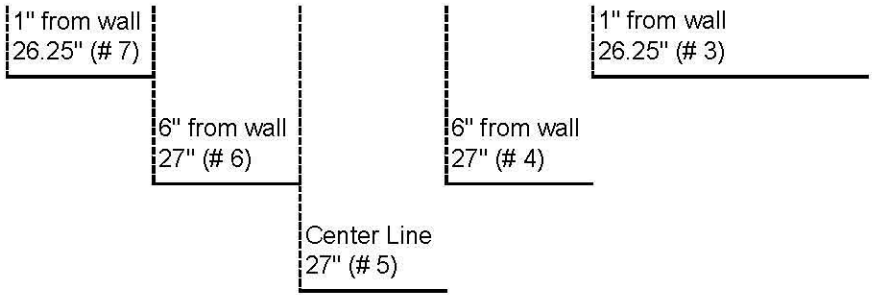

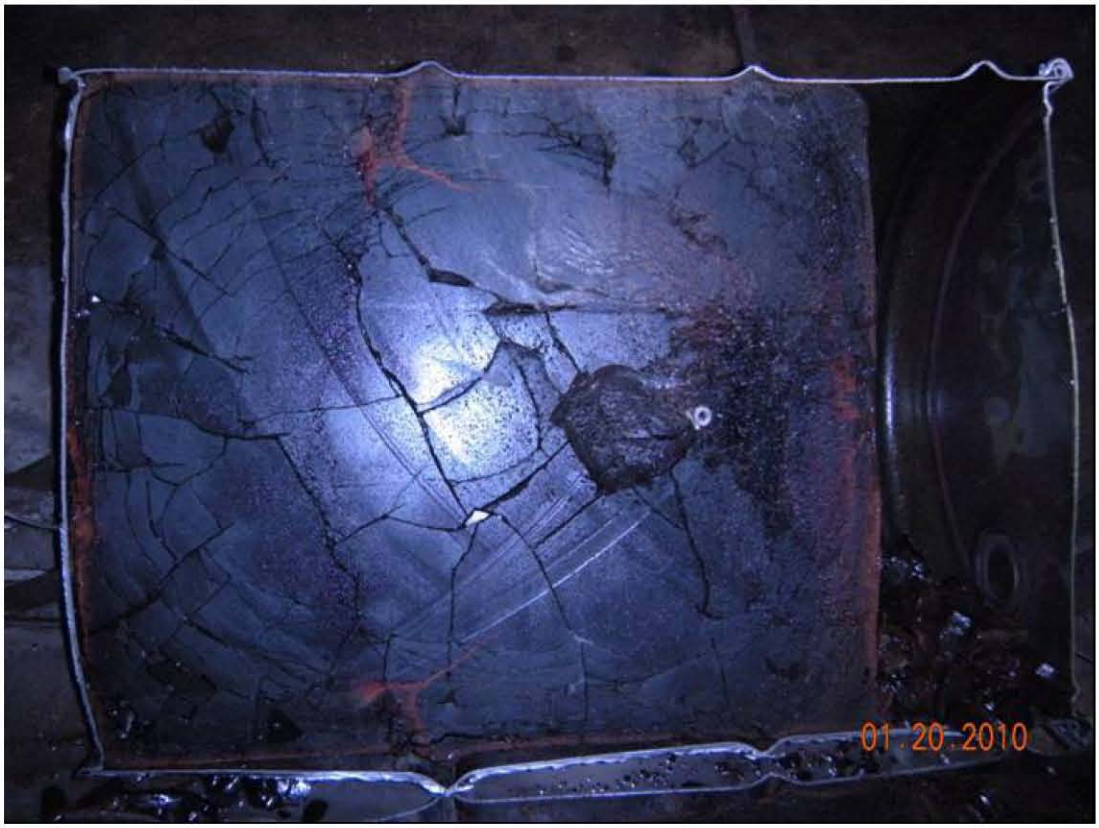

Overall view, left half of drum after cut.

Overall view, right half of drum after cut.

Glass measured @ 1" from right wall of right half of drum.

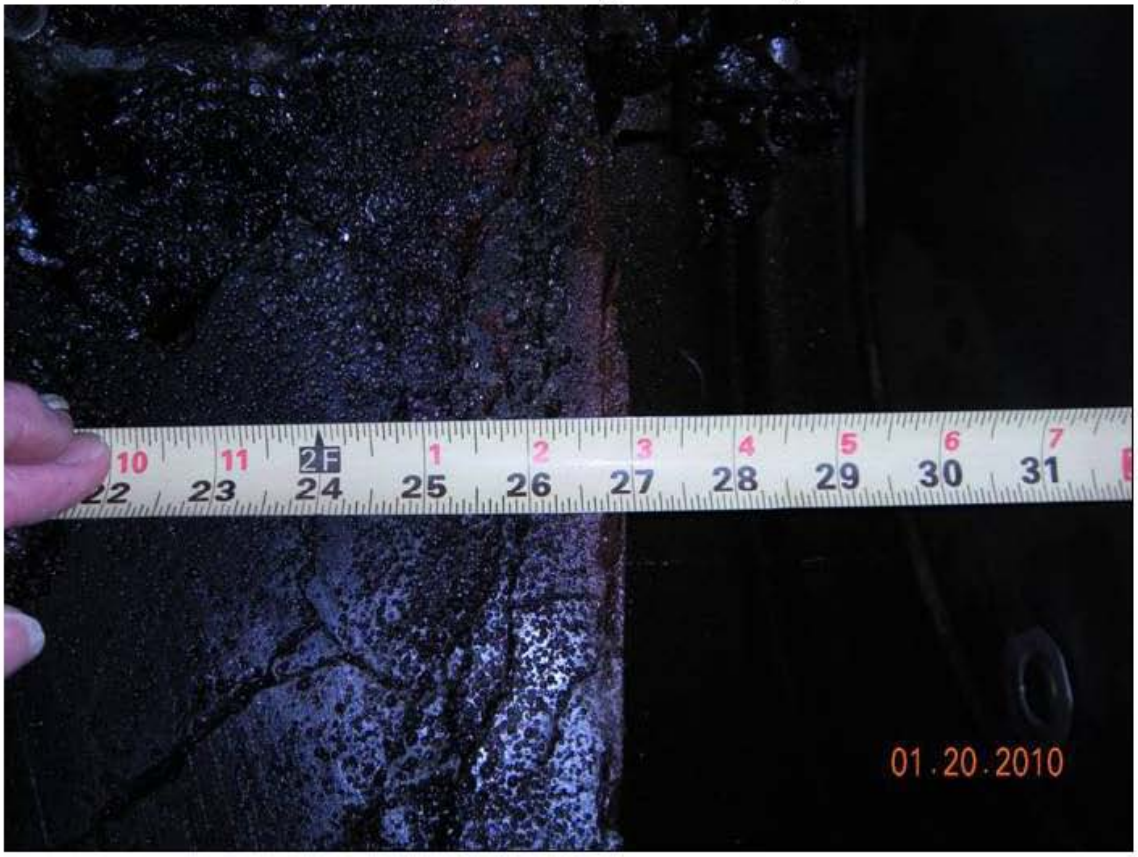

Glass measured @ 1" from right wall of right half of drum.

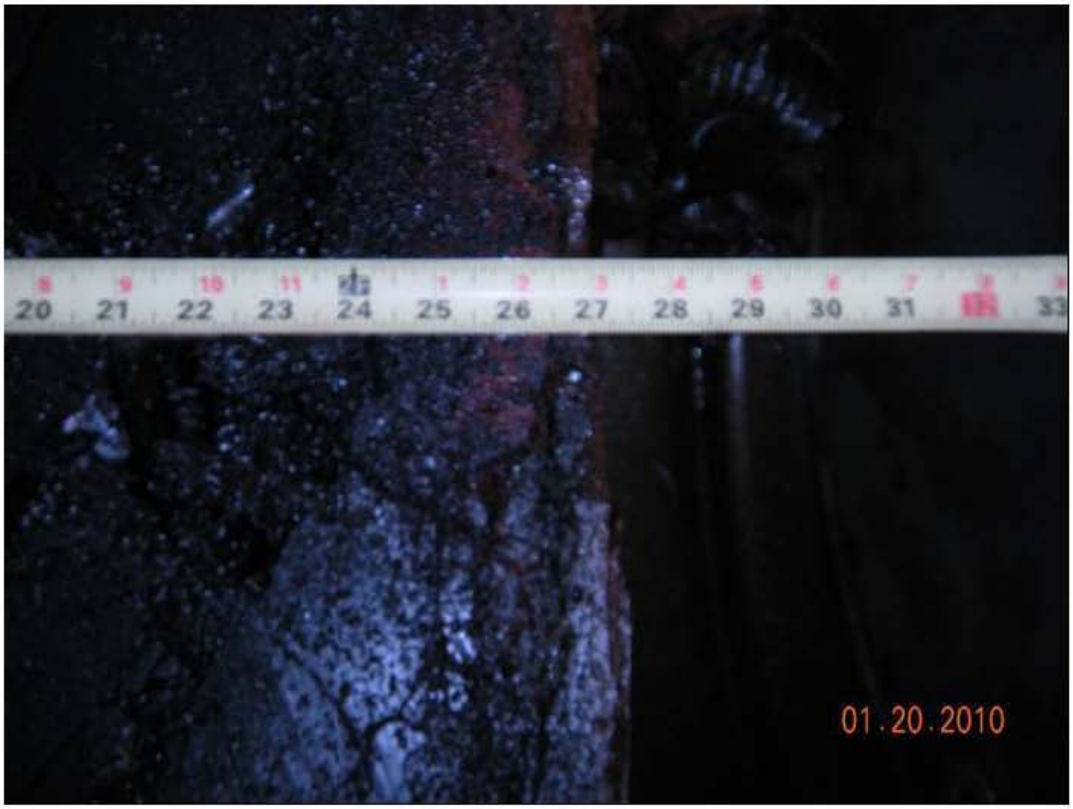

Glass measured @ center line of right half of drum.

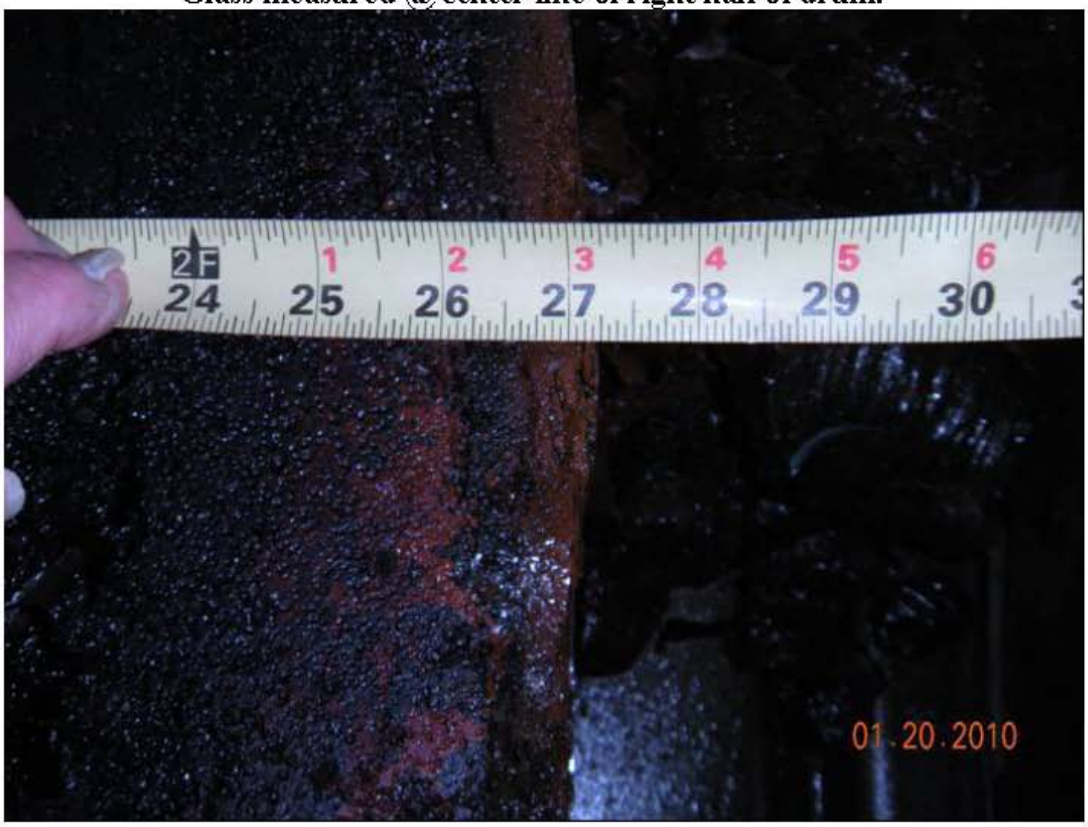

Glass measured @ 6" from left wall of right half of drum.

Glass measured @ 1" from left wall of right half of drum.

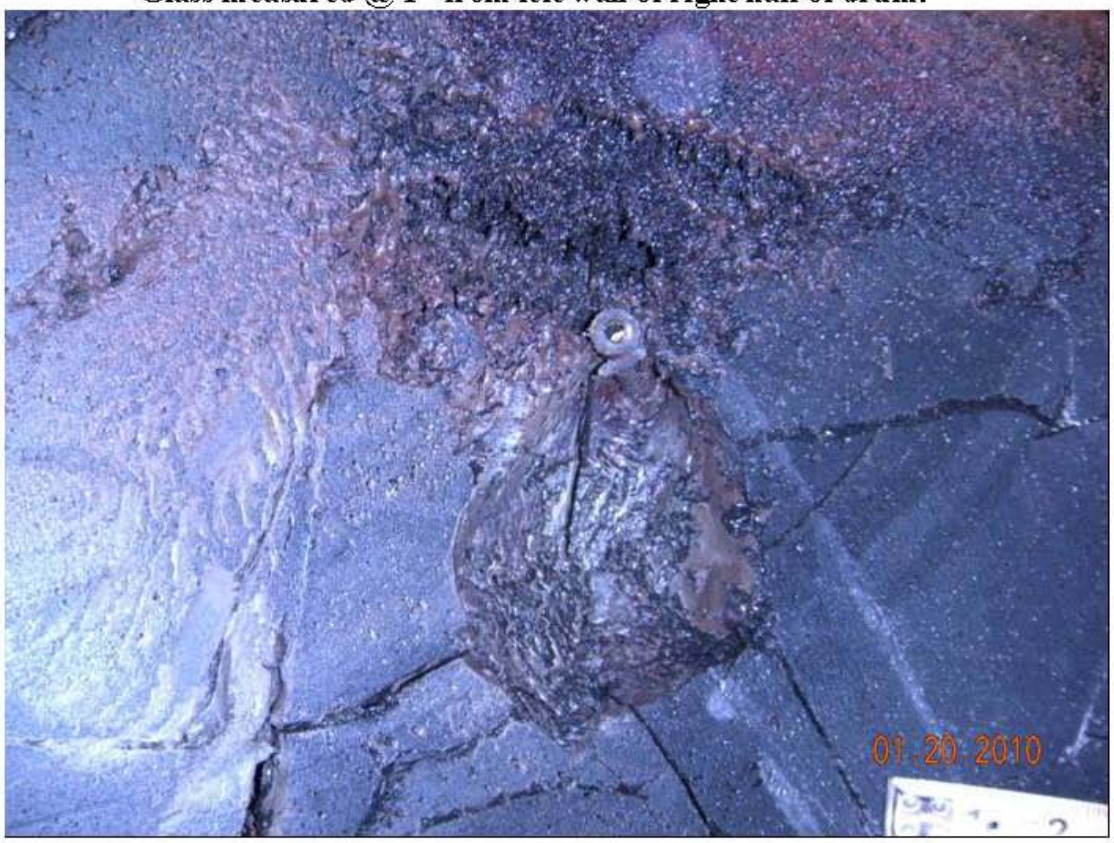

Void area around t/w on right half of drum.

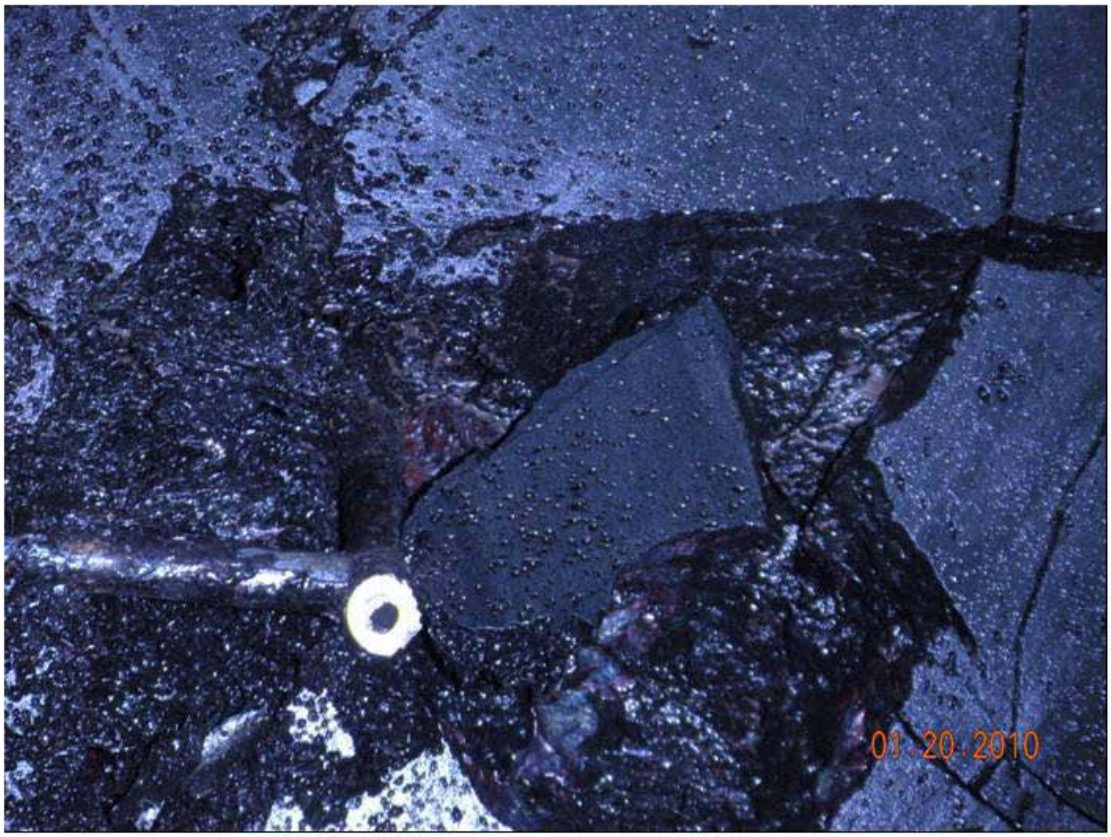

Void area around t/w on right half of drum.

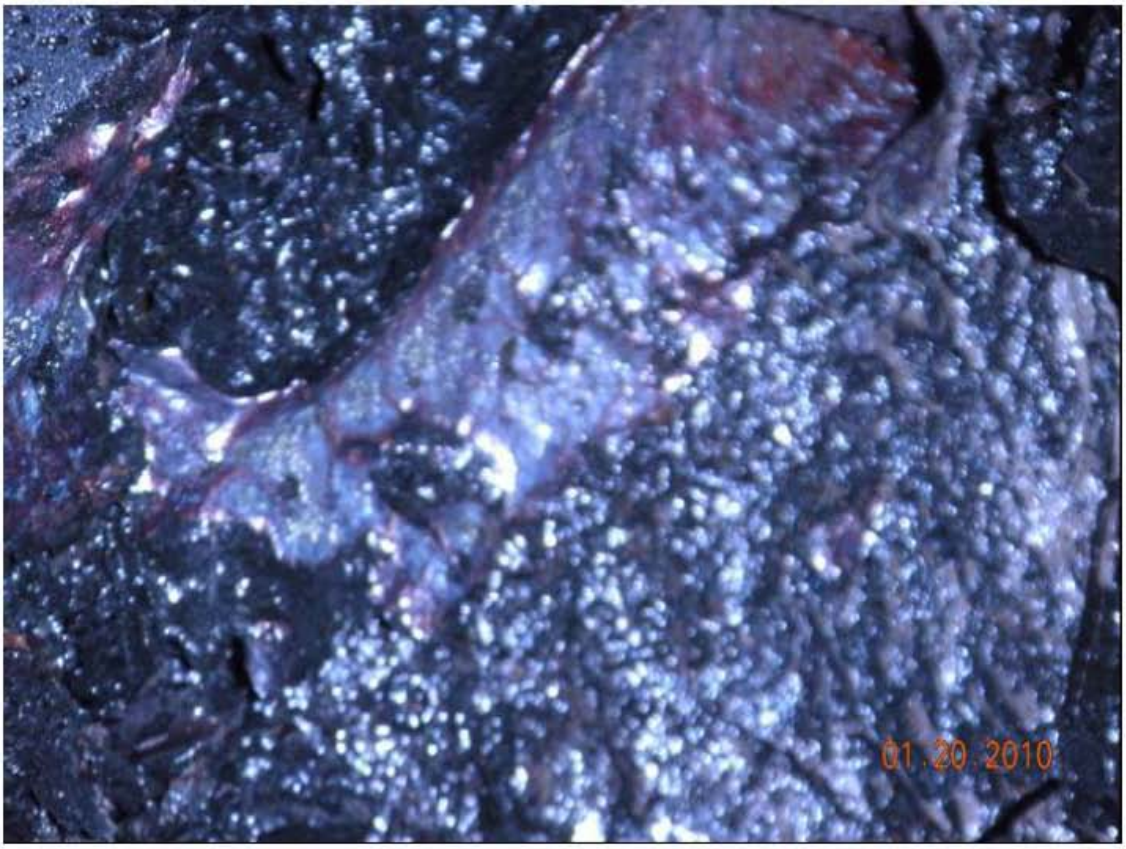

Glazed glass area near center of drum on right half.

Suspect secondary phase where sample: G-12O-150A-4 was collected.

G-120-101A
1/21/10

LEFT HALF

Picture Ref. # 1
overall view of left
half of drum

Note 1: GLASS IS FOAMY THROUGOUT

NOTE 2: NO METALLIC PHASES OBSERVED THROUGHOUT THE GLASS

NOTE 3: NO SECONDARY PHASES OBSERVED THROUGHOUT THE GLASS

NOTE 4: RED/BROWN STRIATIONS OBSERVED AROUND EDGES OF GLASS AND ABOVE T/W

RIGHT HALF

Picture Ref. # 2
overall view of right
half of drum

Picture Ref. # N/A

Note 5: N/A

Measurements of glass from the bottom of the glass to the top of glass in inches.

**** Unable to determine glass height due to complete collapse of glass in area.**

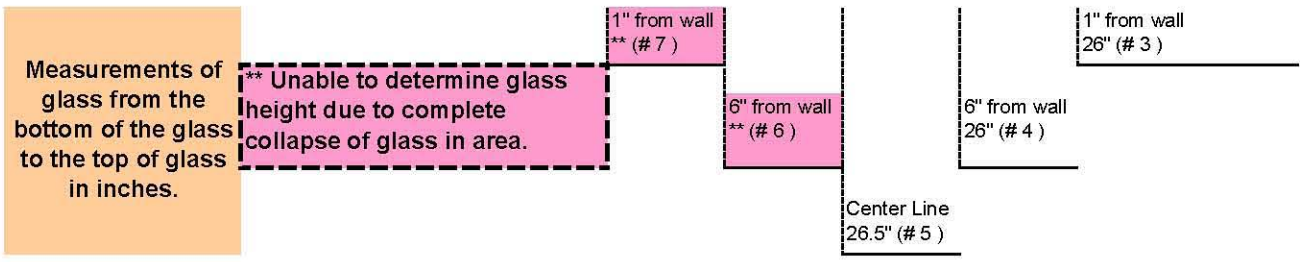

Overall view. left half of drum after cut.

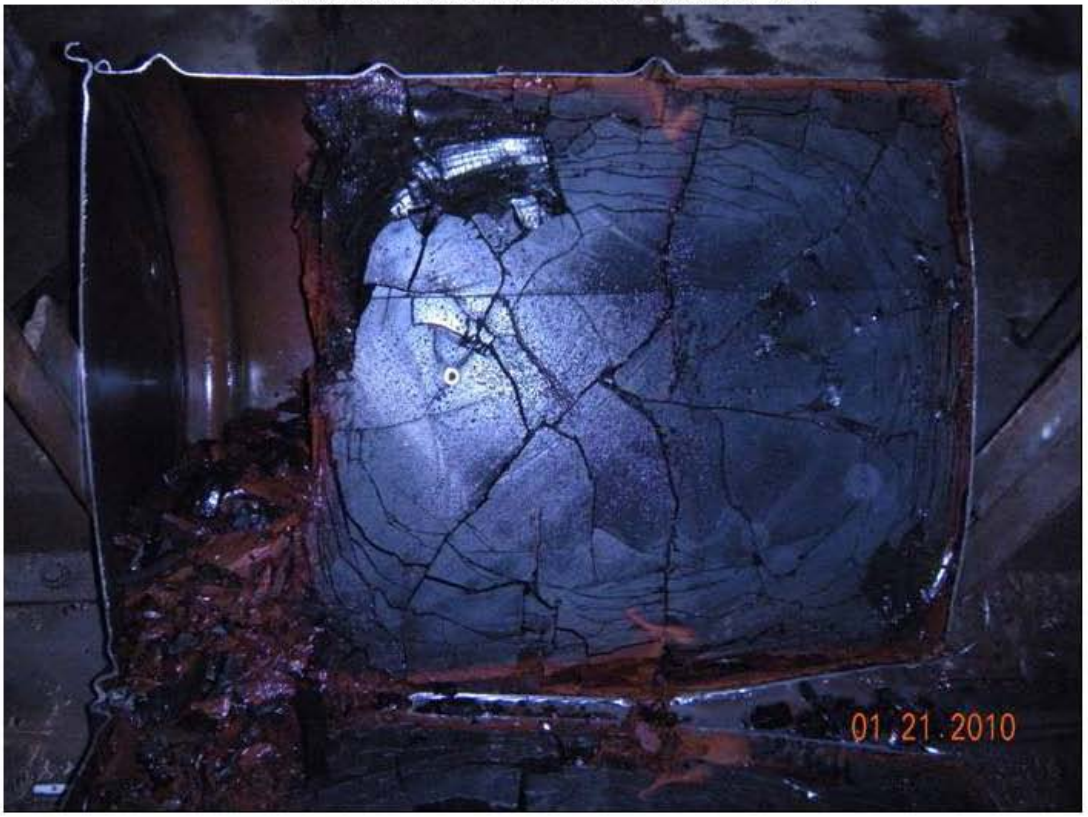

Overall view, right half of drum after cut.

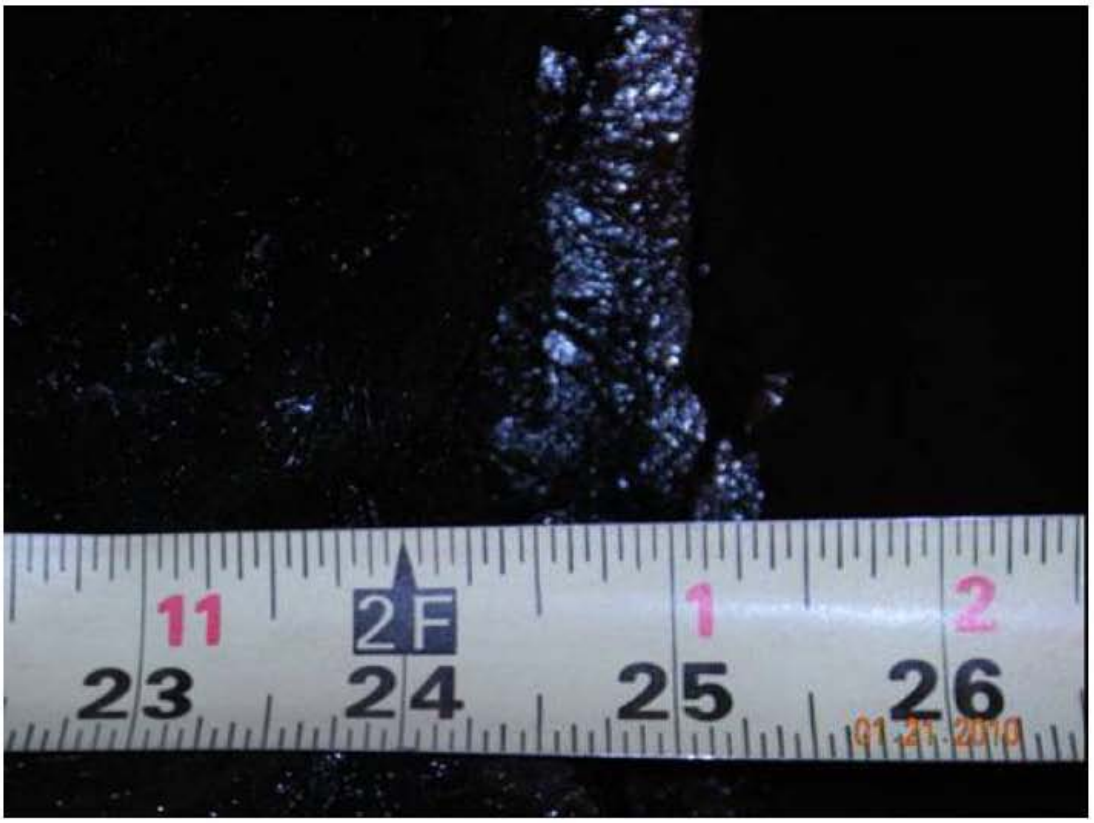

Glass measured @ 1" from right wall of right half of drum.

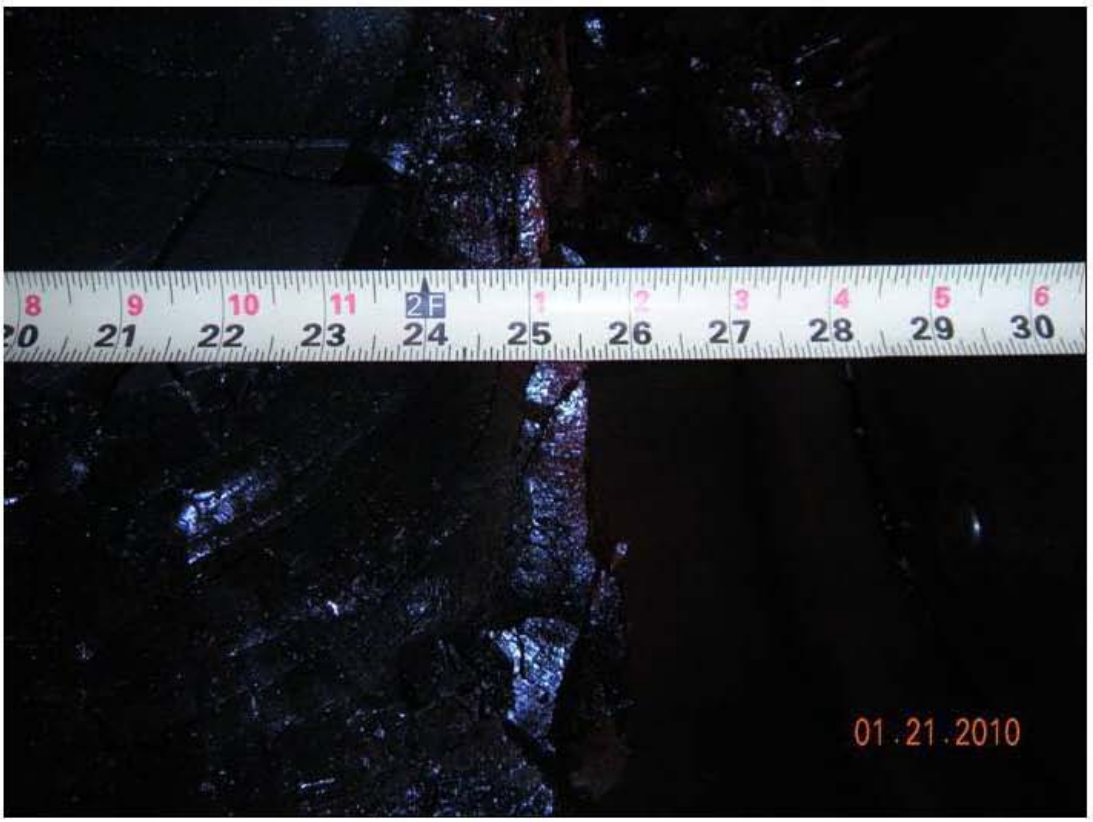

Glass measured @ 6" from right wall of right half of drum.

Glass measured @ center line of right half of drum.

Glass measured @ 6" from left wall of right half of drum.

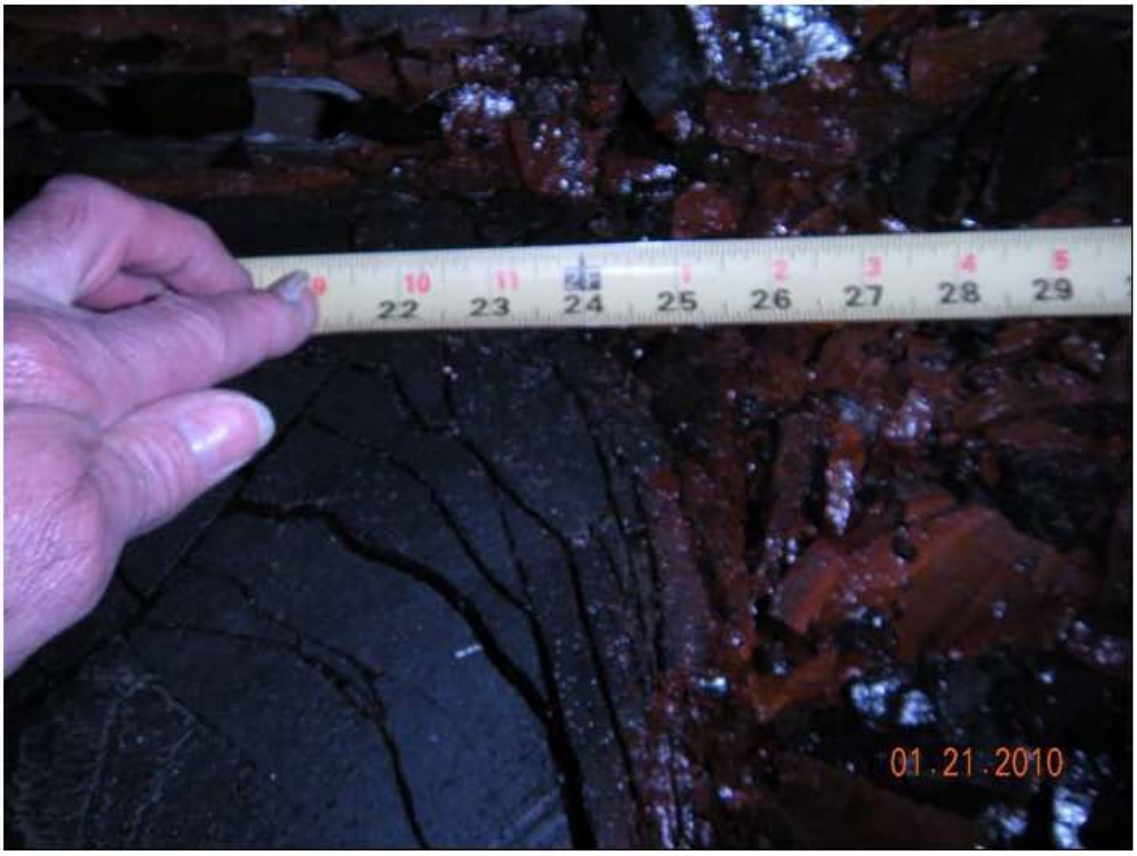

Glass measured @ 1" from left wall of right half of drum.

G-12O-85A
1/21/2010

LEFT HALF

Picture Ref. # 1
overall view of left
half of drum

Note 1: LARGE AREA OF MINIMAL FOAMING NEAR CENTER OF DRUM

NOTE 2: NO METALLIC PHASES OBSERVED THROUGHOUT THE GLASS

NOTE 3: NO SECONDARY PHASES OBSERVED THROUGHOUT THE GLASS

NOTE 4: RED/BROWN STRIATIONS OBSERVED THROUGHOUT BUT HEAVIER AROUND EDGES OF GLASS AND AT SURFACE

RIGHT HALF

Picture Ref. # 2
overall view of right
half of drum

Pictures;
Ref. # 8: Left half of drum, void @ t/w
Ref. #9: Right half of drum, void @ t/w

Note 4: void under t/w is ~ 6" sphere

Measurements of glass from the bottom of the glass to the top of glass in inches.

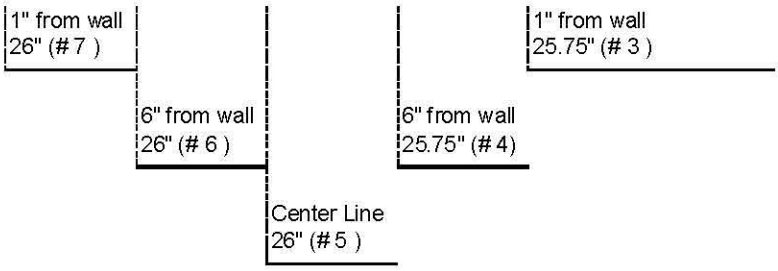

Overall view, left half of drum after cut.

Overall view, right half of drum after cut.

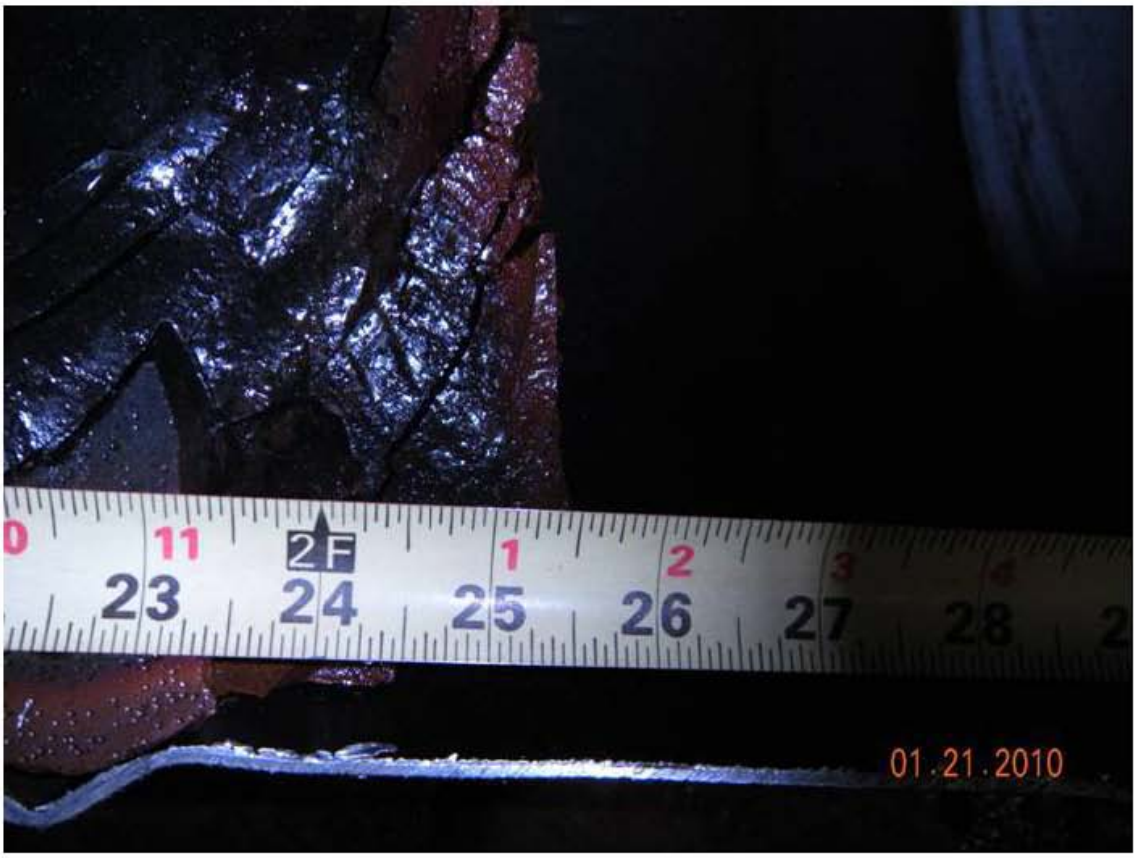

Glass measured @ 1" from right wall of right half of drum.

Glass measured @ 6" from right wall of right half of drum.

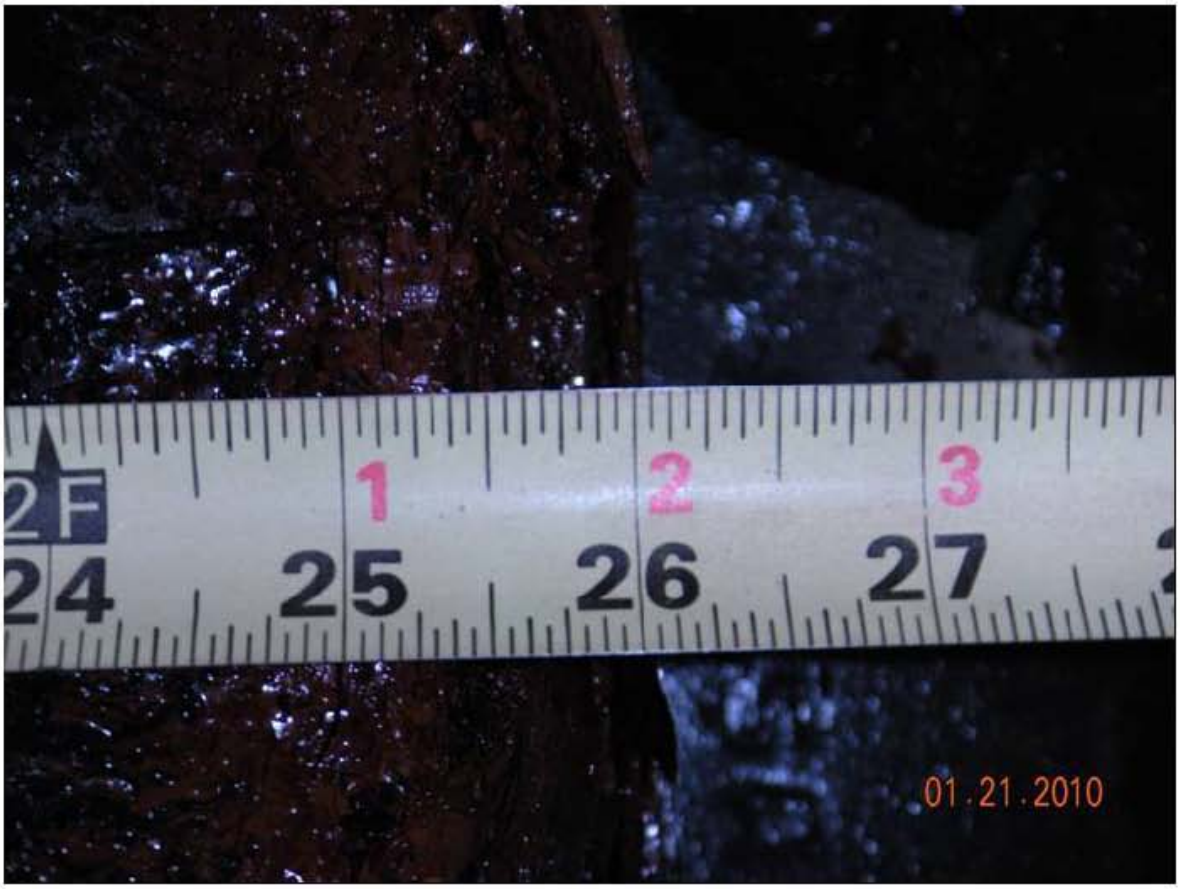

Glass measured @ center line of right half of drum.

Glass measured @ 6" from left wall of right half of drum.

Glass measured @ 1" from left wall of right half of drum.

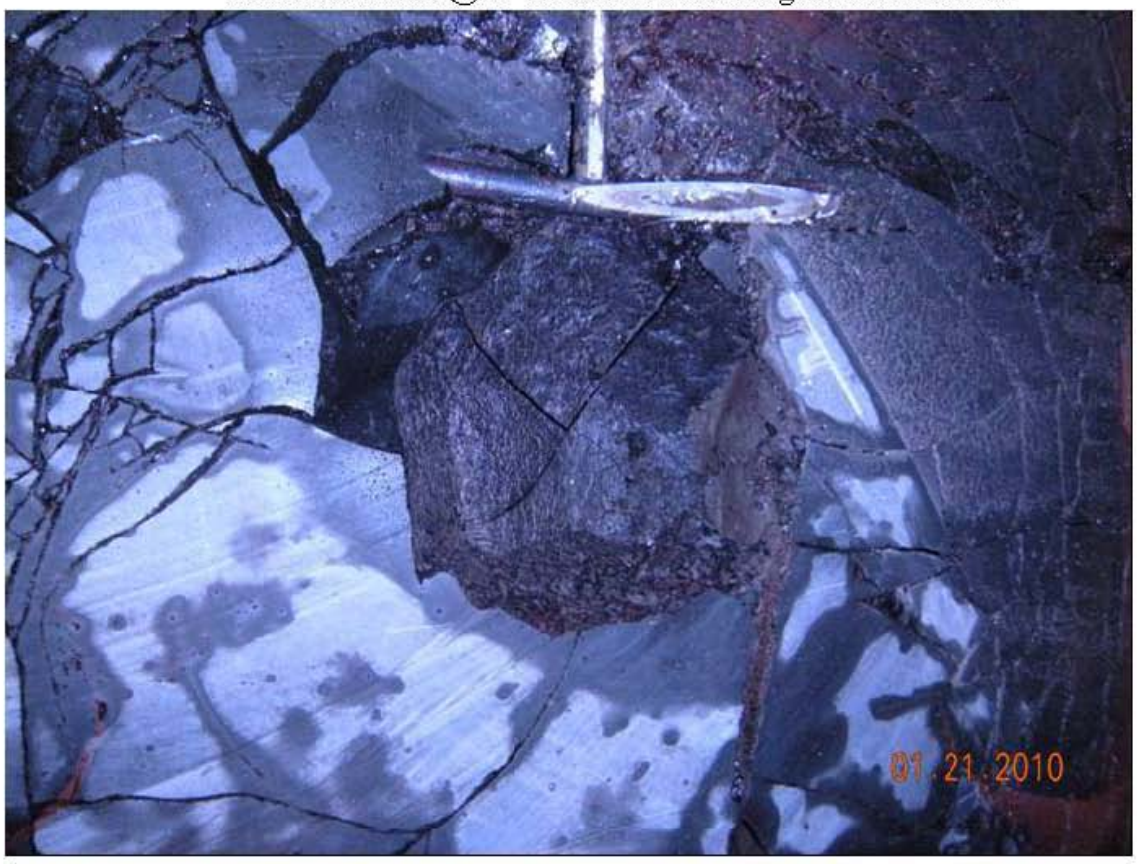

Left half of drum, void area around t/w.

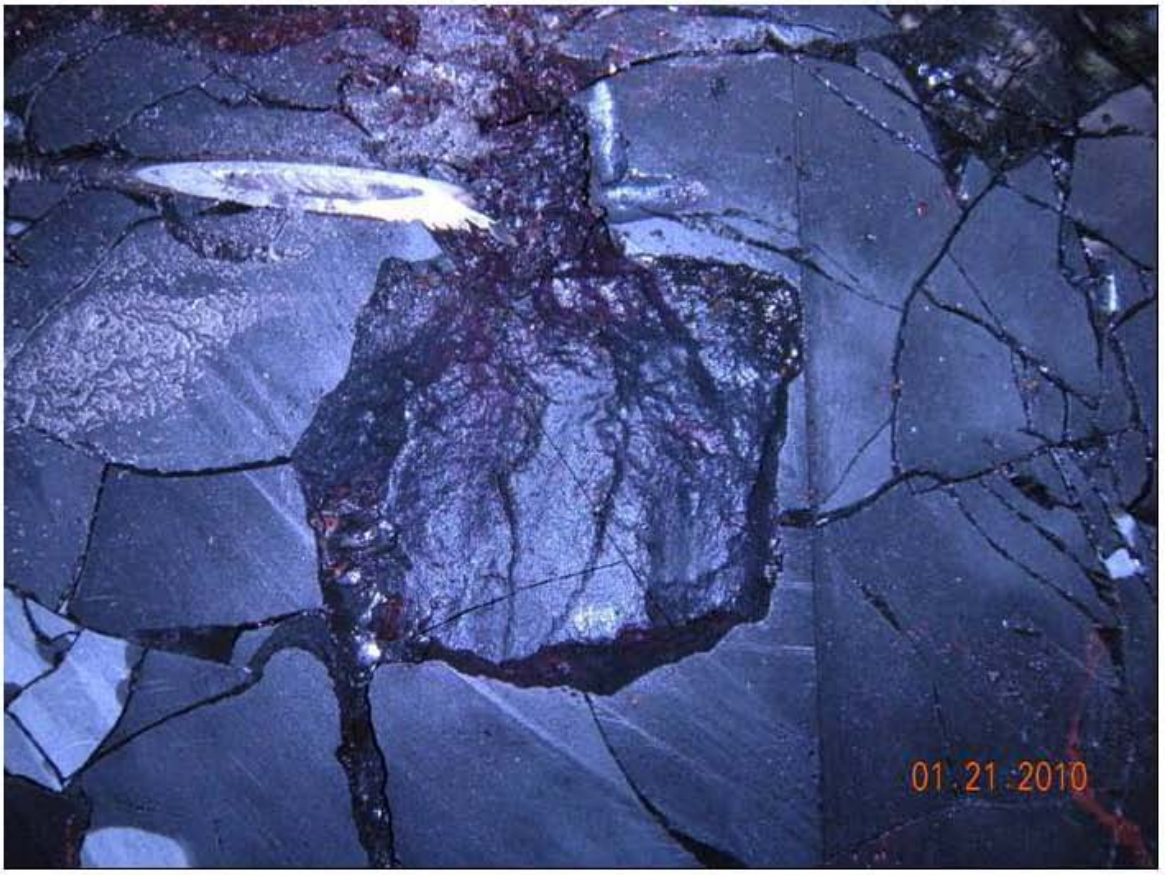

Right half of drum, void area around t/w.

G-12O-69A
1/21/10

LEFT HALF

Picture Ref. # 1
overall view of left half of drum

Note 1: Not as foamy throughout as later discharges

NOTE 2: YES / NO METALLIC PHASES OBSERVED THROUGHOUT THE GLASS

NOTE 3: YES / NO SECONDARY PHASES OBSERVED THROUGHOUT THE GLASS

NOTE 4: RED/BROWN STRIATIONS OBSERVED THROUGHOUT BUT VERY HEAVY IN VOID ABOVE T/W

RIGHT HALF

Picture Ref. # 2
overall view of right half of drum

Pictures;
Ref. # 8: Left half of drum, void @ t/w
Ref. #9: Right half of drum, void @ t/w

Note 4: See drawing below for void around t/w description. Equal depth on each half of drum ~3"

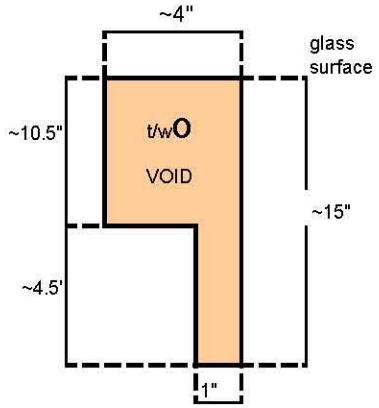

Measurements of glass from the bottom of the glass to the top of glass in inches.

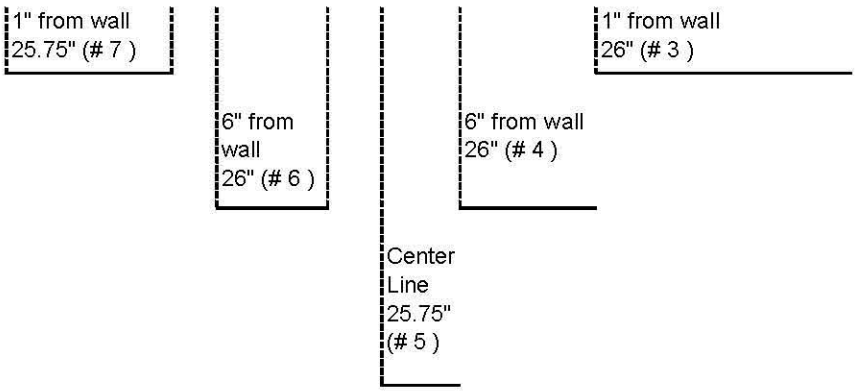

Overall view, left half of drum after cut.

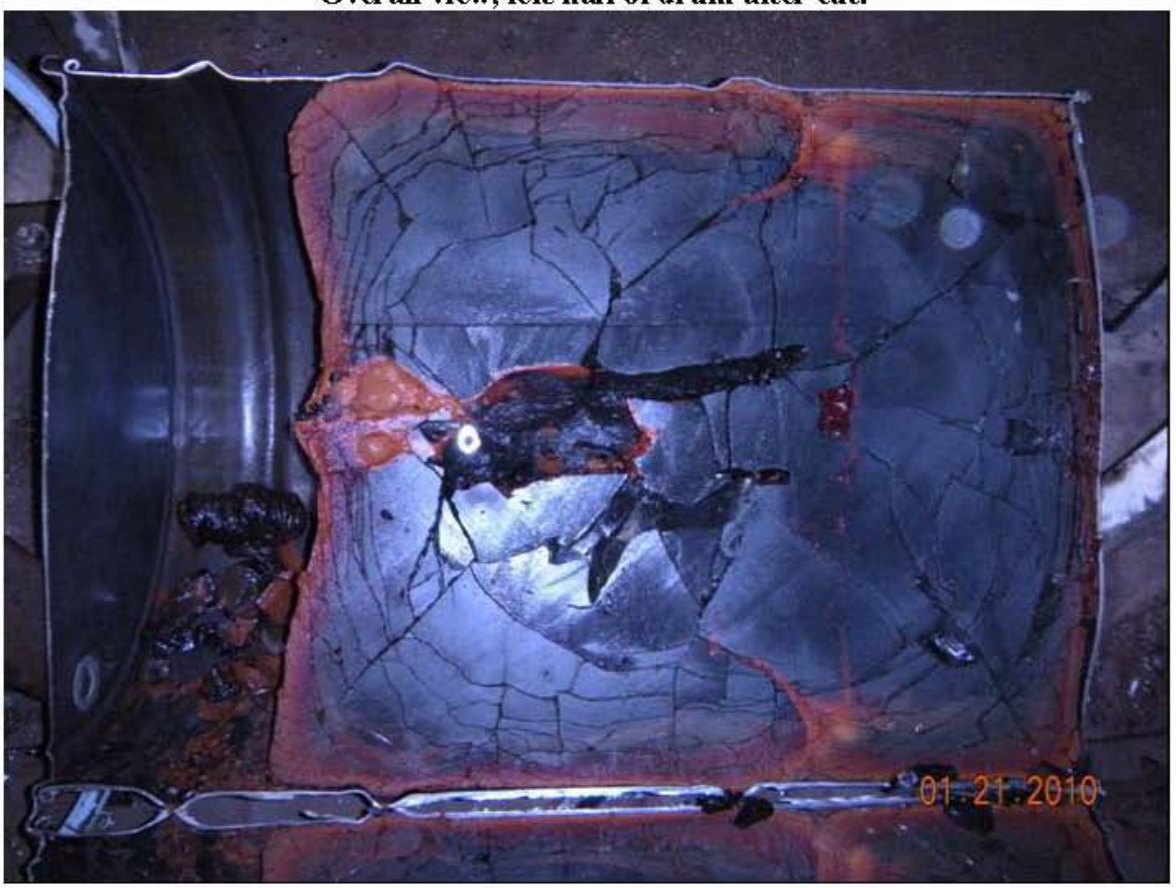

Overall view, right half of drum after cut.

Glass measured @ 1" from right wall of right half of drum.

Glass measured @ 6" from right wall of right half of drum.

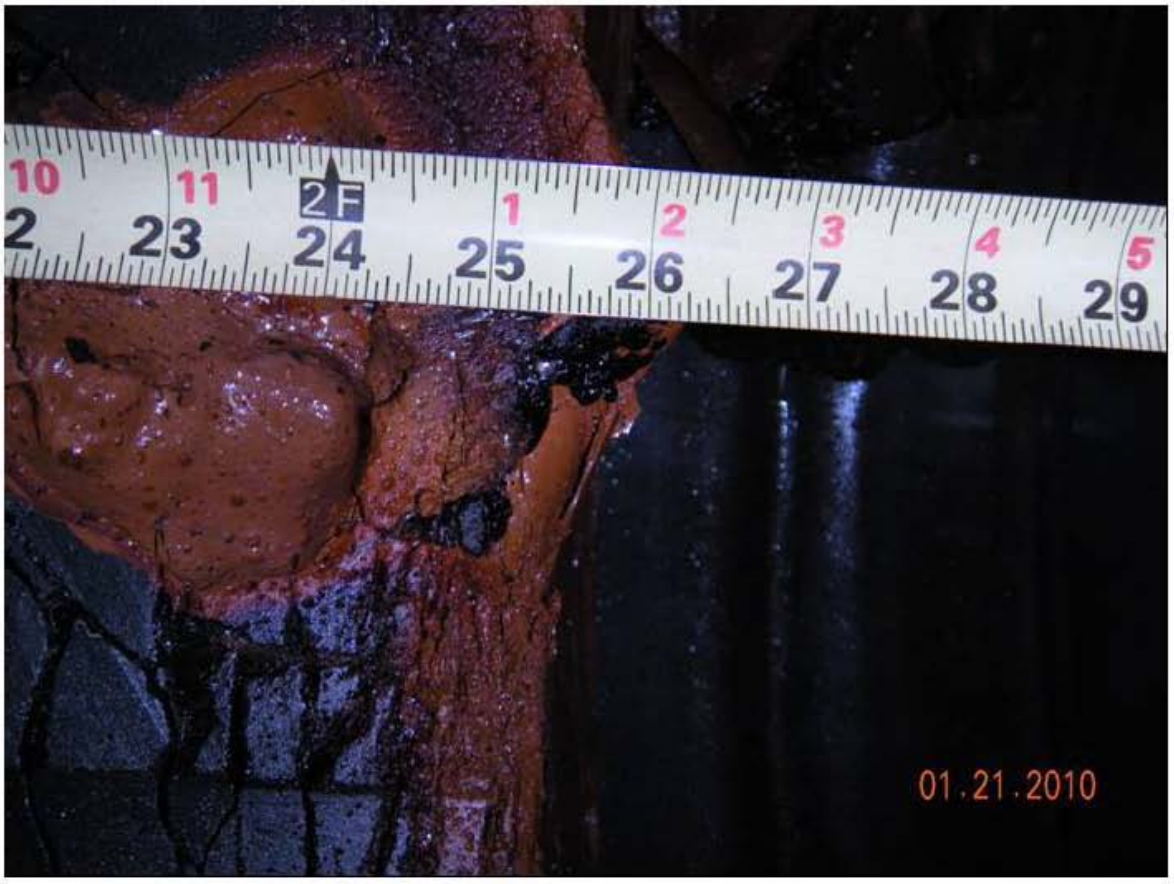

Glass measured @ center line of right half of drum.

Glass measured @ 6" from left wall of right half of drum.

Glass measured @ 1" from left wall of right half of drum.

Left half of drum, void area around t/w.

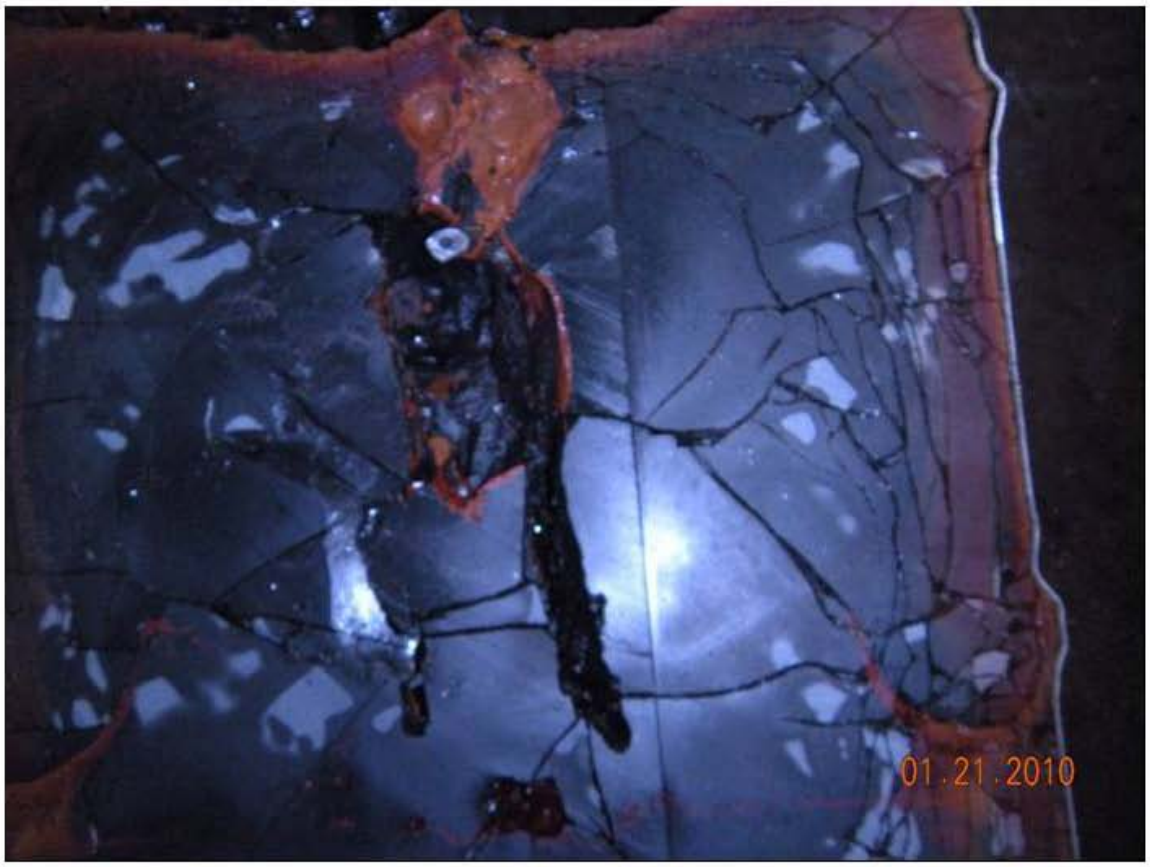

Right half of drum, void area around t/w.

G-12O-53A
1/21/10

LEFT HALF

Picture Ref. # 1
overall view of left
half of drum

Note 1: Minimal foam

NOTE 2: NO METALLIC PHASES OBSERVED THROUGHOUT THE GLASS

NOTE 3: NO SECONDARY PHASES OBSERVED THROUGHOUT THE GLASS

NOTE 4: RED/BROWN STRIATIONS OBSERVED AROUND EDGES OF GLASS AND ~9" FROM BOTTOM OF DRUM

RIGHT HALF

Picture Ref. # 2
overall view of right
half of drum

Picture Ref. # N/A

Note 5: NO voids

Measurements of glass from the bottom of the glass to the top of glass in inches.

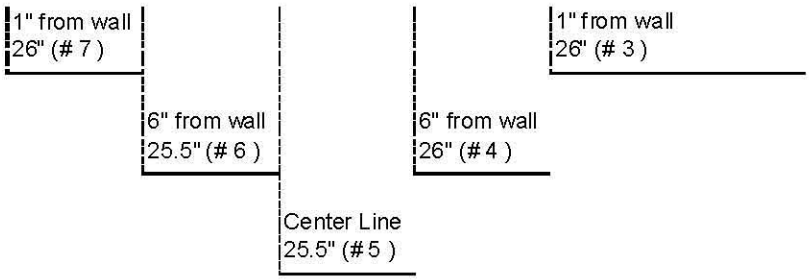

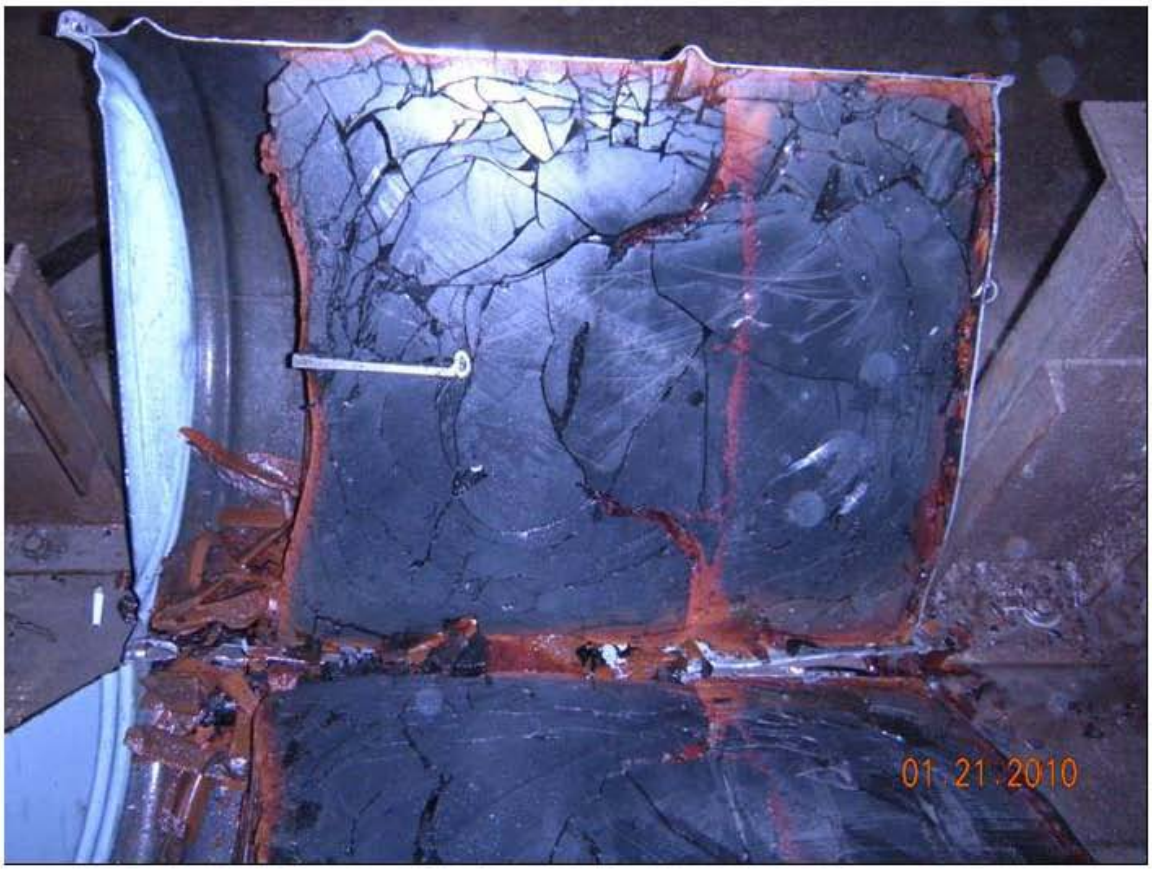

Overall view, left half of drum after cut.

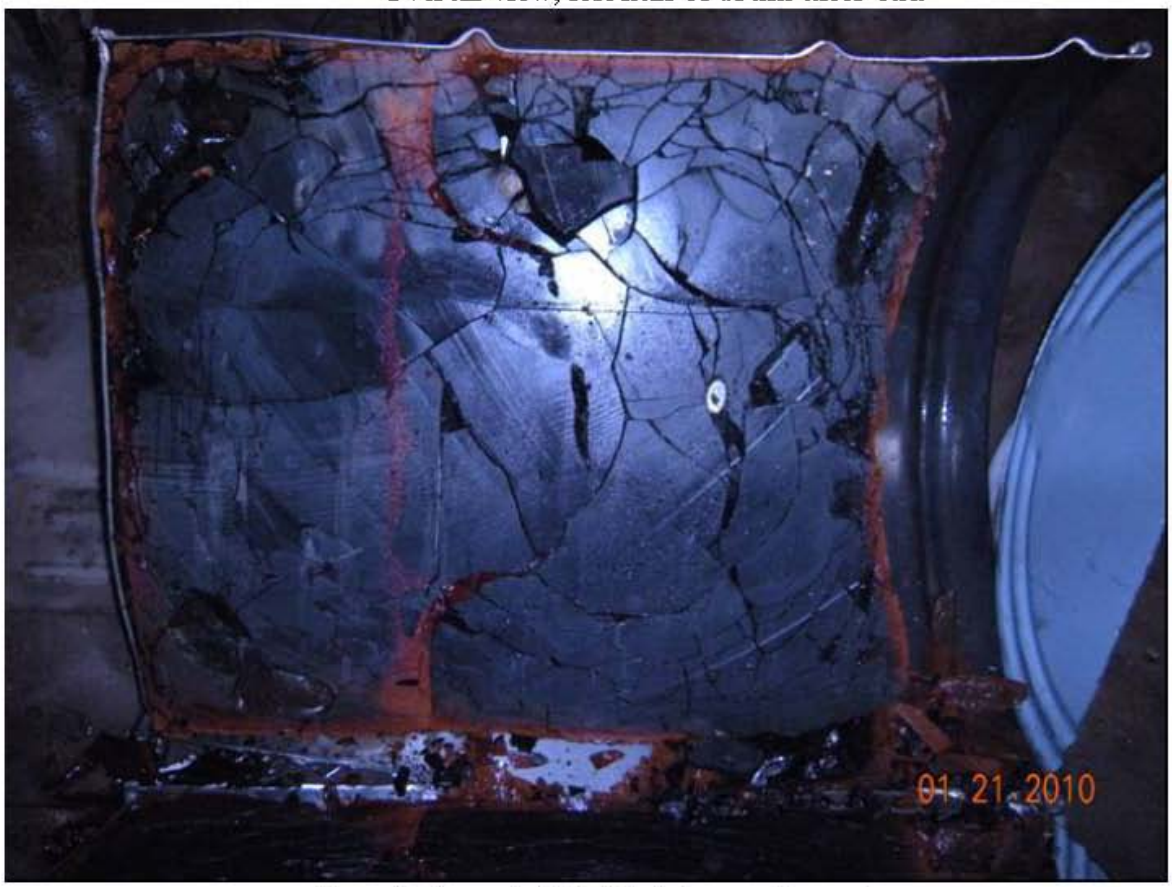

Overall view, right half of drum after cut.

Glass measured @ 1" from right wall of right half of drum.

Glass measured @ 6" from right wall of right half of drum.

Glass measured @ center line of right half of drum.

Glass measured @ 6" from left wall of right half of drum.

Glass measured @ 1" from left wall of right half of drum.